NATIONAL ADVISORY COMMITTEE FOR AERONAUTICS

JPL LIBRARY
CALIFORNIA INSTITUTE OF TECHNOLOGY

WARTIME REPORT

ORIGINALLY ISSUED
December 1943 as
Advance Confidential Report 3L08

WIND-TUNNEL DATA ON THE AERODYNAMIC CHARACTERISTICS OF AIRPLANE CONTROL SURFACES

By Richard I. Sears

Langley Memorial Aeronautical Laboratory
Langley Field, Va.

CASE FILE COPY

NACA

WASHINGTON

NACA WARTIME REPORTS are reprints of papers originally issued to provide rapid distribution of advance research results to an authorized group requiring them for the war effort. They were previously held under a security status but are now unclassified. Some of these reports were not technically edited. All have been reproduced without change in order to expedite general distribution.

NATIONAL ADVISORY COMMITTEE FOR AERONAUTICS

ADVANCE CONFIDENTIAL REPORT

L-653

WIND-TUNNEL DATA ON THE AERODYNAMIC CHARACTERISTICS OF AIRPLANE CONTROL SURFACES

By Richard I. Sears

SUMMARY

A collection of wind-tunnel data on the lift and hinge-moment characteristics of various types of airplane control surface is presented. These data, most of which have been previously published, include a major part of the results of both two- and three-dimensional-flow control-surface tests that have been made in the LMAL 4- by 6-foot vertical tunnel and the LMAL 7- by 10-foot tunnel. Data are included for control surfaces of various airfoil sections both without aerodynamic balance and with aerodynamic balance of the overhang (inset-hinge), horn, internal, and beveled-trailing-edge types. The control surfaces dealt with in this paper are mainly of the wide-chord type suitable for use as elevators or rudders. A summary of data pertaining to narrow-chord flaps is to be presented in another paper dealing with aileron characteristics.

These basic data, supplemented by additional data not included in this paper, have been used to determine curves correlating the results of many tests of the various types of aerodynamic balance. A very limited discussion of the characteristics of several types of balanced control surface is included. A method of applying section data to compute the aerodynamic characteristics of finite control surfaces is briefly outlined and discussed.

INTRODUCTION

The NACA has been conducting an extensive wind-tunnel investigation to determine the aerodynamic characteristics of various types of airplane control surface in order to supply data for design purposes. This investigation has been conducted primarily with two-dimensional-flow models in the LMAL 4- by 6-foot vertical tunnel.

Existing equipment has recently been modified in order to test control surfaces of finite span in three-dimensional flow in the LMAL 7- by 10-foot tunnel. Several airplane tail surfaces have already been tested as finite-span models, and the control-surface investigation is still in progress, both two- and three-dimensional-flow tests being made.

L-663

Two-dimensional-flow pressure-distribution measurements have been made of an NACA 0009 airfoil with various sizes of plain flaps and tabs (references 1 to 3). These data have been analyzed and parameters for determining the aerodynamic section characteristics of a thin symmetrical airfoil with plain, sealed flaps of any chord have been experimentally established (reference 4). Certain theoretical relationships developed by Glauert and Perring (references 5 and 6) from lifting-line theory for a thin airfoil with multiple flaps are reviewed in reference 4.

Force-test measurements have been made in two-dimensional flow to determine the aerodynamic section characteristics of the following control-surface arrangements:

(a) NACA 0009, NACA 0015, and NACA 66-009 airfoils with flaps having a systematic variation of flap nose overhang, flap nose shape, and gap at the flap nose

(b) NACA 0015 and NACA 66-009 airfoil with flaps of straight-line contours

(c) NACA 0009 airfoil with flaps of thickened profile and various beveled trailing-edge shapes

(d) NACA 0009 and NACA 0015 airfoils with flaps having various arrangements of internal aerodynamic balances

The results of most of these tests have been published and are presented in references 7 to 20.

Force tests have been made in three-dimensional flow of a series of horizontal tail surfaces mounted on a typical pursuit fuselage. These tests (references 21 and 22) provided a systematic variation of elevator overhang, elevator nose shape, gap at the elevator nose, and beveled

trailing edges and were made at large angles of attack and large angles of yaw to simulate spin conditions. Two 0.5-scale models of the horizontal tail surface of a torpedo-bomber type airplane have been tested as semi-span models. These tests (unpublished) provided a systematic variation of the unshielded horn types of aerodynamic balance and of elevators with a large overhang and a leading tab. A 0.45-scale vertical tail of a pursuit-type airplane was mounted on a stub fuselage for testing with and without a horizontal tail. These test results (unpublished) furnish data for a rudder with various overhang and internal types of aerodynamic balance.

The purpose of this paper is to assemble in one report the main portion of the experimental data from the various phases, previously mentioned, of the NACA wind-tunnel investigation of control-surface characteristics. The data given in this report are therefore, of necessity, much condensed. Further details and data for each particular phase of the investigation may be obtained by referring to the reports already published on that particular subject. (See list of references.) The section data presented are equally applicable to ailerons and to tail surfaces.

Test data on finite-span ailerons are given in reference 23, but some of the curves presented herein summarizing the characteristics of various types of aerodynamic balance include data from tests of finite-span ailerons.

APPARATUS, MODELS, AND TESTS

Two-Dimensional-Flow Tests

The section data presented in this paper were obtained from tests made in the LMAL 4- by 6-foot vertical tunnel, which is described in reference 24. The test section of this tunnel has been converted from the original open, circular, 5-foot-diameter jet to a closed, rectangular 4- by 6-foot throat. A diagram of the test section and the airfoil installation for two-dimensional flow is presented in references 1 to 3. A three-component balance system has been installed to allow force-test

measurements of lift, drag, and pitching moments to be made. Hinge moments were obtained by measuring electrically the twist of a short torque rod or the strain of a small cantilever beam when subjected to the hinge-moment load.

The force-test models, for which results are presented for two-dimensional-flow tests in figures 1 to 106, were rectangular 2-foot-chord by 4-foot-span wings made of laminated mahogany. The flaps were provided with ball-bearing hinges in order to minimize friction. The models, when mounted in the tunnel, completely spanned the test section. With this type of installation, two-dimensional flow is approximated and section characteristics of the airfoil and flap can be determined. The models were attached to the balance frame by torque tubes that extended through the sides of the tunnel. The angle of attack was set from outside the tunnel by rotating the torque tubes with an electric drive. Flap deflections were set inside the tunnel by templets and were held by friction clamps. L-663

The airfoil profile, flap shape, and gap at the flap nose for each particular control-surface arrangement are illustrated at the top of the figure presenting the data for that arrangement. Further details and dimensions for each arrangement may be found in the original reports listed as references on each figure. The surfaces of all the airfoils were filled and finished with either shellac or lacquer to form a smooth surface.

The two-dimensional-flow tests were made at a dynamic pressure of 15 pounds per square foot, which corresponds to a velocity of about 76 miles per hour at standard sea-level conditions. The test Reynolds number was about 1,430,000. The turbulence factor of the LMAL 4- by 6-foot vertical tunnel being 1.95, the effective Reynolds number of the tests was therefore about 2,700,000.

Three-Dimensional-Flow Tests

The tests of finite-span models, for which data are presented in figures 107 to 139, were made in the LMAL 7- by 10-foot tunnel which is described in reference 25.

The horizontal tail surfaces shown in figures 107 to 122 were of NACA 0009 airfoil section and were mounted

on a 1/6-scale model of a typical pursuit fuselage. The fuselage junctures were filleted. The model had no wing, propeller, or vertical tail and the cut-out for the wing through the fuselage was faired in. The fuselage was mounted in the conventional manner on the balance fork for force-test measurements. Hinge moments were measured electrically by means of a calibrated torque rod inside the fuselage. The tests were made at a dynamic pressure of 16.37 pounds per square foot, which corresponds to a velocity of 80 miles per hour at standard sea-level conditions. Based on the average chord of the horizontal tail, 8.25 inches, the test Reynolds number was 502,000. The effective Reynolds number of the tests was 803,000, the turbulence factor of the tunnel being 1.6.

The horizontal tail surfaces shown in figures 123 to 130 were tested as semispan models by mounting one-half the tail surface vertically in the tunnel with the inboard end adjacent to the floor of the tunnel, which thereby acted as a reflection plane. The model was supported entirely by the balance frame with a small clearance at the tunnel floor so that all the forces and moments acting on the model could be measured. The flow over the model simulated the flow over the semispan of a complete horizontal tail consisting of the test panel joined to its reflection and mounted in a 10- by 14-foot tunnel.

Provisions were made for changing the angle of attack of the model and the elevator deflection while the tunnel was in operation. The elevator hinge moments were measured by means of an electrical strain gage mounted within the model. A dynamic pressure of 16.37 pounds per square foot was maintained for all tests, which corresponds to an air voloctiy of 80 miles per hour at standard sea-level conditions and to a test Reynolds number of 1,920,000 based on the model mean chord of 2.63 feet.

The airfoil section of the horizontal tail surfaces of figures 123 to 130 were modified symmetrical NACA sections about 11-percent chord thick at the root and about 7-percent chord thick at the tip. The airfoil contour back of the hinge axis was a straight line.

The vertical tail surfaces shown in figures 131 to 139 were mounted on a stub fuselage. All arrangements were tested with a dummy horizontal tail surface except that of figure 133, which was tested without the horizontal

tail surface. The vertical surface was derived from NACA 65-series airfoil profiles modified by extending the tip sections and shortening the root sections to give an airfoil section about 10.5-percent chord thick at the root and about 9.5-percent chord thick near the tip. The airfoil contour back of the hinge axis was a straight line. The horizontal tail surface had a flat-plate rather than an airfoil contour and had a conventional plan form with about 2:1 taper ratio and circular tips. The rudder was slotted to clear the horizontal tail. The gap at the nose of the rudder, when unsealed, was 0.113 inch and was constant along the span. The cut-outs for the hinge arms were unsealed for all tests except for the sealed internal balance (fig. 138).

The aerodynamic characteristics presented in figures 131 to 139 are those for the vertical tail alone plus interferences, the contribution of the stub fuselage and horizontal tail having been deducted. A dynamic pressure of 16.87 pounds per square foot was maintained for these tests, which corresponds to an air velocity of 80 miles per hour at standard sea-level conditions and to a test Reynolds number of 1,510,000 based on the model mean chord of 2.06 feet.

SYMBOLS

The symbols used in this paper are:

C_L airfoil lift coefficient (L/qS)

c_l airfoil section lift coefficient $(l/qc = dL/qcdb)$

c_{l_o} airfoil section lift coefficient at $\alpha = \delta = 0$

C_h hinge-moment coefficient of control surface $(H/q\bar{c}_f{}^2 b_f)$

$C_{h'}$ elevator hinge-moment coefficient (figs. 107 to 122 only) $(H/q\bar{c}_e S_e)$

c_{h_f} flap section hinge-moment coefficient $(h/qc_f{}^2 = dH/qc_f{}^2 db)$

c_H flap section hinge-moment coefficient $(h/qc^2 = dH/qc^2 db)$

P	pressure coefficient $\left(\frac{p - p_o}{q}\right)$
P_R	resultant pressure coefficient $\left[P_{lower} - P_{upper}\right]$
L	airfoil lift
l	airfoil section lift (dL)
H	flap hinge moment
h	flap section hinge moment (dH)
p	static pressure at point on airfoil surface
p_o	static pressure in free air stream
q	dynamic pressure of free air stream
S	wing area
S_f	flap area
c	chord of airfoil section
c_f	chord of flap measured at any airfoil section from hinge axis to trailing edge of airfoil
$\bar{c}_f$	root-mean-square chord of flap
c_b	chord of overhang (balancing surface)
α	angle of attack of finite-span wing
α_o	angle of attack for infinite aspect ratio
ψ	angle of yaw
δ	control-surface deflection
δ_f	deflection of flap with respect to airfoil
δ_t	deflection of tab with respect to flap
b	span of surface
y	spanwise dimension of wing
x	chordwise location of vent measured from airfoil nose

A aspect ratio

t thickness of control surface at hinge

R test Reynolds number

M Mach number

λ ratio of tip chord to root chord

$$C_{L_\alpha} = (C_{L_\alpha})_\delta = \left(\frac{\partial C_L}{\partial \alpha}\right)_\delta$$

$$c_{l_\alpha} = (c_{l_\alpha})_\delta = \left(\frac{\partial c_l}{\partial \alpha_o}\right)_\delta$$

$$\alpha_\delta = (\alpha_\delta)_{c_l} = \left(\frac{\partial \alpha}{\partial \delta}\right)_{c_l}$$

$$C_{h_\alpha} = (C_{h_\alpha})_\delta = \left(\frac{\partial C_h}{\partial \alpha}\right)_\delta$$

$$C_{h_\delta} = (C_{h_\delta})_\alpha = \left(\frac{\partial C_h}{\partial \delta}\right)_\alpha$$

$$c_{h_\alpha} = (c_{h_\alpha})_\delta = \left(\frac{\partial c_h}{\partial \alpha_o}\right)_\delta$$

$$c_{h_\delta} = (c_{h_\delta})_\alpha = \left(\frac{\partial c_h}{\partial \delta}\right)_\alpha$$

$$P_\alpha = (P_\alpha)_\delta = \left(\frac{\partial P}{\partial \alpha}\right)_\delta$$

$$P_\delta = (P_\delta)_\alpha = \left(\frac{\partial P}{\partial \delta}\right)_\alpha$$

$c_{l_{\alpha_3}}$ rate of change of section lift coefficient with angle of attack of entire finite-span wing

$c_{l_{\delta_3}}$ rate of change of section lift coefficient with deflection of entire flap on finite-span wing

$$\left.\begin{matrix} c_{l_{a_1}} \\ c_{l_{b_1}} \end{matrix}\right\}$$ span-load distribution factors defined by equation (12)

$$\left(c_{h_{c_l}}\right)_{\delta} = \left(\frac{\partial c_h}{\partial c_l}\right)_{\delta}$$

$$\left(c_{h_{\delta}}\right)_{c_l} = \left(\frac{\partial c_h}{\partial \delta}\right)_{c_l}$$

Subscripts:

f	flap
t	tab
e	elevator
r	rudder
b	balance (overhang)
s	control stick

Subscripts outside the parentheses around the partial derivatives indicate the variables held constant when the derivatives are taken. The term "flap" is used as a general expression for any movable control surface such as a rudder, elevator, aileron, or tab. The term "control stick" is used as a general expression for the pilot's control-surface-actuating device whether it be a stick, a wheel, or pedals.

PRESENTATION OF DATA

A summary of information for convenience in locating the data is presented in tables I to III.

Lift and flap hinge-moment characteristics are presented as functions of angle of attack (or angle of yaw) at various flap deflections for the control-surface arrangements previously discussed (figs. 1 to 139). Insofar as has been practical, the same symbols for each flap deflection and the same scales have been used on each

figure. In some cases, however, it has been necessary to halve the scale of ordinates or abscissas in order to be able to include all the data.

Figures 140 to 142 pertain to plain flaps with sealed gaps on the NACA 0009 airfoil. Figure 140 shows the chordwise distribution of the resultant pressure-coefficient parameters P_{R_α} and P_{R_δ}. These distributions were experimentally determined in the two-dimensional-flow pressure-distribution investigations reported in references 1 to 3. The hinge-moment parameters c_{h_α} and c_{h_δ} and the lift-effectiveness parameters α_δ measured from the same series of tests are plotted in figures 141 and 142 as functions of the ratio of flap chord to airfoil chord. A few points from more recent force tests have also been plotted on these curves.

Figures 143 to 146 pertain to the overhang (inset-hinge) type of aerodynamic balance. The hinge-moment and lift parameters plotted as functions of overhang were measured from some of the data presented in figures 1 to 139. The slopes were measured at zero flap deflection and hence the values are valid only at these points unless the curves are linear. The original data, therefore, rather than the measured slopes, should be used for design purposes; the curves of figures 143 to 146 are merely indicative of the relative merits of various arrangements of aerodynamic balances.

Figures 147 and 148 pertain to the characteristics of tabs on plain flaps with sealed gaps. Figure 147 presents the parameter $c_{h_{f_{\delta_t}}}$ as a function of tab size for various sizes of flaps. These data were obtained by integrating the pressure-distribution diagrams (fig. 140) about the appropriate axes. The curves of figure 148 show the computed characteristics of various sizes of balancing tabs on a 0.30c and a 0.50c plain flap.

Figure 149, derived from unpublished data, presents pressure-distribution characteristics typical of beveled-trailing-edge control surfaces. Figure 150, based on the correlation presented in reference 26, summarizes available data from references 11, 16, 27, and 28 and unpublished data on the hinge moments of flaps with beveled

trailing edges. The increments of c_{h_α} and c_{h_δ} caused by the bevels are plotted as functions of the included angle at the trailing edge of the airfoil.

Figures 151 and 152, taken from reference 29, summarize available experimental data from references 30, 31, and 32 and unpublished data on the characteristics of flaps with internal aerodynamic balance. Values of ΔC_{h_α} and ΔC_{h_δ} are plotted as a function of parameters defining the geometric dimensions of the balancing plate and of the flap to be balanced.

Figures 153 and 154, adapted from reference 33, pertain to the horn type of aerodynamic balance. Increments of C_{h_α} and C_{h_δ} from the data of figures 123 to 136, supplemented by other test data from references 34 to 39, are plotted in figure 154 as a function of the square root of the ratio of horn area times mean horn chord to control area times mean control chord.

DISCUSSION

Tunnel corrections to section data.- The section data presented have been partly corrected for tunnel effects. An experimentally determined correction has been applied only to lift. Recent theoretical analysis of the corrections for the streamline curvature caused by the tunnel walls indicates that the experimental correction applied to c_{l_α} is in reasonable agreement with the calculated value. The calculated correction to c_{l_δ} was less than that actually applied, which fact indicates that the values of α_δ presented may be about 5 percent too small.

The tunnel correction that should be applied to hinge moments is dependent on the chord of the flap and the size and type of aerodynamic balance employed. The correction may be expressed as

$$\Delta c_{h_{c_l}} = 0.6 \frac{c_{l_\alpha}(c/g)^2}{(c_f/c)^2} F$$

although some tests have been made with modifications to these basic shapes. The data (figs. 144 and 146) indicate that on all airfoils tested, for a given amount of overhang, greatest balance is secured with a blunt-nose shape and progressively less balance is obtained as the nose shape becomes sharper. Regardless of nose shape, flaps with large overhangs were not so closely balanced at small deflections as at moderate deflections up to the deflection at which the flap nose unported. When the flap nose unported, large increases in hinge moment and large losses in lift resulted with all nose shapes. At negative angles of attack and positive flap deflections (the attitude at which the pilot must hold the elevator when landing or the rudder when causing sideslip), overhang types of aerodynamic balances are most closely balanced and the lift effectiveness of the control is maintained to 5° or 10° beyond the unporting angle of the control. At zero or positive angles of attack with positive flap deflection (position of rudder to overcome yaw due to asymmetrical power conditions) control surfaces with large overhangs cannot be relied on to maintain lift effectiveness beyond the unporting angle. Further deflection causes air-flow separation over the flap. This separation of flow gives a large increase in hinge moment and no increase (often even a decrease) in lift. At positive angles of attack far above the airfoil stall, flaps with overhangs tended to float at greater negative deflections than did plain unbalanced flaps (figs. 107 to 116) but generally required less force to hold zero or positive deflections under this condition.

The lift effectiveness of flaps generally increased slightly with increases in the size of the flap nose overhang (figs. 143 and 145), but the lift effectiveness of a flap with overhang was still primarily determined by the ratio of the chord of movable surface behind the hinge to the total airfoil chord. Unsealing the gap at the flap nose generally improved the lift effectiveness of a flap with overhang; whereas, it decreased the lift effectiveness of a plain flap.

Medium flap nose shapes generally gave more satisfactory characteristics for a control surface than did either the blunt or sharp nose shapes. The blunt shape gave more balance but produced greater losses in lift and balancing moment when the flap unported. The drag of a flap with sharp nose shape was excessive.

trailing edges. The increments of c_{h_α} and c_{h_δ} caused by the bevels are plotted as functions of the included angle at the trailing edge of the airfoil.

Figures 151 and 152, taken from reference 29, summarize available experimental data from references 30, 31, and 32 and unpublished data on the characteristics of flaps with internal aerodynamic balance. Values of ΔC_{h_α} and ΔC_{h_δ} are plotted as a function of parameters defining the geometric dimensions of the balancing plate and of the flap to be balanced.

Figures 153 and 154, adapted from reference 33, pertain to the horn type of aerodynamic balance. Increments of C_{h_α} and C_{h_δ} from the data of figures 123 to 126, supplemented by other test data from references 34 to 39, are plotted in figure 154 as a function of the square root of the ratio of horn area times mean horn chord to control area times mean control chord.

DISCUSSION

Tunnel corrections to section data.- The section data presented have been partly corrected for tunnel effects. An experimentally determined correction has been applied only to lift. Recent theoretical analysis of the corrections for the streamline curvature caused by the tunnel walls indicates that the experimental correction applied to c_{l_α} is in reasonable agreement with the calculated value. The calculated correction to c_{l_δ} was less than that actually applied, which fact indicates that the values of α_δ presented may be about 5 percent too small.

The tunnel correction that should be applied to hinge moments is dependent on the chord of the flap and the size and type of aerodynamic balance employed. The correction may be expressed as

$$\Delta c_{h_{c_l}} = 0.6 \frac{c_{l_\alpha}(c/g)^2}{(c_f/c)^2} F$$

The term c/g is the ratio of the chord of the model to the tunnel gap. This ratio was 1/2 for the pressure-distribution test results shown in figures 140 to 142, and was 1/3 for all other section data presented. The factor F is dependent on the size and type of aerodynamic balance and has been evaluated for only the overhang type of balance. Values of F for plain flaps of various chords and for a 0.30c flap with various amounts of overhang have been obtained from reference 40 and are presented in figure 155. The increments of slope to be added to the section slopes presented in this paper in order to correct them to free-air values are:

$$\Delta c_{h_\alpha} = \Delta c_{h_{c_l}} c_{l_\alpha}$$

$$\Delta c_{h_\delta} = \Delta c_{h_\alpha} (-\alpha_\delta)$$

These tunnel corrections, which decrease in magnitude with increasing flap overhang, tend to make the hinge-moment slopes more positive. The corrections for beveled-trailing-edge flaps are similar to but somewhat smaller than those for plain flaps and the corrections for flaps with internal balance are similar to those with overhang.

Plain flaps.- The lift characteristics of plain flaps on the various airfoils tested are nearly independent of the airfoil shape, but the flap hinge moments vary markedly with airfoil thickness. A plain flap on the NACA 0015 airfoil gave values of c_{h_δ} that were about two-thirds and values of c_{h_α} that were about one-third of the corresponding values for a similar flap on the NACA 0009 airfoil (cf. figs. 5 and 59). These results indicate that there must be quite a difference in the distribution of pressure over the region near the trailing edge of the two airfoils. Part of this difference may be attributed to the greater included angle at the trailing edge of the thicker airfoil.

Recent unpublished tests made by the NACA and tests by the British (reference 41) indicate that the turbulence in the air stream, the boundary-layer thickness, and the location of the transition region have considerable effect upon slopes of both the lift and hinge-moment curves. The slopes of these curves decreased progressively as the tran-

sition region was fixed nearer and nearer the leading edge by means of small wires. The reduction in the slopes of c_{l_α} and c_{h_α} was greater for thicker airfoils than for thinner airfoils. The data presented in this paper, having been obtained in turbulent wind tunnels, should therefore be more applicable to tail surfaces, which are generally located in a region of fairly turbulent air flow, than to ailerons, which are usually well away from the slipstream and fuselage wake.

The chordwise distribution of the rate of change of resultant pressure coefficient with angle of attack P_{R_α} and with flap deflection P_{R_δ} (fig. 140) should not be expected to apply to airfoils other than the NACA 0009, for which the data were obtained. Because of separation phenomena the variation of P_R with α has the slope P_{R_α} only between the limits $\alpha = \pm 10^\circ$ and the variation of P_R with δ has the slope P_{R_δ} only within $\delta = \pm 10^\circ$. By graphical integration of pressure-distribution data (references 1 to 3) the variation of c_{h_α}, c_{h_δ}, and α_δ with flap chord was obtained for plain sealed flaps on the NACA 0009 airfoil (figs. 141 and 142). These figures, derived from the same pressure-distribution data as figures 1 and 2 of reference 4, have plotted on them the experimentally determined parameter values that define the curves. These data indicate that, between the limits specified, the parameters vary in the following manner with ratio of flap chord to airfoil chord:

$$c_{h_\alpha} \propto (c_f/c)^{1.00} \quad \text{for} \quad 0 < c_f/c < 0.8$$

$$c_{h_\delta} \propto (c_f/c)^{0.37} \quad \text{for} \quad 0.2 < c_f/c < 0.5$$

$$\alpha_\delta \propto (c_f/c)^{0.59} \quad \text{for} \quad 0.09 < c_f/c < 0.6$$

Increasing the gap at the flap nose adversely affected the lift effectiveness of plain flaps.

Overhang type of aerodynamic balance.- In general, three shapes of flap nose overhang have been investigated - namely, the blunt, the medium, and the sharp shapes.-

although some tests have been made with modifications to these basic shapes. The data (figs. 144 and 146) indicate that on all airfoils tested, for a given amount of overhang, greatest balance is secured with a blunt-nose shape and progressively less balance is obtained as the nose shape becomes sharper. Regardless of nose shape, flaps with large overhangs were not so closely balanced at small deflections as at moderate deflections up to the deflection at which the flap nose unported. When the flap nose unported, large increases in hinge moment and large losses in lift resulted with all nose shapes. At negative angles of attack and positive flap deflections (the attitude at which the pilot must hold the elevator when landing or the rudder when causing sideslip), overhang types of aerodynamic balances are most closely balanced and the lift effectiveness of the control is maintained to 5° or 10° beyond the unporting angle of the control. At zero or positive angles of attack with positive flap deflection (position of rudder to overcome yaw due to asymmetrical power conditions) control surfaces with large overhangs cannot be relied on to maintain lift effectiveness beyond the unporting angle. Further deflection causes air-flow separation over the flap. This separation of flow gives a large increase in hinge moment and no increase (often even a decrease) in lift. At positive angles of attack far above the airfoil stall, flaps with overhangs tended to float at greater negative deflections than did plain unbalanced flaps (figs. 107 to 116) but generally required less force to hold zero or positive deflections under this condition.

The lift effectiveness of flaps generally increased slightly with increases in the size of the flap nose overhang (figs. 143 and 145), but the lift effectiveness of a flap with overhang was still primarily determined by the ratio of the chord of movable surface behind the hinge to the total airfoil chord. Unsealing the gap at the flap nose generally improved the lift effectiveness of a flap with overhang; whereas, it decreased the lift effectiveness of a plain flap.

Medium flap nose shapes generally gave more satisfactory characteristics for a control surface than did either the blunt or sharp nose shapes. The blunt shape gave more balance but produced greater losses in lift and balancing moment when the flap unported. The drag of a flap with sharp nose shape was excessive.

It was pointed out in reference 8 that a flap with an overhang sufficiently large to give overbalance might be used in conjunction with a leading tab to correct the overbalanced condition of the flap and to increase the lift effectiveness of the control. This arrangement has been tested on a finite-span model (figs. 127 to 130). The data indicate that satisfactory control-surface characteristics can be obtained in this manner. Such an arrangement offers the possibility of utilizing the large overhang as a mass balance for the control so that metal-covered control surfaces may be utilized even with a saving in weight over conventional fabric-covered surfaces with conventional mass balance. This same idea of leading tab has been carried one step further by applying it to an all-movable tail surface (reference 42). By use of a leading tab or a flap with an all-movable tail surface, the free-floating tendency of the tail surface can be controlled in much the same manner as that for the tail surfaces of figures 127 to 130. The analysis and flight tests reported in reference 42 indicate this type of all-movable tail to be an aerodynamically desirable control-surface arrangement.

Control surfaces with large overhangs, especially those with relatively blunt nose shapes, may be unsatisfactory at high speeds because of excessive pressure peaks over the nose of the balance. Reference 43, which reports the results of tests of ailerons with various sizes and shapes of overhang, presents some data on the magnitude of the peak pressures measured over the nose of ailerons having the overhang type of aerodynamic balance.

<u>Tabs</u>.- The rates of change of flap hinge-moment coefficient with tab deflection plotted in figure 147 as a function of the ratio of tab chord to flap chord were obtained from the pressure-distribution curves presented in figure 140. The data, therefore, pertain to plain sealed flaps and tabs on the NACA 0009 airfoil. The value of $c_{h_{f_{\delta_t}}}$ for a 0.30c plain flap with a $0.20c_f$ tab was found from force-test measurements to be -0.010 on both the NACA 0009 and the NACA 0015 airfoils and to be -0.013 on the NACA 66-009 airfoil (references 7, 12, and 19). These values are somewhat smaller than those given by the curves of figure 147, which indicates that the absolute magnitude of the parameters presented in

figure 147 may be somewhat high. The relative magnitudes of the parameters of this figure and hence the variation with tab size are believed reliable.

The data of figure 147 indicate that a tab of which the chord is about 50 percent of the flap chord causes the greatest change in flap hinge moment per unit tab deflection. A tab of this size should therefore be most effective as a trimming tab.

The optimum size of balancing tab must be determined from considerations of lift and tab hinge moment as well as of flap hinge moment. When it is desired to estimate the characteristics of a flap and tab linked to deflect at a given rate with respect to each other, it is convenient to refer the rate of deflection of each and the overall characteristics of the system to a common basis such as the control stick. Thus, if c_{H_s} is the hinge-moment coefficient of the control stick and α_{δ_s} is the lift effectiveness of the control surface per unit stick deflection, the following relations can be shown to hold for a serially hinged flap and tab system:

$$c_{H_{s_{\delta_s}}} = c_{H_{f_{\delta_f}}}\left(\frac{\partial\delta_f}{\partial\delta_s}\right)^2 + \left(c_{H_{f_{\delta_t}}} + c_{H_{t_{\delta_f}}}\right)\frac{\partial\delta_f}{\partial\delta_s}\,\frac{\partial\delta_t}{\partial\delta_s} + c_{H_{t_{\delta_t}}}\left(\frac{\partial\delta_t}{\partial\delta_s}\right)^2 \quad (1)$$

$$c_{H_{s_\alpha}} = c_{H_{f_\alpha}}\frac{\partial\delta_f}{\partial\delta_s} + c_{H_{t_\alpha}}\frac{\partial\delta_t}{\partial\delta_s} \quad (2)$$

$$\alpha_{\delta_s} = \alpha_{\delta_f}\frac{\partial\delta_f}{\partial\delta_s} + \alpha_{\delta_t}\frac{\partial\delta_t}{\partial\delta_s} \quad (3)$$

The rates of balancing tab deflection to make $c_{H_{s_{\delta_s}}} = 0$ and the corresponding values of $c_{H_{s_\alpha}}$ and α_{δ_s} have been computed from the data of figures 141 and 147 by use of equations (1) to (3). The results of the computations are presented in figure 148 for a 0.30c and a 0.50c flap. The solution of equation (1) yields two roots, the first of which is plotted as a solid line in figure 148 and corresponds to the conventional balancing tab. It can be seen that, for either size flap, the optimum size of balancing tab is about a $0.20c_f$ tab. For complete c_{H_δ}

balance, the lift effectiveness of the resulting combination is about two-thirds that of the flap without tab.

The reciprocals of the second roots of equation (1) are plotted as dashed curves in figure 148. In this case the lift is obtained from the tab and the balancing is accomplished by the flap through the linkage system. It can be seen that, as might be expected, a $0.50c_f$ tab is the optimum size of balancing tab for this type of arrangement. For a given amount of movable control surface the lift effectiveness of the $0.50c_f$ tab combination is slightly less than that of the conventional balancing tab arrangement but c_{H_α} as well as c_{H_δ} is completely balanced. The calculations indicate, therefore, that a 0.50c and a 0.25c flap can be linked to give complete c_{H_α} and c_{H_δ} balance, the smaller flap serving as the elevator and the larger flap, which moves only slightly, serving as a balancing and trimming surface, the trimming control being 77 percent as effective as an adjustable stabilizer. This arrangement is worthy of further investigation because of its aerodynamic characteristics and because mass balance of the system can probably be obtained without additions of concentrated weights.

<u>Beveled-trailing-edge type of aerodynamic balance</u>.- When a beveled trailing edge is added to a flap of thickened profile, the lift, pitching-moment, and hinge-moment characteristics of the airfoil are markedly changed from those with a flap of airfoil contour. The slope of the lift curve c_{l_α} and the lift effectiveness α_δ are decreased. The aerodynamic centers of the lift due to angle of attack and of the lift due to flap deflection are both moved forward. The rates of change of hinge-moment coefficient both with angle of attack c_{h_α} and with flap deflection c_{h_δ} are increased positively. When the flap is deflected, the bevel at small deflections tends to have the same effect on hinge moments as a balancing tab, but at large deflections its effect is more nearly like that of a trim tab. The effect of gap at the flap nose is critical, the parameter c_{h_δ} being much more positive at small deflections with an open gap than with a sealed gap. This effect generally causes the hinge-moment characteristics of a

flap with beveled trailing edge to be undesirably nonlinear unless the gap at the flap nose is sealed. Figures 46 to 56 and 117 to 122 illustrate the lift and hinge-moment characteristics discussed.

Figure 149 was derived from unpublished pressure-distribution section data for an NACA 0009 airfoil with a 0.30c flap having a 0.15c, (30°) beveled trailing edge, the same control arrangement for which force-test data are presented in figure 50. The rates of change of pressure coefficient with angle of attack and with flap deflection are plotted as functions of chordwise position for both the upper and the lower surfaces of the airfoil. The zero-lift pressure distribution of $\alpha = \delta = 0^{\circ}$ is also presented. From these data, the pressure-distribution diagrams for angles of attack and flap deflections below 10° can be estimated for this flap arrangement with sealed or open gap. The pressure-distribution curves are typical of beveled-trailing-edge flaps.

A preliminary correlation of hinge-moment data for sealed flaps with beveled trailing edges has been made in reference 28. Figures 150 has been adapted from figure 1 of this reference. It has been found that the trailing-edge angle is of fundamental importance in determining the hinge-moment slopes of beveled flaps. The result of correlating the hinge-moment characteristics of 16 different flap arrangements indicates that the effect of a beveled trailing edge may be expressed by the following relations:

$$\Delta C_{h_\alpha} = 0.00113\Delta\phi C_{L_\alpha}(c_f/c)^{-1.0} \tag{4}$$

$$\Delta C_{h_\delta} = 0.011\Delta\phi C_{L_\delta}(c_f/c)^{0.4} \tag{5}$$

The parameters ΔC_{h_α} and ΔC_{h_δ} are the increments in hinge-moment-coefficient slopes caused by changing the trailing-edge angle of a flap by the amount $\Delta\phi$ degrees. The slopes C_{L_α} and C_{L_δ} are those for the wing with an airfoil-contour flap. Equations (4) and (5) were obtained from the equations for the curves of figure 150, faired through the experimentally determined points. The hinge-moment characteristics of a beveled-trailing-edge flap can be predicted, provided the hinge-moment slopes of the

similar flap without bevel are known, by adding to these slopes the increment contributed by the bevel as computed from equations (4) and (5). Reference 26 discusses more fully the method of correlation and the method of predicting the hinge-moment characteristics of a flap with beveled trailing edges.

Internal type of aerodynamic balance.- The internal type of aerodynamic balance, being completely enclosed within the airfoil covering, does not affect the lift, drag, or pitching-moment characteristics of the airfoil but does furnish a means of balancing the control surface. Several types of internal balance are discussed in reference 15. The most commonly used, although not necessarily the most aerodynamically desirable type of internal balance, is that with a balancing plate rigidly attached to the flap and with the vents located near the hinge axis. Lift and hinge-moment data for internally balanced flaps are presented in figures 57, 58, 76 to 96, 138, and 139. The data cover the effects of changes in vent location, gap or amount of leak at the nose of the balance, length of cover plates, and alinement of cover plates. A correlation of data from wind-tunnel tests of internally balanced ailerons is presented in reference 29, from which figures 151 and 152 are taken. Increments of C_{h_α} and C_{h_δ} caused by the internal balance have been plotted as functions of the geometric dimensions of the control arrangement. As determined by the lines faired through the experimental points of figure 151, the increments of hinge-moment-coefficient slope caused by a sealed internal balance vented near the hinge may be expressed as:

$$\Delta C_{h_\alpha} = 0.0237\left[\left(\frac{c_b}{c_f}\right)^2 - \left(\frac{t/2}{c_f}\right)^2\right]\frac{c_f}{c} \tag{6}$$

$$\Delta C_{h_\delta} = 0.359\left[\left(\frac{c_b}{c_f}\right)^2 - \left(\frac{t/2}{c_f}\right)^2\right]\left(\frac{c_f}{c}\right)^{1.4} \tag{7}$$

Figure 152 shows the loss in balancing moment ΔC_{h_δ} caused by air leakage from one side of the balancing surface to the other. Insufficient data were available to present a similar curve for ΔC_{h_α}, but the variation should be similar. The characteristics of internally

balanced ailerons can be estimated, provided the hinge-moment slopes for the surface without balance are known, by adding to these slopes the increment due to the balance, which can be calculated from equations (6) and (7) and corrected for air leakage in accordance with figure 152. Misalinement of the cover plates causes a change in the slopes of the hinge-moment curves (figs. 88 to 96).

Horn type of aerodynamic balance.- In general, as suggested in reference 33, the horn type of aerodynamic balance may be divided into three classifications, each having different balancing characteristics. Control surfaces such as those of figures 123 to 126 and of figure 153(a) may be called type A. Type A horns may be considered as those formed by converting a spanwise portion of the fixed surface ahead of the hinge axis into movable surface. Type B horns (fig. 153(b)) may be considered as those formed by adding area at the tip, generally, both ahead and behind the hinge axis, in such a manner as to increase the span of the unbalanced control surface. The leading and trailing edges of control surfaces with type B horn, therefore, are joined by a broken curve rather than a continuous one as for type A horns. Type C horns are shielded horns, which may be considered as those formed by providing the movable surface with a large amount of overhang concentrated near the tip behind a portion of the fixed surface.

Figure 154 from reference 33 presents a correlation of hinge-moment data for type A and type B horns obtained from references 34 to 39. Insufficient data are available to present a correlation of type C horns. Increments of C_{h_α} and C_{h_δ} caused by the horn have been plotted as a function of a horn-balance factor, defined as the square root of the ratio of horn area times horn mean chord to control area times control mean chord. The plan forms of the control surfaces considered in the correlation are sketched in figure 153 and are numbered to identify the test points of figure 154. Further details and dimensions are generally available in the appropriate reference listed on figure 153.

The data presented in figure 154 indicate the balancing effectiveness of type B horn to be considerably greater than that of type A horn. Probably because of the dissimilarity of air flow over the odd-shaped tips of the control surfaces with type B horns, the scatter

of points about the faired curve is considerably greater for type B than for type A horns. For either type of horn, however, ΔC_{h_α} and ΔC_{h_δ} were approximately equal for nearly all the control surfaces for which data were available. A more complete analysis of the hinge-moment characteristics of horn-balanced control surfaces is presented in reference 33.

Application of section data to finite-span control surfaces.- The lifting-line theory can be used as a basis for applying the section data to estimate the lift and hinge-moment characteristics of control surfaces of finite span. For such application, lift and hinge-moment characteristics are written in the form of parameters, which, according to lifting-line theory, are independent of aspect ratio (reference 4). Thus:

$$(\alpha_\delta)_{c_l} = -\frac{\left(c_{l_\delta}\right)_\alpha}{\left(c_{l_\alpha}\right)_\delta} \tag{8}$$

$$(c_{h_{c_l}})_\delta = \frac{\left(c_{h_\alpha}\right)_\delta}{\left(c_{l_\alpha}\right)_\delta} \tag{9}$$

$$(c_{h_\delta})_{c_l} = (c_{h_\delta})_\alpha + (c_{h_\alpha})_\delta (\alpha_\delta)_{c_l} \tag{10}$$

Lifting-line theory assumes that the induced downwash is constant along the chord and, therefore, that the chordwise distribution of resultant pressure at a section of a finite wing is the same as that of a wing of infinite span at a lower angle of attack. Because the distribution of downwash varies along the chord, however, the effective streamline curvature induced at a section of a wing in three-dimensional flow causes the parameters $(\alpha_\delta)_{c_l}$, $(c_{h_{c_l}})_\delta$, and $(c_{h_\delta})_{c_l}$ to vary slightly with aspect ratio rather than to be independent of it as lifting-line theory assumes. This fact apparently has small effect on the over-all lift but, for small aspect ratios, introduces a possible source of error in the calculation of hinge moments, because they are dependent upon the distribution as well as upon the magnitude of resultant pressure.

Therefore, until lifting-surface theory provides a more exact method, or until empirical correction factors are experimentally determined, the lift and hinge-moment characteristics of a finite-span control surface calculated from section data must be subject to all the assumptions and limitations of the lifting-line theory.

Reference 4 presents the method of applying section data to compute the characteristics of a control surface having an elliptical load distribution, which, in effect, is a surface of elliptical chord distribution with a constant percentage airfoil chord flap. This method, when applied to wings of other plan forms and flap chord ratios, becomes the so-called "strip" method and, in general, does not give satisfactory results. This method, however, when augmented by experimentally determined correction factors, may provide a more accurate and practical solution than the more general method described in the following paragraphs.

In order to expand the method of reference 4 to apply to the general case, it is necessary to take account of aerodynamic induction by calculating the spanwise lift distribution per unit change in angle of attack of the whole wing and per unit change in flap deflection. This is, at best, a tedious process but can be accomplished by methods presented in references 44 or 45. Values of α_δ for the particular flap-chord ratio at each spanwise station can be determined from section data to define the spanwise distribution of effective angle of attack in order to compute the lift distribution per unit change in flap deflection.

For the special case of a control surface with a full-span flap having a chord that is a constant percentage of the wing chord, the span-lift distribution per unit change in flap deflection is similar to that per unit change in angle of attack of the wing. If the surface is rectangular or linearly tapered, the span-lift distribution can be easily calculated from the tables presented in reference 46 and the hinge-moment characteristics, therefore, can be more readily estimated.

The lift coefficient at a section of a wing of finite span may be expressed as:

$$c_l = c_{l_0} + c_{l_{a_1}} C_{L_\alpha} \alpha + c_{l_{b_1}} C_{L_\delta} \delta \qquad (11)$$

The rates of change of the section lift-coefficient slope with angle of attack of the whole wing and with deflection of the entire flap are therefore

$$\left.\begin{aligned} c_{l_{\alpha_3}} &= c_{l_{a_1}} C_{L_\alpha} \\ c_{l_{\delta_3}} &= c_{l_{b_1}} C_{L_\delta} \end{aligned}\right\} \tag{12}$$

The wing lift coefficient may be expressed as:

$$C_L = \frac{1}{S} \int_0^b c_l c\,dy \tag{13}$$

The lift-curve slopes for the entire wing can be found by integrating the calculated lift-distribution curves, $c_{l_{\alpha_3}} c = f(y)$ and $c_{l_{\delta_3}} c = f'(y)$. Thus:

$$\left.\begin{aligned} C_{L_\alpha} &= \frac{1}{S} \int_0^b c_{l_{\alpha_3}} c\,dy \\ C_{L_\delta} &= \frac{1}{S} \int_0^b c_{l_{\delta_3}} c\,dy \end{aligned}\right\} \tag{14}$$

The lift-effectiveness parameter for the entire wing is obtained from the ratio of the calculated lift-curve slopes. Thus:

$$(\alpha_\delta)_{C_L} = \frac{C_{L_\delta}}{C_{L_\alpha}} \tag{15}$$

The hinge-moment slopes are found by performing mechanically the integrations indicated by the following expressions:

$$\left.\begin{aligned} C_{h_\alpha} &= \frac{1}{b_f \bar{c}_f^2} \int_0^b (c_{h_{c_l}})_\delta c_f^2 c_{l_{\alpha_3}}\,dy \\ C_{h_\delta} &= \frac{1}{b_f \bar{c}_f^2}\left[\int_0^b (c_{h_\delta})_{c_l} c_f^2\,dy + \int_0^b (c_{h_{c_l}})_\delta c_f^2 c_{l_{\delta_3}}\,dy\right] \end{aligned}\right\} \tag{16}$$

Values of $(c_{h_{c_l}})_\delta$ and $(c_{h_\delta})_{c_l}$ for each spanwise station are obtained by means of equations (9) and (10) from available section data. The section data presented in this paper give the variation of section hinge-moment parameters with ratio of flap chord to airfoil chord for scaled plain flaps and with overhang for a 0.30c flap on several airfoils. These data should be corrected for tunnel-wall effect in the manner already indicated. Until more data become available, the hinge-moment parameters of balanced flaps may be assumed to vary in the same manner with ratio of flap chord to airfoil chord as do the parameters for plain flaps.

Recent wind-tunnel tests (unpublished) have indicated that manufacturing imperfections on the flap such as rib stiching and the sagging of fabric between the ribs of a control surface have considerable effect upon the hinge-moment characteristics. This fact should be realized when computing the hinge moments of an airplane control surface from section data obtained from a model wing of true airfoil contour. It is imperative that the section data applied are those for exactly the same airfoil profile as the sections of the finite-span control surface. Arbitrary modifications to an airfoil profile, such as shortening or lengthening the distance from a hinge axis to the trailing edge, are apt to cause large changes in the hinge-moment characteristics from those of the basic airfoil section.

The aerodynamic section characteristics of an isolated horizontal tail surface (reference 47), tested in the NACA full-scale tunnel have been estimated from section data in the manner already outlined. The horizontal tail surface had the following geometric characteristics:

Airfoil section	NACA 0009
Aspect ratio	4.7
Taper ratio (rounded tips)	2:1
S_e/S (nearly constant percentage chord elevator)	0.41
Blunt-nose overhang	$0.10c_e$
Gap	0.005c

The span load distribution per unit angle of attack was calculated from the tables of reference 46 and was arbitrarily altered at the center section to account for the effect of a cut-out made in the elevator for the rudder.

Because the elevator was nearly a constant percentage of the airfoil chord along the span, the span load distribution per unit elevator deflection was assumed similar to that per unit angle of attack; that is, $c_{l_{b_1}}$ was assumed equal to $c_{l_{a_1}}$. The section hinge-moment-coefficient data were obtained from figure 144(c) by assuming that the slopes for a balanced flap vary with flap-chord ratio in a manner similar to those for an unbalanced flap (fig. 142). Section lift characteristics were obtained from figures 143 and 141 by making this same assumption. The theoretically derived correction for the streamline curvature induced by the tunnel walls, which has already been discussed, was applied to the hinge-moment parameter $(c_{h_{c_l}})_\delta$. This correction reduced the value of $(c_{h_{c_l}})_\delta$ for the 0.45c flap by 8 percent. The parameter $(c_{h_\delta})_{c_l}$ was negligibly affected by this tunnel-wall correction.

A comparison of the calculated with the measured values is presented in the following table:

Parameter	Calculated value	Measured value
C_{L_α}	0.063	0.060
α_δ	-.71	-.70
C_{h_α}	-.0031	-.0045
C_{h_δ}	-.0106	-.0080

The calculated lift characteristics are in reasonably good agreement with the measured values. The parameter C_{h_α} was calculated to be 0.0016 more negative and the parameter C_{h_δ}, 0.0026 more negative than the corresponding measured values. It would be expected, however, that the computed values should be more positive than the measured values. The section data were obtained in a turbulent tunnel and the transition region should therefore be further forward; thus, the section hinge-moment

slopes should be more positive than those measured in the less turbulent full-scale tunnel. The effect of streamline curvature caused by the finite-span airfoil probably accounts for a large part of the discrepancy between the computed and the measured values. A streamline-curvature correction theoretically derived from lifting-surface theory for an elliptical wing indicates that a reduction of about 14 percent, for this case, in the value of $(c_{h_{c_l}})_\delta$ is justified for this aspect ratio. When this aspect-ratio correction is applied, a slightly closer agreement with the measured values is obtained, the calculated value of C_{h_α} then being -0.0053 and that of C_{h_δ} being -0.0102.

The limitations of the lifting-line theory as a basis for estimating the aerodynamic characteristics of a finite-span control surface from section data are indicated by the example cited. Unfortunately the margin of error, which for hinge-moment slopes amounted to about 20 percent of the slope values of the unbalanced surface, is not tolerable for purposes of estimating the characteristics of a closely balanced surface for a large high-speed airplane. Suitable correction factors must be obtained, either theoretically or experimentally, before the hinge-moment characteristics of a finite-span control surface can be accurately predicted from section data. The determination of these factors remains a project for future investigation.

CONCLUDING REMARKS

A large quantity of data, much of which has been previously published, has been gathered and presented in one report for convenient reference. It is beyond the scope of this paper to draw conclusions concerning the merits of various types of airplane control surfaces, only a very limited analysis of the accumulated data having been made. The basic data presented and the curves correlating the results of many tests of several types of aerodynamic balances should facilitate the design of balanced control surfaces.

Langley Memorial Aeronautical Laboratory,
National Advisory Committee for Aeronautics,
Langley Field, Va.

REFERENCES

1. Street, William G., and Ames, Milton B., Jr.: Pressure-Distribution Investigation of an N.A.C.A. 0009 Airfoil with a 50-Percent-Chord Plain Flap and Three Tabs. T.N. No. 734, NACA, 1939.

2. Ames, Milton B., Jr., and Sears, Richard I.: Pressure-Distribution Investigation of an N.A.C.A. 0009 Airfoil with a 30-Percent-Chord Plain Flap and Three Tabs. T.N. No. 759, NACA, 1940.

3. Ames, Milton B., Jr., and Sears, Richard I.: Pressure-Distribution Investigation of an N.A.C.A. 0009 Airfoil with an 80-Percent-Chord Plain Flap and Three Tabs. T.N. No. 761, NACA, 1940.

4. Ames, Milton B., Jr., and Sears, Richard I.: Determination of Control-Surface Characteristics from NACA Plain-Flap and Tab Data. Rep. No. 721, NACA, 1941.

5. Glauert, H.: Theoretical Relationships for an Aerofoil with Hinged Flap. R. & M. No. 1095, British A.R.C., 1927.

6. Perring, W. G. A.: The Theoretical Relationships for an Aerofoil with a Multiply Hinged Flap System. R. & M. No. 1171, British A.R.C., 1928.

7. Sears, Richard I.: Wind-Tunnel Investigation of Control-Surface Characteristics. I - Effect of Gap on the Aerodynamic Characteristics of an NACA 0009 Airfoil with a 30-Percent-Chord Plain Flap. NACA A.R.R., June 1941.

8. Sears, Richard I., and Hoggard, H. Page, Jr.: Wind-Tunnel Investigation of Control-Surface Characteristics. II - A Large Aerodynamic Balance of Various Nose Shapes with a 30-Percent-Chord Flap on an NACA 0009 Airfoil. NACA A.R.R., Aug. 1941.

9. Ames, Milton B., Jr.: Wind-Tunnel Investigation of Control-Surface Characteristics. III - A Small Aerodynamic Balance of Various Nose Shapes Used with a 30-Percent-Chord Flap on an NACA 0009 Airfoil. NACA A.R.R., Aug. 1941.

10. Ames, Milton B., Jr., and Eastman, Donald R., Jr.: Wind-Tunnel Investigation of Control-Surface Characteristics. IV - A Medium Aerodynamic Balance of Various Nose Shapes Used with a 30-Percent-Chord Flap on an NACA 0009 Airfoil. NACA A.R.R., Sept. 1941.

11. Jones, Robert T., and Ames, Milton B., Jr.: Wind-Tunnel Investigation of Control-Surface Characteristics. V - The Use of a Beveled Trailing Edge to Reduce the Hinge Moment of a Control Surface. NACA A.R.R., March 1942.

12. Sears, Richard I., and Liddell, Robert B.: Wind-Tunnel Investigation of Control-Surface Characteristics. VI - A 30-Percent-Chord Plain Flap on the NACA 0015 Airfoil. NACA A.R.R., June 1942.

13. Sears, Richard I., and Hoggard, H. Page, Jr.: Wind-Tunnel Investigation of Control-Surface Characteristics. VII - A Medium Aerodynamic Balance of Two Nose Shapes Used with a 30-Percent-Chord Flap on an NACA 0015 Airfoil. NACA A.R.R., July 1942.

14. Sears, Richard I., and Gillis, Clarence L.: Wind-Tunnel Investigation of Control-Surface Characteristics. VIII - A Large Aerodynamic Balance of Two Nose Shapes Used with a 30-Percent-Chord Flap on an NACA 0015 Airfoil. NACA A.R.R., July 1942.

15. Sears, Richard I.: Wind-Tunnel Investigation of Control-Surface Characteristics. IX - Some Analytical Considerations and Experimental Test Results for an Internally Balanced Flap. NACA A.R.R., July 1942.

16. Hoggard, H. Page, Jr.: Wind-Tunnel Investigation of Control-Surface Characteristics. X - A 30-Percent-Chord Plain Flap with Straight Contour on the NACA 0015 Airfoil. NACA A.R.R., Sept. 1942.

17. Sears, Richard I., and Hoggard, H. Page, Jr.: Wind-Tunnel Investigation of Control-Surface Characteristics. XI - Various Large Overhang and Internal-Type Aerodynamic Balances for a Straight-Contour Flap on the NACA 0015 Airfoil. NACA A.R.R., Jan. 1943.

18. Hoggard, H. Page, Jr.: Wind-Tunnel Investigation of Control-Surface Characteristics. XII - Various Cover-Plate Alinements on the NACA 0015 Airfoil with a 30-Percent-Chord Flap and Large Sealed Internal Balance. NACA A.R.R., Jan. 1943.

19. Gillis, Clarence L., and Lockwood, Vernard E.: Wind-Tunnel Investigation of Control-Surface Characteristics. XIII - Various Flap Overhangs Used with a 30-Percent-Chord Flap on an NACA 66-009 Airfoil. NACA A.C.R., No. 3G20, July 1943.

20. Sears, Richard I., and Purser, Paul E.: Wind-Tunnel Investigation of Control-Surface Characteristics. XIV - NACA 0009 Airfoil with a 20-Percent-Chord Double Plain Flap. NACA A.R.R., No. 3F29, June 1943.

21. Sears, Richard I., and Hoggard, H. Page, Jr.: Characteristics of Plain and Balanced Elevators on a Typical Pursuit Fuselage at Attitudes Simulating Normal-Flight and Spin Conditions. NACA A.R.R., March 1942.

22. Gillis, Clarence L.: Characteristics of Beveled-Trailing-Edge Elevators on a Typical Pursuit Fuselage at Attitudes Simulating Normal Flight and Spin Conditions. NACA A.R.R., Dec. 1942.

23. Rogallo, F. M.: Collection of Balanced Aileron Data. NACA A.C.R. No.4A11, 1944.

24. Wenzinger, Carl J., and Harris, Thomas A.: The Vertical Wind Tunnel of the National Advisory Committee for Aeronautics. Rep. No. 387, NACA, 1931.

25. Wenzinger, Carl J., and Harris, Thomas A.: Wind-Tunnel Investigation of an N.A.C.A. 23012 Airfoil with Various Arrangements of Slotted Flaps. Rep. No. 664, NACA, 1939.

26. Purser, Paul E., and Gillis, Clarence L.: Preliminary Correlation of the Effects of Beveled Trailing Edges on the Hinge-Moment Characteristics of Control Surfaces. NACA C.R., No. 3E14, 1943.

27. Rogallo, F. M., and Purser, Paul E.: Wind-Tunnel Investigation of a Plain Aileron with Various Trailing-Edge Modifications on a Tapered Wing. II - Ailerons with Thickened and Beveled Trailing Edges. NACA A.R.R., Oct. 1942.

28. Purser, Paul E., and McKee, John W.: Wind-Tunnel Investigation of a Plain Aileron with Thickened and Beveled Trailing Edges on a Tapered Low-Drag Wing. NACA A.C.R., Jan. 1943.

29. Rogallo, F. M., and Lowry, John G.: Résumé of Data for Internally Balanced Ailerons. NACA R.B., March 1945.

30. Rogallo, F. M., and Lowry, John G.: Wind-Tunnel Investigation of a Plain Aileron and a Balanced Aileron on a Tapered Wing with Full-Span Duplex Flaps. NACA A.R.R., July 1942.

31. Rogallo, F. M., and Lowry, John G.: Wind-Tunnel Development of Ailerons for the Curtiss XP-60 Airplane. NACA A.C.R., Sept. 1942.

32. Harris, Thomas A., and Purser, Paul E.: Wind-Tunnel Investigation of Plain Ailerons for a Wing with a Full-Span Flap Consisting of an Inboard Fowler and an Outboard Retractable Split Flap. NACA A.C.R., March 1941.

33. Lowry, John G.: Résumé of Hinge-Moment Data for Unshielded Horn-Balanced Control Surfaces. NACA R.B., No. 3F19, 1943.

34. Priestley, E.: An Analysis of Model Hinge Moments on Set-Back Hinge and Horn-Balanced Controls. B.A. Dept. Note - Performance No. 10, British A.R.C. (British Confidential - U. S. Restricted), Jan. 1940.

35. Gorsky, V. P.: Aerodynamic Investigations of Tail Surfaces with Balanced and Unbalanced Elevators. Rep. No. 49, Central Aero-Hydrodynamical Inst. (Moscow), 1930, pp. 49-90, 92.

36. Fannell, J. R., and Campbell, N. R.: The Balancing of Wing Flaps. R. & M. No. 200, British A.C.A., 1916.

37. Sivells, James C.: Tests in the 19-Foot Pressure Tunnel of a Rectangular NACA 0012 Horizontal Tail Plane with Plain and Horn-Balanced Elevators. NACA A.R.R., Oct. 1942.

38. Harris, Thomas A.: Reduction of Hinge Moments of Airplane Control Surfaces by Tabs. Rep. No. 528, NACA, 1935.

39. Bradfield, F. B.: A Collection of Wind Tunnel Data on the Balancing of Controls. R. & M. No. 1420, British A.R.C., 1932.

40. Swanson, Robert S., and Toll, Thomas A.: Jet-Boundary Corrections for Reflection-Plane Models in Rectangular Wind Tunnels. NACA A.R.R., No. 3E22, May 1943.

41. The Effect of Boundary Layer Thickness on the Normal Force Distribution of Aerofoils, with Particular Reference to Control Problems:

Batson, A. S., Preston, J. H., Warsap, J. H., and Hopwood, M. L.: Part I. The Relation between Lift and Hinge Moment, Estimated from the Pressure Distribution, When These Factors Are Varied by Fitting Turbulence Wires and Trailing Edge Strips. 5724, S. & C. 1341, N.P.L. (British Confidential - U. S. Restricted), April 8, 1942.

Preston, J. H., Batson, A. S., Warsap, J. H., and Brown, T. W.: Part II. Wake Exploration near the Trailing Edge. 7525, N.P.L. (British Confidential - U. S. Restricted), April 9, 1942.

Preston, J. H., Sweeting, N. E., and Brown, T. W.: Part III. Measurements of the Transition Region. 5726, N.P.L. (British Confidential - U. S. Restricted), April 9, 1942.

Batson, A. S., and Preston, J. H.: Part IV. The Effect of Changes in Transition Point on Characteristics of Aerofoils, with Particular Reference to Lift and Hinge Moment on a Control. 5727, S. & C. 1341a, N.P.L. (British Confidential - U. S. Restricted), April 8, 1942.

42. Jones, Robert T., and Kleckner, Herold F.: Theory and Preliminary Flight Tests of an All-Movable Vertical Tail Surface. NACA A.R.R., Jan. 1943.

43. Purser, Paul E., and Toll, Thomas A.: Wind-Tunnel Investigation of the Characteristics of Blunt-Nose Ailerons on a Tapered Wing. NACA A.R.R., Feb. 1943.

44. Pearson, Henry A., and Jones, Robert T.: Theoretical Stability and Control Characteristics of Wings with Various Amounts of Taper and Twist. Rep. No. 635, NACA, 1938.

45. Anon.: Spanwise Air-Load Distribution. ANC-1(1), Army-Navy-Commerce Committee on Aircraft Requirements. U. S. Govt. Printing Office, April 1938.

46. Pearson, H. A.: Span Load Distribution for Tapered Wings with Partial-Span Flaps. Rep. No. 585, NACA, 1937.

47. Goett, Harry J., and Reeder, J. P.: Effects of Elevator Nose Shape, Gap, Balance, and Tabs on the Aerodynamic Characteristics of a Horizontal Tail Surface. Rep. No. 675, NACA, 1939.

INDEX TO FIGURES

Subject	Figures
I - Section data	1-106
1. Airfoils	
(a) NACA 0009	1-58
(b) NACA 0015	59-96
(c) NACA 66-009	97-106
2. Aerodynamic balance	
(a) Plain flaps	1-8, 59-60, 69-70, 97-98, 140
(b) Overhang (inset hinge)	9-45, 61-68 71-75, 99-106
(c) Beveled trailing edge	47-56, 149
(d) Internal balance	57-58, 76-96
3. Pressure distribution	
(a) Plain flaps	140
(b) Beveled trailing edge	149
II - Finite span data	107-139
1. Aerodynamic balance	
(a) Plain flaps	107-108, 131-133
(b) Overhang (inset hinge)	109-116, 127-130, 134-137
(c) Beveled trailing edge	117-122
(d) Internal balance	138-139
(e) Horn balance	123-126
III - Parameters	140-155
1. Aerodynamic balance	
(a) Plain flaps	141, 142
(b) Overhangs	143-146
(c) Tabs	147-148
(d) Beveled trailing edge	150
(e) Internal balance	151-152
(f) Horn Balance	153-154
2. Tunnel correction factor	155

Note: Variables not specifically assigned values on the various figures of this paper are held constant at zero magnitude for the data presented in each figure, even though certain variables, such as tab deflection or angle of yaw, may have been varied in the investigations reported originally in the reference quoted on each figure.

NATIONAL ADVISORY
COMMITTEE FOR AERONAUTICS

TABLE I.- INFORMATION REGARDING TWO-DIMENSIONAL-FLOW MODELS

TESTED IN NACA 4- BY 6-FOOT VERTICAL TUNNEL

[Test Reynolds number, 1,430,000; Mach number, 0.1; turbulence factor, 1.93.
Experimental tunnel wall corrections applied to lift only.]

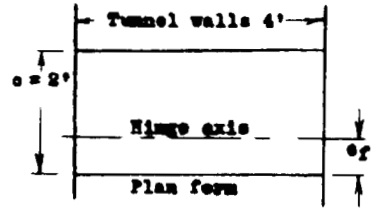

Flap section	NACA airfoil designation	c_f/c	c_b/c_f	Type of balance	Description of balance	Nose gap	Reference	Figure
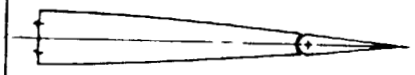	0009	0.15	0.10	Unbalanced plain flap	Circular arc	Sealed, 0.005c	20	1,2
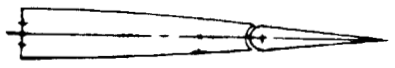	0009	0.20	0.10	Unbalanced plain flap	Circular arc	Sealed, 0.005c	20	3,4
	0009	0.30	0.09	Unbalanced plain flap	Circular arc	Sealed, 0.001c, 0.005c, 0.010c	7	5 to 8
	0009	0.30	0.20	Overhang	Blunt nose	Sealed, 0.001c, 0.005c, 0.010c	9	9 to 12
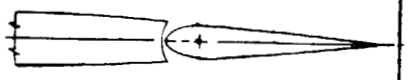	0009	0.30	0.20	Overhang	Modified blunt nose	0.005c	9	13
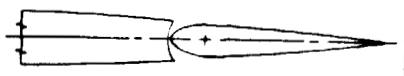	0009	0.30	0.20	Overhang	Medium nose	Sealed, 0.001c, 0.005c, 0.010c	9	14 to 17
	0009	0.30	0.20	Overhang	Modified medium nose	0.005c	9	18

NATIONAL ADVISORY
COMMITTEE FOR AERONAUTICS

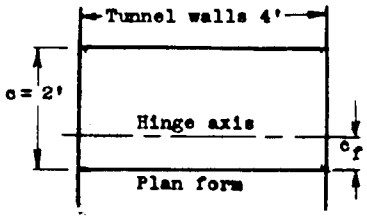

TABLE I.- INFORMATION REGARDING TWO-DIMENSIONAL-FLOW MODELS

TESTED IN NACA 4- BY 6-FOOT VERTICAL TUNNEL - Continued

[Test Reynolds number, 1,430,000; Mach number, 0.1; turbulence factor, 1.93. Experimental tunnel wall corrections applied to lift only.]

Flap section	NACA airfoil designation	c_f/c	c_b/c_f	Type of balance	Description of balance	Nose gap	Reference	Figure
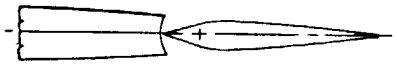	0009	0.30	0.20	Overhang	Sharp nose	Sealed, 0.001c, 0.005c, 0.010c	9	19 to 22
	0009	0.30	0.20	Overhang	Modified sharp nose	0.005c	9	23
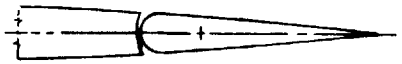	0009	0.30	0.35	Overhang	Blunt nose	Sealed, 0.001c, 0.005c, 0.010c	10	24 to 27
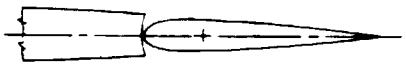	0009	0.30	0.35	Overhang	Medium nose	Sealed, 0.001c, 0.005c, 0.010c	10	28 to 31
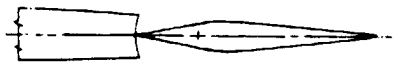	0009	0.30	0.35	Overhang	Sharp nose	Sealed, 0.001c, 0.005c, 0.010c	10	32 to 35
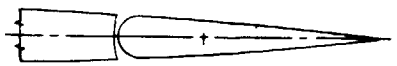	0009	0.30	0.50	Overhang	Blunt nose	Sealed 0.0015c	8	36, 37
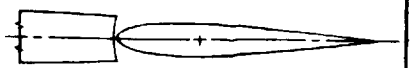	0009	0.30	0.50	Overhang	Medium nose	Sealed 0.0015c	8	38, 39

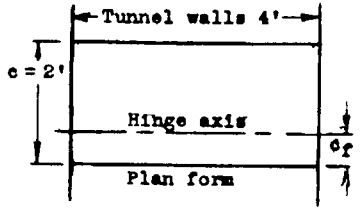

NATIONAL ADVISORY
COMMITTEE FOR AERONAUTICS

TABLE I.- INFORMATION REGARDING TWO-DIMENSIONAL-FLOW MODELS

TESTED IN NACA 4- BY 6-FOOT VERTICAL TUNNEL - Continued

[Test Reynolds number, 1,430,000; Mach number, 0.1; turbulence factor, 1.93. Experimental tunnel wall corrections applied to lift only.]

Flap section	NACA airfoil designation	c_f/c	c_b/c_f	Type of balance	Description of balance	Nose gap	Reference	Figure
	0009	0.30	0.50	Overhang	Modified medium nose	Sealed 0.0015c	Unpublished	40, 41
	0009	0.30	0.50	Overhang	Sharp nose	Sealed 0.0015c	8	42, 43
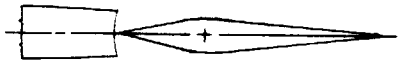	0009	0.30	0.50	Overhang	Modified sharp nose	Sealed 0.0015c	Unpublished	44, 45
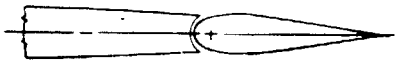	0009	0.30	0.09	Profile modification	Bulged flap profile	Sealed 0.005c	11	46, 47
	0009	0.30	0.09	Profile modification	Beveled trailing edge	Sealed 0.005c	11	48 to 53
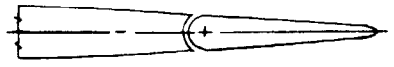	0009	0.30	0.09	Profile modification	Elliptical trailing edge	Sealed	11	54, 55
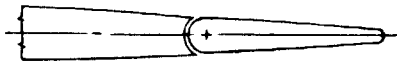	0009	0.30	0.09	Profile modification	Circular trailing edge	Sealed	11	56

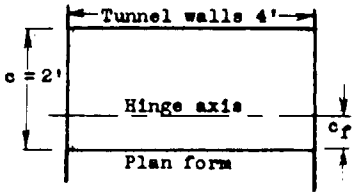

NATIONAL ADVISORY
COMMITTEE FOR AERONAUTICS

TABLE I.- INFORMATION REGARDING TWO-DIMENSIONAL-FLOW MODELS

TESTED IN NACA 4- BY 6-FOOT VERTICAL TUNNEL - Continued

[Test Reynolds number, 1,430,000; Mach number, 0.1; turbulence factor, 1.93. Experimental tunnel wall corrections applied to lift only.]

Flap section	NACA airfoil designation	c_f/c	c_b/c_f	Type of balance	Description of balance	Nose gap	Reference	Figure
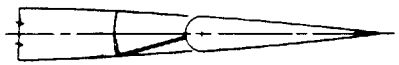	0009	0.30	0.50	Internal	Vent at 0.56c and at 0.69c	Sealed	15	57, 58
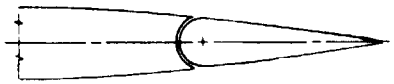	0015	0.30	0.15	Unbalanced plain flap	Circular arc	Sealed 0.005c	12, 16	59, 60 69, 70
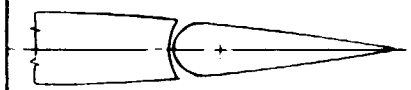	0015	0.30	0.35	Overhang	Blunt nose	Sealed 0.005c	13	61, 62
	0015	0.30	0.35	Overhang	Medium nose	Sealed 0.005c	13	63, 64
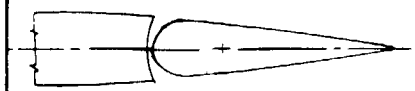	0015	0.30	0.50	Overhang	Blunt nose	Sealed 0.005c	14, 17	65, 66, 71
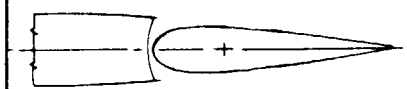	0015	0.30	0.50	Overhang	Medium nose	Sealed 0.005c	14	67, 68
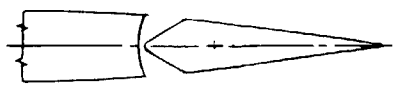	0015	0.30	0.50	Overhang	Blunt nose, modification 1	0.005c	17	72

NATIONAL ADVISORY
COMMITTEE FOR AERONAUTICS

TABLE I.- INFORMATION REGARDING TWO-DIMENSIONAL-FLOW MODELS

TESTED IN NACA 4- BY 6-FOOT VERTICAL TUNNEL - Continued

[Test Reynolds number, 1,430,000; Mach number, 0.1; turbulence factor, 1.93. Experimental tunnel wall corrections applied to lift only.]

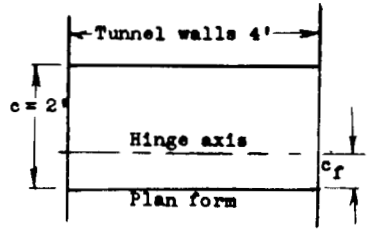

Flap section	NACA airfoil designation	c_f/c	c_b/c_f	Type of balance	Description of balance	Nose gap	Reference	Figure
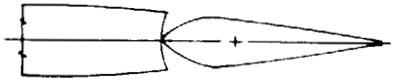	0015	0.30	0.50	Overhang	Blunt nose, modification 2	0.005c	17	73
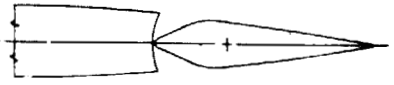	0015	0.30	0.50	Overhang	Blunt nose, modification 3	0.005c	17	74
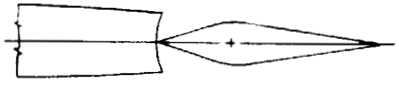	0015	0.30	0.50	Overhang	Sharp nose	0.005c	17	75
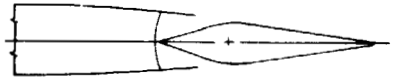	0015	0.30	0.50	Internal	Narrow cover plates	Sealed, 0.0011c, 0.0023c, 0.005c	17	76 to 79
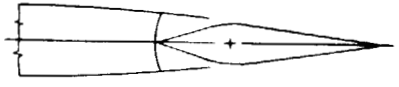	0015	0.30	0.50	Internal	Medium cover plates	Sealed, 0.0011c, 0.0023c, 0.005c	17	80 to 83
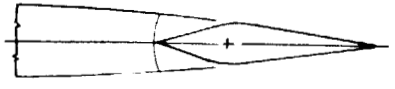	0015	0.30	0.50	Internal	Large cover plates	Sealed, 0.0011c, 0.0023c, 0.005c	17	84 to 87
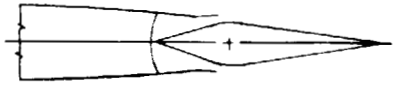	0015	0.30	0.50	Internal	Cover plates bent in and out at 0.63c station	Sealed	18	88 to 93

NATIONAL ADVISORY
COMMITTEE FOR AERONAUTICS

TABLE I.- INFORMATION REGARDING TWO-DIMENSIONAL-FLOW MODELS

TESTED IN NACA 4- BY 6-FOOT VERTICAL TUNNEL - Concluded

[Test Reynolds number, 1,430,000; Mach number, 0.1; turbulence factor, 1.93. Experimental tunnel wall corrections applied to lift only.]

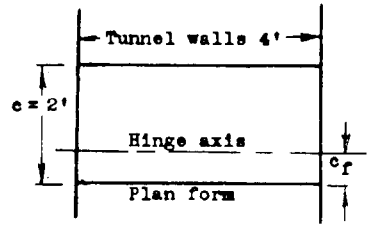

Flap section	NACA airfoil designation	c_f/c	c_b/c_f	Type of balance	Description of balance	Nose gap	Reference	Figure
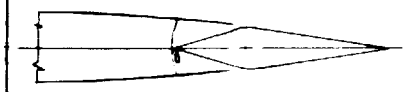	0015	0.30	0.50	Internal	Cover plates bent in and out at 0.50c station	Sealed	18	94 to 96
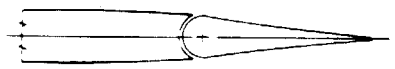	66-009	0.30	0.11	Unbalanced plain flap	Circular arc	Sealed 0.005c	19	97, 98
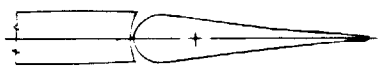	66-009	0.30	0.35	Overhang	Blunt nose	Sealed 0.005c	19	99, 100
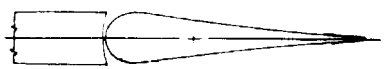	66-009	0.30	0.50	Overhang	Blunt nose	Sealed 0.005c	19	101, 102
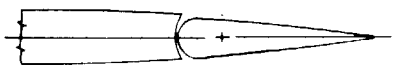	66-009	0.26	0.30	Overhang	Blunt nose	Sealed 0.001c	Unpublished	103, 104
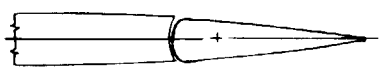	66-009	0.26	0.30	Overhang	Modified blunt nose	0.001c	Unpublished	105
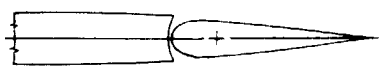	66-009	0.26	0.30	Overhang	Medium nose	0.001c	Unpublished	106

TABLE II.- INFORMATION REGARDING THREE-DIMENSIONAL-FLOW MODELS

TESTED IN THE LMAL 7- BY 10-FOOT TUNNEL

[Turbulence factor, 1.6. Tunnel-wall corrections applied in accordance with reference 40.]

NATIONAL ADVISORY
COMMITTEE FOR AERONAUTICS

Plan form	Typical section of control surface	Aspect ratio, A	Taper ratio, λ	S_e/S	S_b/S_e	Airfoil section	Test condition	Gap	Reference	Figure
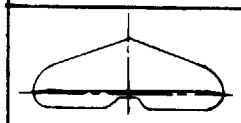	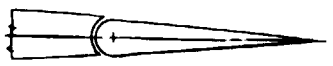 Unbalanced elevator	3.7	0.57	0.27	0.09	NACA 0009	Horizontal tail on pursuit fuselage R = 502,000 M = 0.1	Sealed 0.005c	21	107, 108
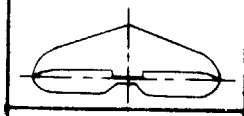	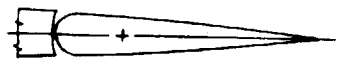 Blunt-nose elevator	3.7	0.57	0.27	0.35	NACA 0009	Horizontal tail on pursuit fuselage R = 502,000 M = 0.1	Sealed 0.005c	21	109, 110
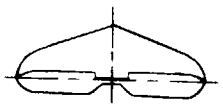	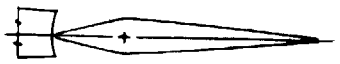 Sharp-nose elevator	3.7	0.57	0.27	0.35	NACA 0009	Horizontal tail on pursuit fuselage R = 502,000 M = 0.1	Sealed 0.005c	21	111, 112
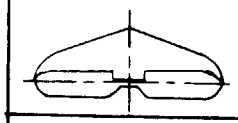	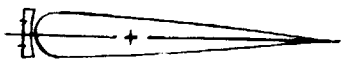 Blunt-nose elevator	3.7	0.57	0.27	0.50	NACA 0009	Horizontal tail on pursuit fuselage R = 502,000 M = 0.1	Sealed 0.005c	21	113, 114
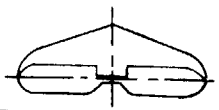	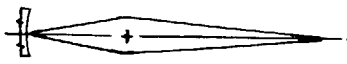 Sharp-nose elevator	3.7	0.57	0.27	0.50	NACA 0009	Horizontal tail on pursuit fuselage R = 502,000 M = 0.1	Sealed 0.005c	21	115, 116
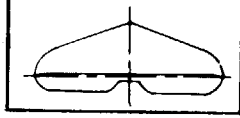	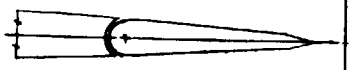 Beveled-trailing-edge elevator	3.7	0.57	0.27	0.09	NACA 0009	Horizontal tail on pursuit fuselage R = 502,000 M = 0.1	Sealed 0.005c	22	117 to 122

TABLE II.- INFORMATION REGARDING THREE-DIMENSIONAL-FLOW MODELS

TESTED IN THE LMAL 7- BY 10-FOOT TUNNEL - Concluded

[Turbulence factor, 1.6. Tunnel-wall corrections applied in accordance with reference 40.]

NATIONAL ADVISORY
COMMITTEE FOR AERONAUTICS

Plan form	Typical section of control surface	Aspect ratio, A	Taper ratio, λ	S_e/S or S_r/S	S_b/S_e or S_b/S_r	Airfoil section	Test condition	Gap	Reference	Figure
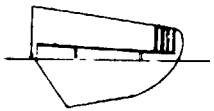	Medium-nose elevator	3.96	0.58	0.43	0.41 .40 .38 .36	Modified NACA symmetrical	Semispan model R = 1,920,000 M = 0.1	0.02c	Unpublished data	123 to 126
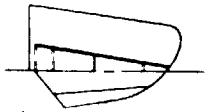	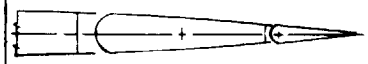 Blunt-nose elevator	3.96	0.58	0.30	0.50	Modified NACA symmetrical	Semispan model R = 1,920,000 M = 0.1	0.02c	Unpublished data	127 to 130
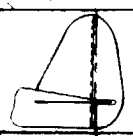	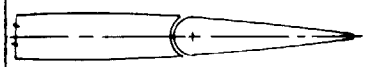 Unbalanced rudder	2.41	0.47	0.42	0.13	Modified NACA 66 series	Complete tail on stub fuselage R = 1,510,000 M = 0.1	Sealed 0.113 inch	Unpublished data	131 to 133
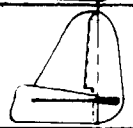	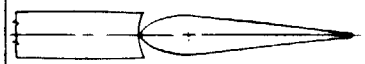 Medium-nose rudder	2.41	0.47	0.42	0.20	Modified NACA 66 series	Complete tail on stub fuselage R = 1,510,000 M = 0.1	Sealed 0.113 inch	Unpublished data	134, 135
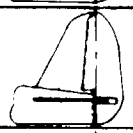	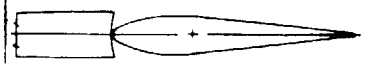 Medium-nose rudder	2.41	0.47	0.42	0.31	Modified NACA 66 series	Complete tail on stub fuselage R = 1,510,000 M = 0.1	Sealed 0.113 inch	Unpublished data	136, 137
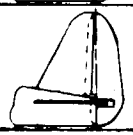	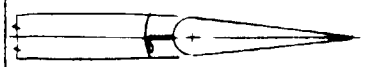 Internally balanced rudder	2.41	0.47	0.42	0.20	Modified NACA 66 series	Complete tail on stub fuselage R = 1,510,000 M = 0.1	Sealed	Unpublished data	138, 139

NATIONAL ADVISORY
COMMITTEE FOR AERONAUTICS

TABLE III.- AERODYNAMIC PARAMETERS AND CORRELATION CHARTS

Type of balance	Subject	Airfoil	Type of data	Reference	Figure
Plain flaps	Pressure distribution Lift Hinge moment	0009	Section	1, 2, 3 1, 2, 3, 7, 20 1, 2, 3, 7, 20	140 141 142
Overhangs	Lift	0009 0015 66-009	Section	7, 8, 9, 10 12, 13, 14 19	143(a) to (d) 143(e), (f) 143(g), (h)
		0009	Finite span	21	145
	Hinge moment	0009 0015 66-009	Section	7, 8, 9, 10 12, 13, 14 19	144(a) to (d) 144(e), (f) 144(g), (h)
		0009	Finite span	21	146
Tabs	Hinge moment and lift	0009	Section	1, 2, 3	147, 148
Beveled trailing edge	Pressure distribution	0009	Section	Unpublished	149
	Hinge moment	Many	Section and finite span	26	150
Internal	Hinge moment	Many	Section and finite span	29	151, 152
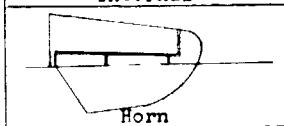 Horn	Hinge moment	Many	Finite	33	153, 154
Plain flaps and overhangs	Tunnel correction factors for hinge moment	Any	Section	40	155

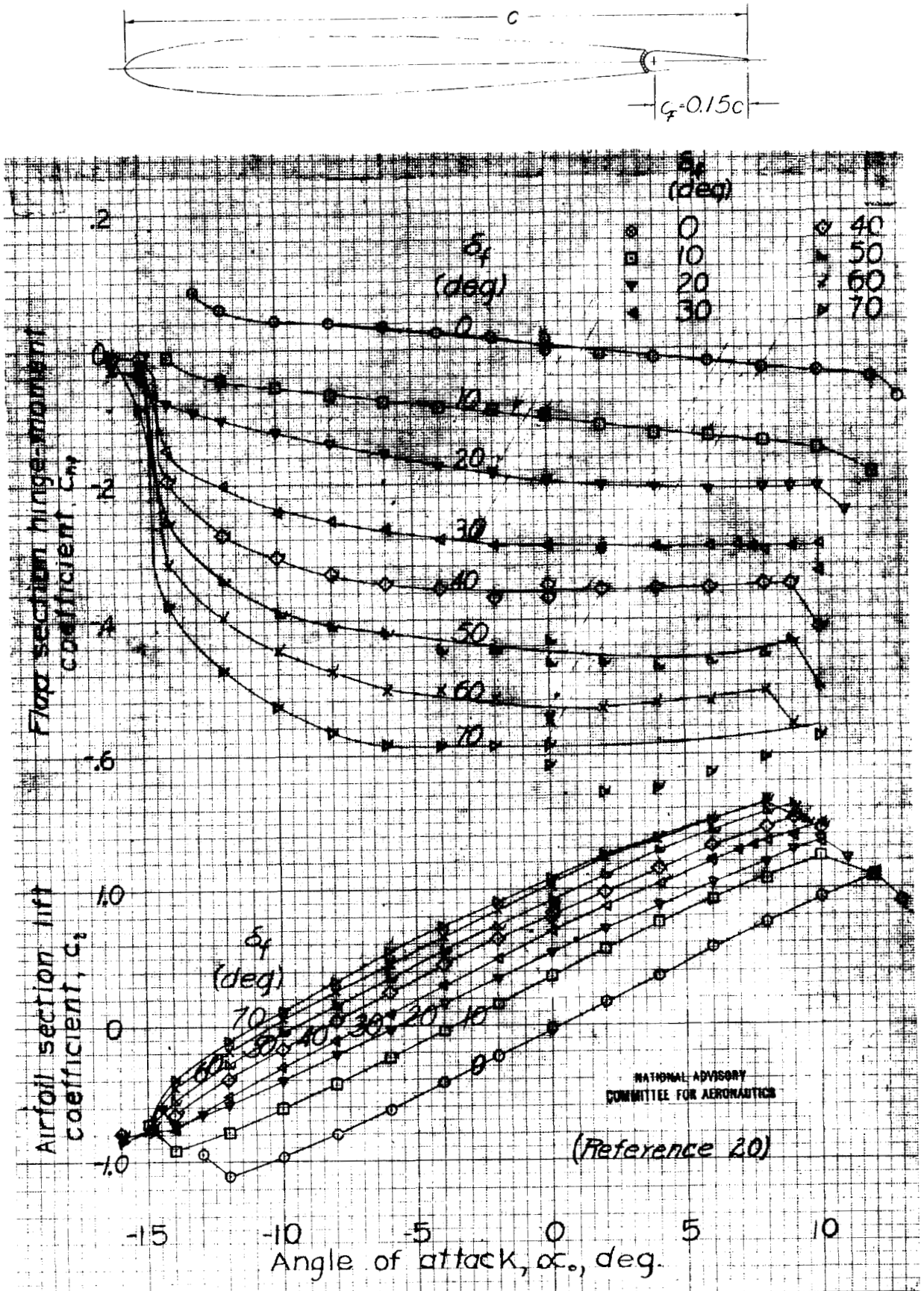

Figure 1.- NACA 0009 airfoil, 0.15c plain flap, sealed gap.

L-663

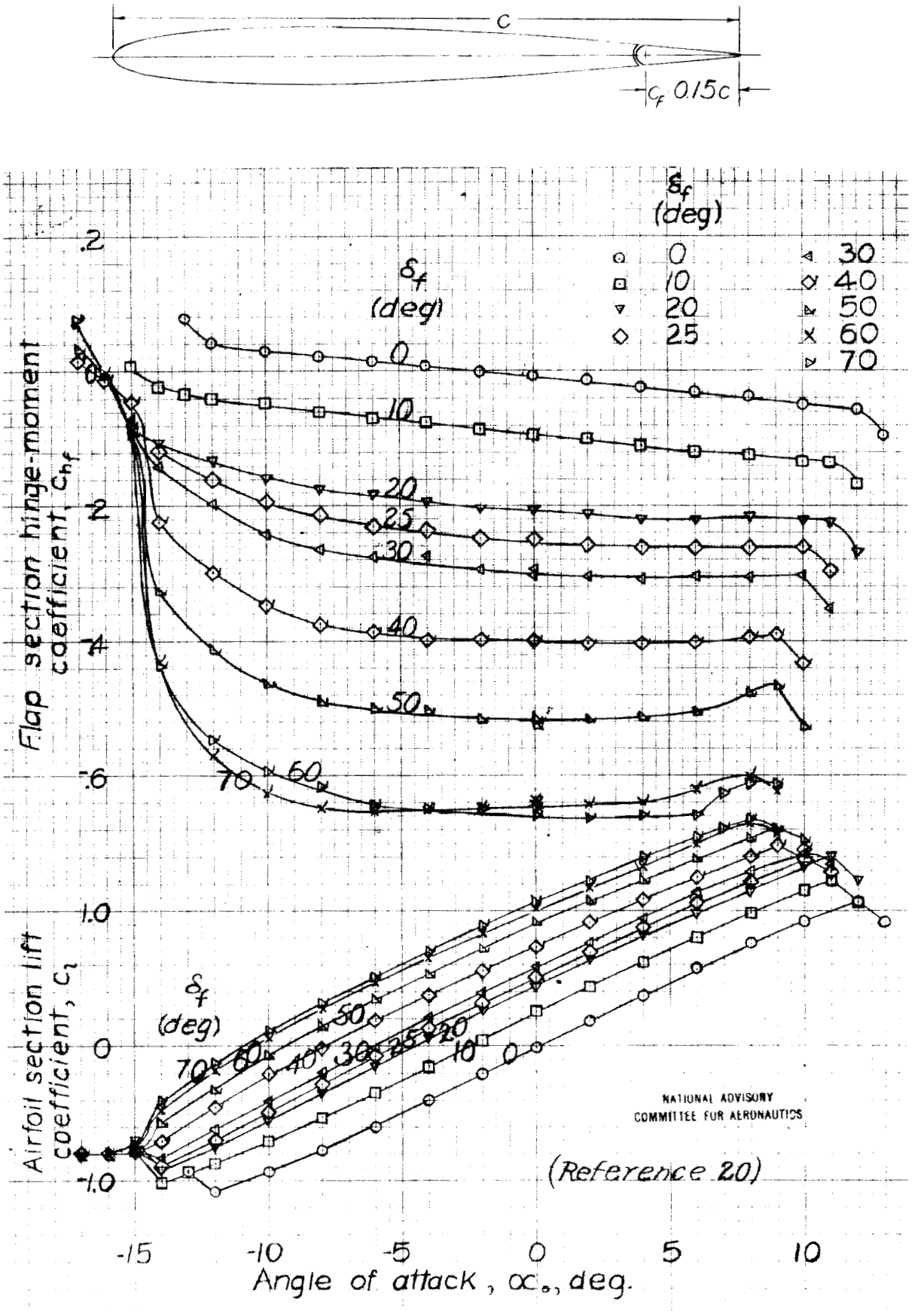

Figure 2.- NACA 0009 airfoil, 0.15c plain flap, 0.005c gap.

L-663

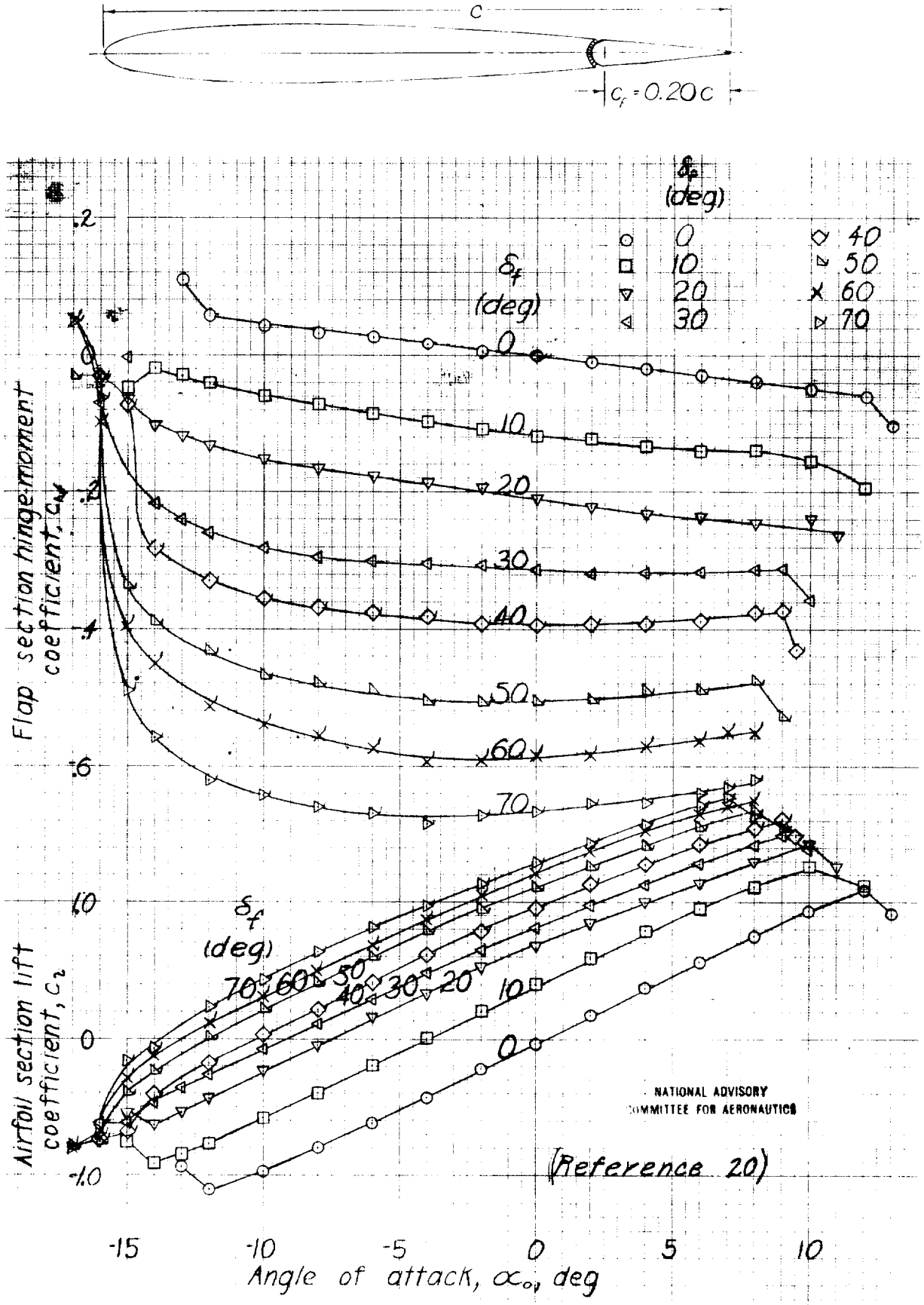

Figure 3.- NACA 0009 airfoil, 0.20c plain flap, sealed gap.

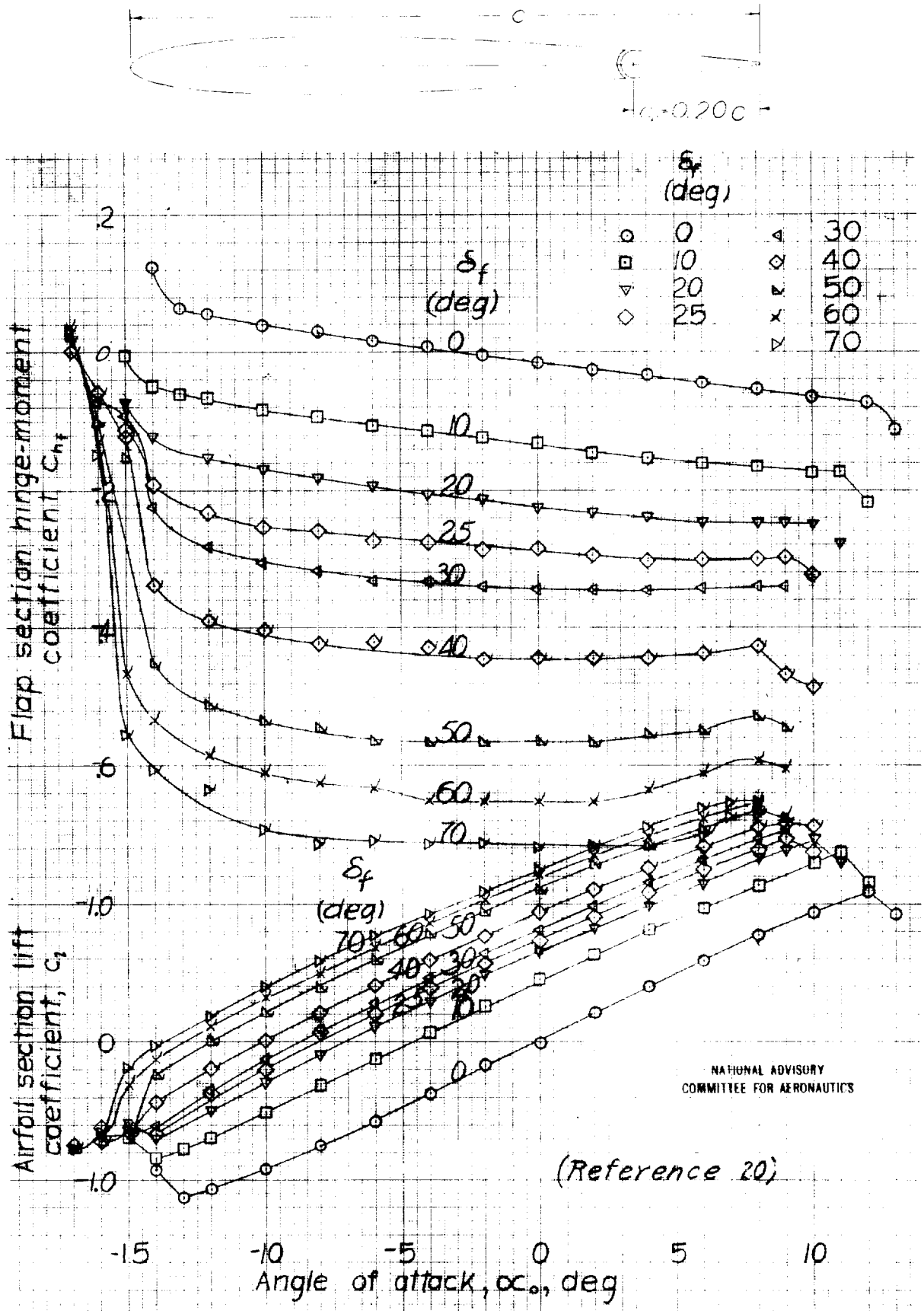

Figure 4.- NACA 0009 airfoil, 0.20c plain flap. 0.005c gap.

L-663

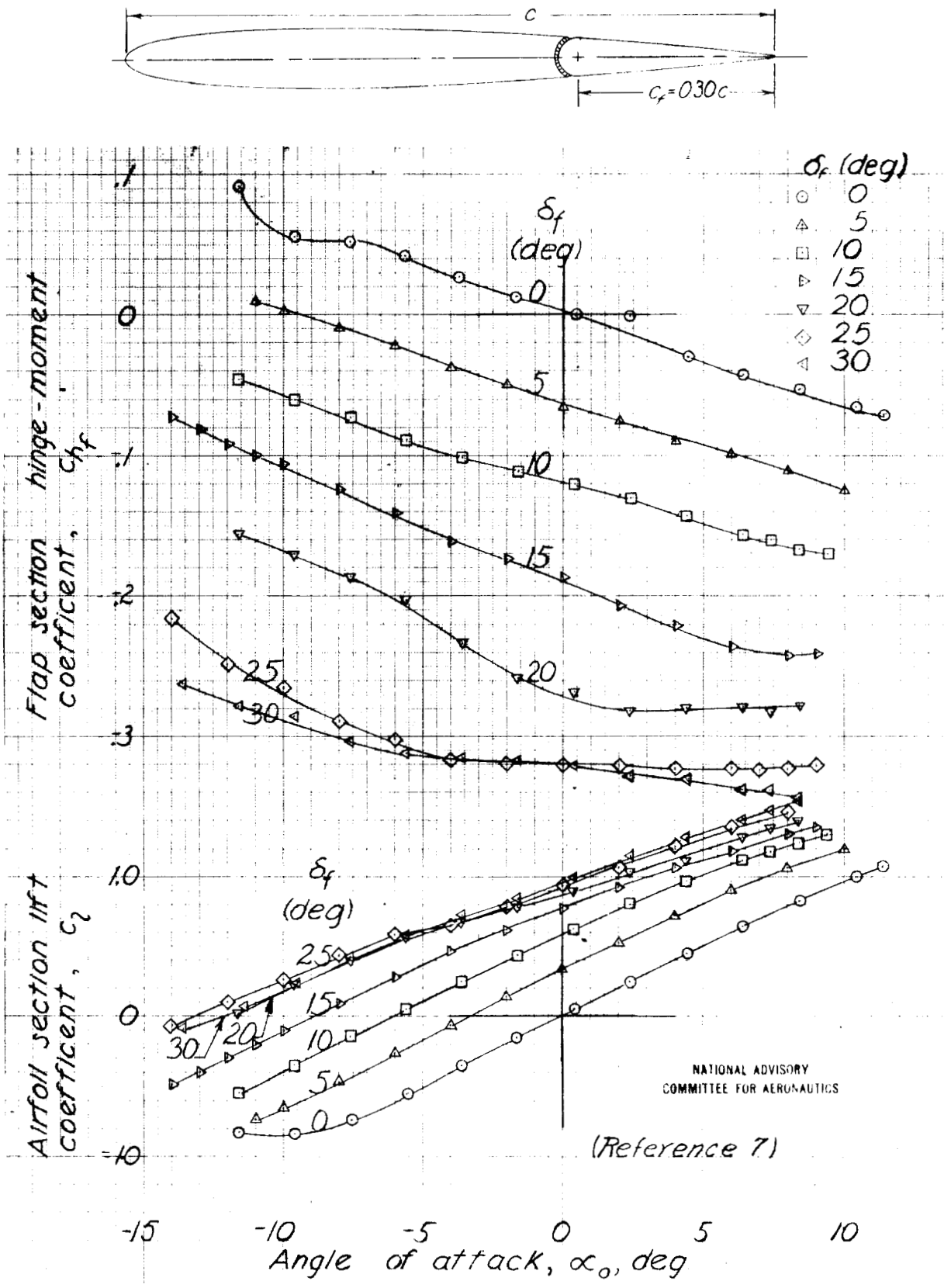

Figure 5.- NACA 0009 airfoil, 0.30c plain flap, sealed gap.

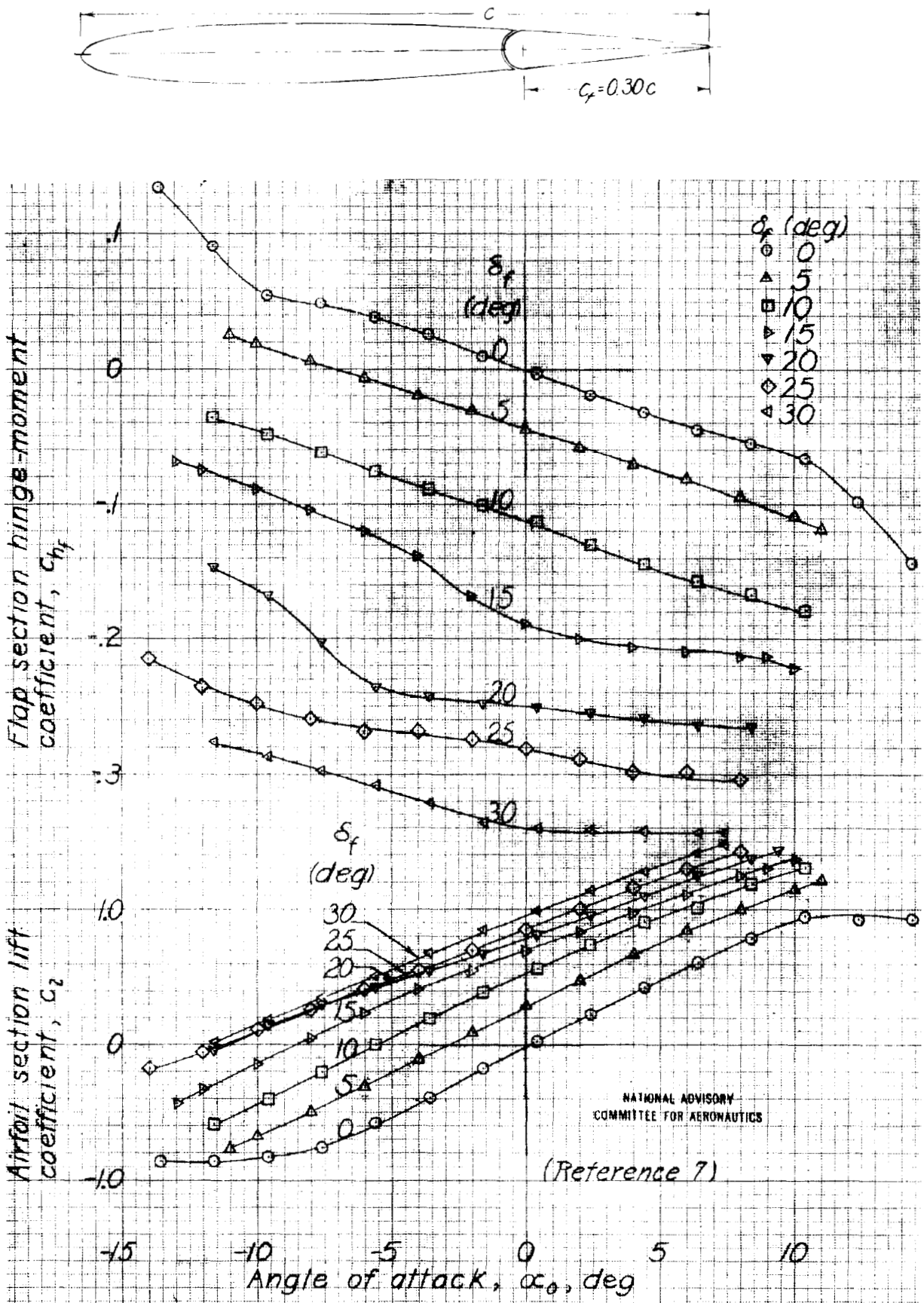

Figure 6.- NACA 0009 airfoil, 0.30c plain flap, 0.001c gap.

L-663

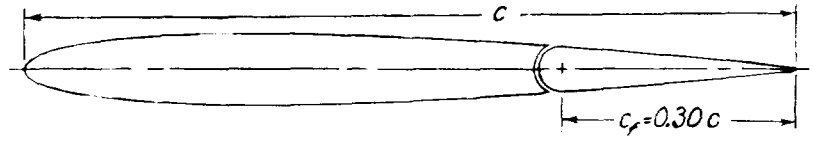

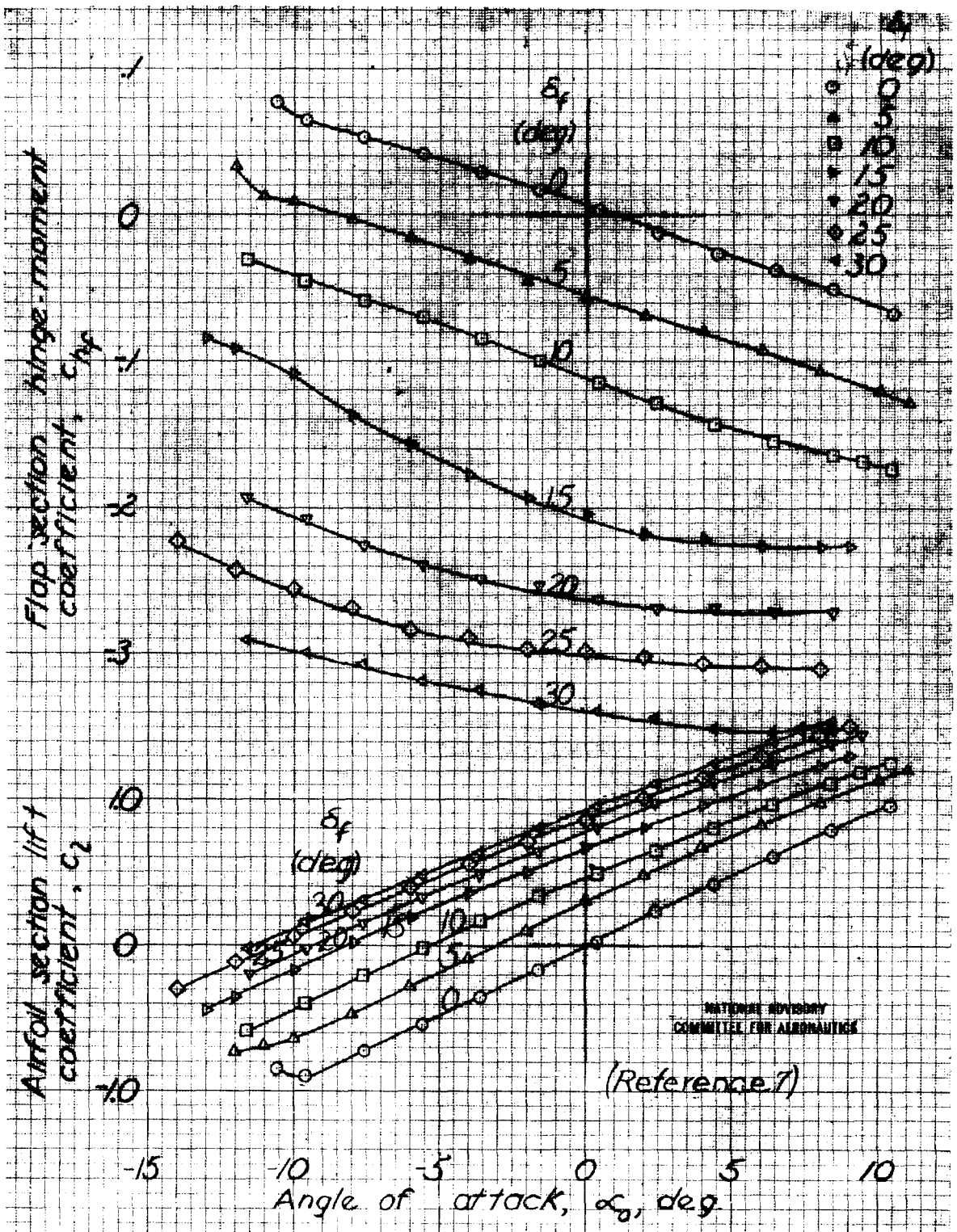

Figure 7.- NACA 0009 airfoil, 0.30c plain flap, 0.005c gap.

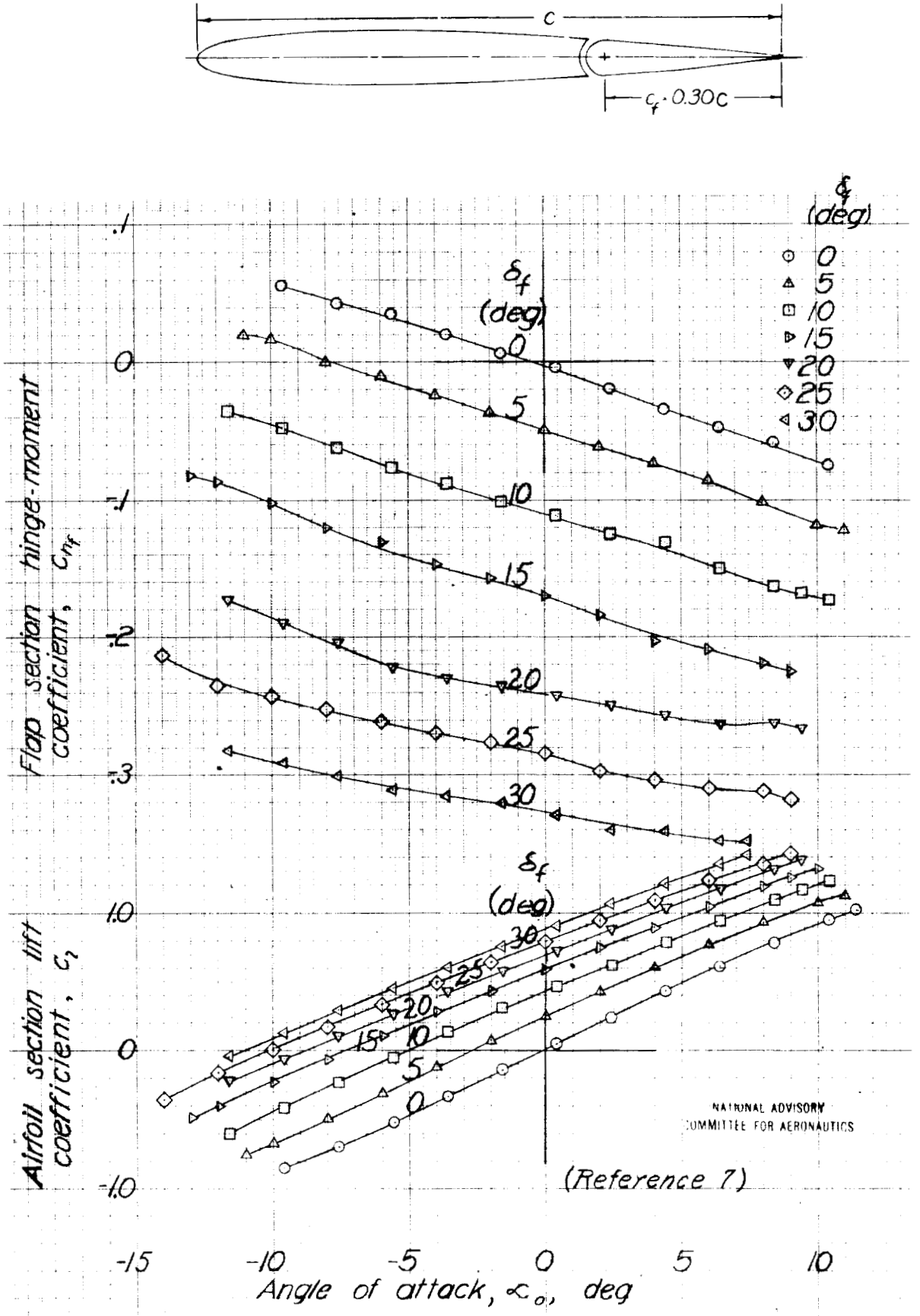

Figure 8.- NACA 0009 airfoil, 0.30c plain flap, 0.010c gap.

L-663

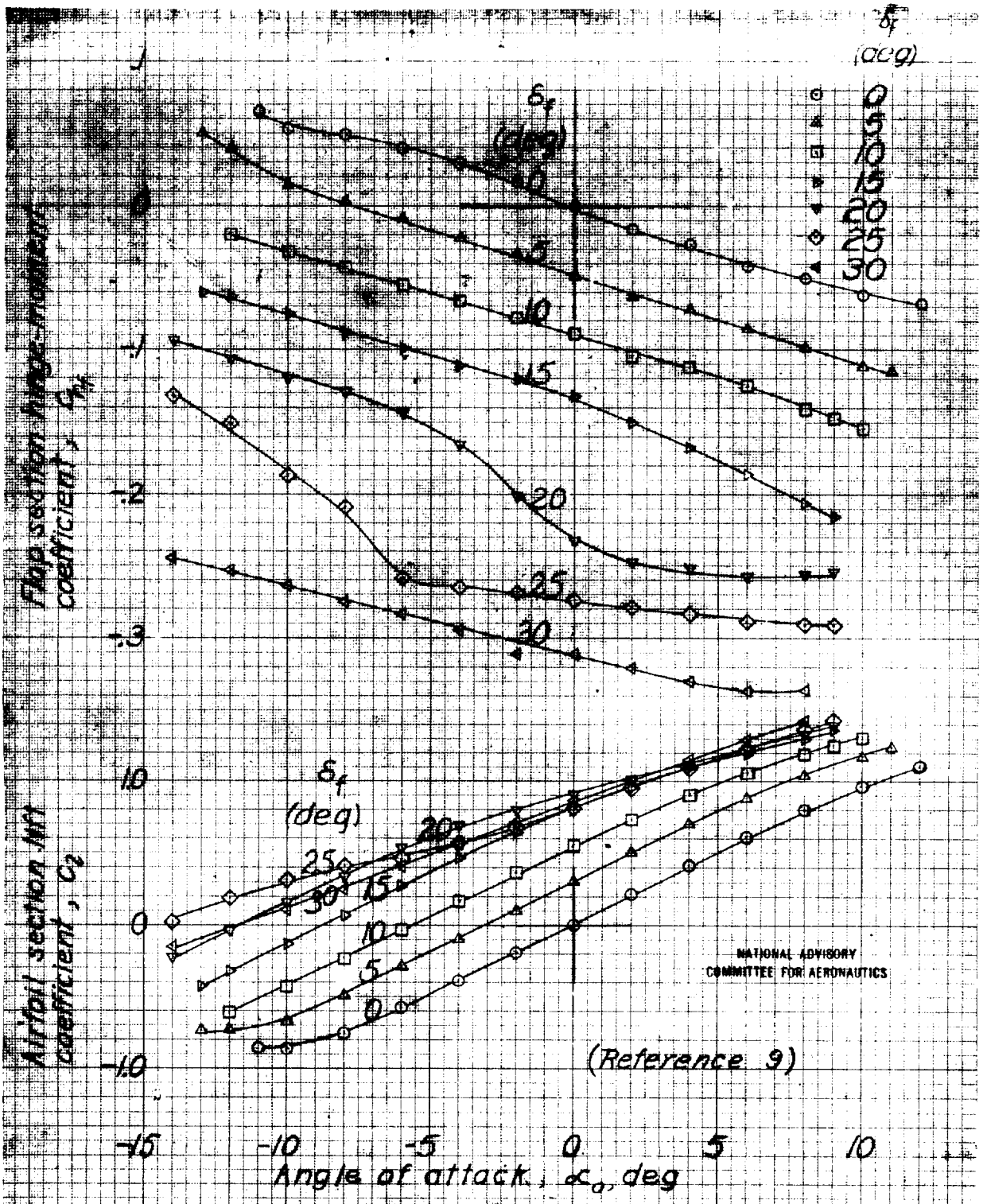

Figure 9.- NACA 0009 airfoil, 0.30c flap, with 0.20c_f blunt-nose overhang, sealed gap.

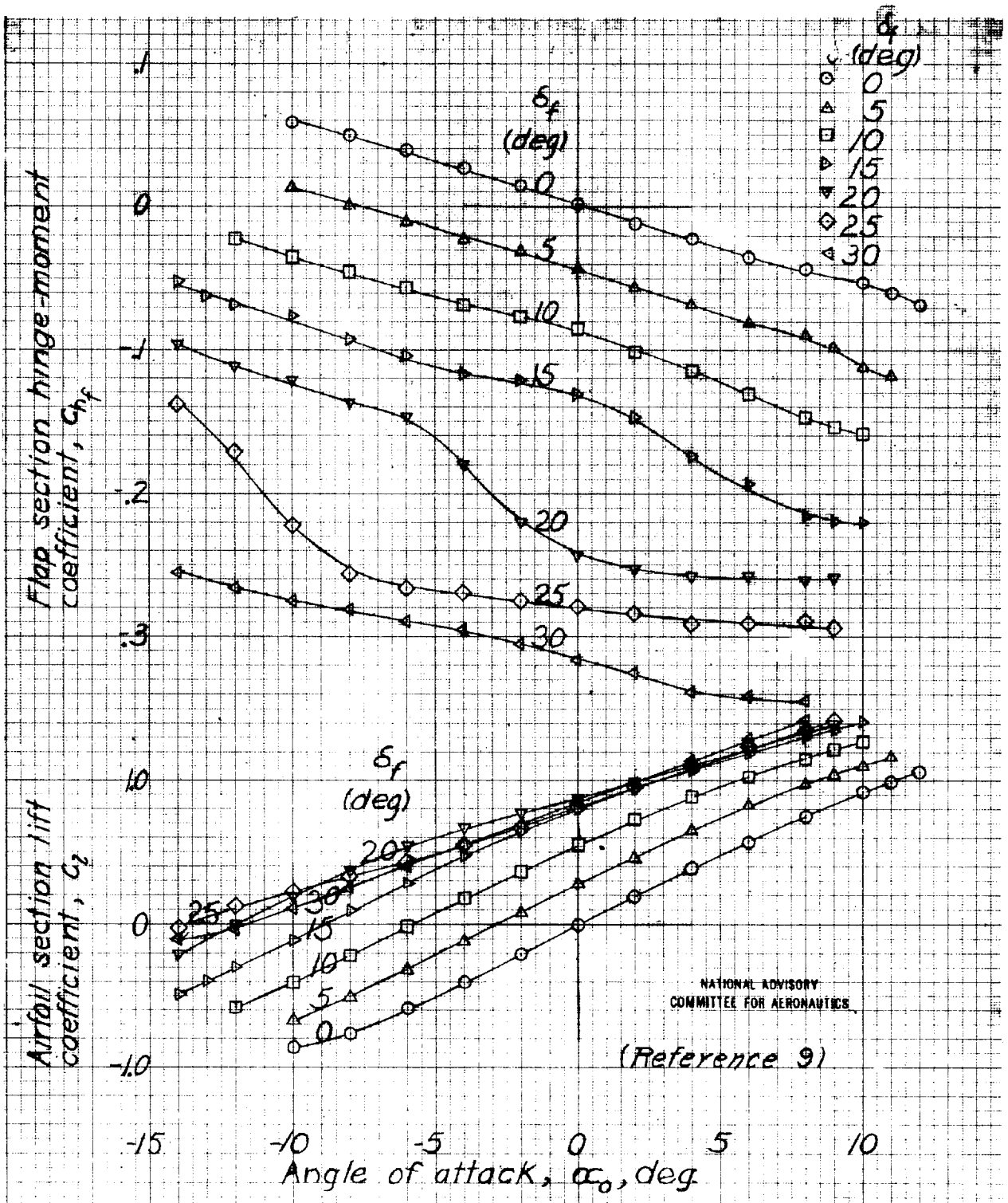

Figure 10.- NACA 0009 airfoil, 0.30c flap with 0.20c_f blunt nose overhang 0.001c gap.

L-663

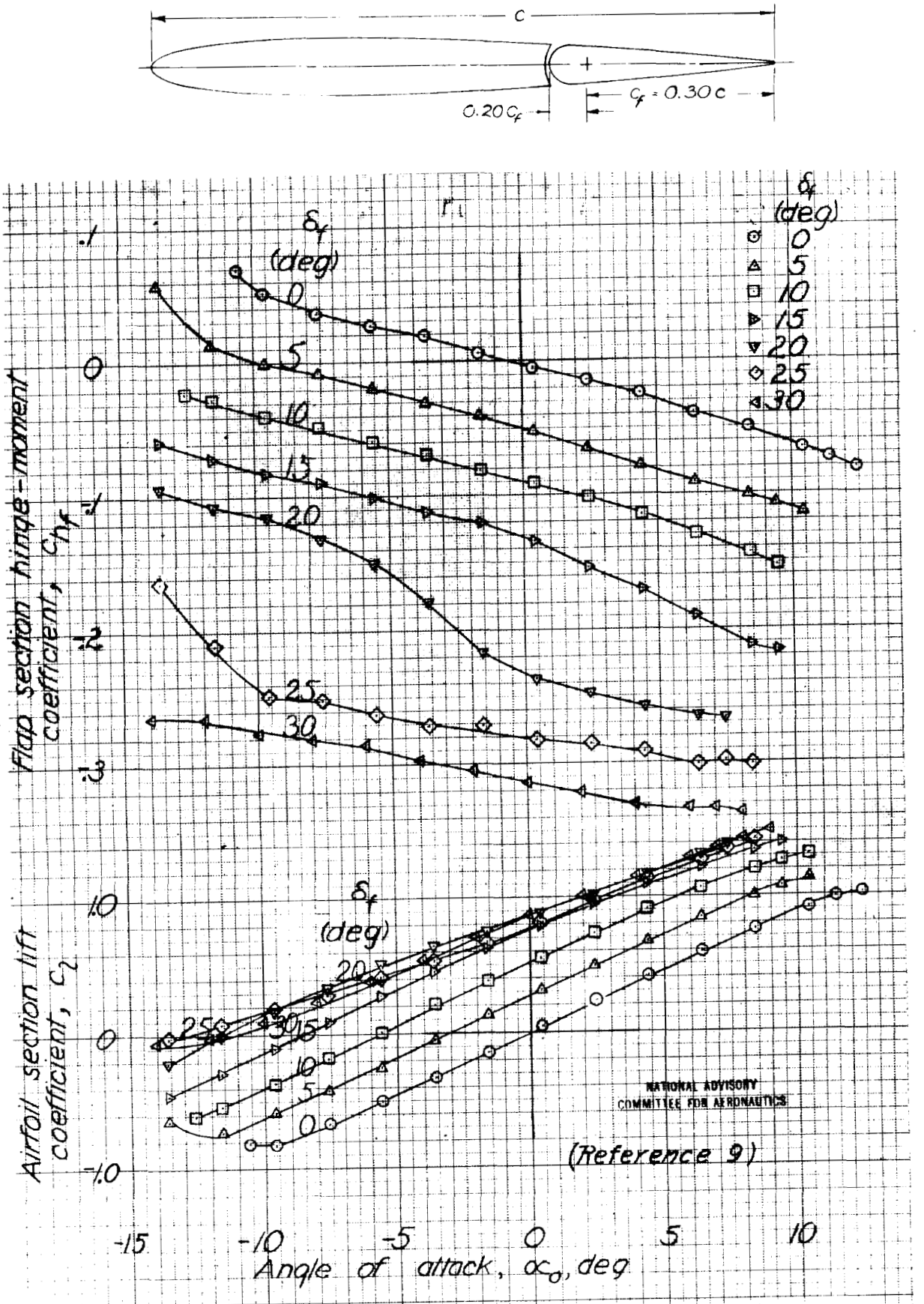

Figure 11.- NACA 0009 airfoil, 0.30c flap, with $0.20c_f$ blunt-nose overhang, 0.005c gap.

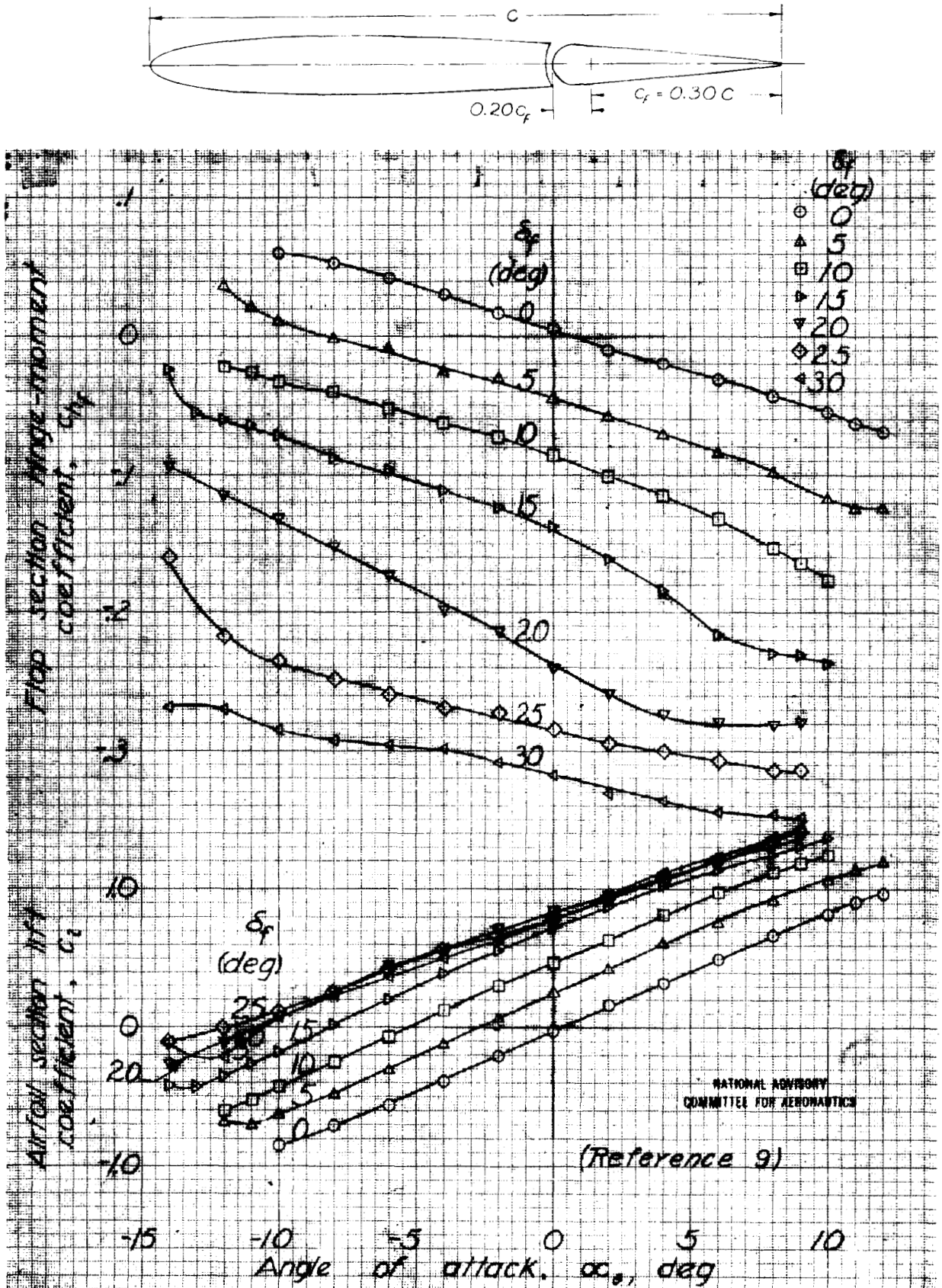

Figure 12.- NACA 0009 airfoil, 0.30c flap with 0.20 c_f blunt-nose overhang, 0.010c gap.

L-663

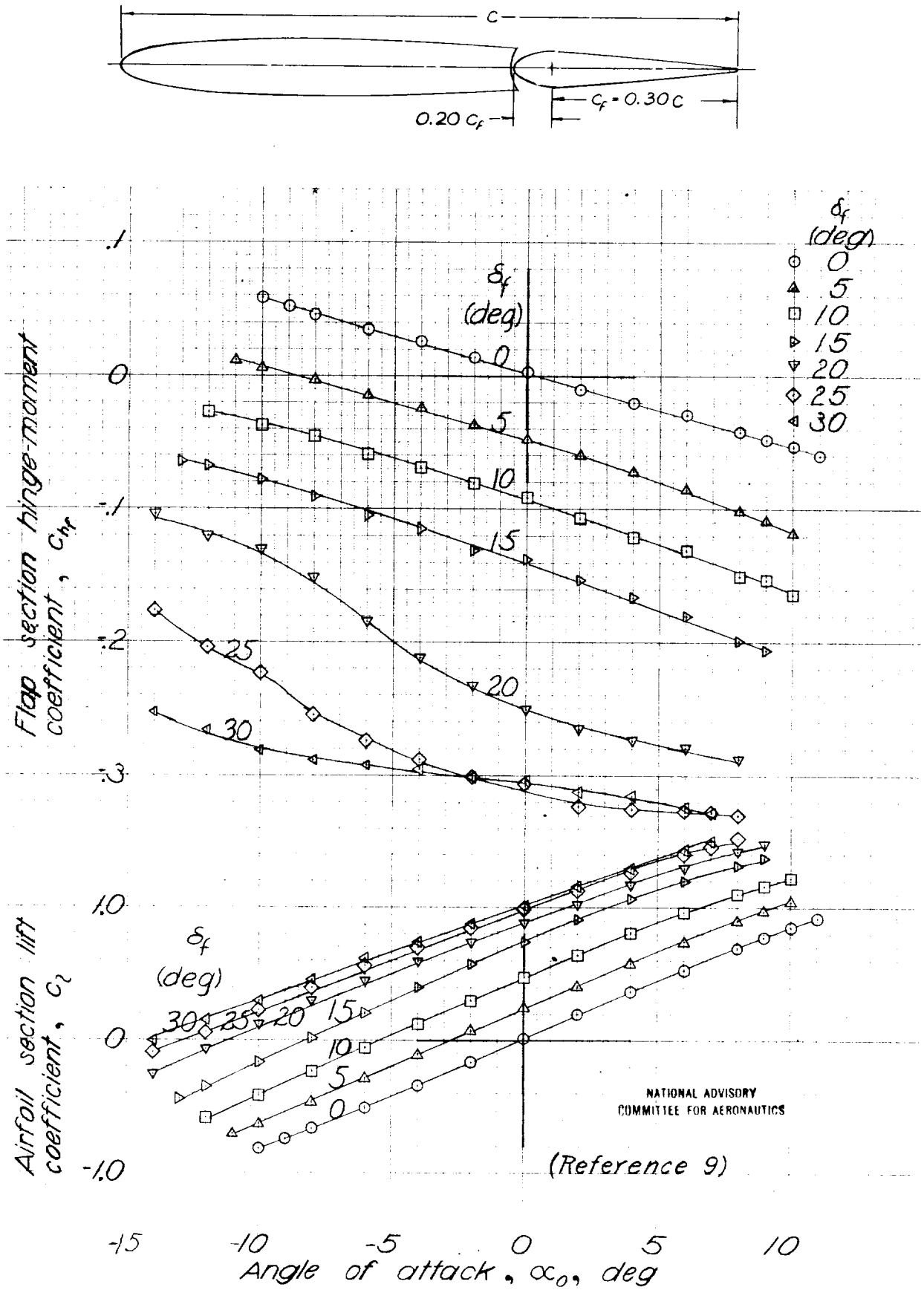

Figure 13.- NACA 0009 airfoil, 0.30 c flap with $0.20c_f$ modified blunt-nose overhang, 0.005c gap.

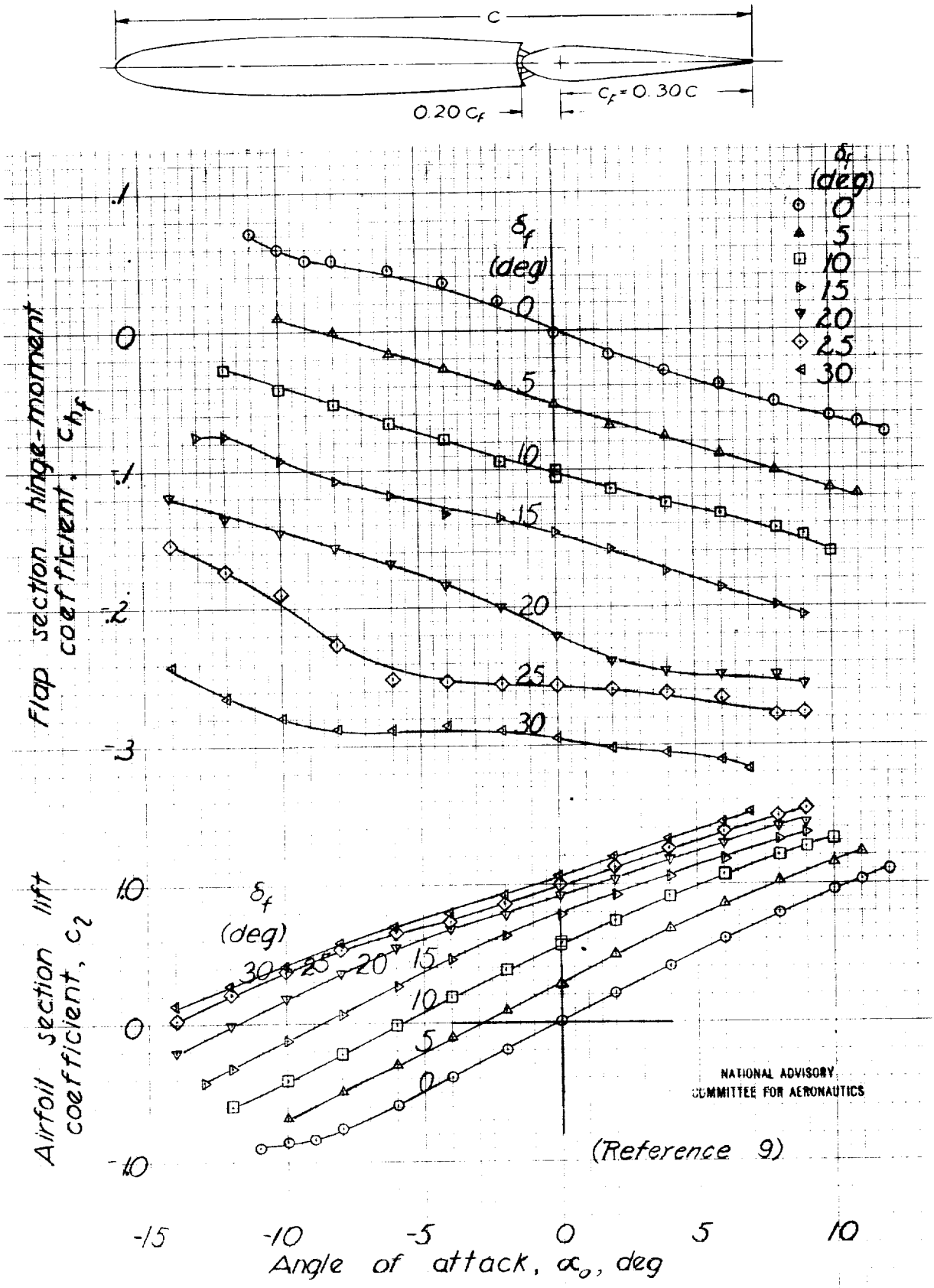

Figure 14.- NACA 0009 airfoil, 0.30c flap with 0.20 c_f medium-nose overhang, sealed gap.

L-663

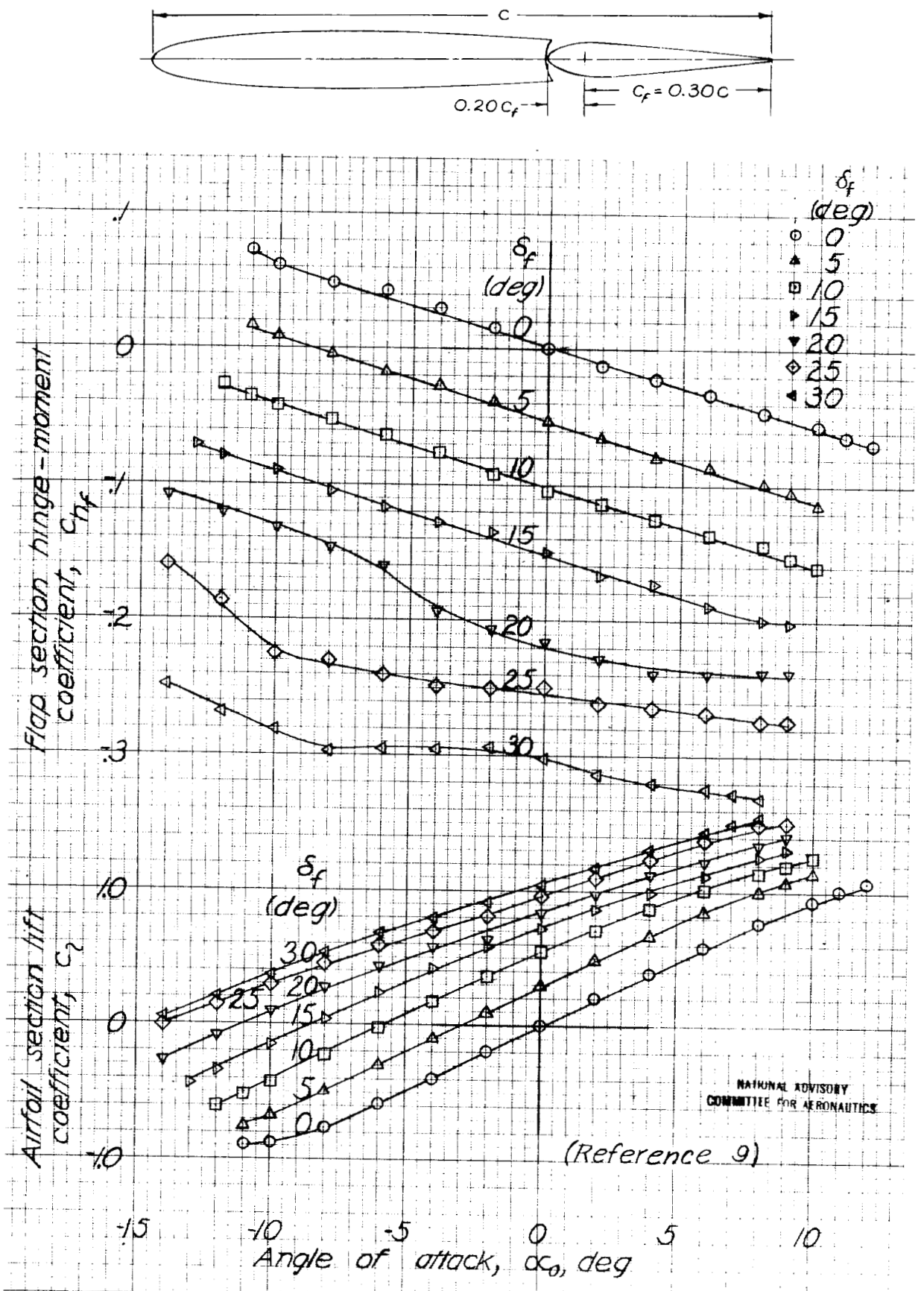

Figure 15.-NACA 0009 airfoil, 0.30c flap with 0.20c_f medium-nose overhang, 0.001c gap.

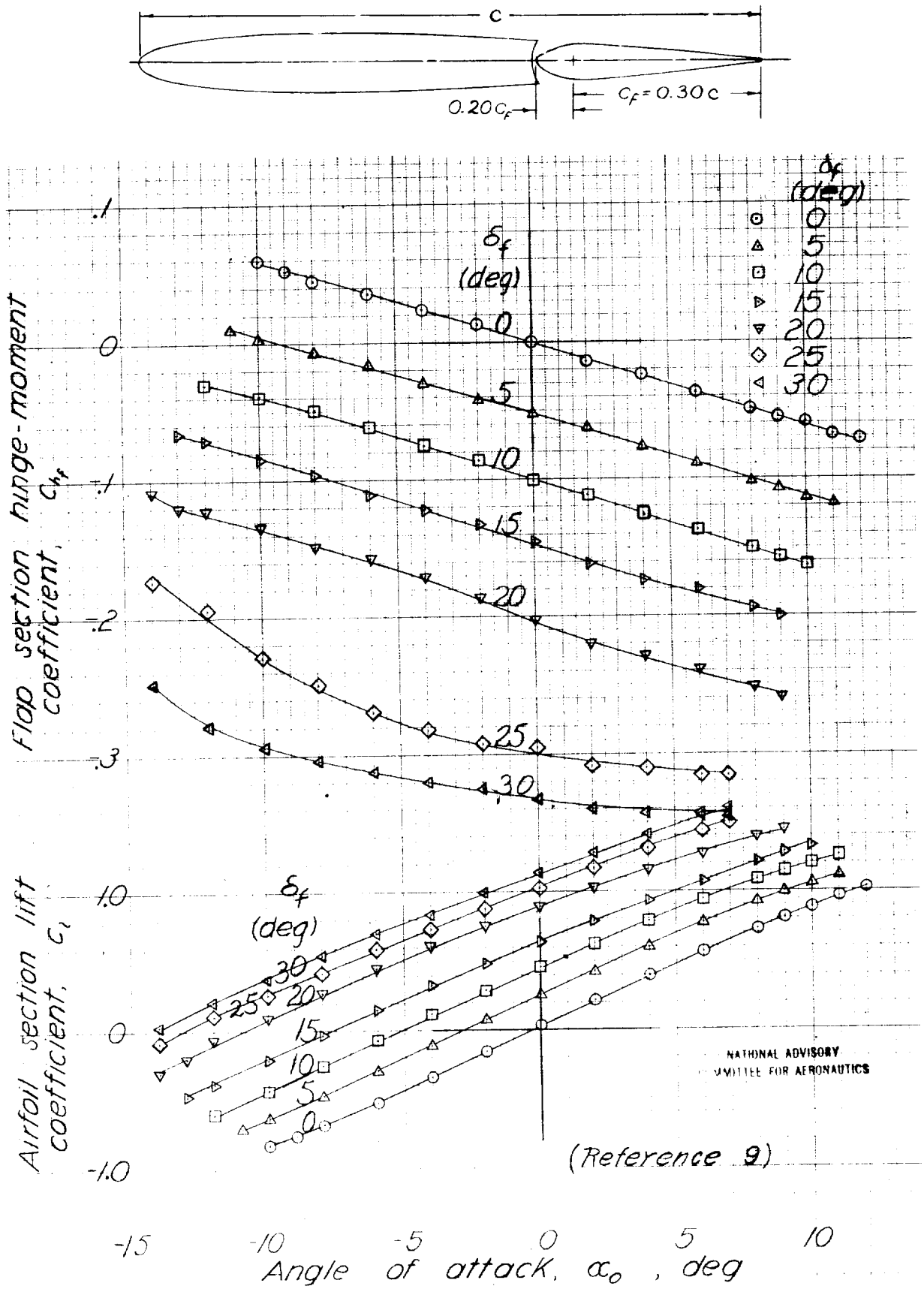

Figure 16.- NACA 0009 airfoil, 0.30c flap with 0.20 c_f medium-nose overhang, 0.005c gap.

L-663

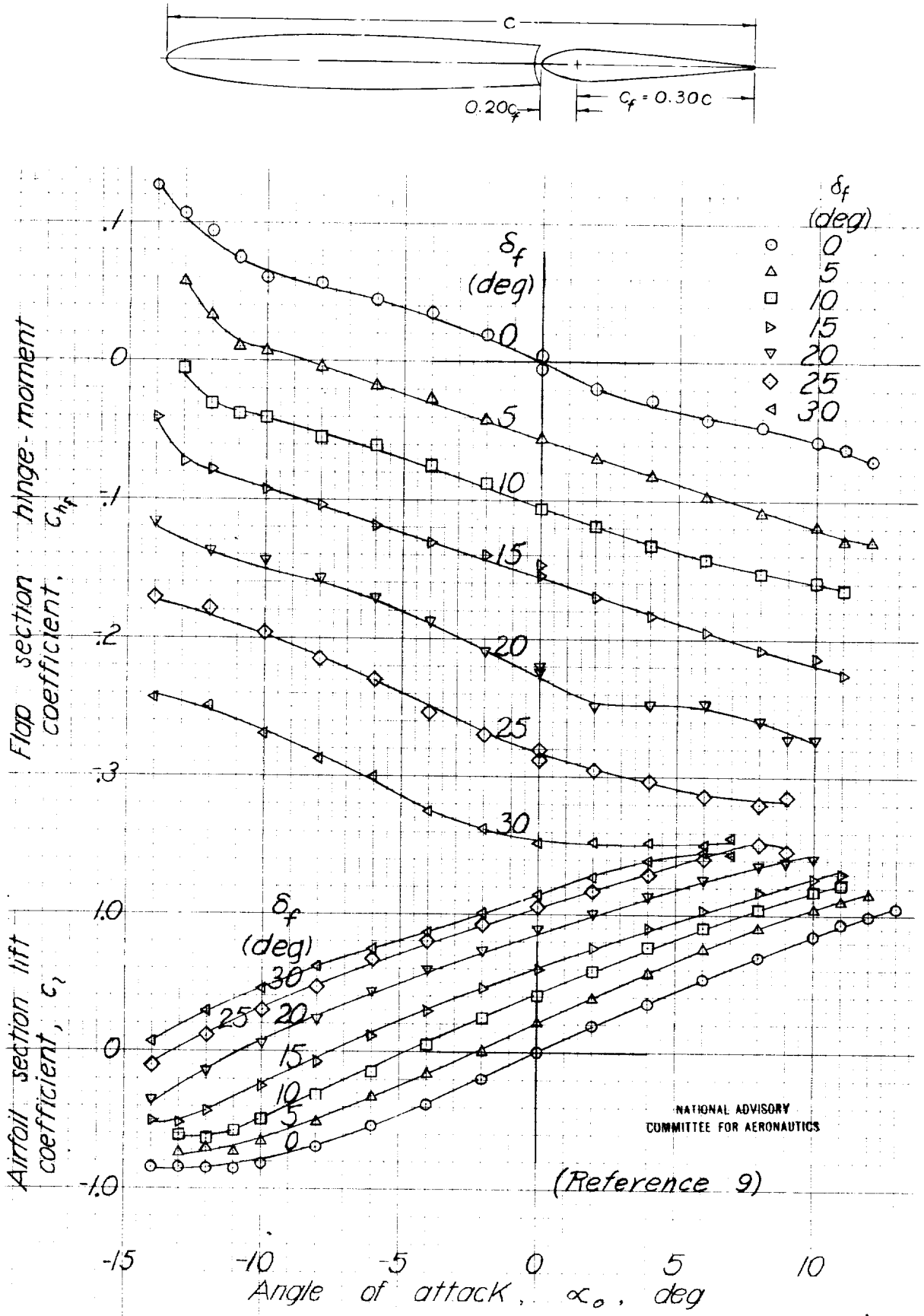

Figure 17.- NACA 0009 airfoil, 0.30c flap with 0.20 c_f medium-nose overhang, 0.010c gap.

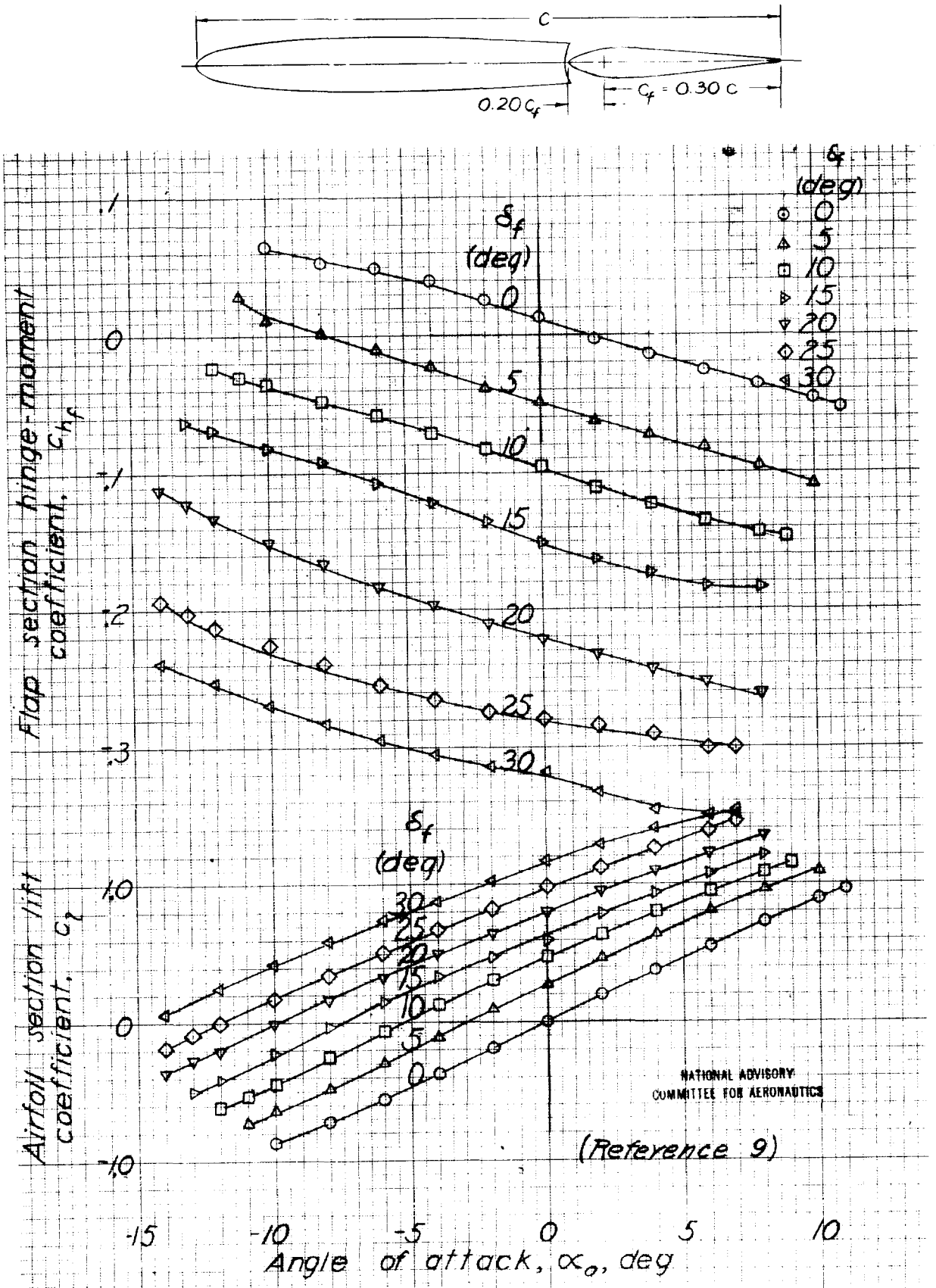

Figure 18.-NACA 0009 airfoil, 0.30c flap with 0.20c_f modified medium-nose overhang, 0.005c gap.

L-663

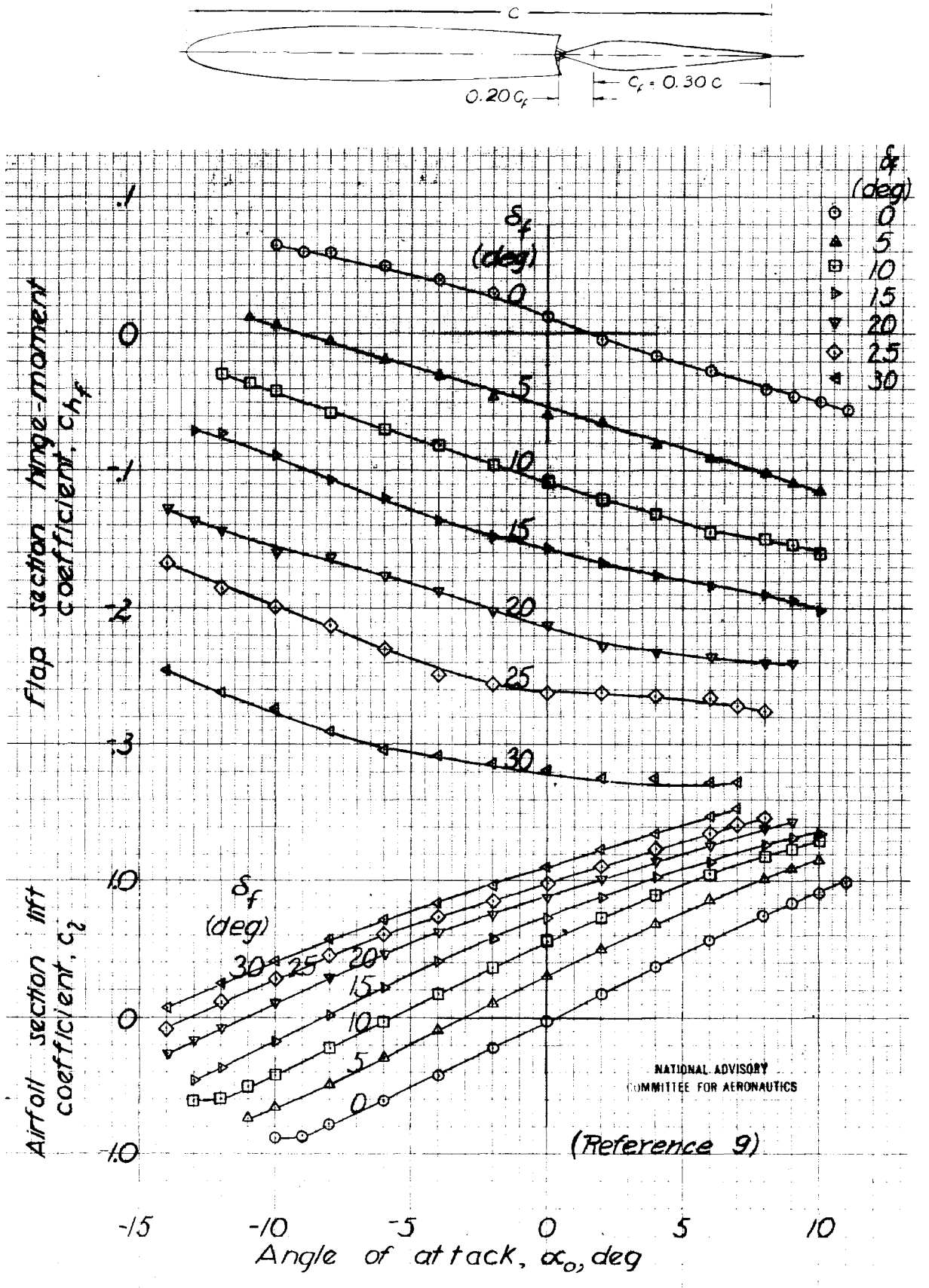

Figure 19.- NACA 0009 airfoil, 0.30c flap with 0.20c_f sharp-nose overhang, sealed gap.

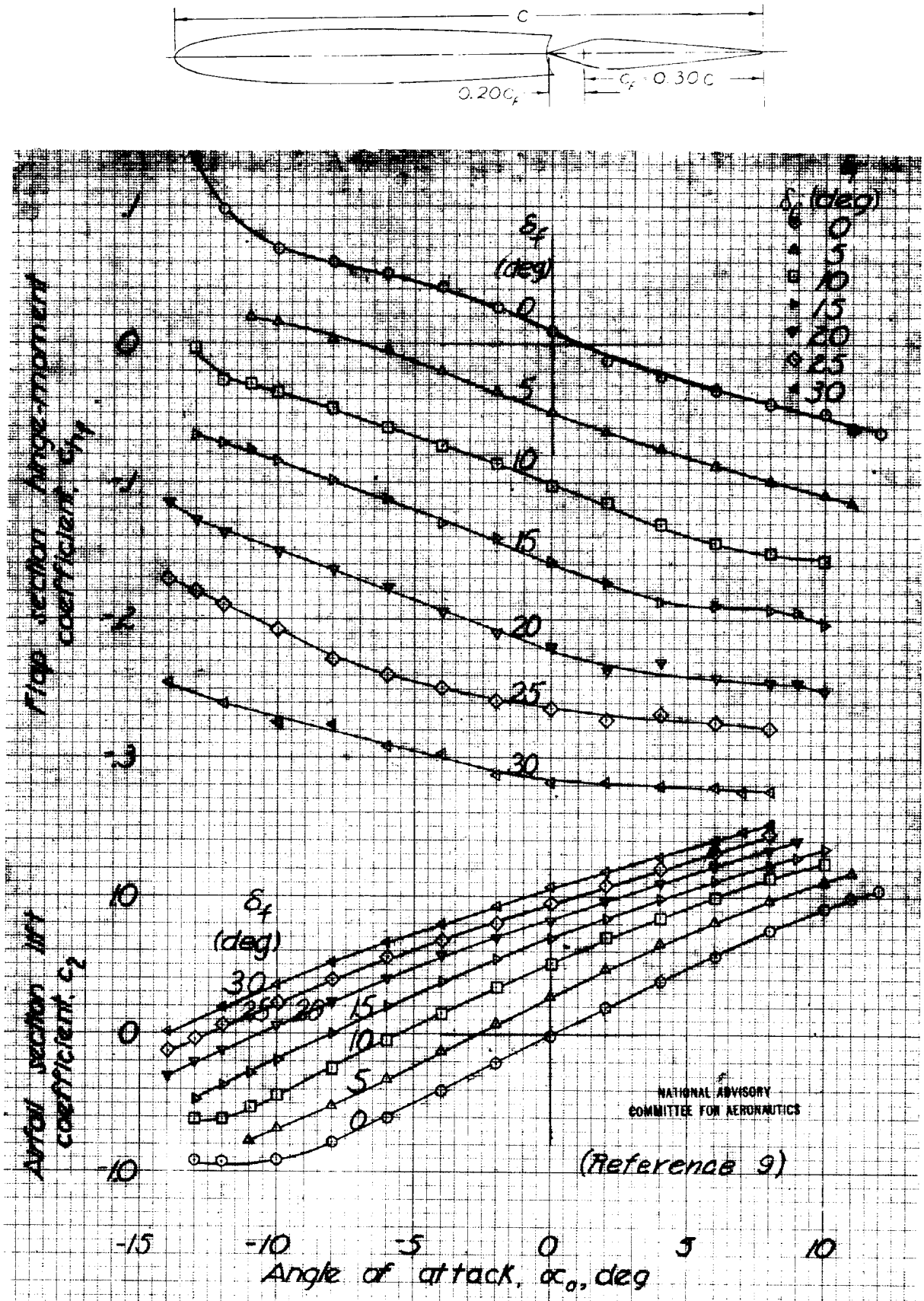

Figure 20.- NACA 0009 airfoil, 0.30c flap with 0.20c$_f$ sharp-nose overhang, 0.001c gap.

L-663

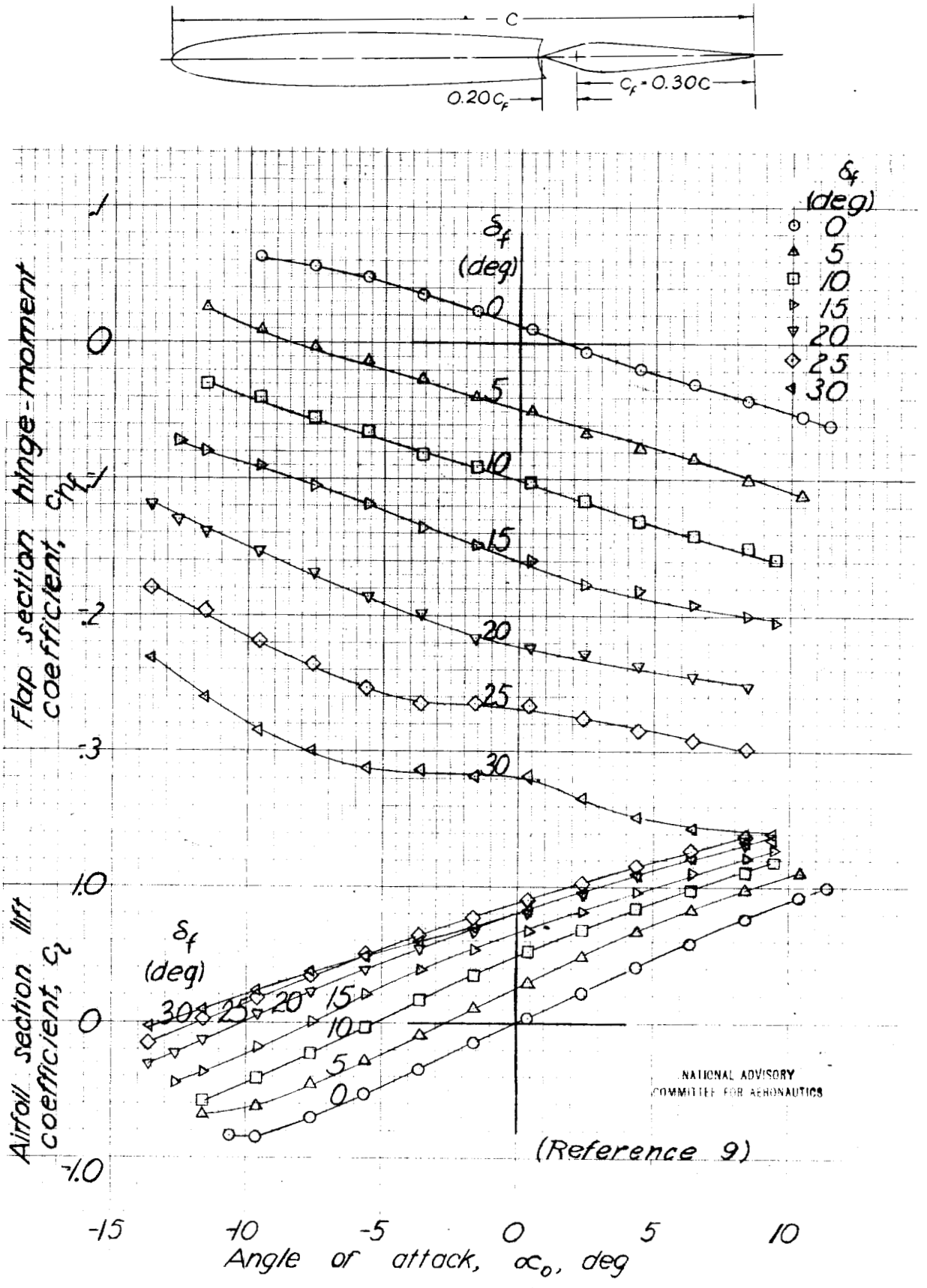

Figure 21.- NACA 0009 airfoil, 0.30c flap with 0.20c_f sharp-nose overhang, 0.005c gap.

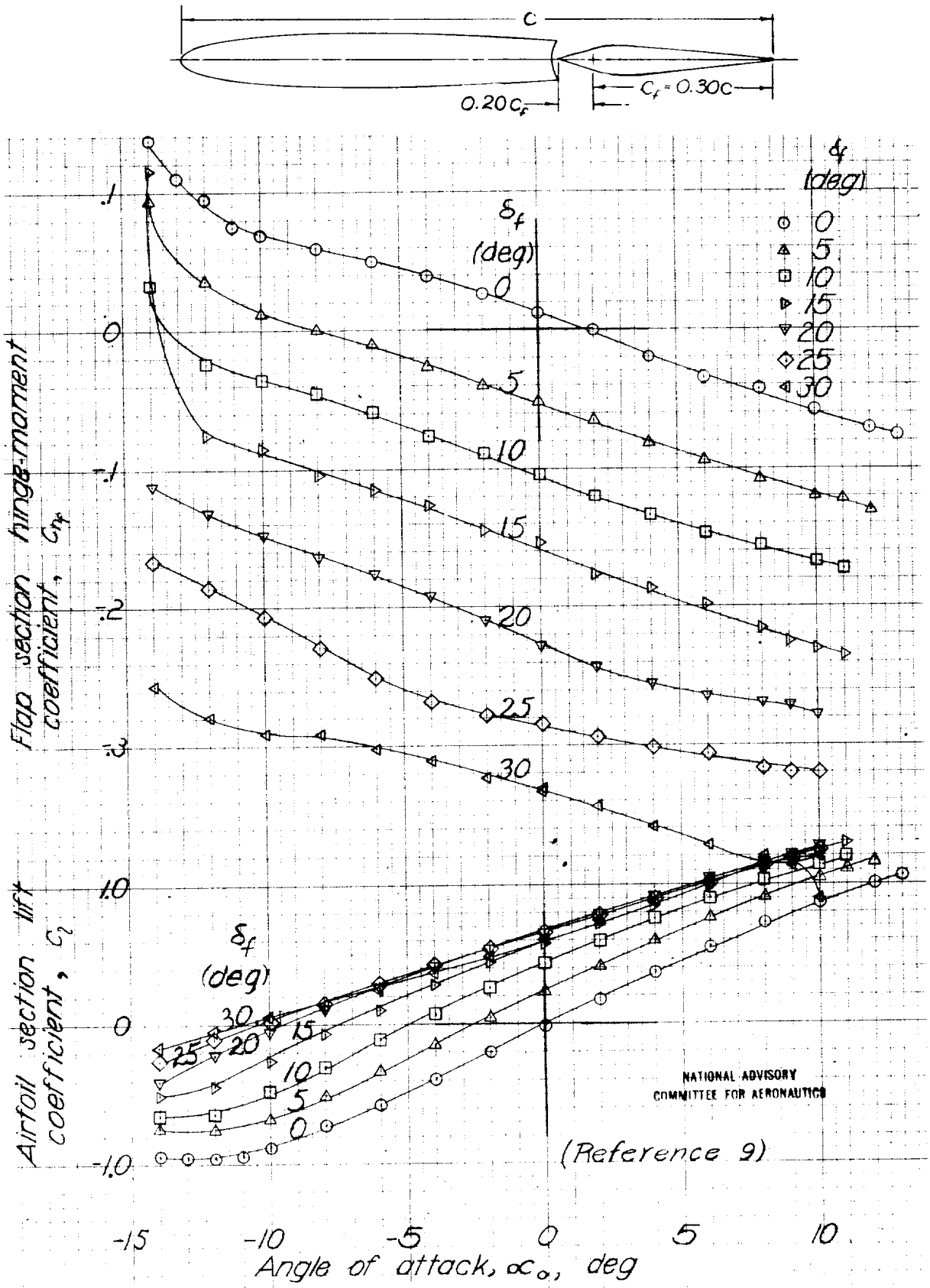

Figure 22.- NACA 0009 airfoil, 0.30 c flap with 0.20c_f sharp-nose overhang, 0.010 c gap.

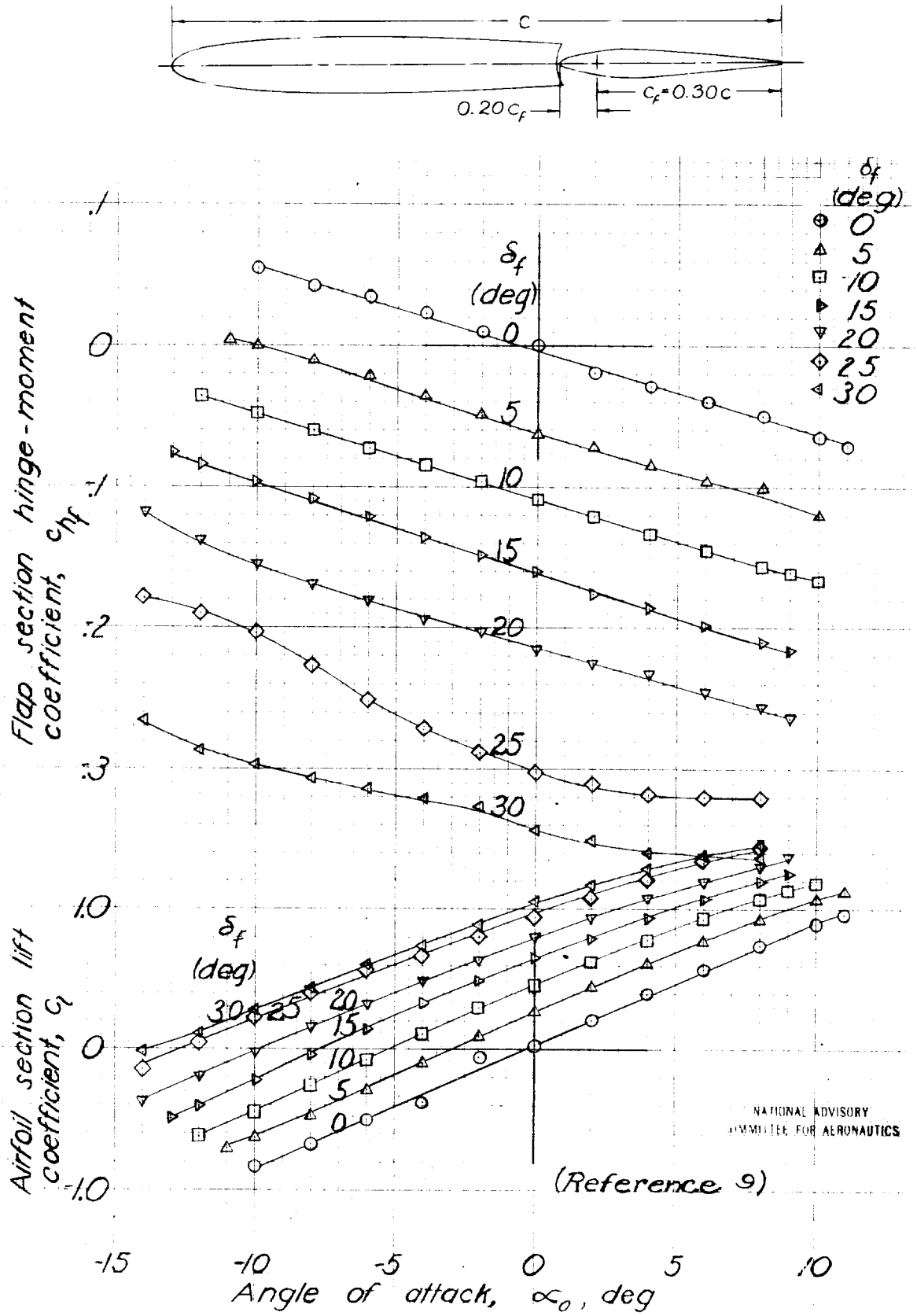

Figure 23.- NACA 0009 airfoil, 0.30c flap with 0.20c_f modified sharp-nose overhang, 0.005c gap.

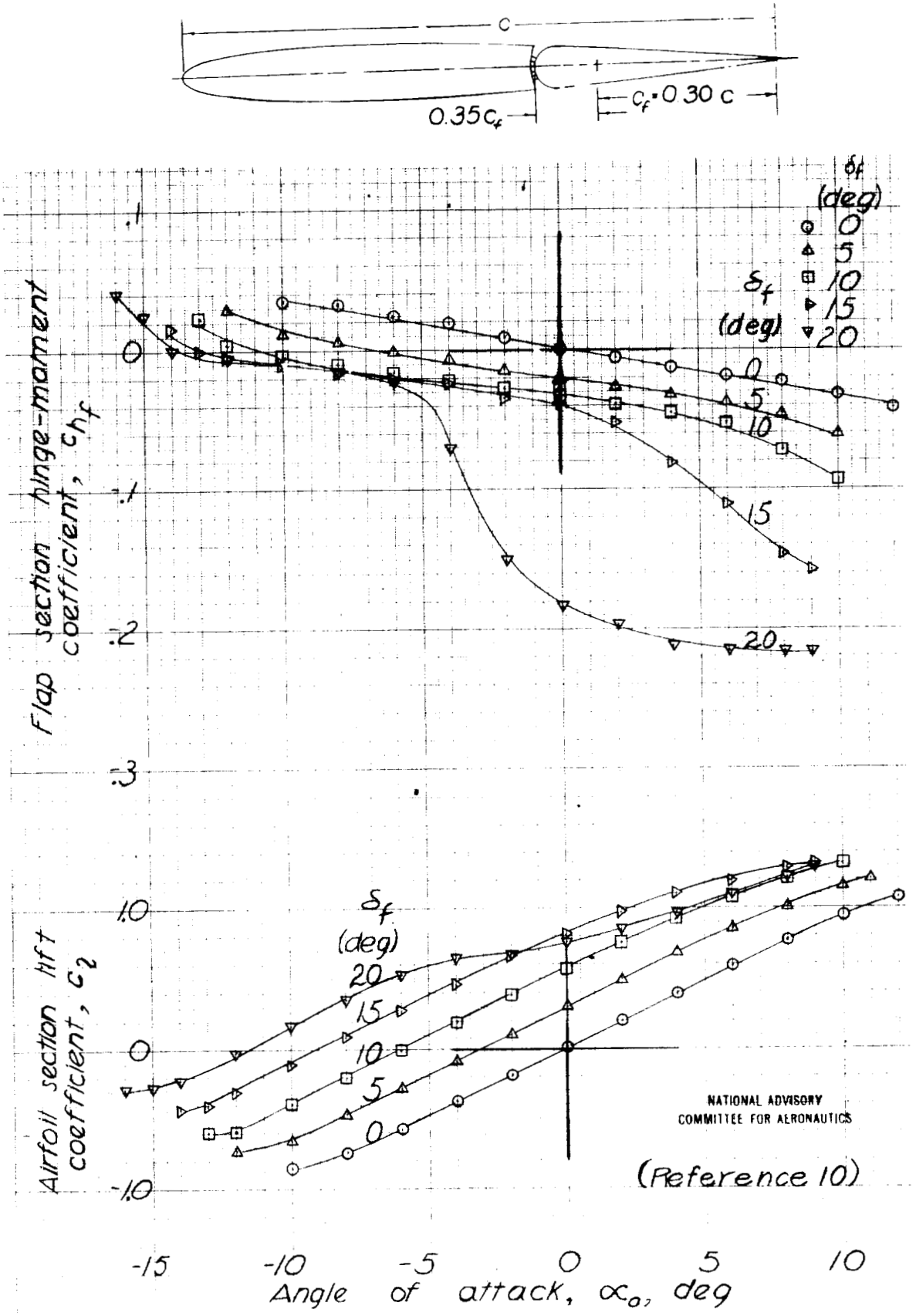

Figure 24.- NACA 0009 airfoil, 0.30 c flap with 0.35 c_f blunt-nose overhang, sealed gap.

L-663

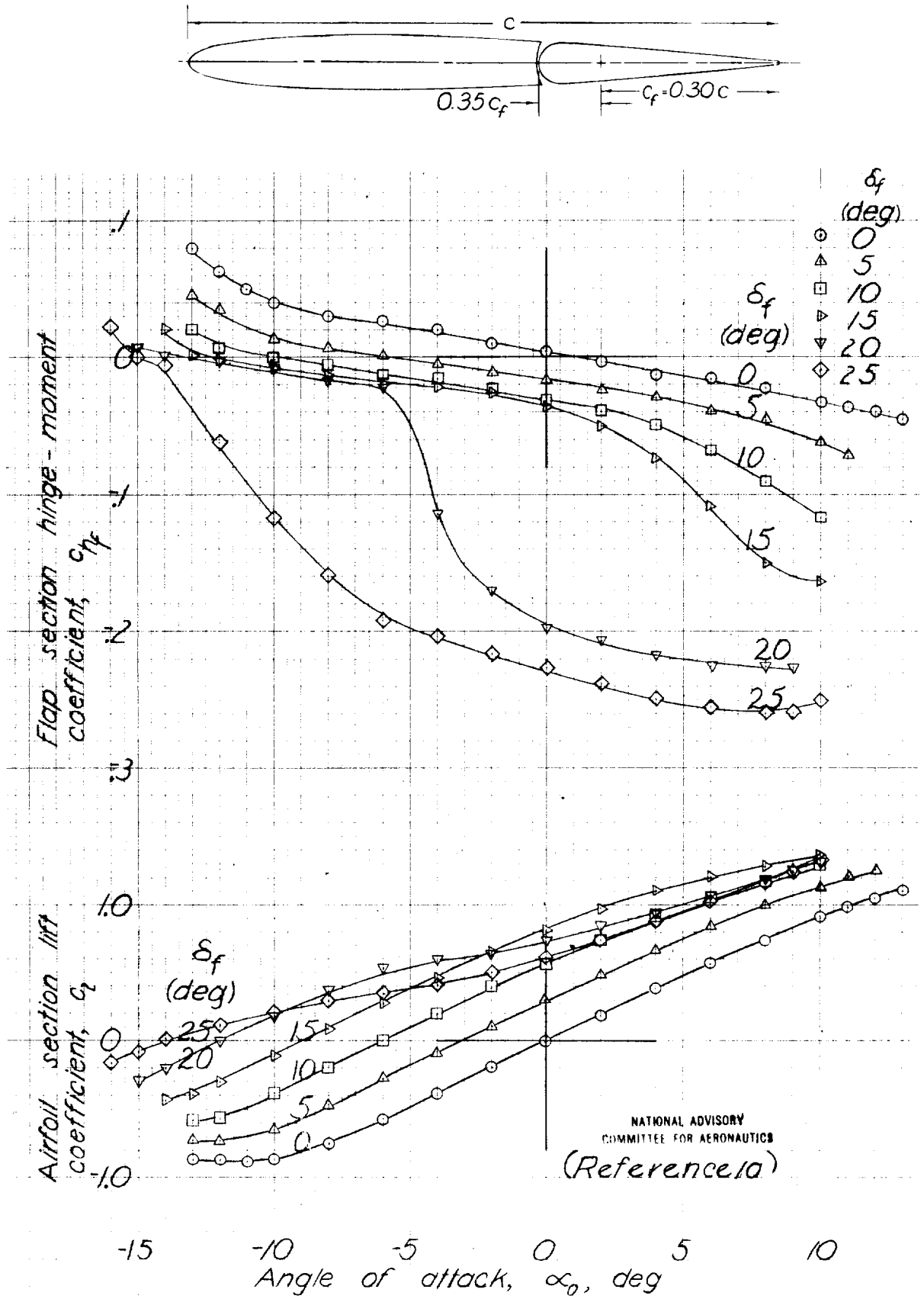

Figure 25.- NACA 0009 airfoil, 0.30c flap with 0.35c_f blunt-nose overhang, 0.001c gap.

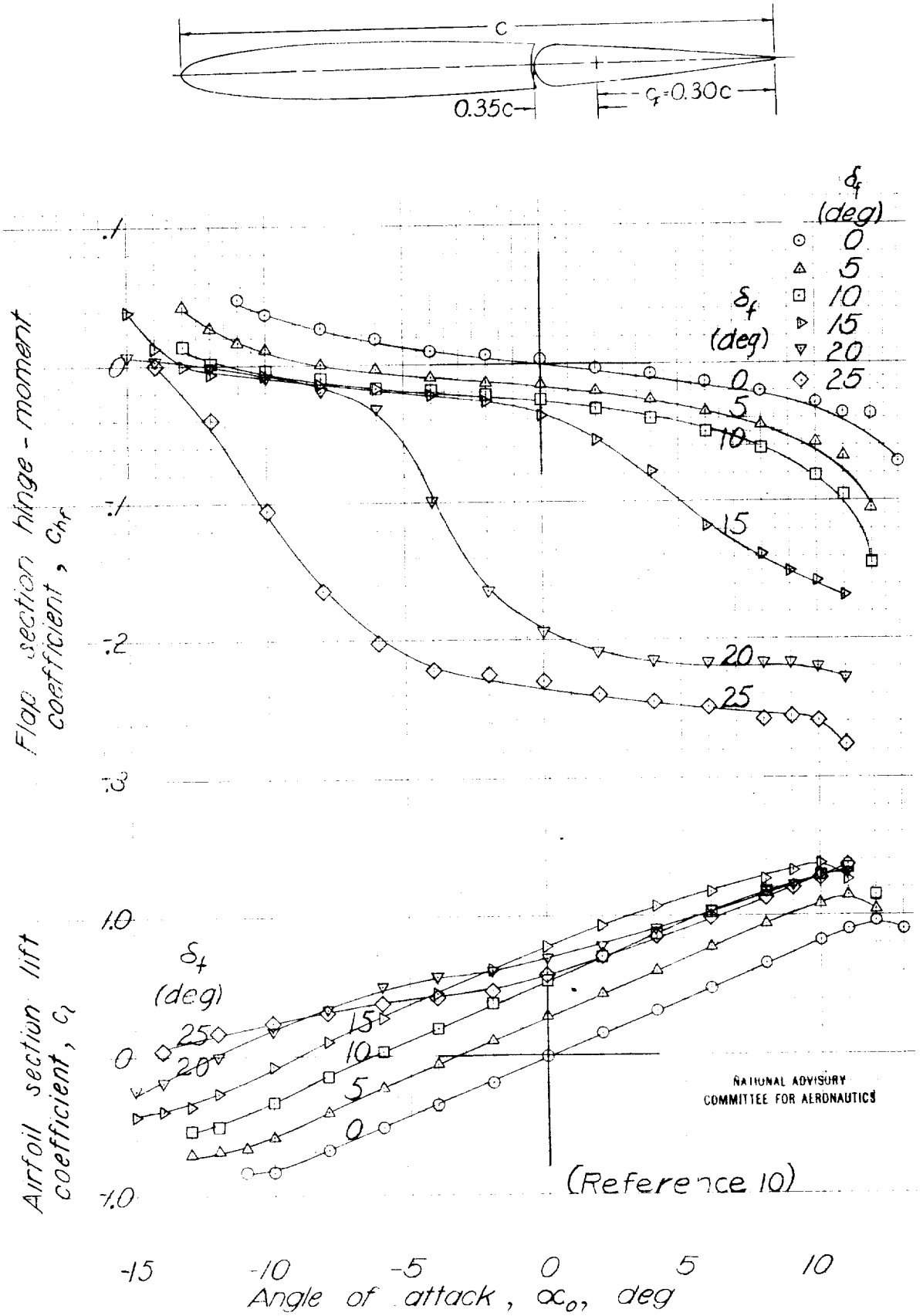

Figure 26.- NACA 0009 airfoil, 0.30c flap with 0.35c_f blunt-nose overhang, 0.005c gap.

L-663

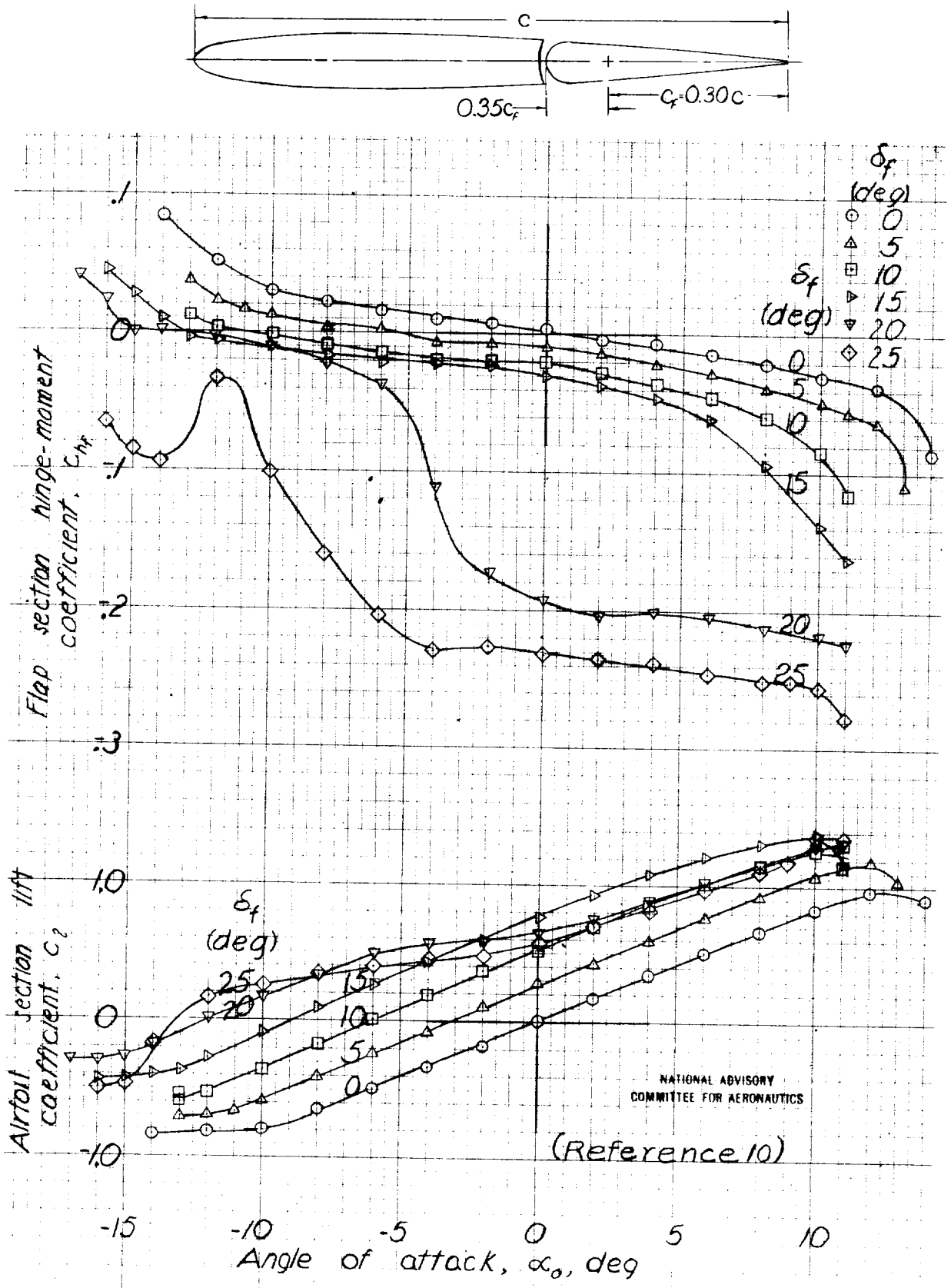

Figure 27.- NACA 0009 airfoil, 0.30c flap with 0.35 c_f blunt-nose overhang, 0.010c gap.

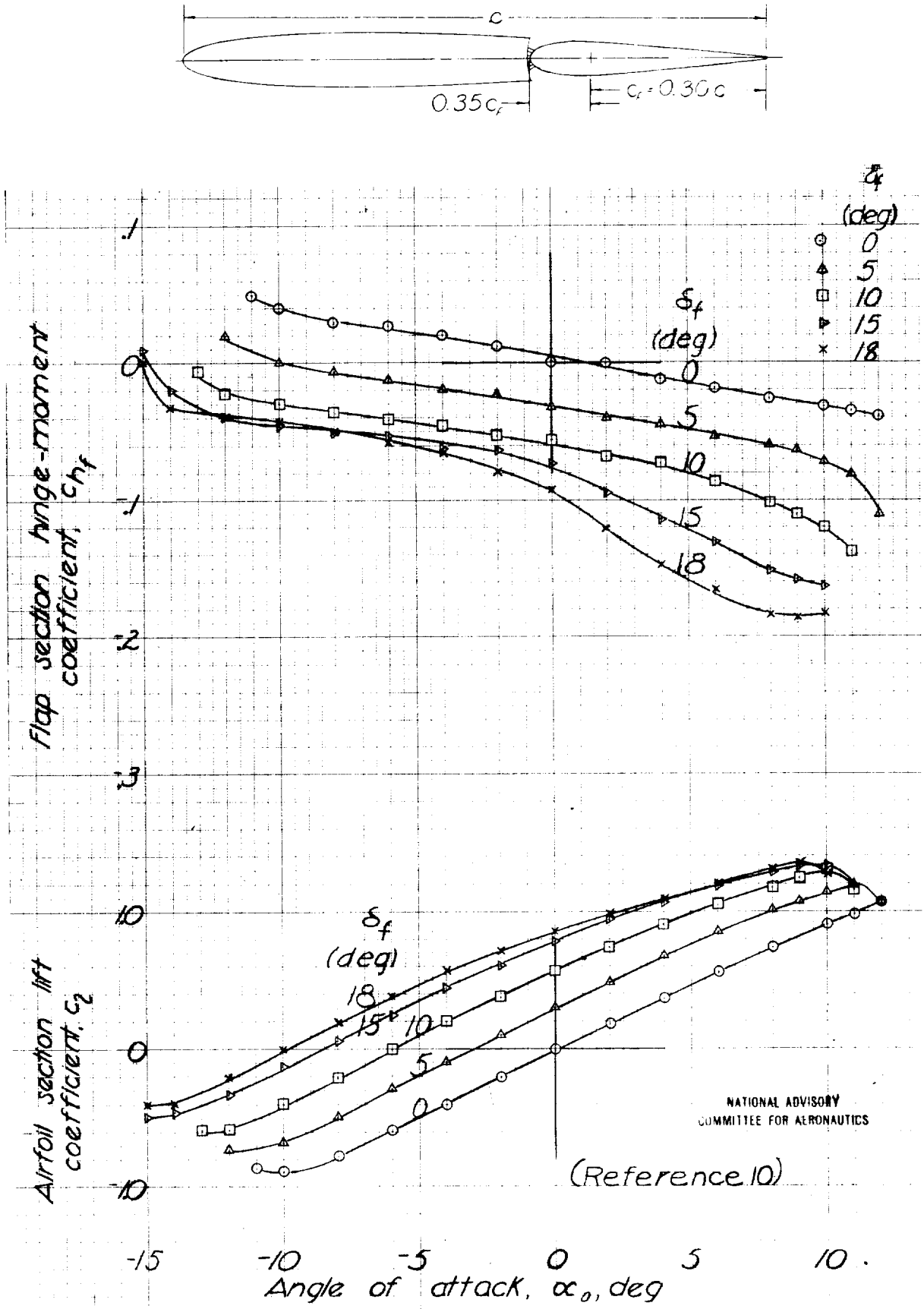

Figure 28.- NACA 0009 airfoil, 0.30c flap with $0.35c_f$ medium-nose overhang, sealed gap.

L-663

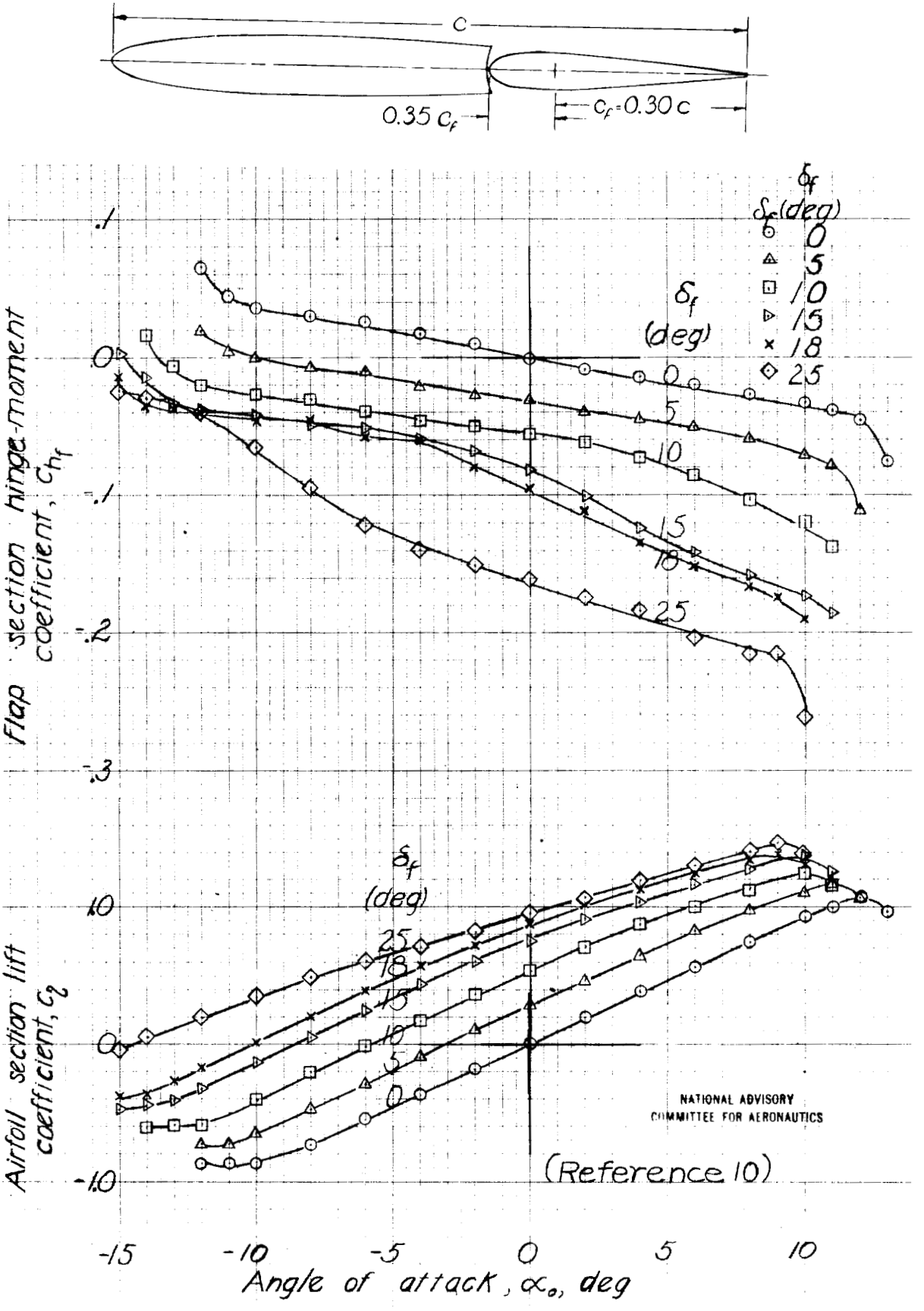

Figure 29.- NACA 0009 airfoil, 0.30c flap with 0.35c_f medium-nose overhang, 0.001c gap.

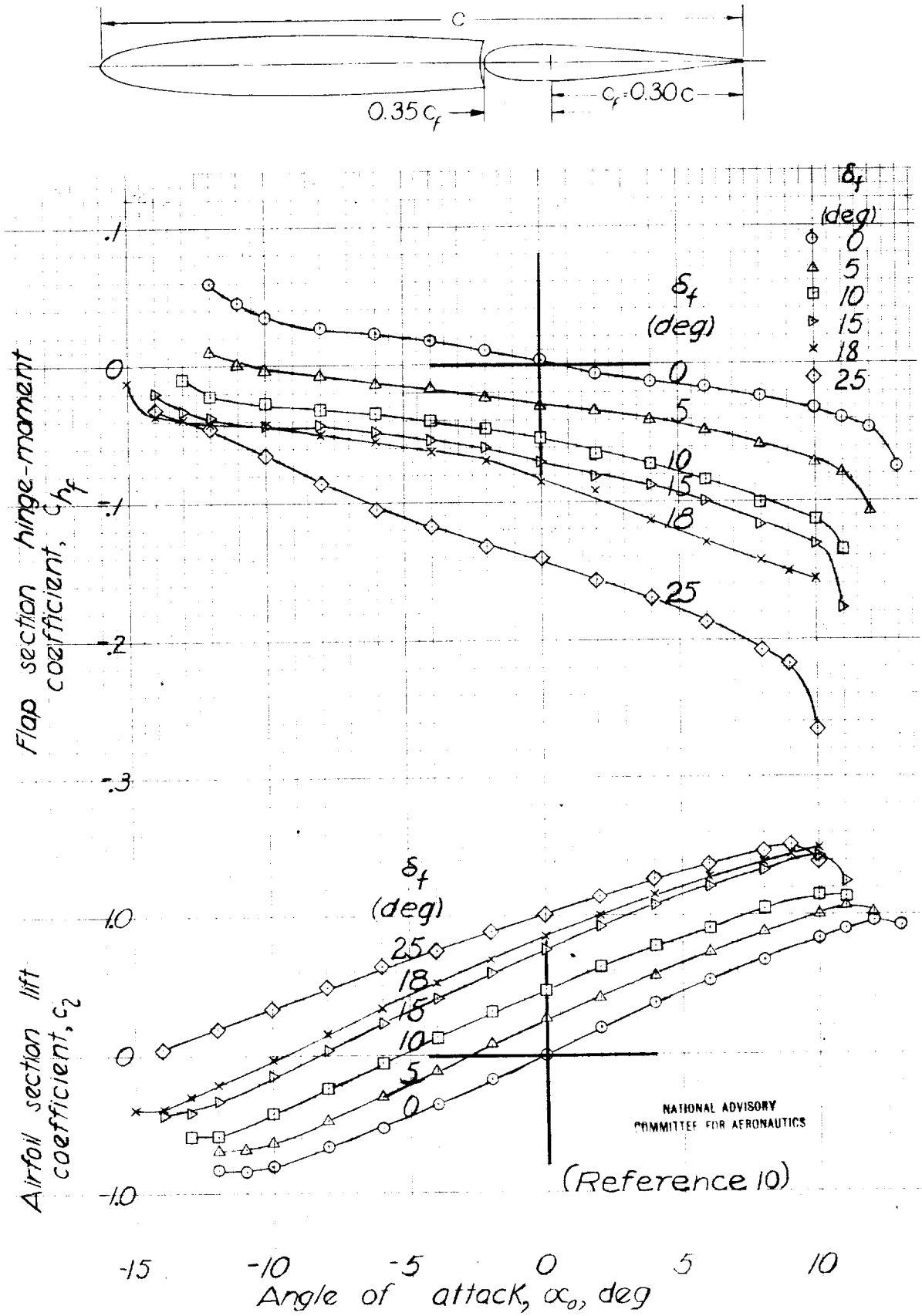

Figure 30.–NACA 0009 airfoil, 0.30c flap with 0.35c_f medium-nose overhang, 0.005c gap.

L-663

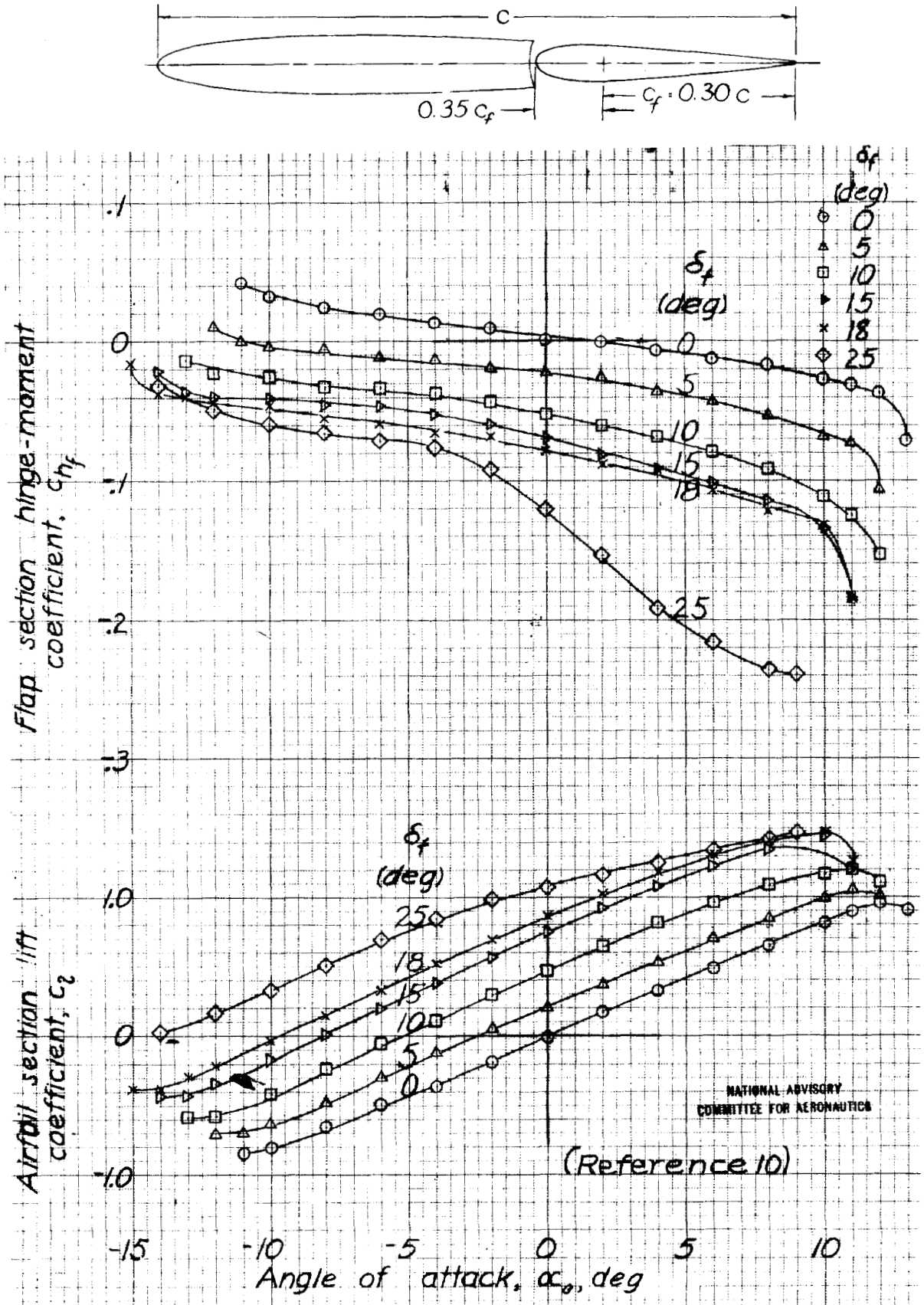

Figure 31.- NACA 0009 airfoil, 0.30c flap with 0.35c_f medium-nose overhang, 0.010c gap.

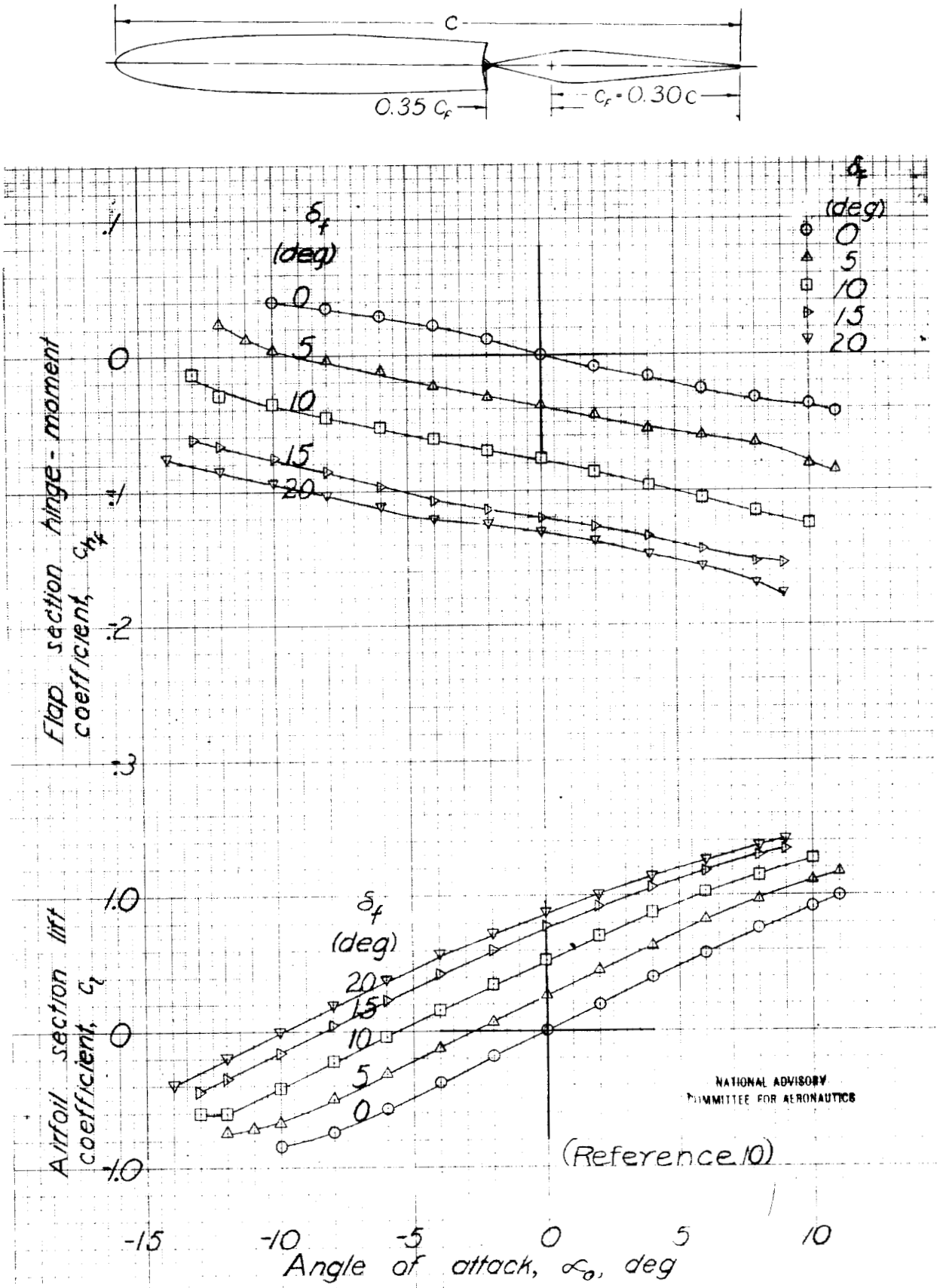

Figure 32.- NACA 0009 airfoil, 0.30c flap with 0.35c_f sharp-nose overhang, sealed gap.

L-663

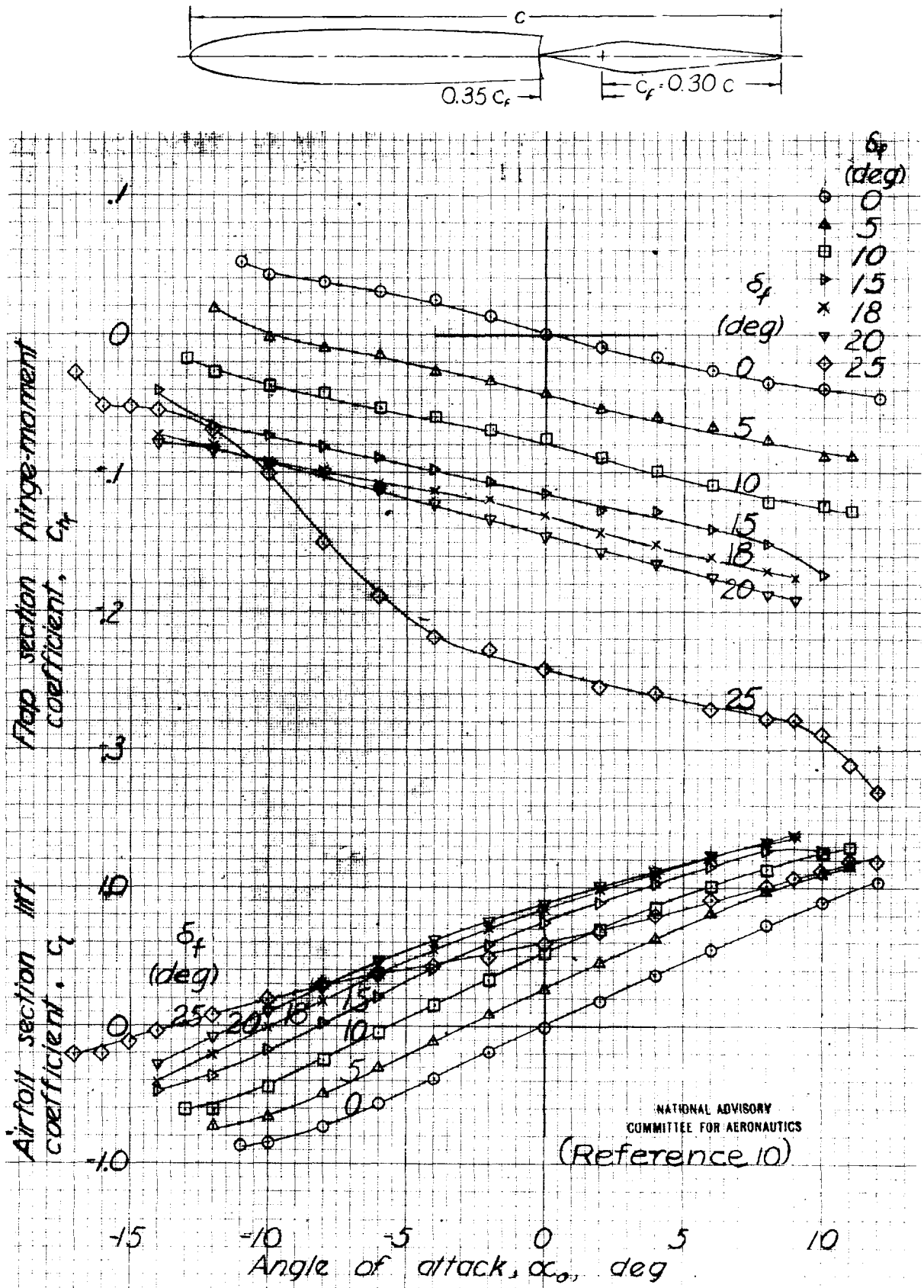

Figure 33.- NACA 0009 airfoil, 0.30 c flap with 0.35c_f sharp-nose overhang, 0.001c gap.

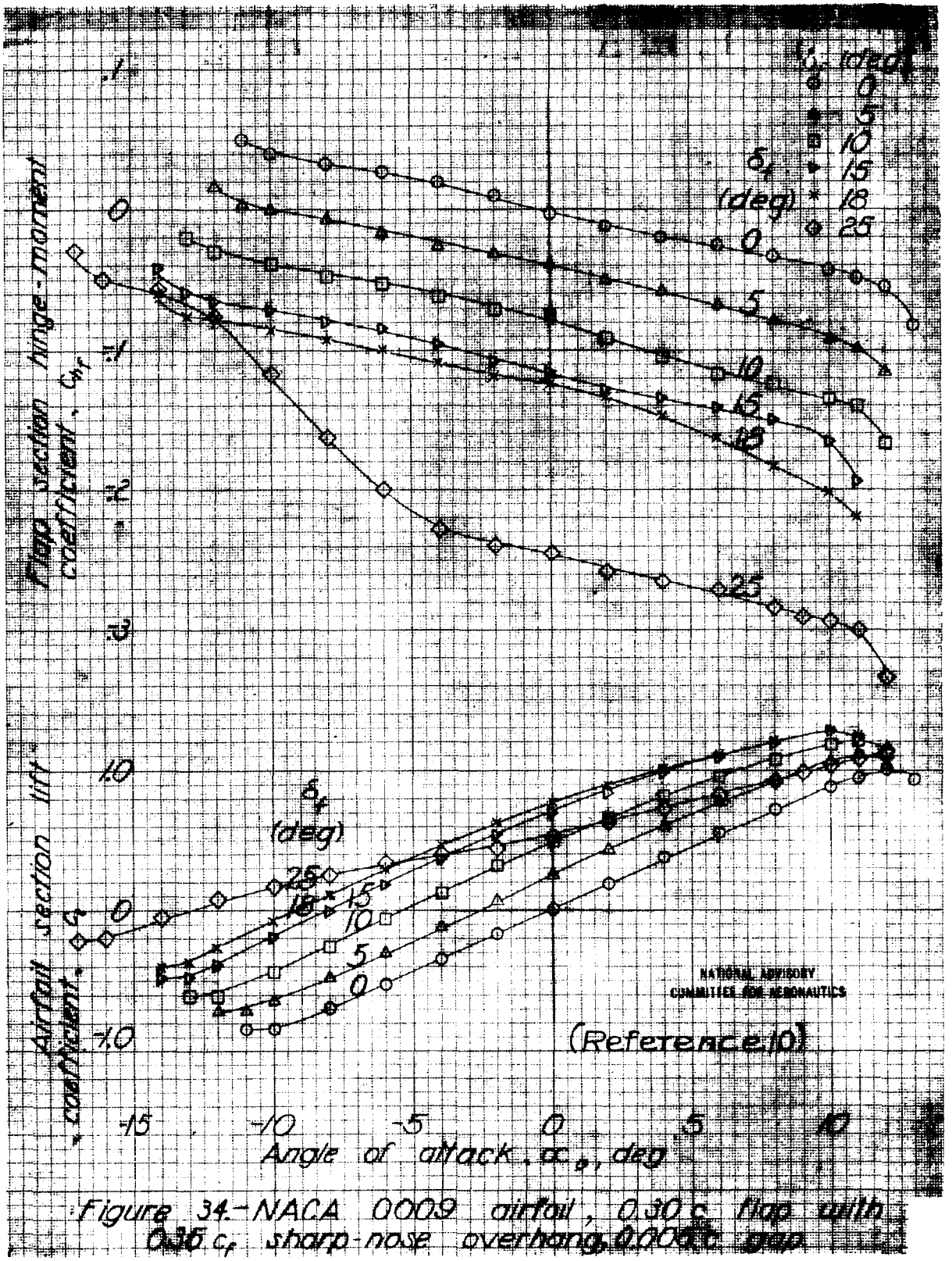

Figure 34.- NACA 0009 airfoil, 0.30c flap with 0.35 c_f sharp-nose overhang, 0.002c gap.

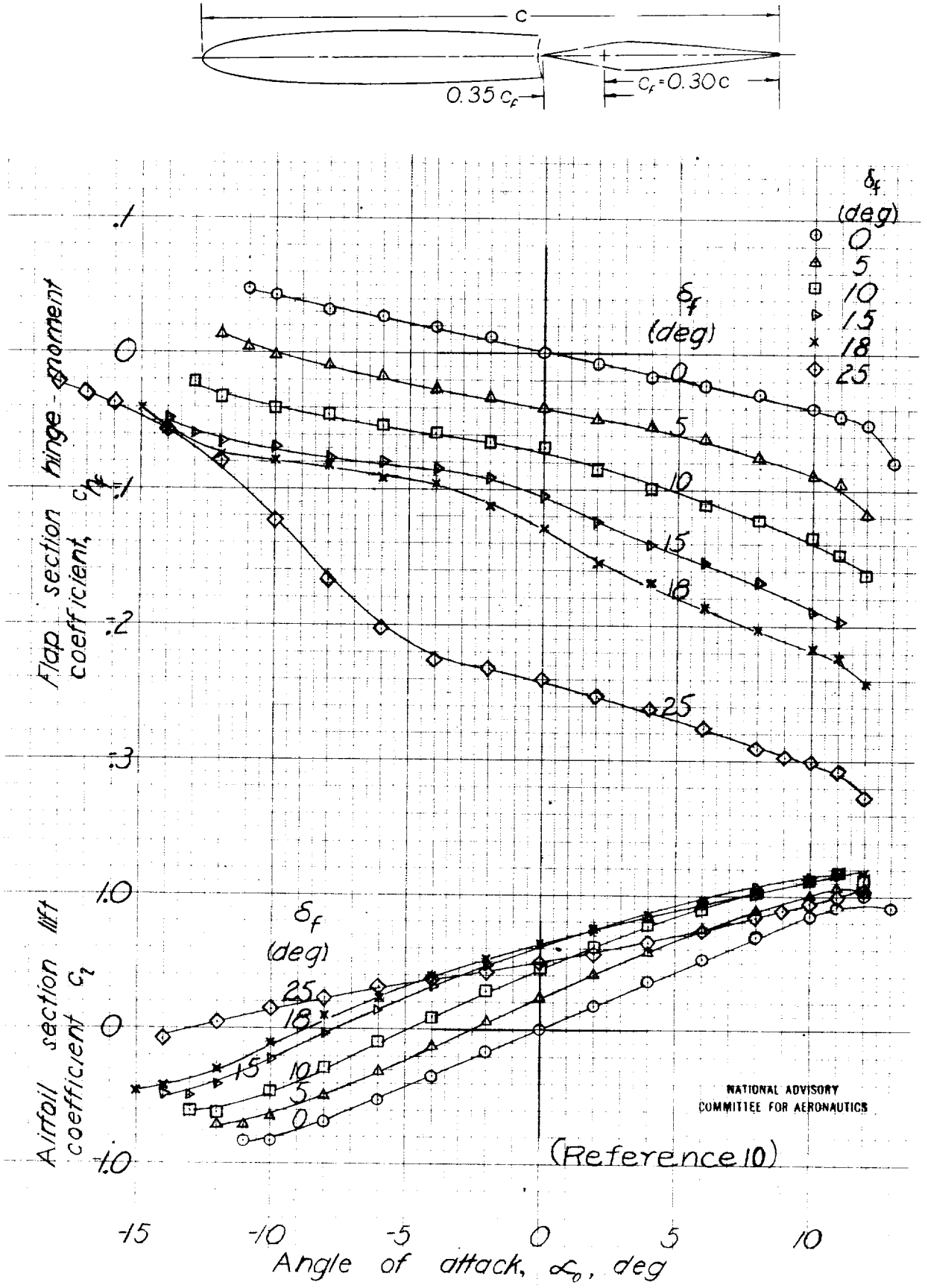

Figure 35.-NACA 0009 airfoil, 0.30c flap with 0.35c_f sharp-nose overhang, 0.010c gap.

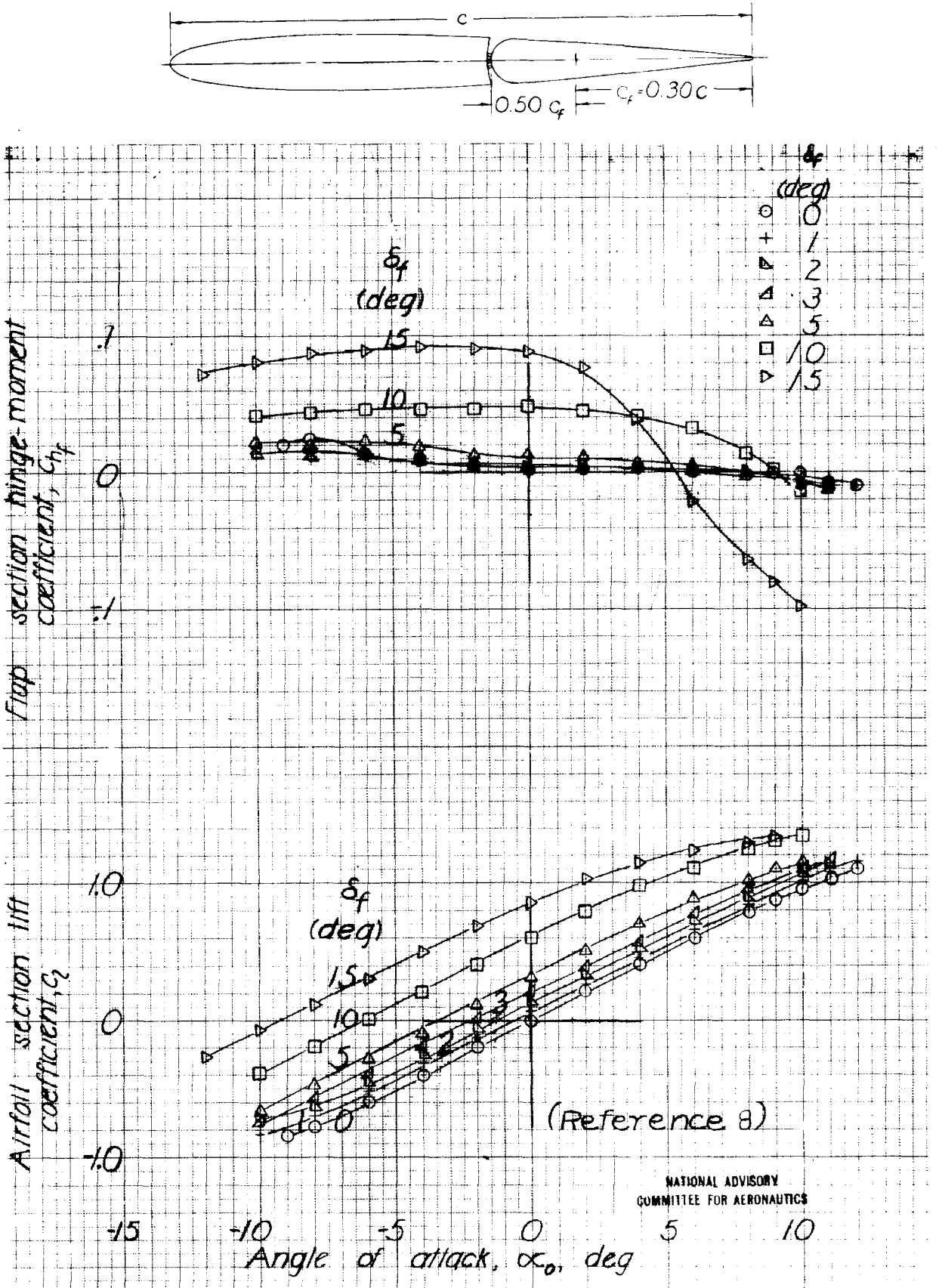

Figure 36.- NACA 0009 airfoil, 0.30c flap with $0.50c_f$ blunt-nose overhang, sealed gap.

L-663

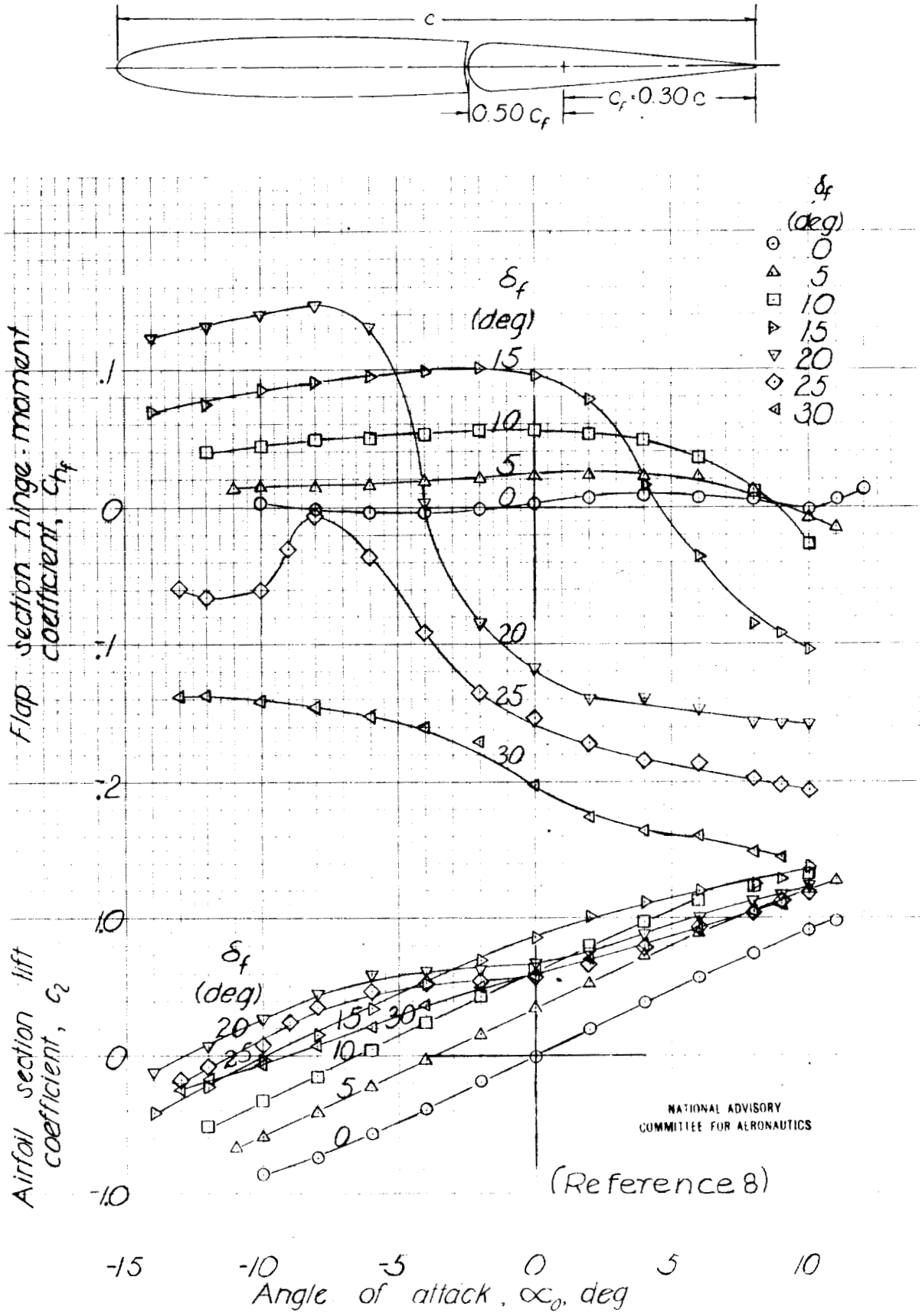

Figure 37.- NACA 0009 airfoil, 0.30c flap with 0.50c_f blunt-nose overhang, 0.0015c gap.

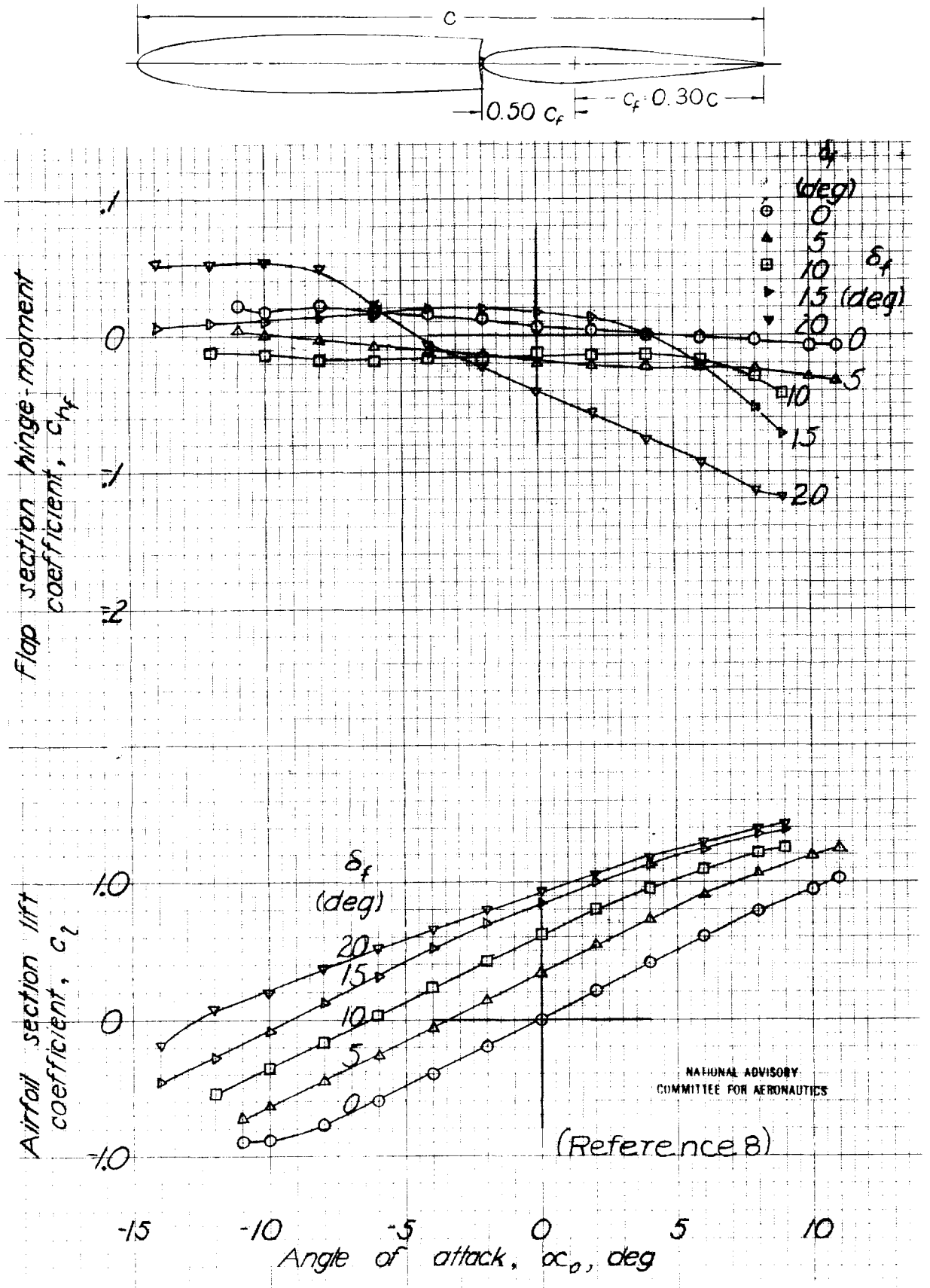

Figure 38.- NACA 0009 airfoil, 0.30c flap with 0.50c_f medium-nose overhang, sealed gap.

L-663

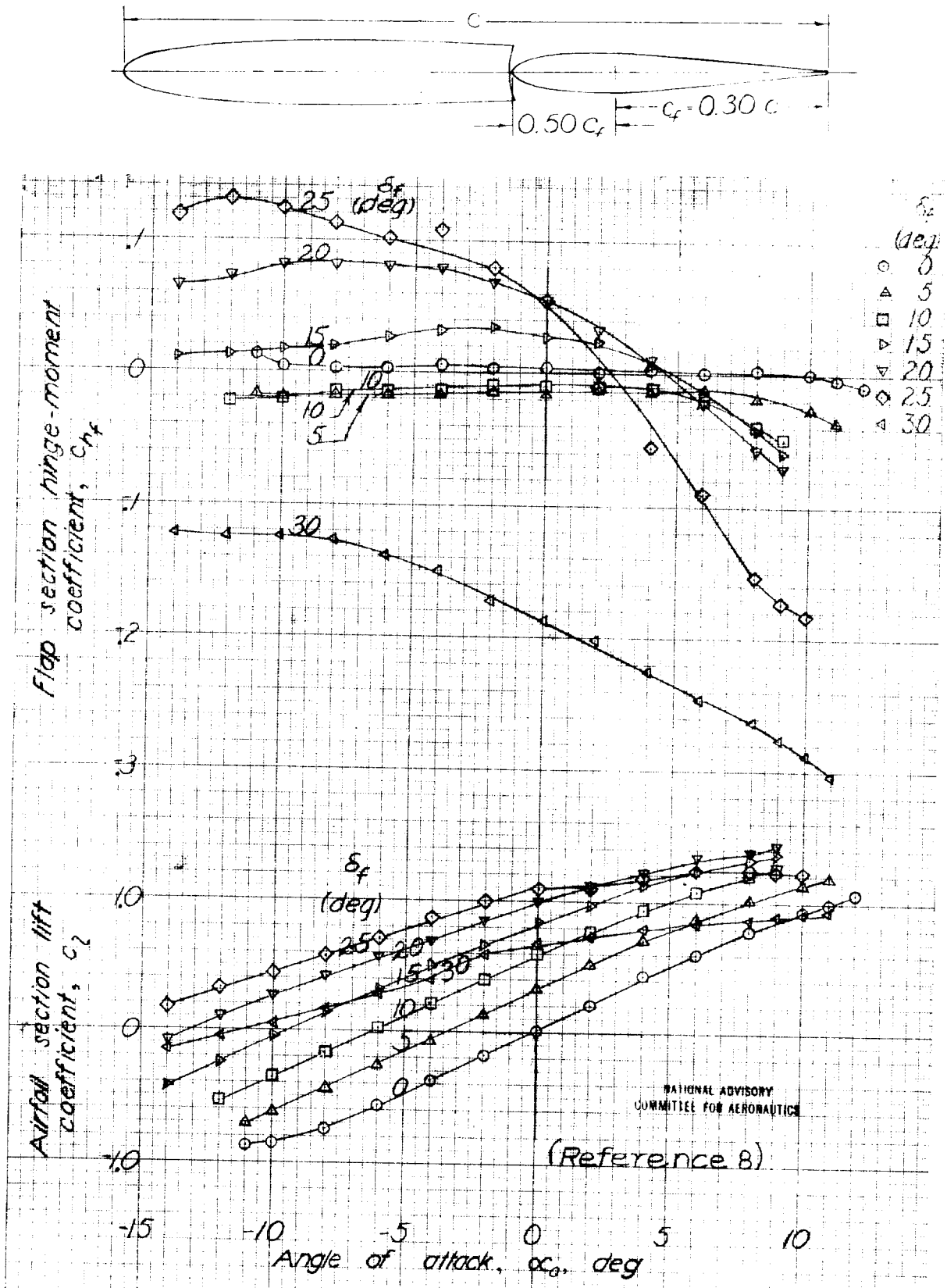

Figure 39.-NACA 0009 airfoil, 0.30c flap with 0.50 c_f medium-nose overhang, 0.0015c gap.

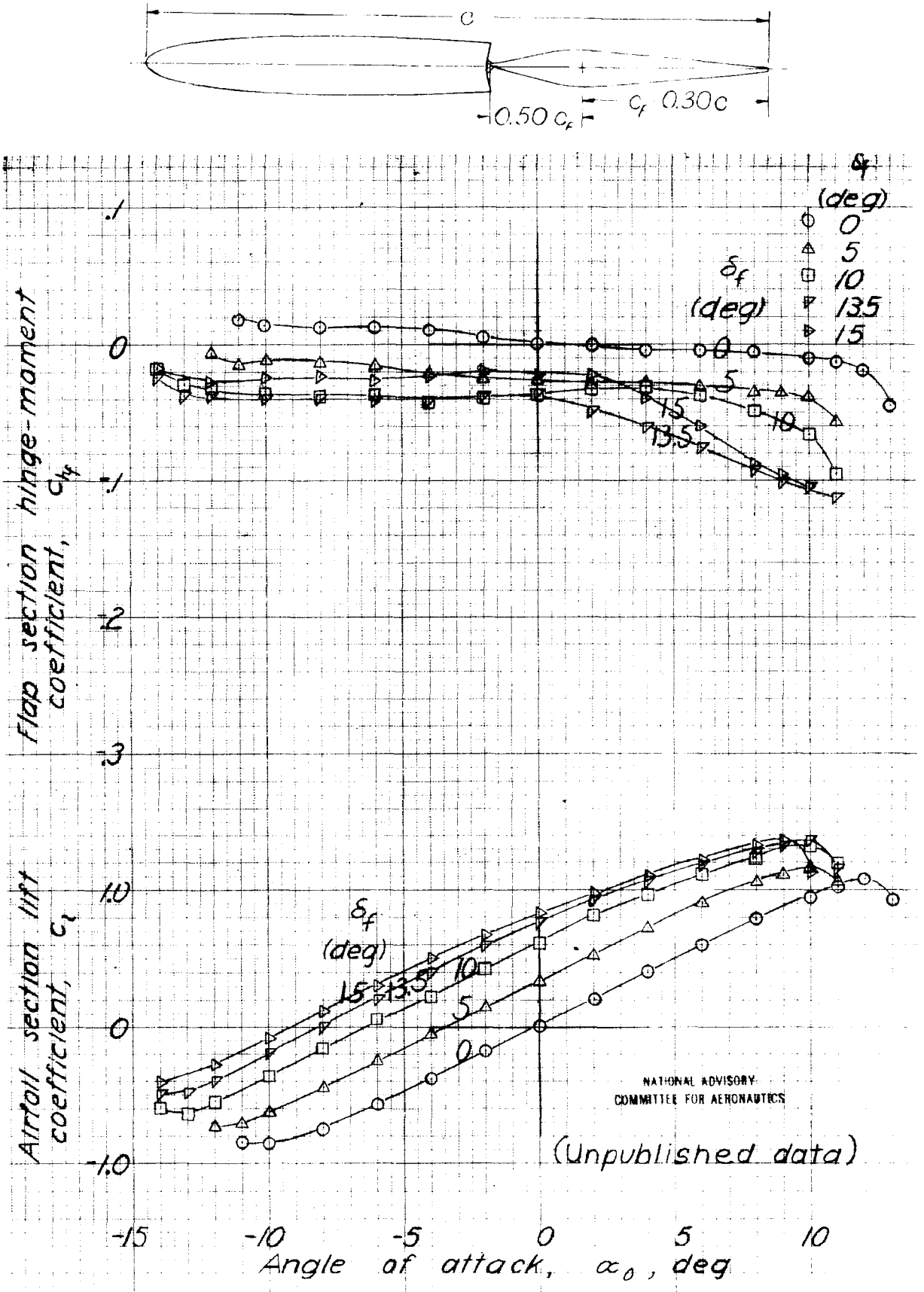

Figure 40.-NACA 0009 airfoil, 0.30c flap with 0.50c_f medium-nose overhang, modification 1, sealed gap.

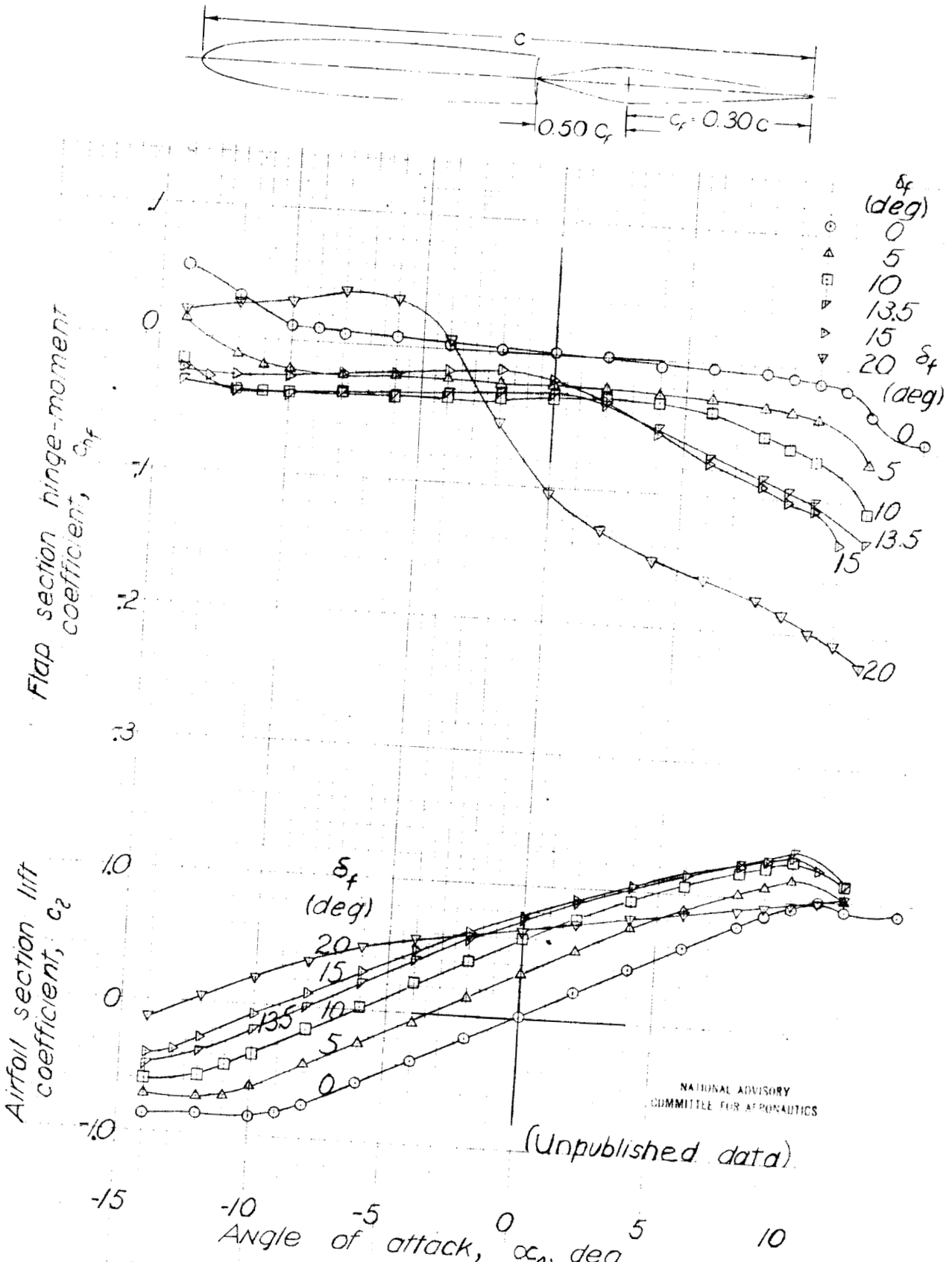

Figure 41.- NACA 0009 airfoil, 0.30c flap with 0.50c_f medium-nose overhang, modification 1, 0.0015c gap.

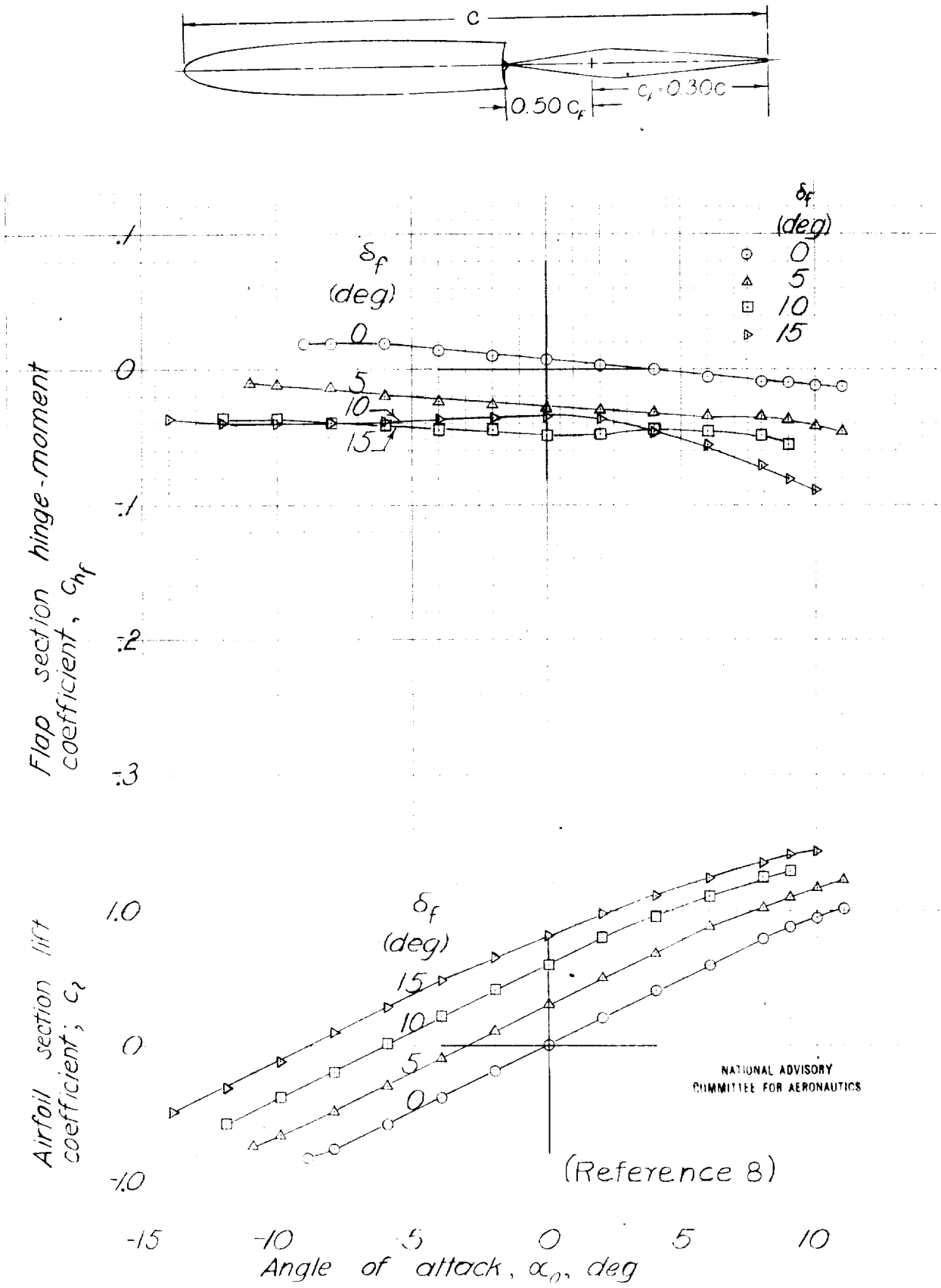

Figure 42.- NACA 0009 airfoil, 0.30 c flap with 0.50 c_f sharp-nose overhang, sealed gap.

L-663

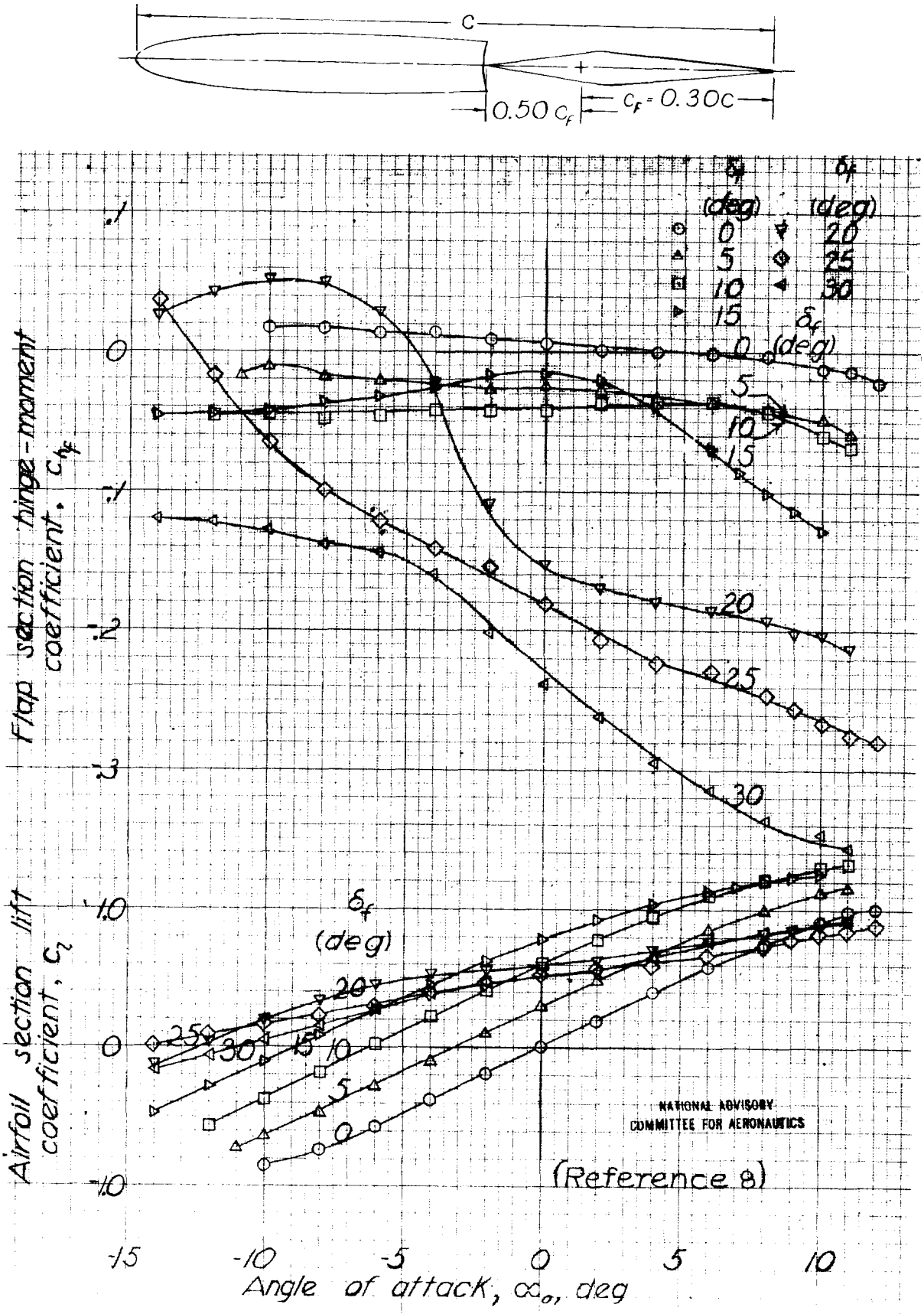

Figure 43.- NACA 0009 airfoil, 0.30c flap with 0.50 c_f sharp-nose overhang, 0.0015c gap.

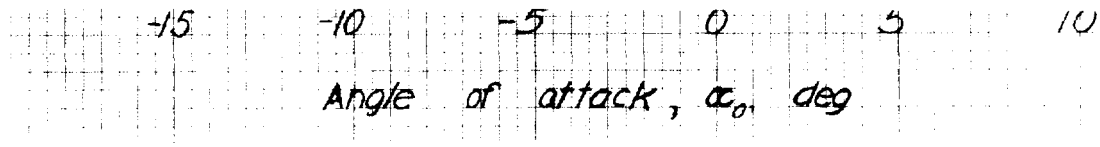

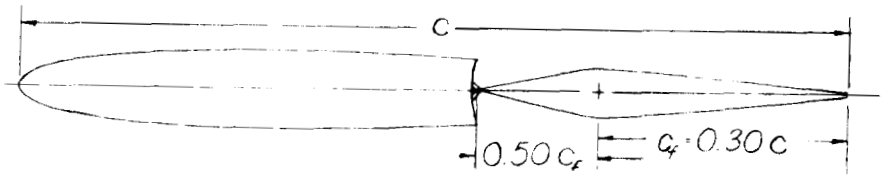
c
0.50 c_f
c_f = 0.30 c

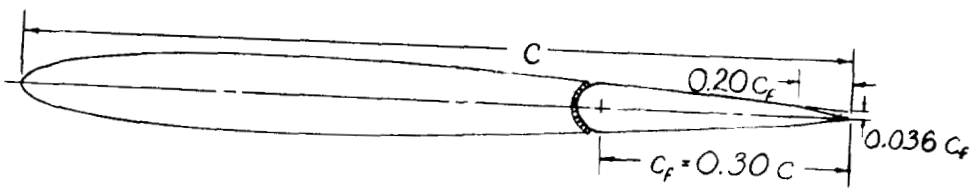
c
0.20 c_f
0.036 c_f
c_f = 0.30 c

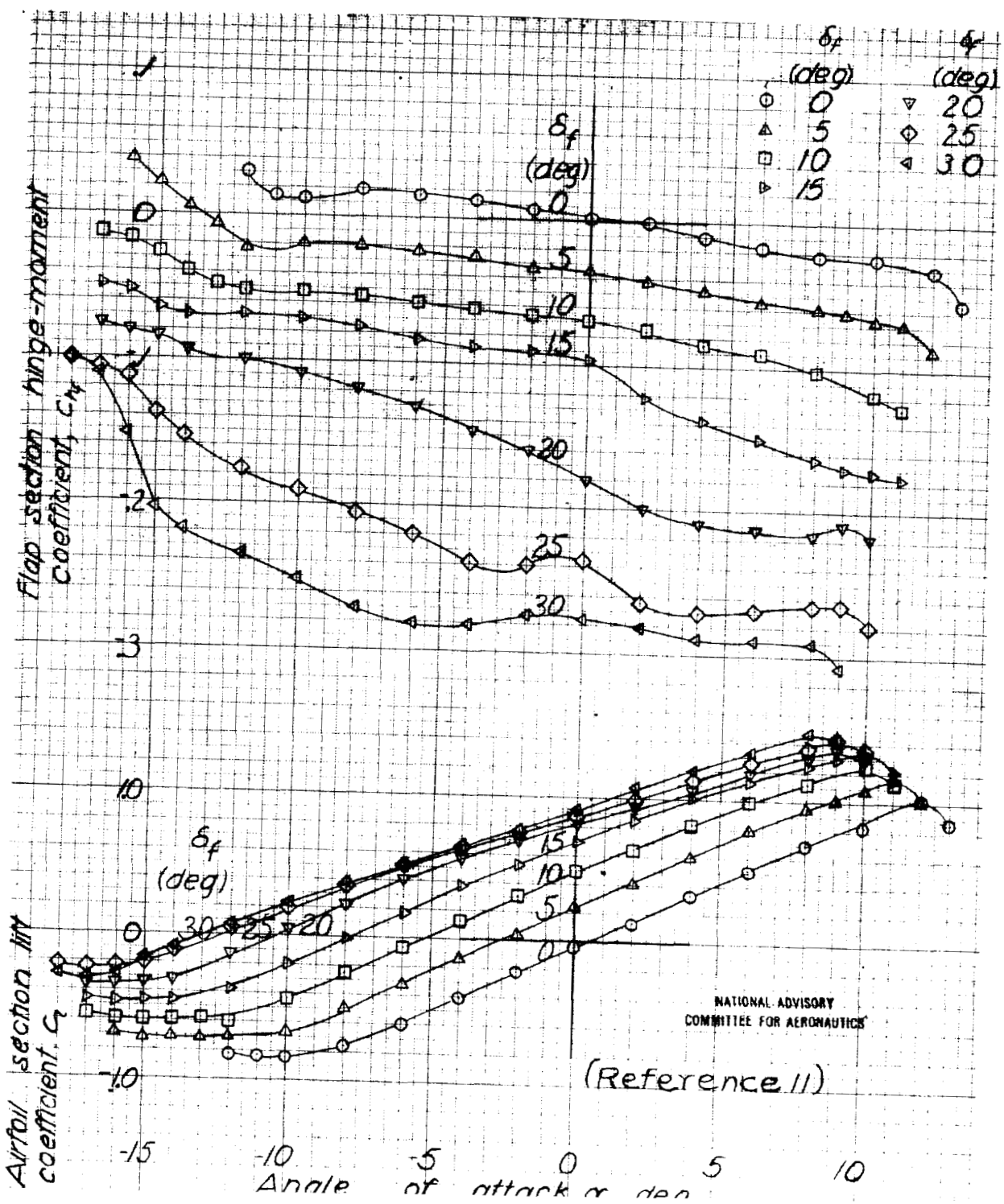
δ_f (deg)
0
5
10
15
20
25
30
Flap section hinge-moment coefficient, c_{h_f}
Airfoil section lift coefficient, c_l
-.2
-.3
1.0
0
-1.0
-15
-10
-5
0
5
10
Angle of attack, α, deg
NATIONAL ADVISORY COMMITTEE FOR AERONAUTICS
(Reference 11)

L-663

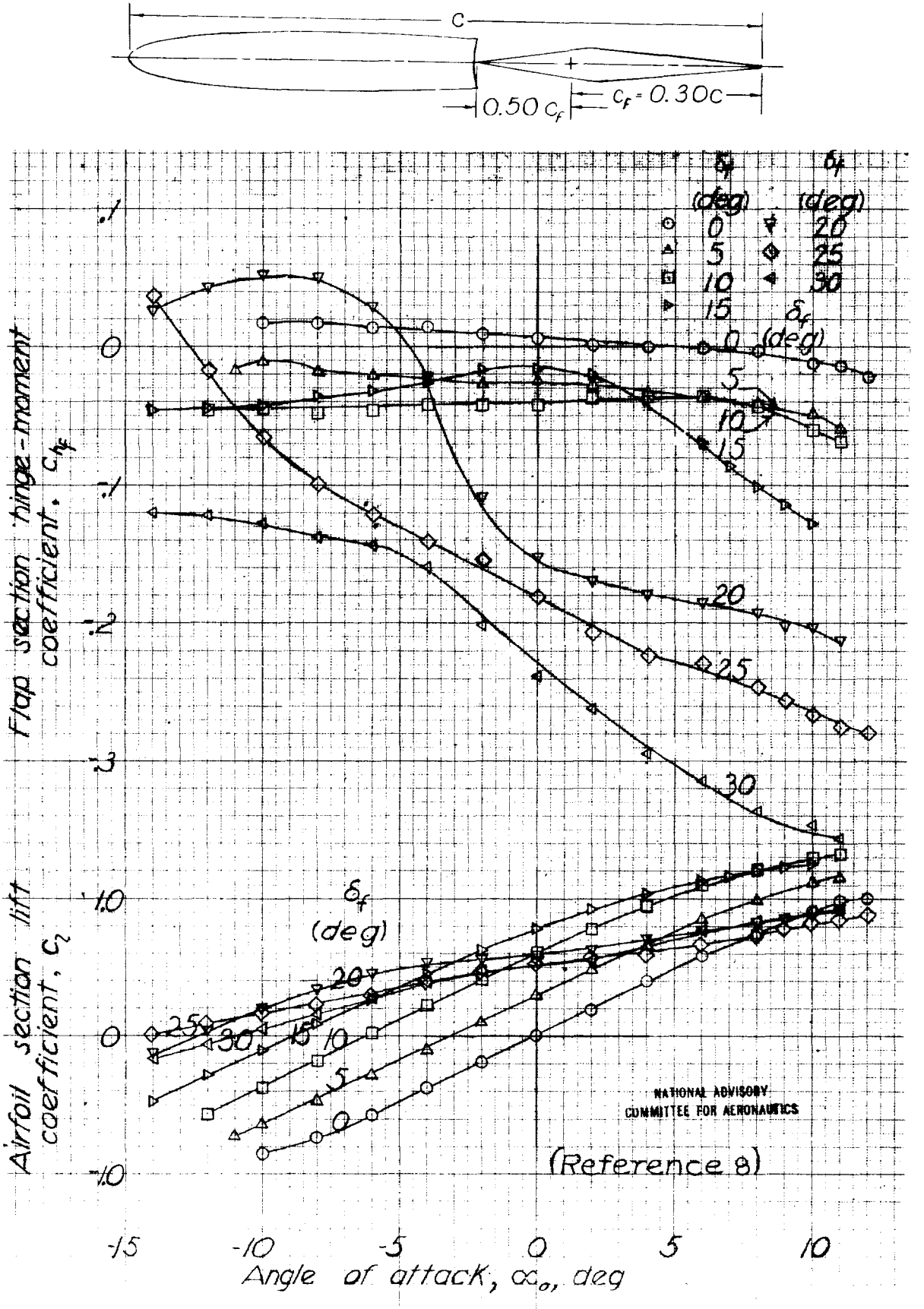

Figure 43.- NACA 0009 airfoil, 0.30c flap with 0.50 c_f sharp-nose overhang, 0.0015c gap.

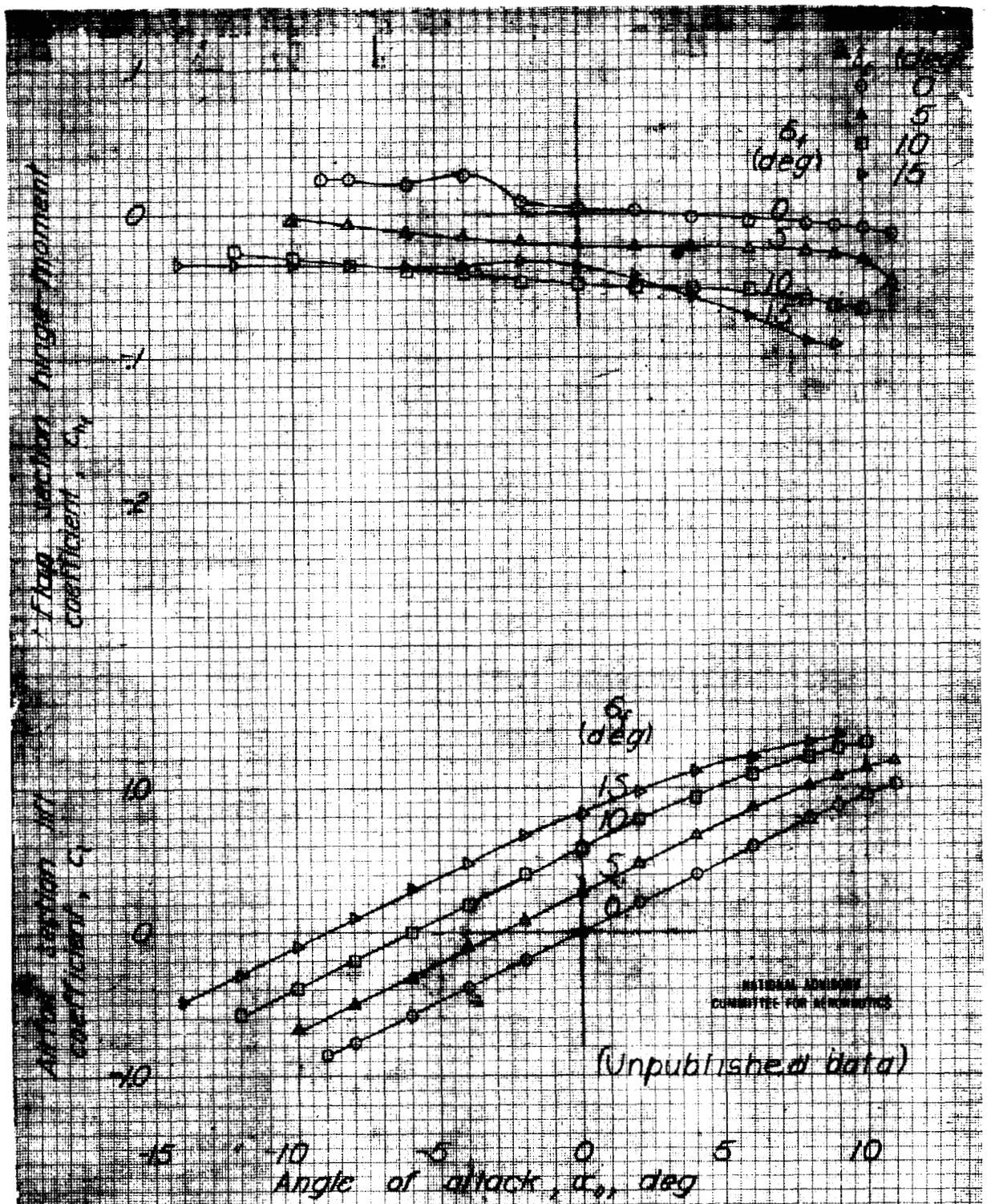

Figure 16.- NACA 0009 airfoil, 0.30 c flap with 0.50 c_f [illegible] overhang, modification 1, sealed gap.

L-663

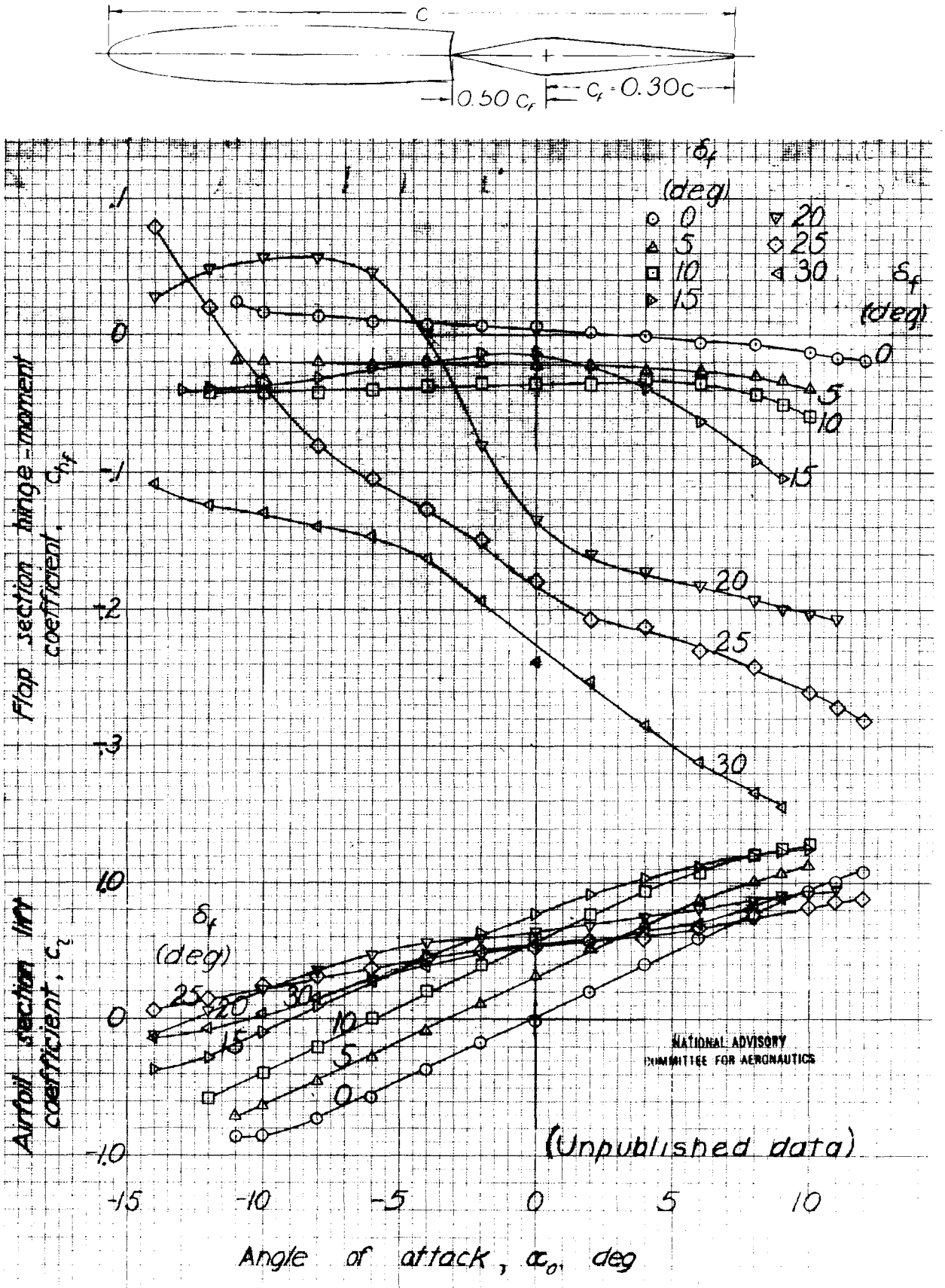

Figure 45.-NACA 0009 airfoil, 0.30c flap with 0.50c_f sharp-nose overhang, modification 1, 0.0015 gap.

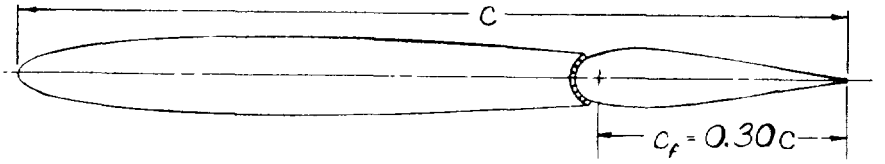

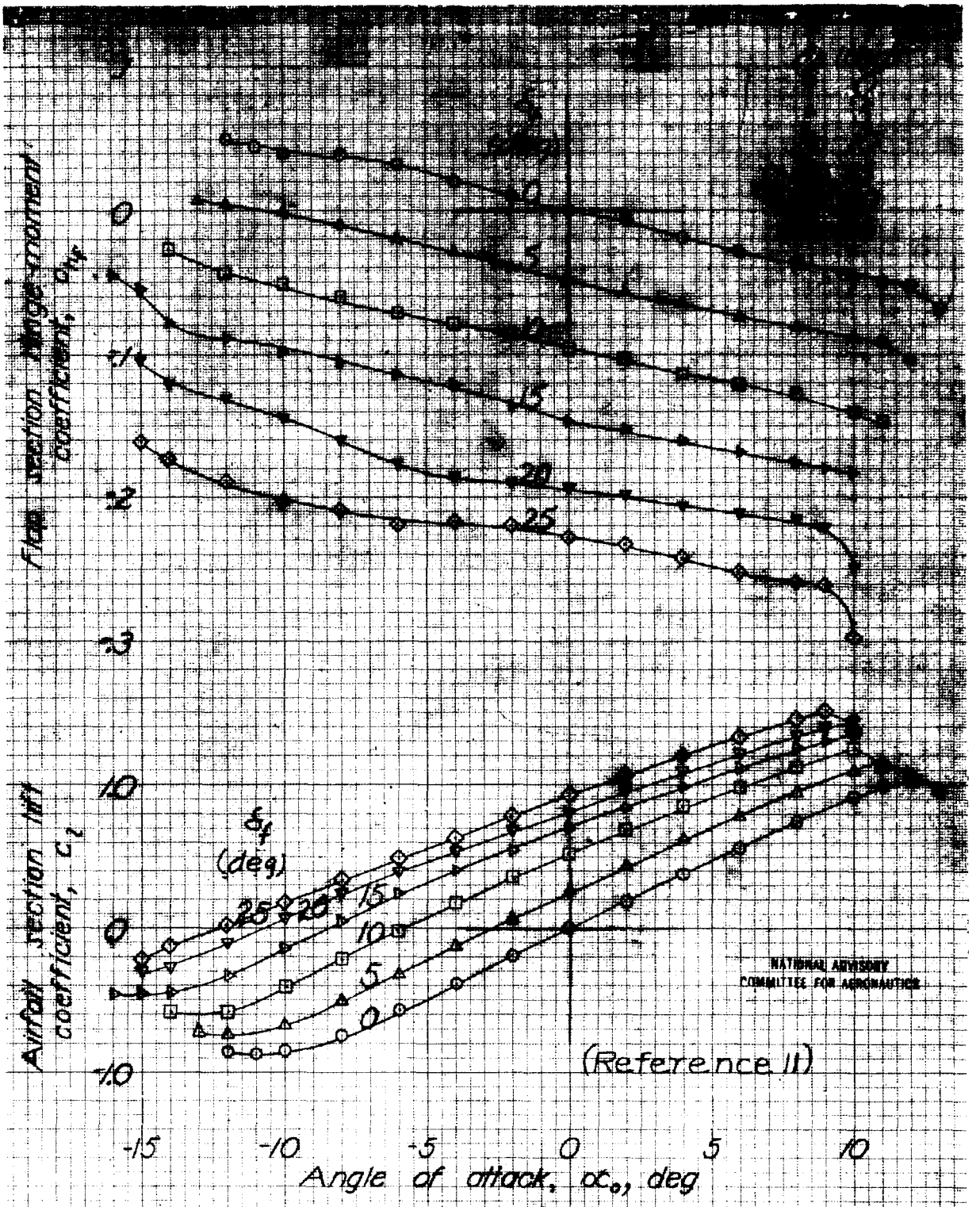

Figure 46.- NACA 0009 airfoil, 0.30c flap with bulged profile, sealed gap.

L-663

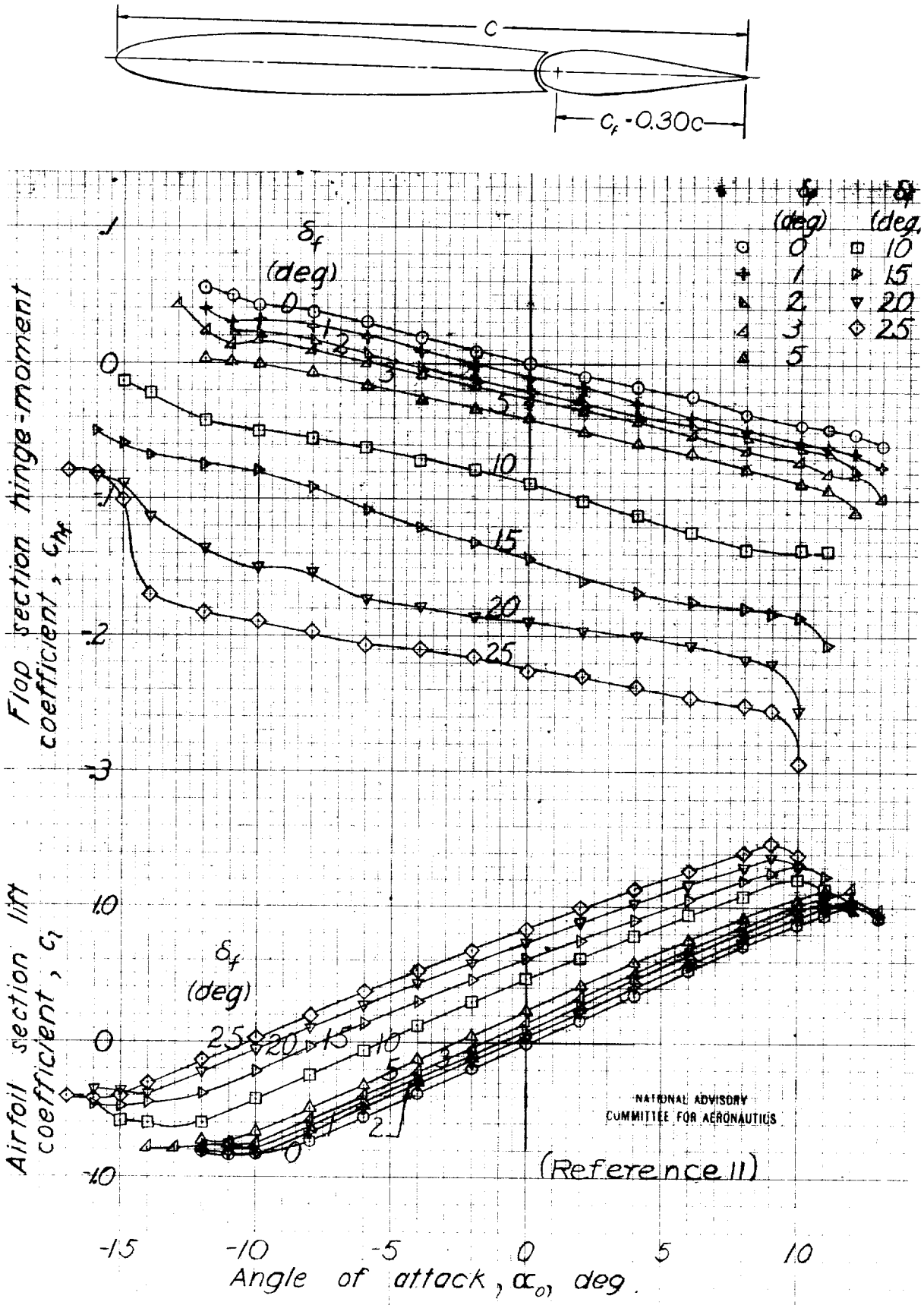

Figure 47.- NACA 0009 airfoil, 0.30c flap with bulged profile, 0.005c gap.

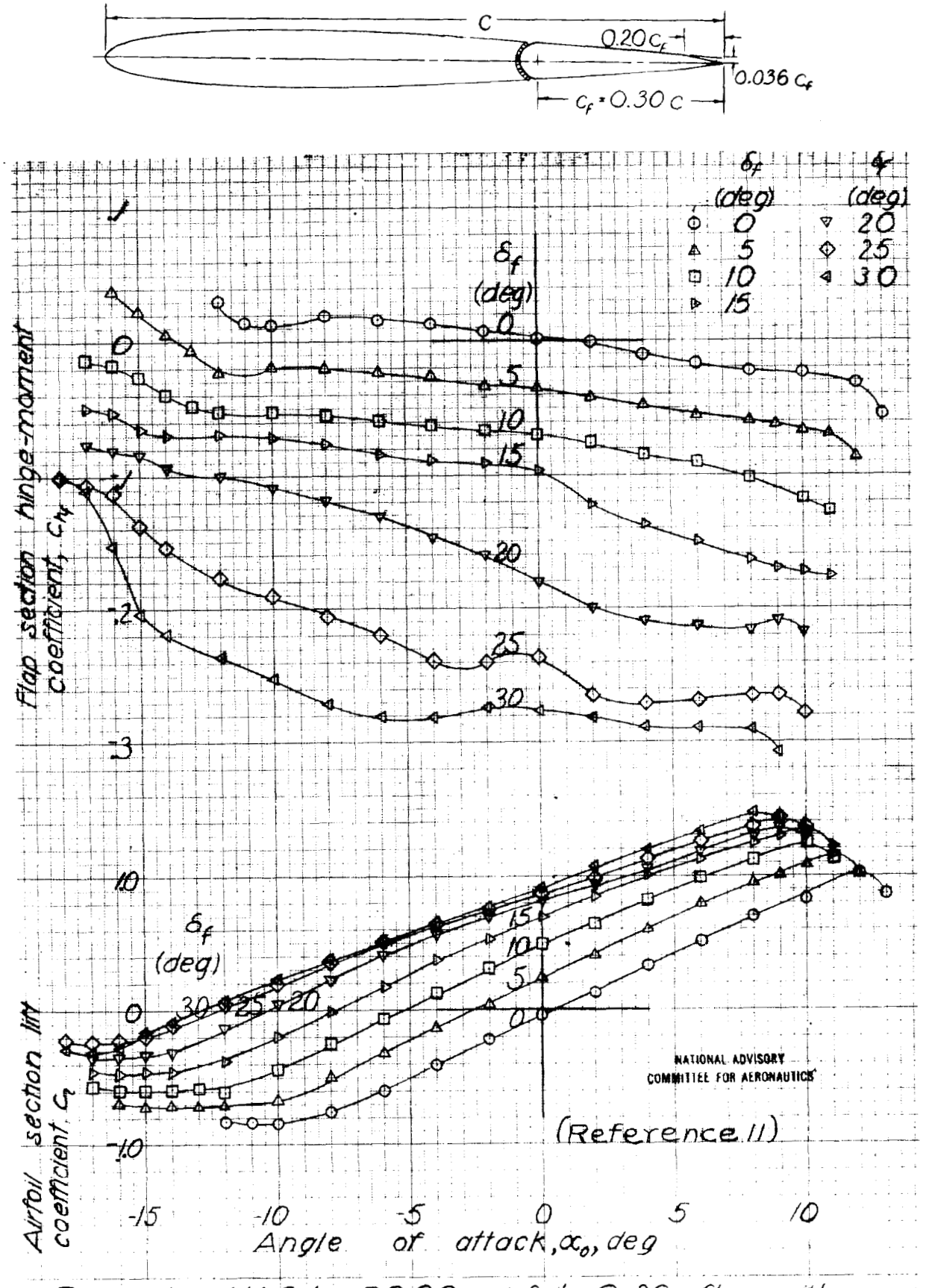

Figure 48.- NACA 0009 airfoil, 0.30c flap with 0.20c_f beveled trailing edge, sealed gap.

L-663

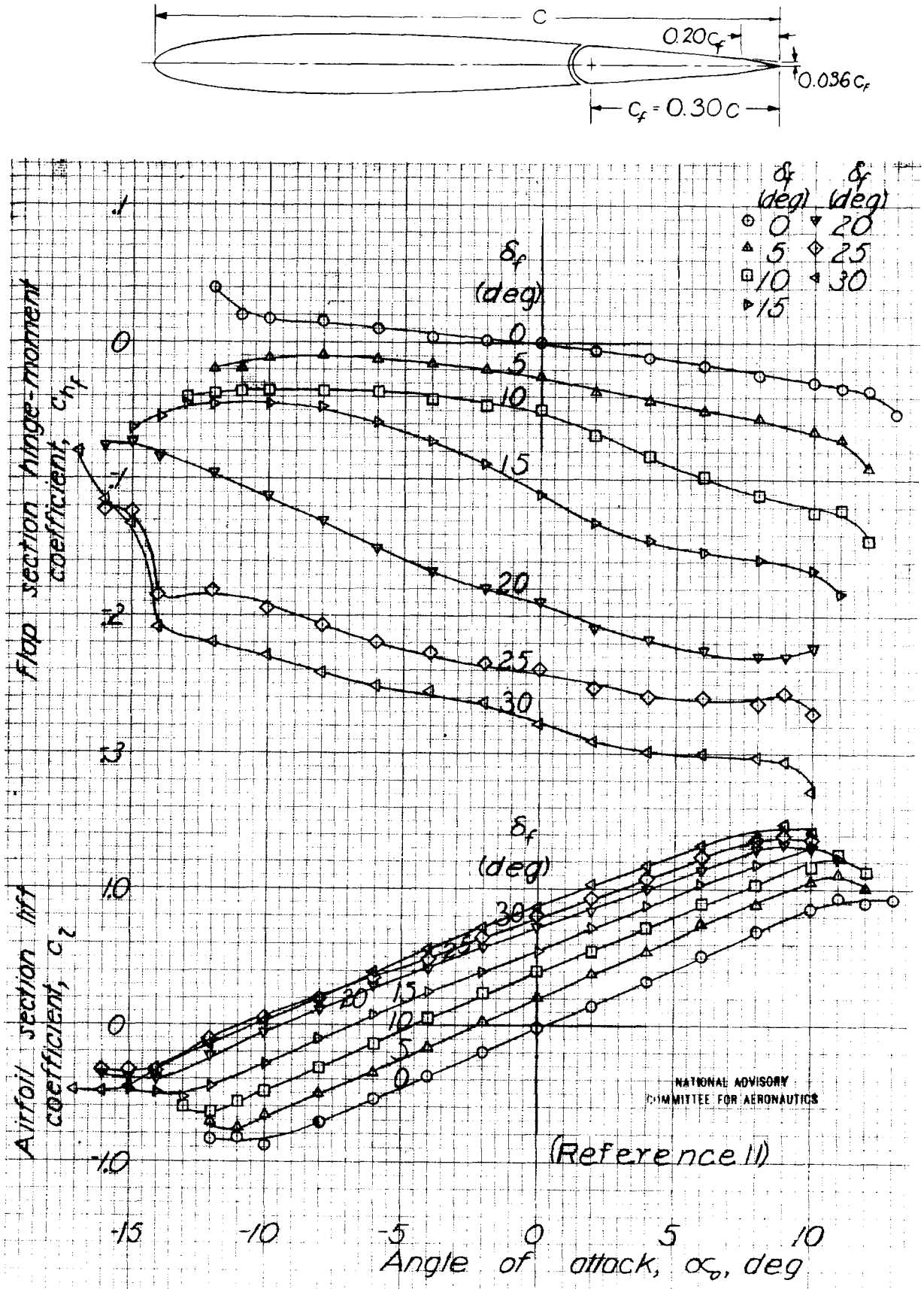

Figure 49.-NACA 0009 airfoil, 0.30c flap with 0.20c_f beveled trailing edge, 0.005c gap.

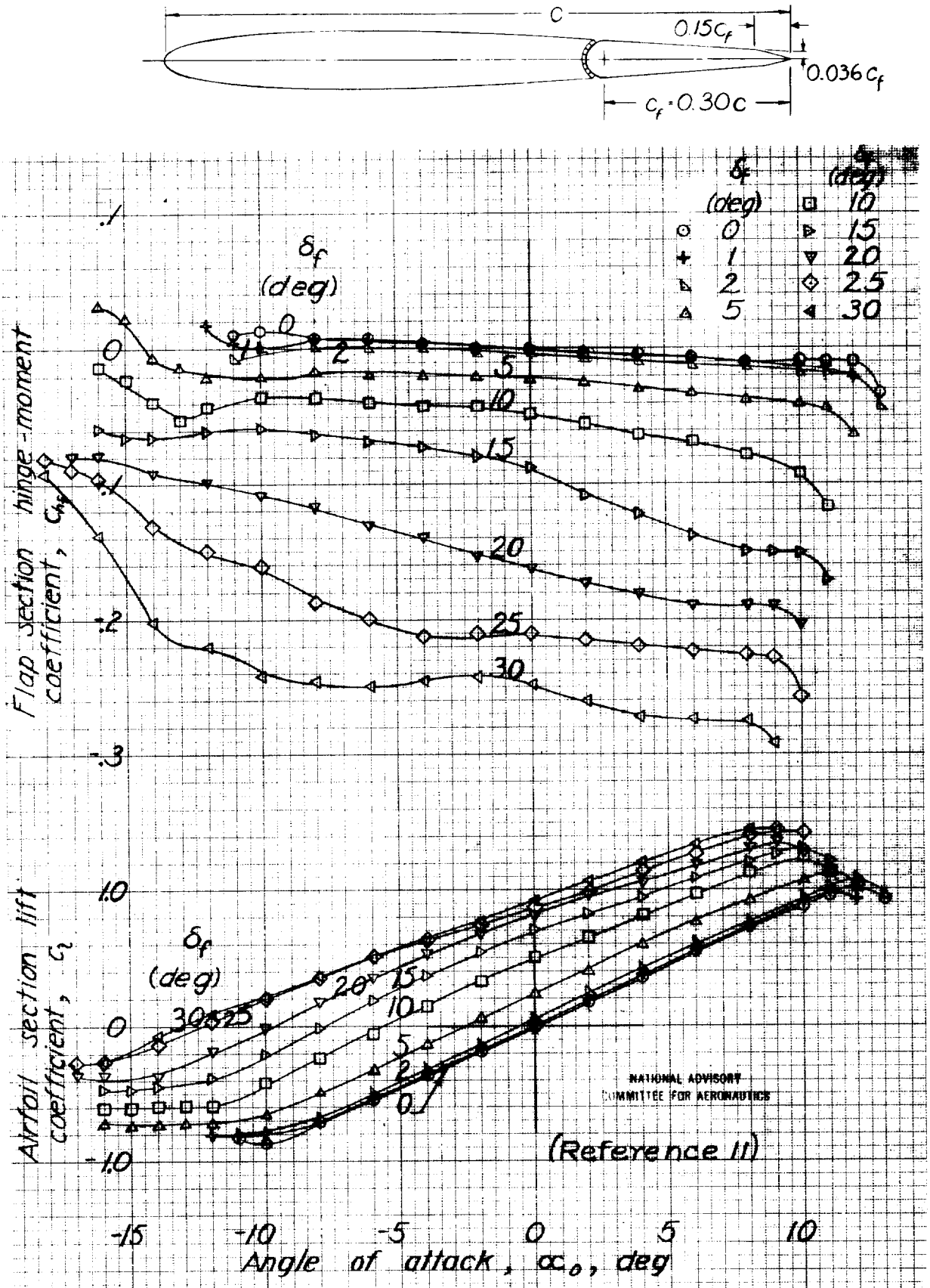

Figure 50.- NACA 0009 airfoil, 0.30c flap with 0.15 c_f beveled trailing edge, sealed gap.

L-663

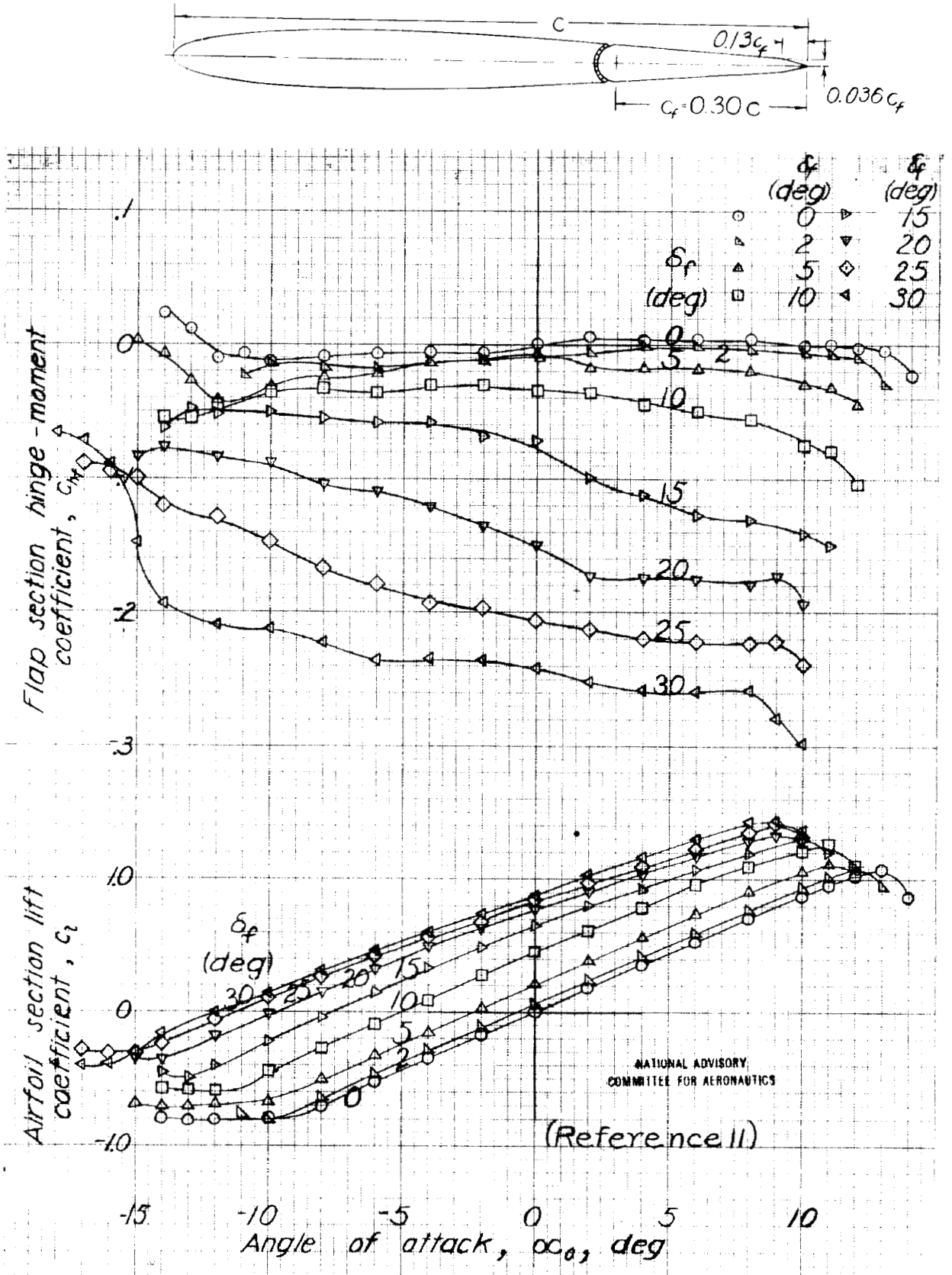

Figure 51.- NACA 0009 airfoil, 0.30c flap with 0.13 c_f beveled trailing edge, sealed gap.

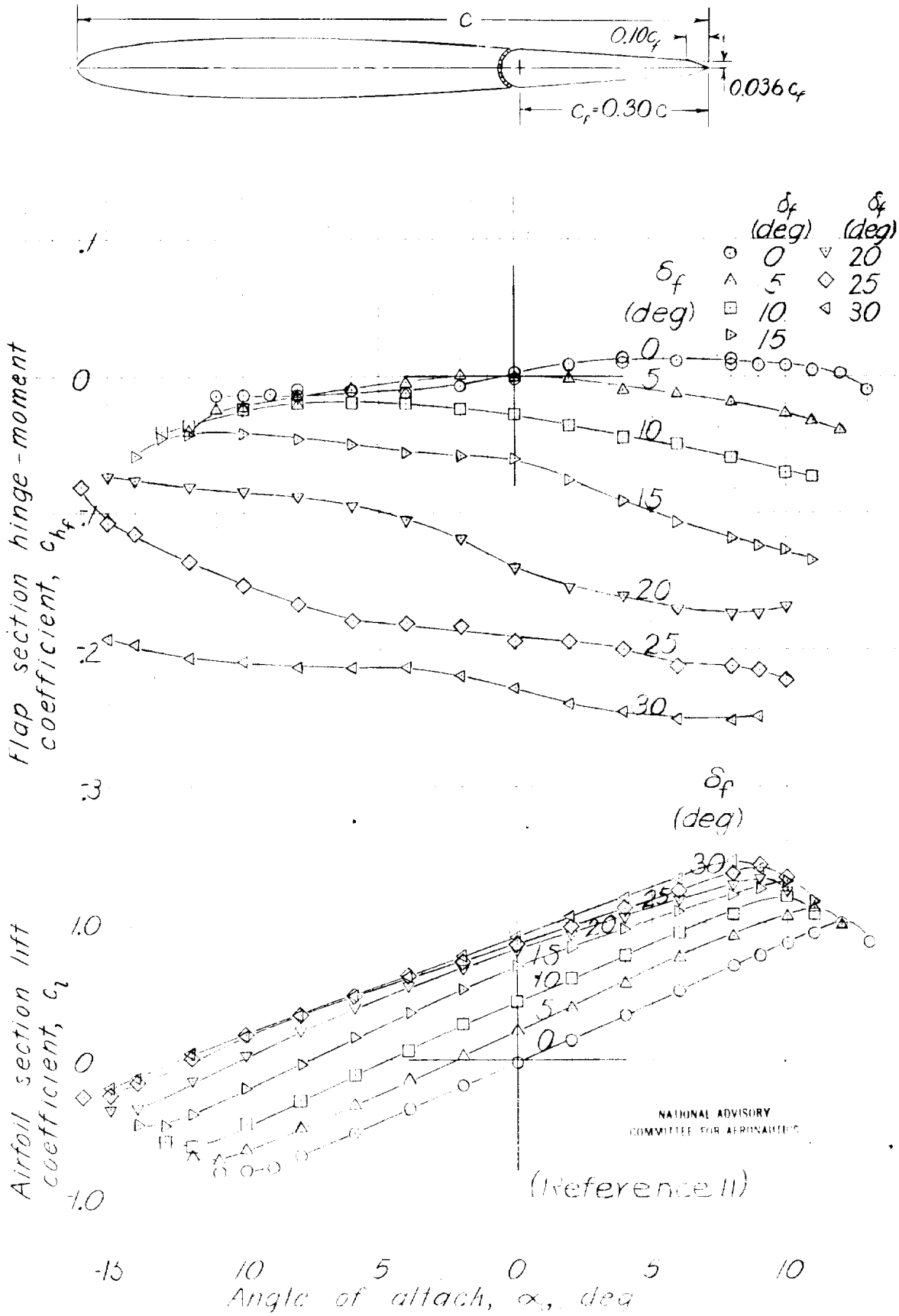

Figure 12. NACA 0009 airfoil, 0.30c flap with 0.10c_f beveled trailing edge sealed gap

L-663

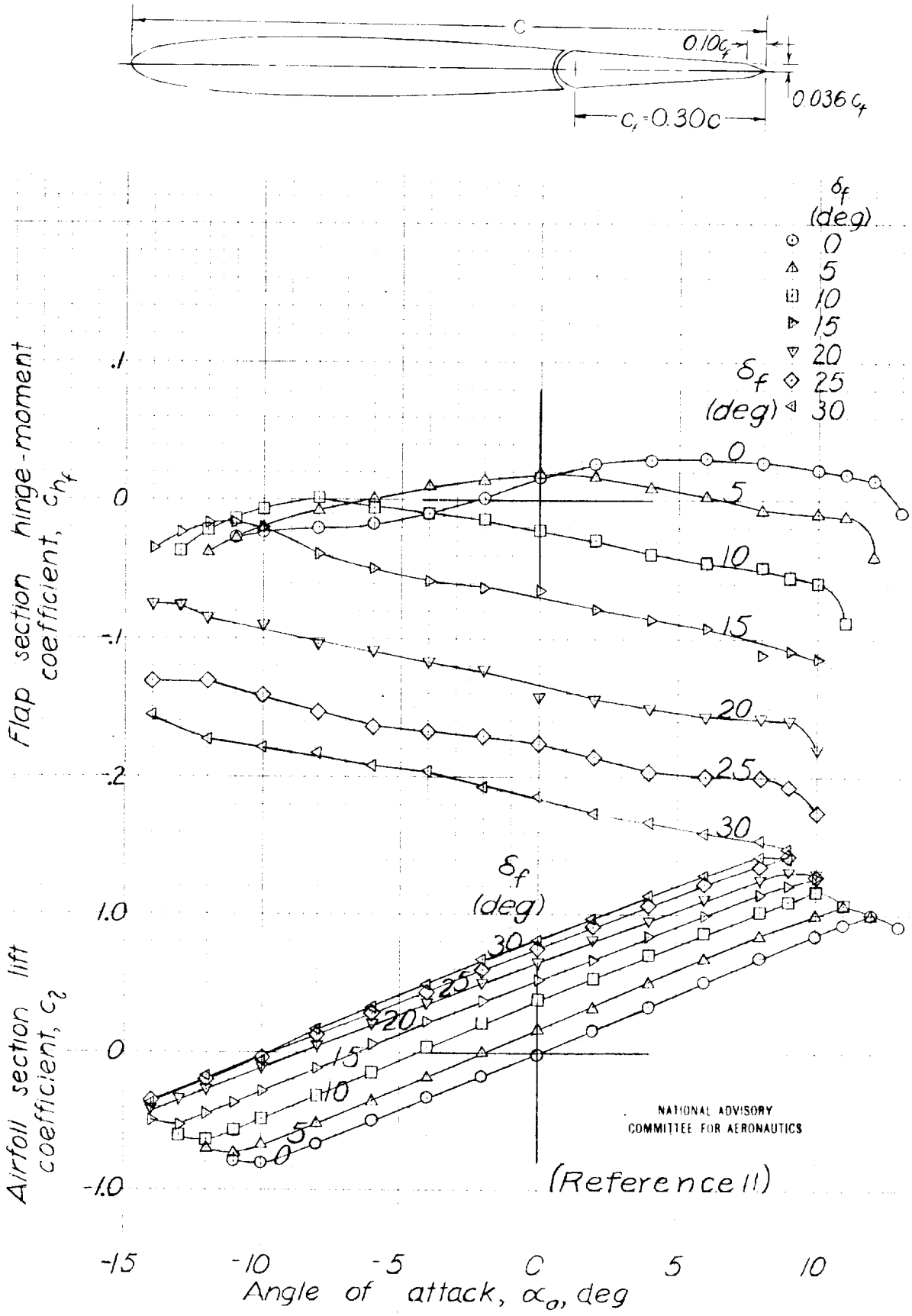

Figure 53.- NACA 0009 airfoil, 0.30c flap with 0.10c_f beveled trailing edge, 0.005c gap.

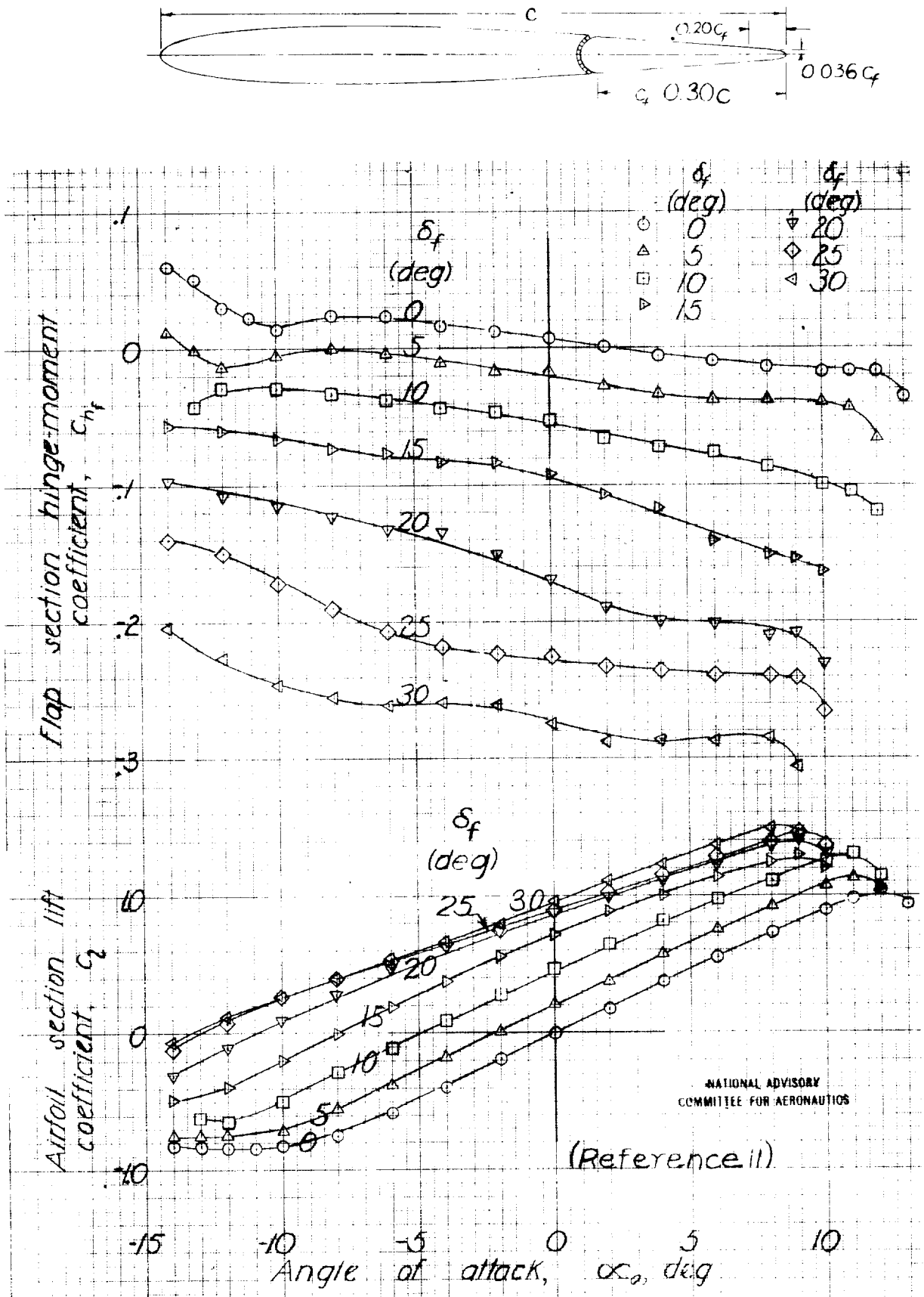

Figure 54.- NACA 0009 airfoil, 0.30c flap with 0.20 c_f elliptical trailing edge, sealed gap.

L-663

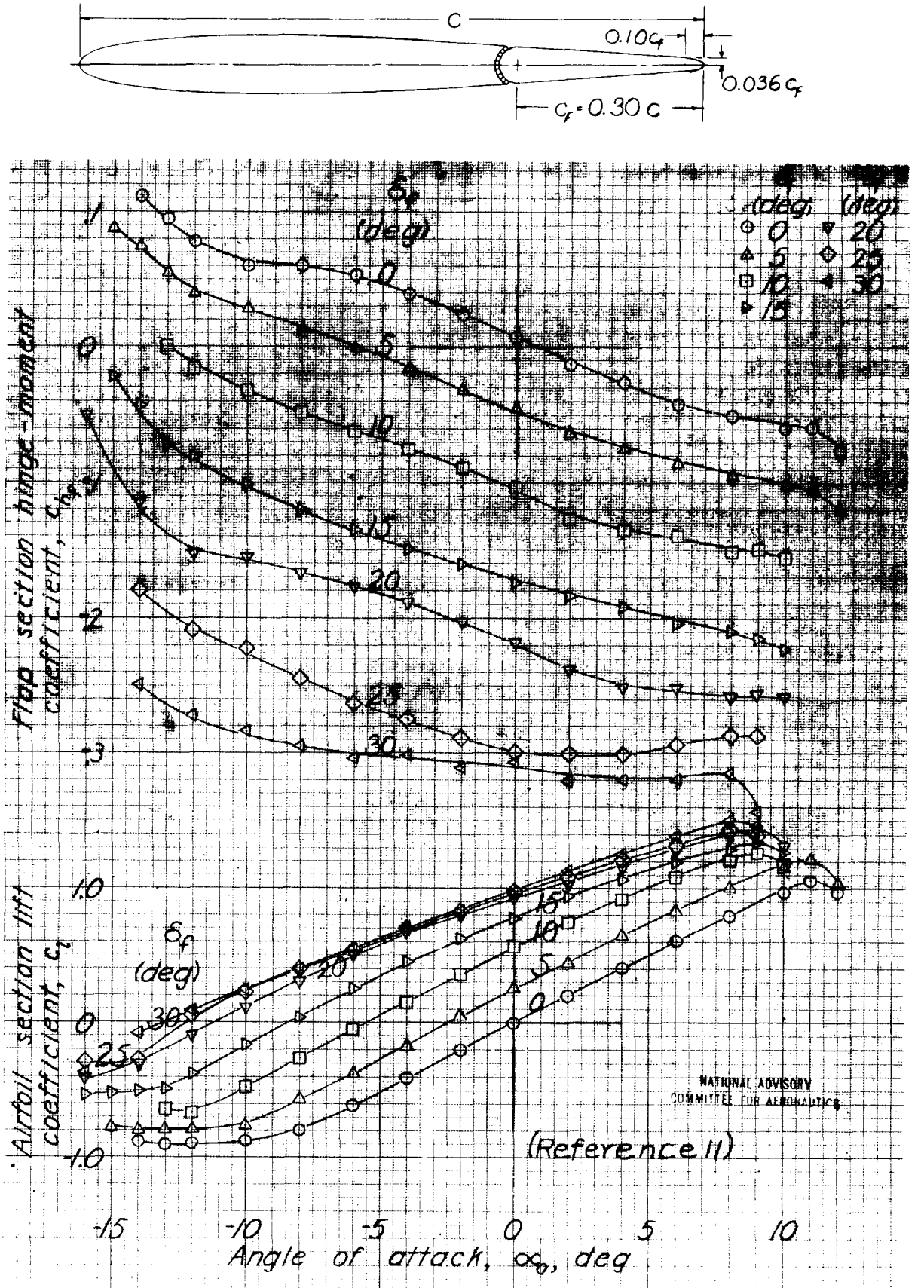

Figure 55.- NACA 0009 airfoil, 0.30c flap with 0.10c_f elliptical trailing edge, sealed gap.

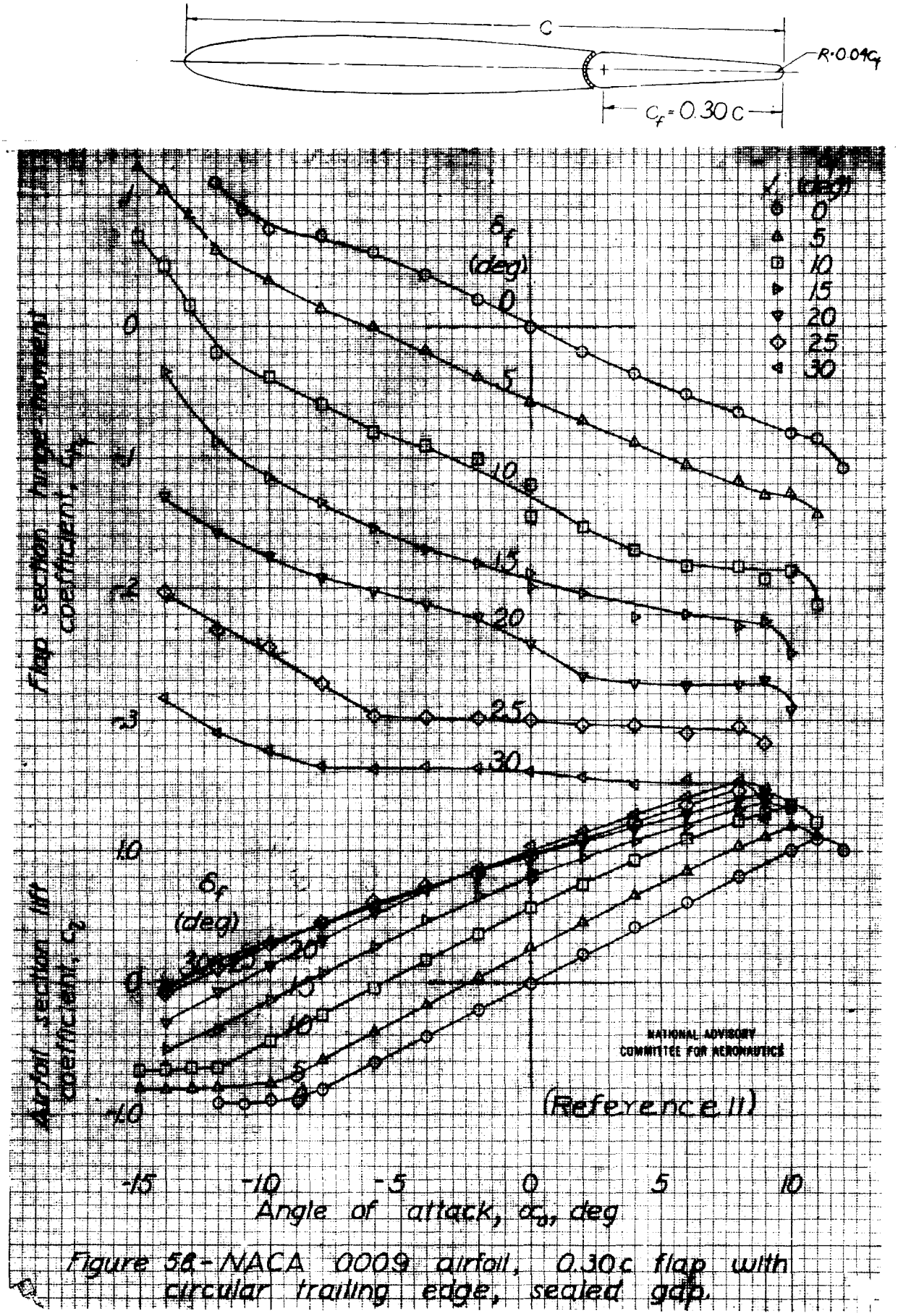

Figure 58.- NACA 0009 airfoil, 0.30c flap with circular trailing edge, sealed gap.

L-663

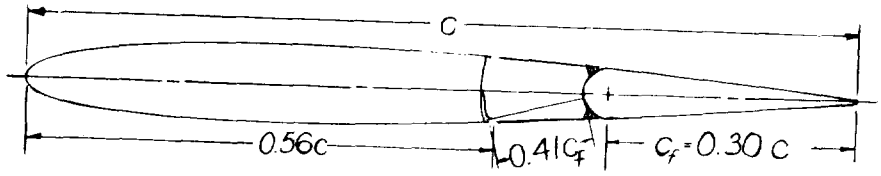

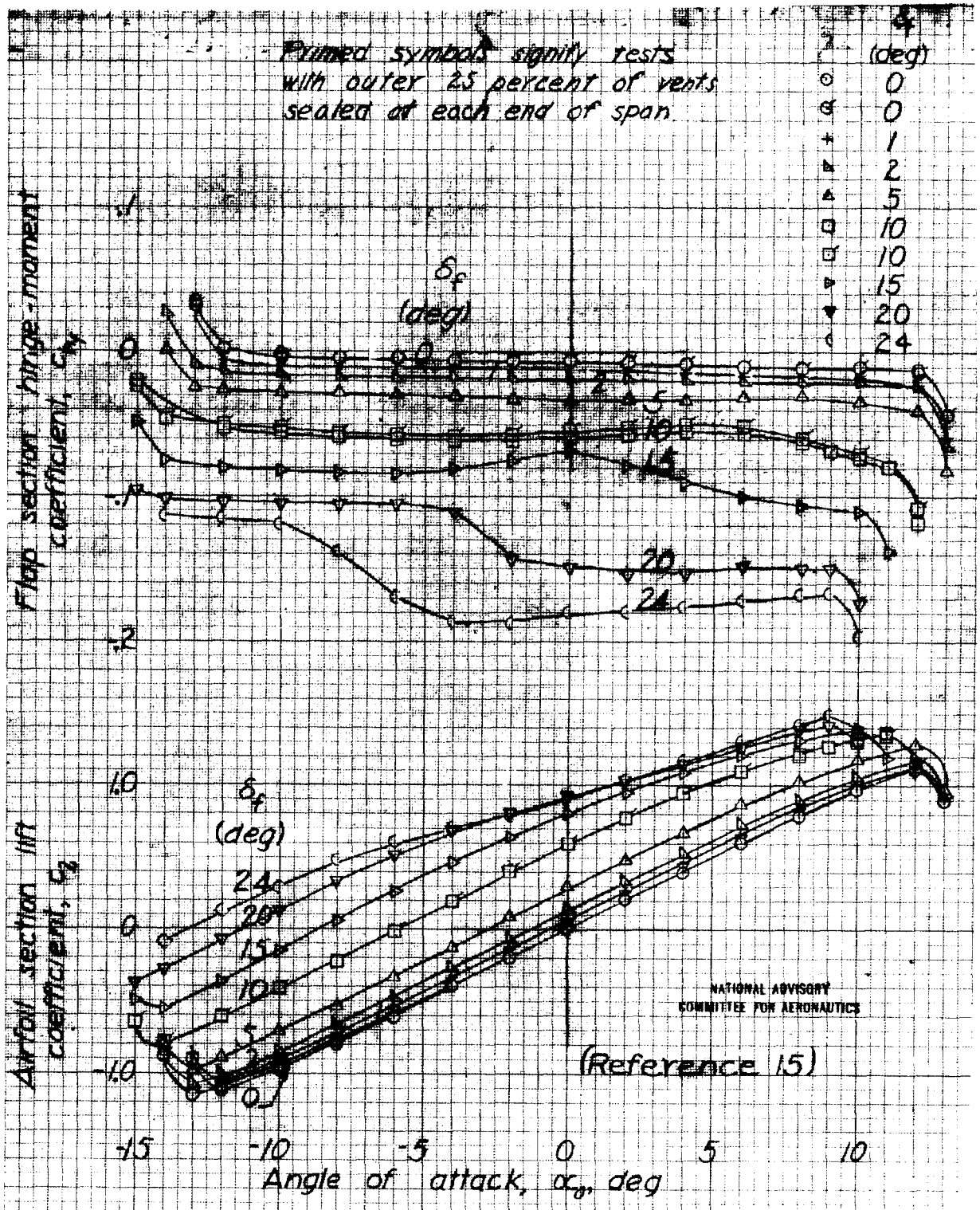

Figure 57.- NACA 0009 airfoil, 0.30c internally balanced flap, vent at 0.56c.

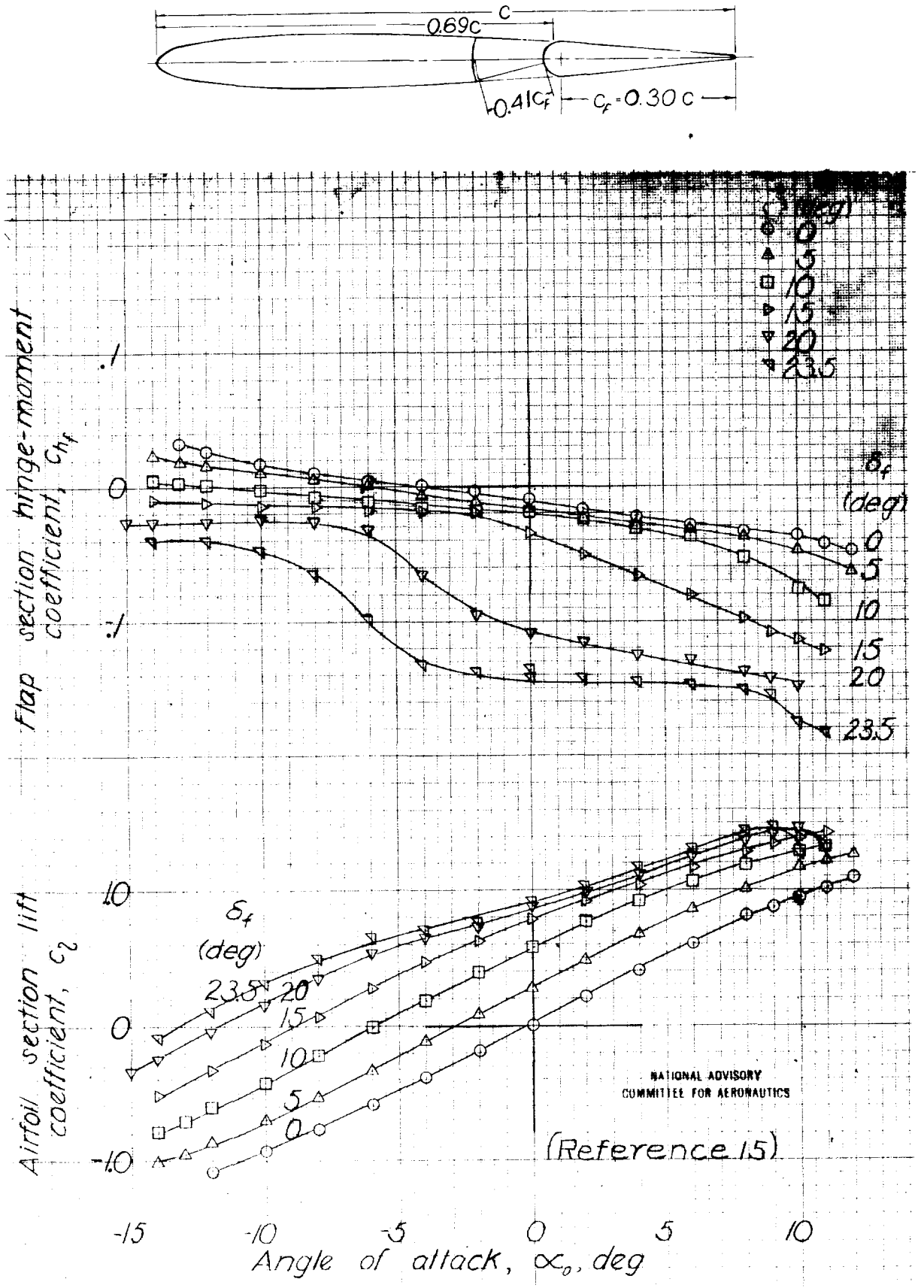

Figure 58.- NACA 0009 airfoil, 0.30c internally balanced flap, vent at 0.69c.

L-663

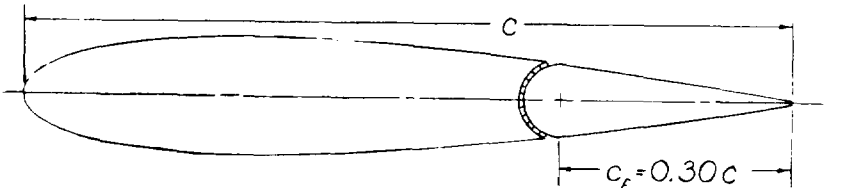

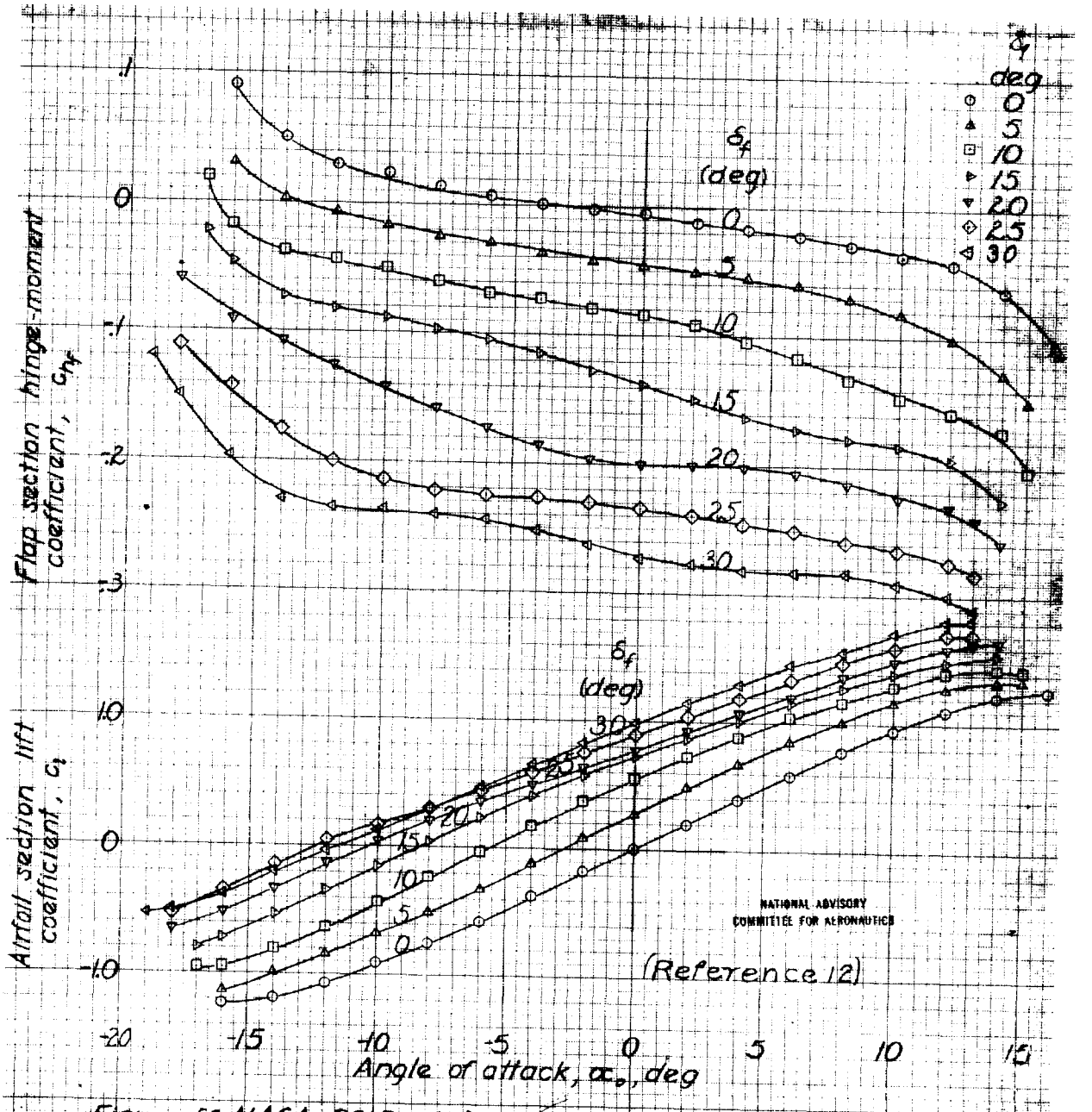

Figure 59.-NACA 0015 airfoil, 0.30c plain flap, sealed gap.

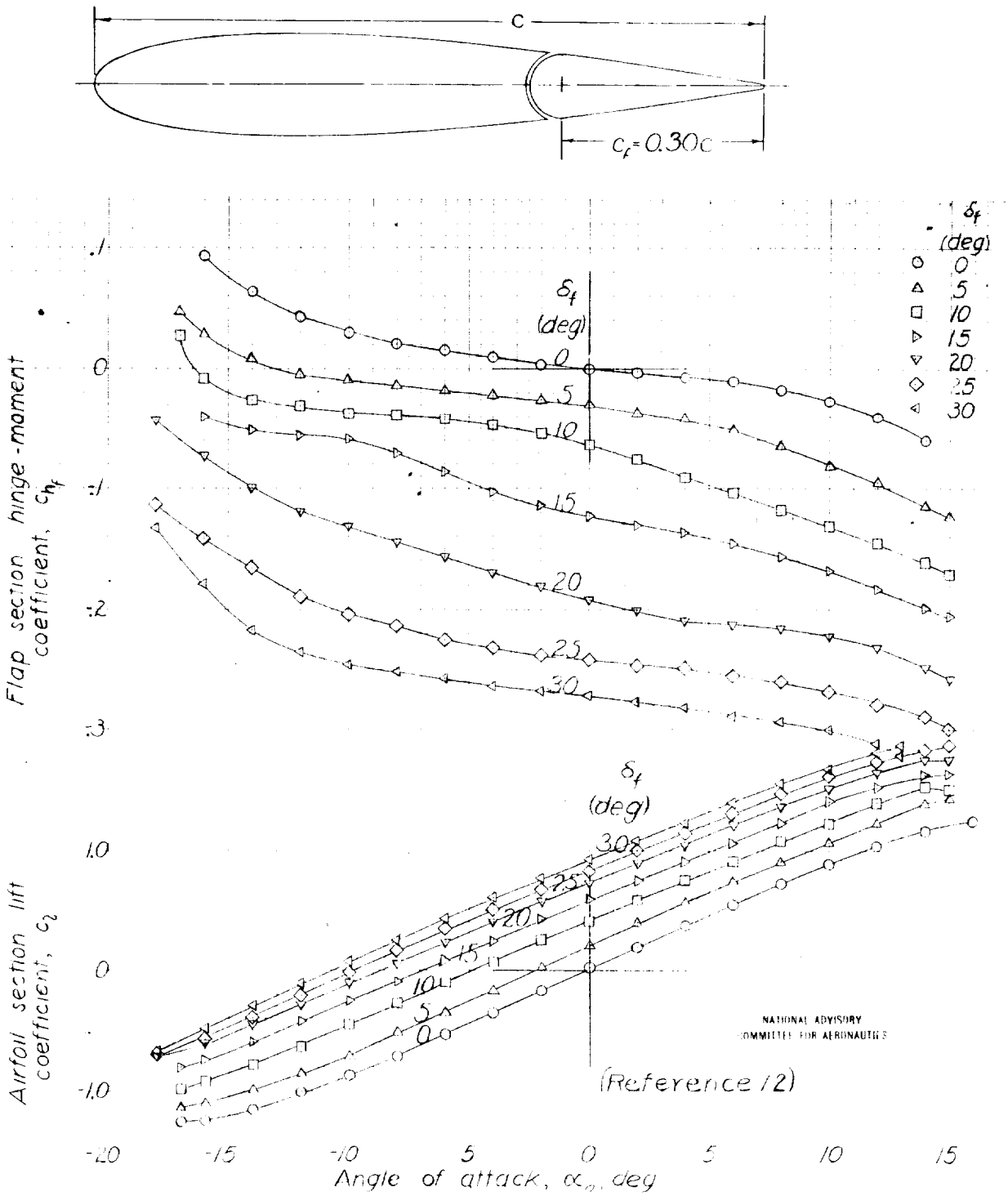

Figure 60.- NACA 0015 airfoil, 0.30c plain flap, 0.005c gap

L-663

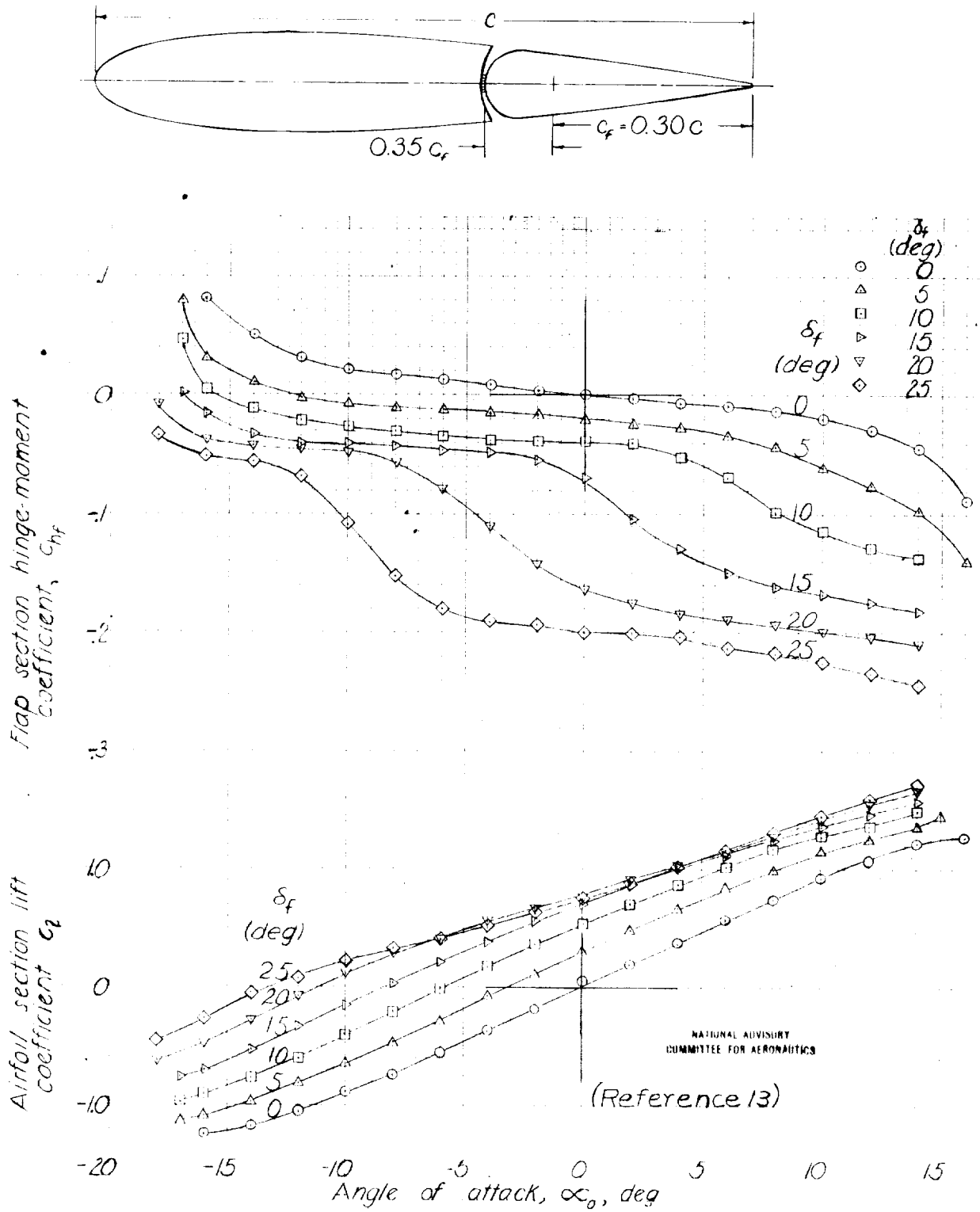

Figure 61.-NACA 0015 airfoil, 0.30c flap with 0.35 c_f blunt nose overhang, sealed gap.

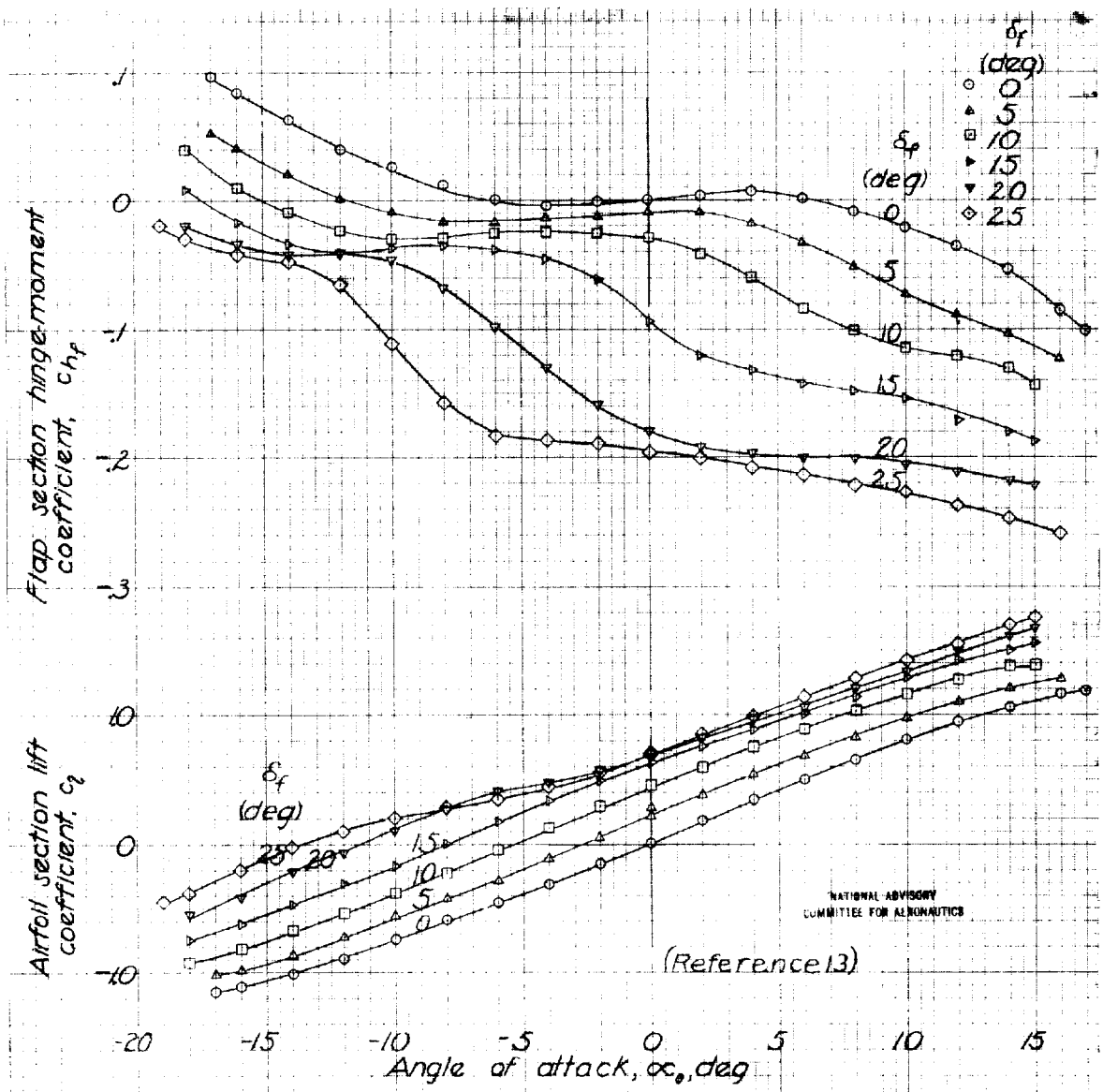

Figure 62.-NACA 0015 airfoil, 0.30c flap with 0.35c_f blunt-nose overhang, 0.005c gap.

L-663

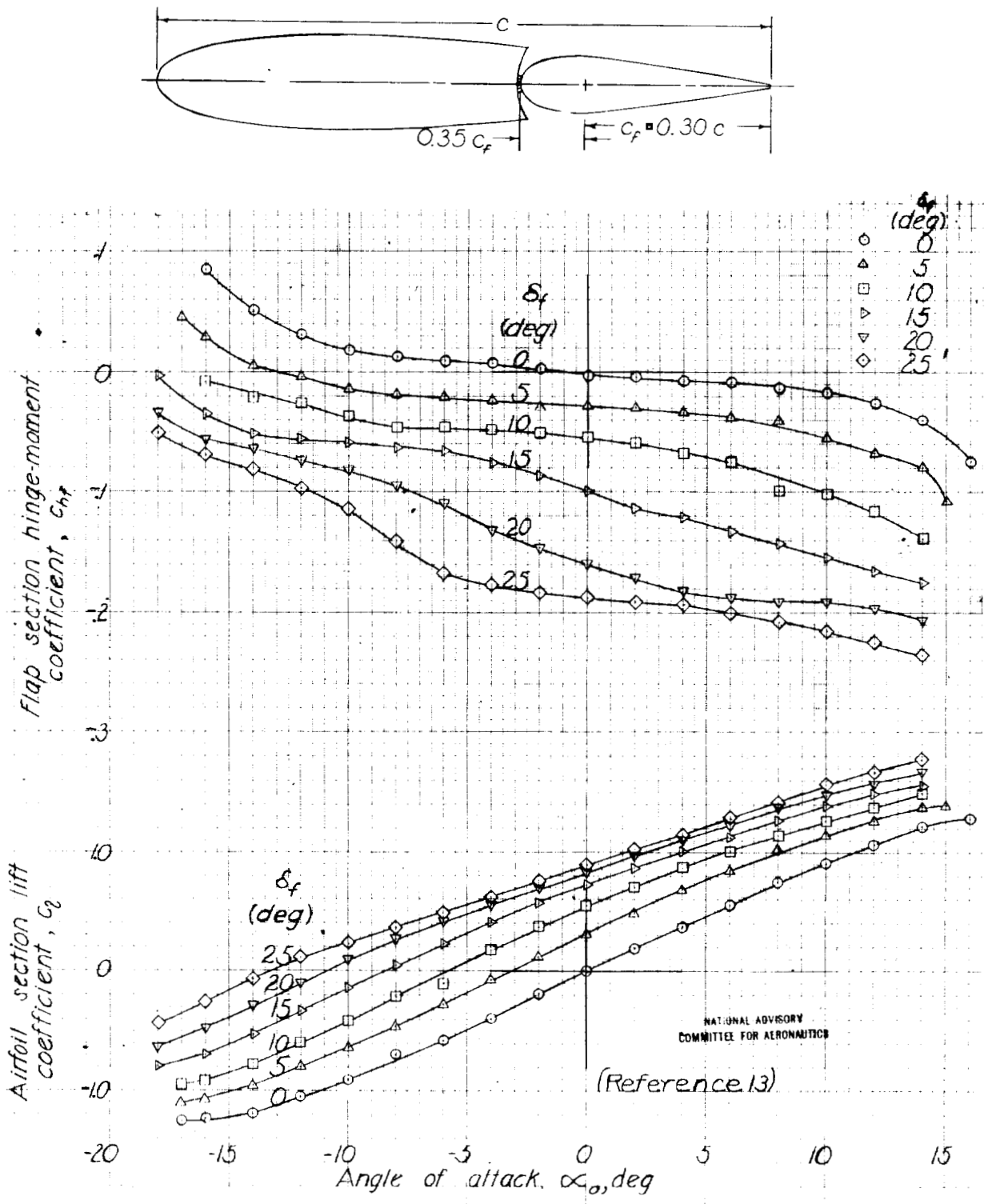

Figure 63.-NACA 0015 airfoil, 0.30c flap with 0.35c_f medium-nose overhang, sealed gap.

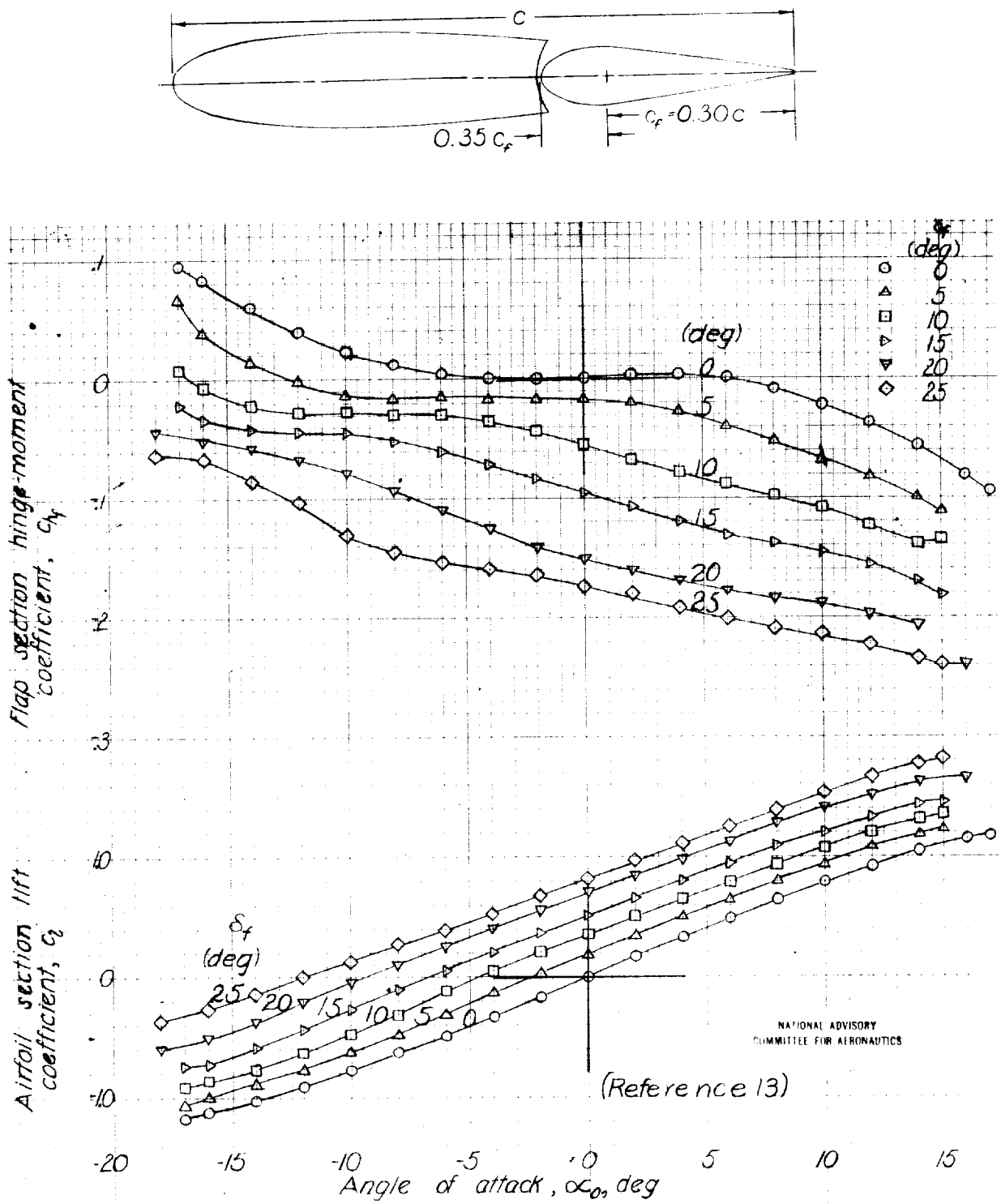

Figure 64.-NACA 0015 airfoil, 0.30c flap with 0.35c_f medium-nose overhang, 0.005c gap.

L-663

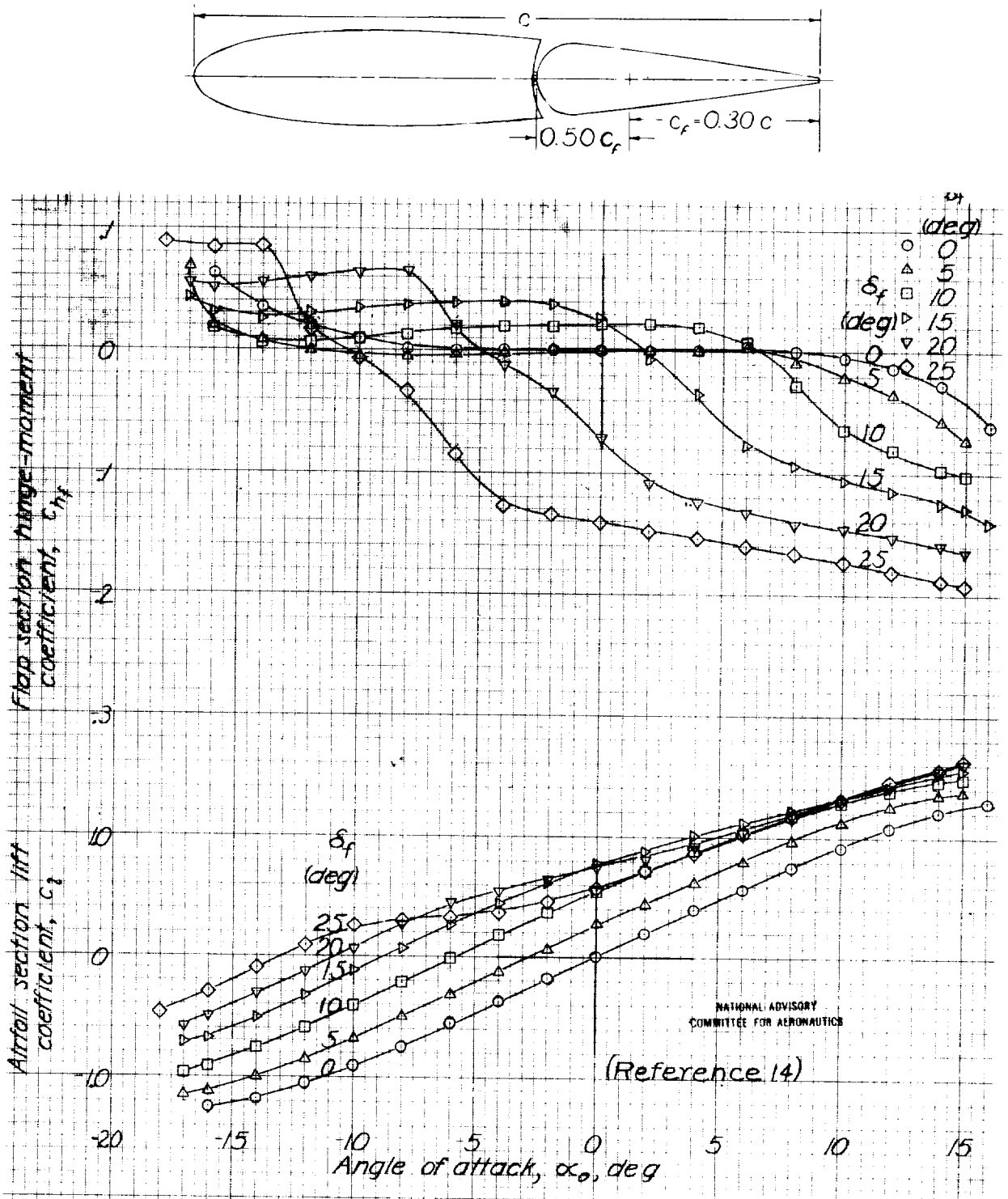

Figure 65.-NACA 0015 airfoil, 0.30c flap with 0.50 c_f blunt-nose overhang, sealed gap.

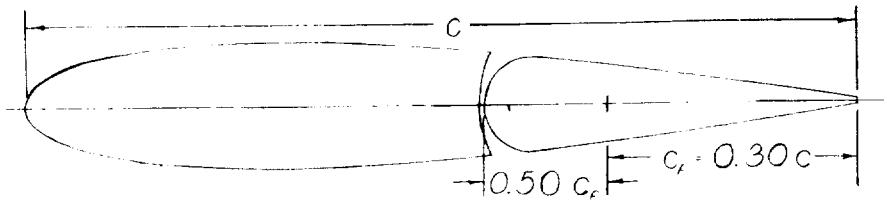

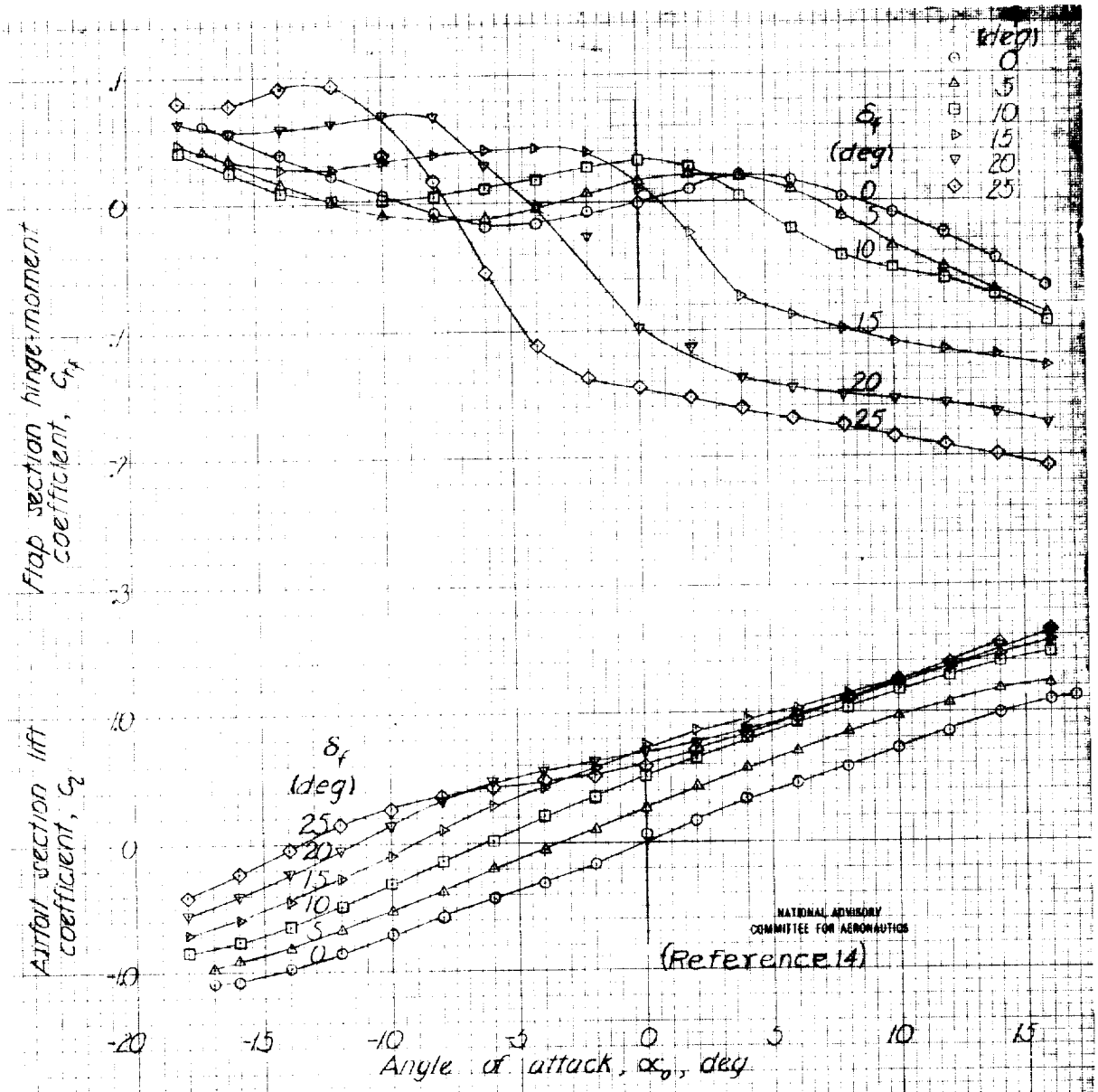

Figure 66-NACA 0015 airfoil, 0.30c flap with 0.50c_f blunt-nose overhang, 0.005c gap.

L-663

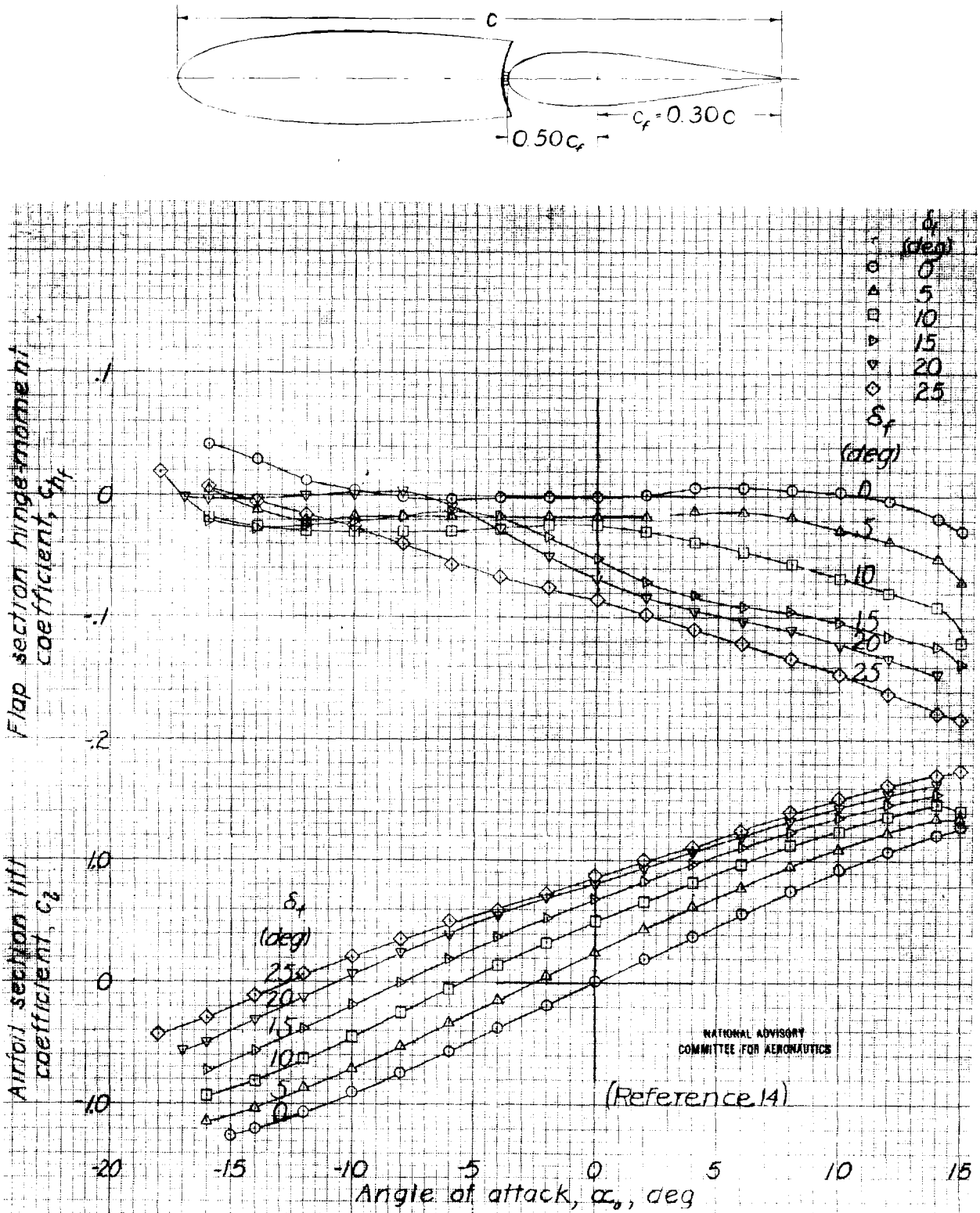

Figure 67.-NACA 0015 airfoil, 0.30c flap with 0.50c_f medium-nose overhang, sealed gap.

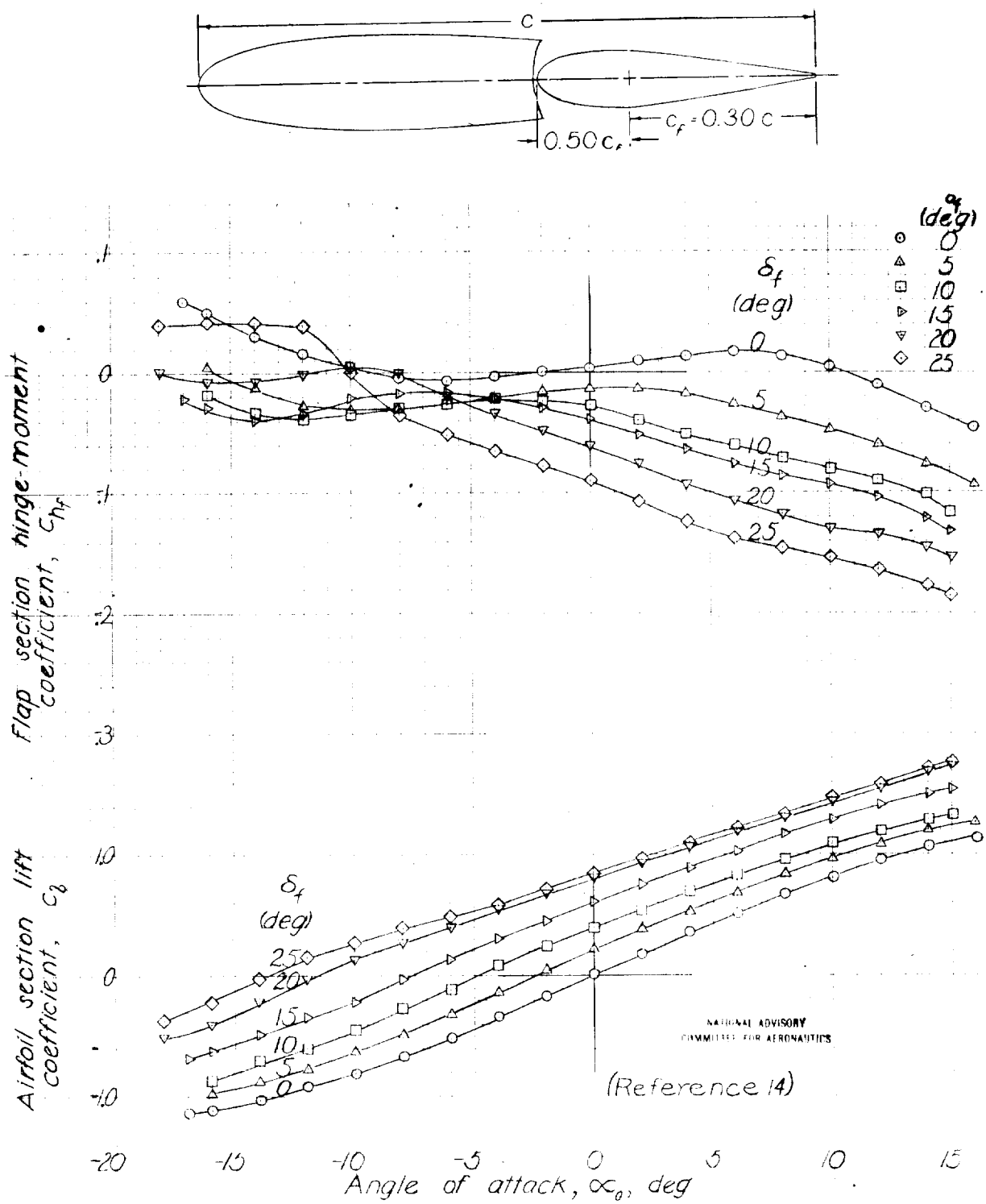

Figure 68.-NACA 0015 airfoil, 0.30c flap with 0.50c_f medium-nose overhang, 0.005c gap.

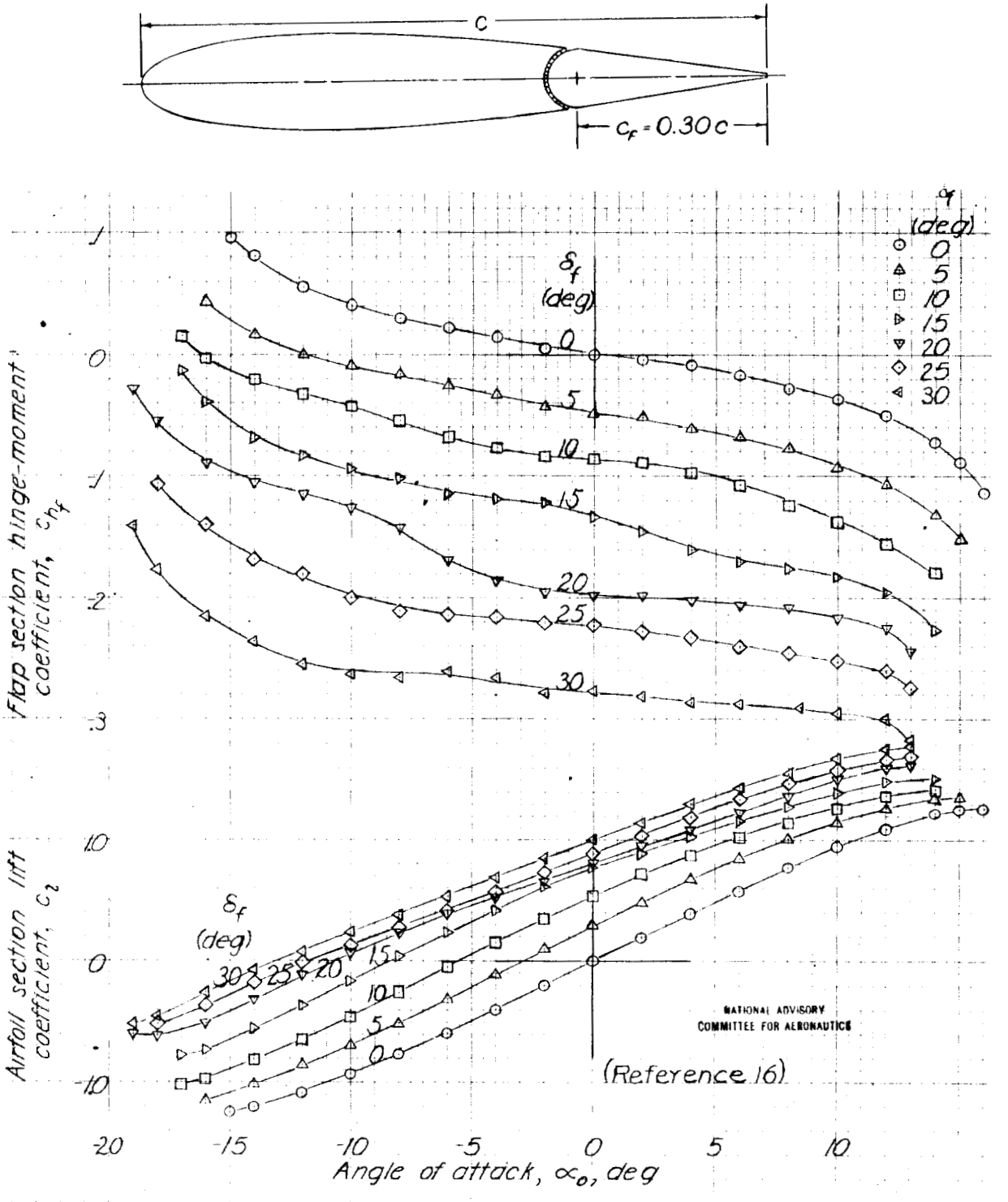

Figure 69.-NACA 0015 airfoil, 0.30c straight-contour plain flap, sealed gap.

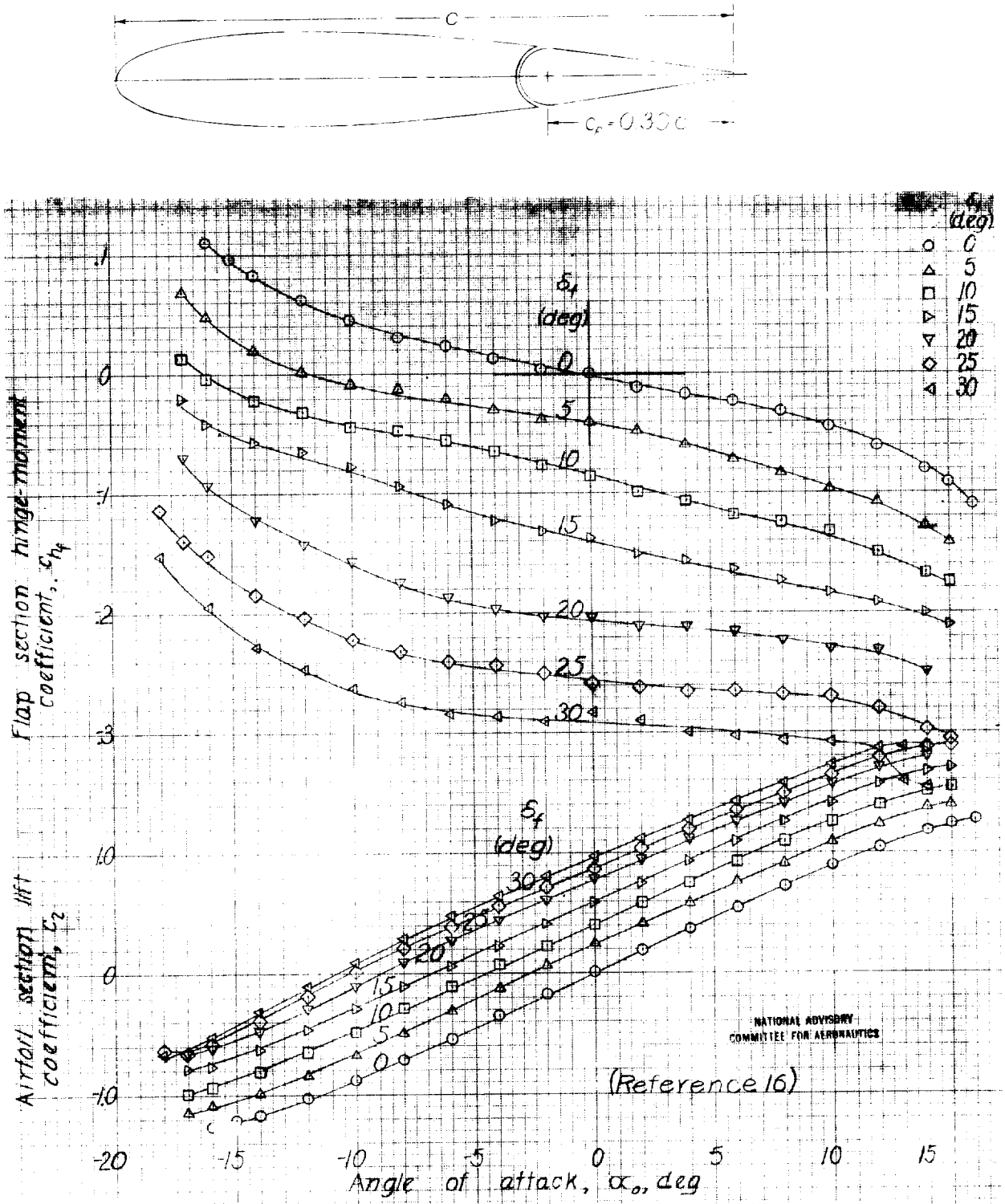

Figure 70.-NACA 0015 airfoil, 0.30c straight-contour plain flap, 0.005c gap.

L-663

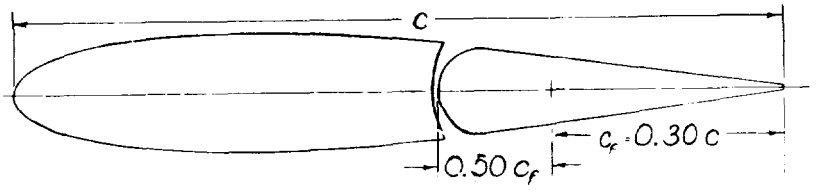

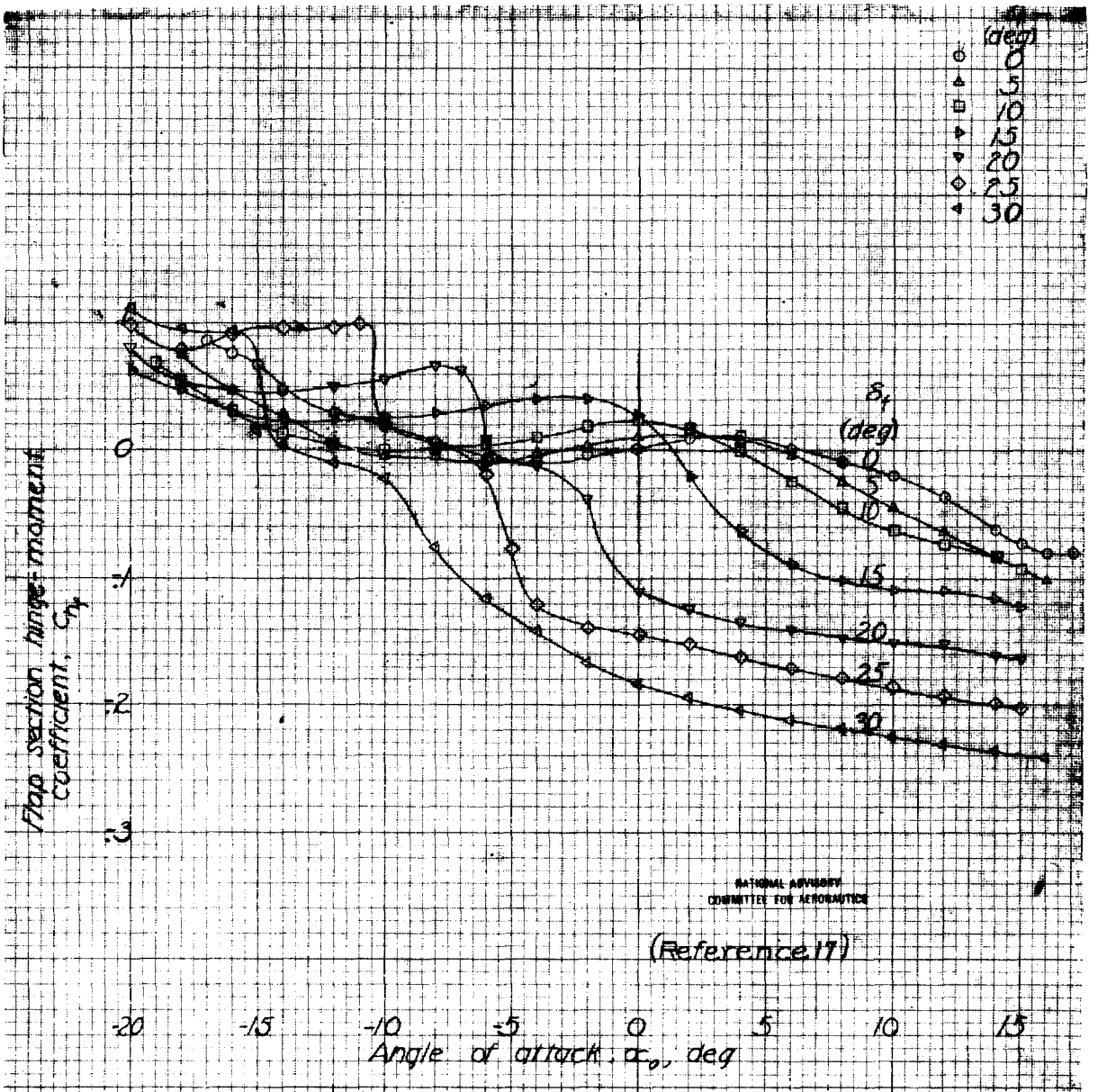

Figure 71.- NACA 0015 airfoil, 0.30c straight-contour flap with $0.50c_f$ blunt-nose overhang, 0.005c gap.

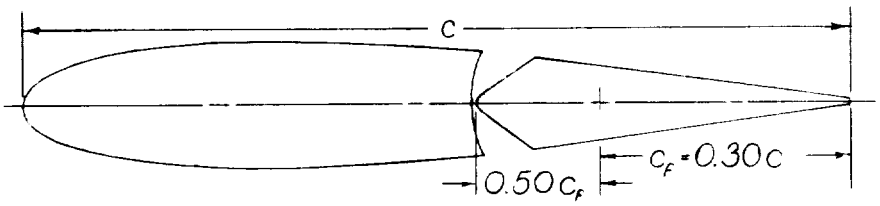

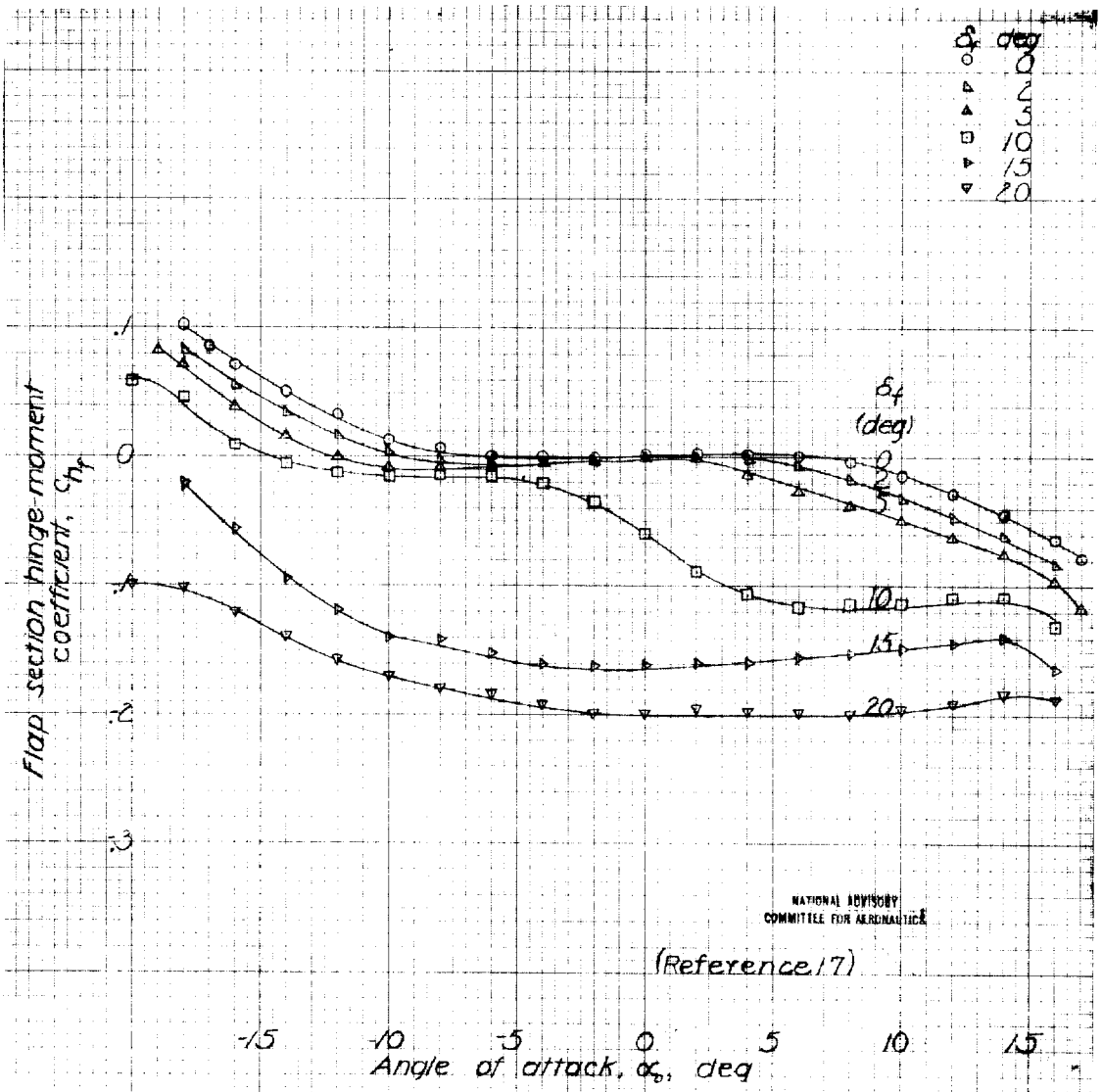

Figure 72.-NACA 0015 airfoil, 0.30c straight contour flap with 0.50c_f blunt-base overhang, modification 1, 0.005c gap.

L-663

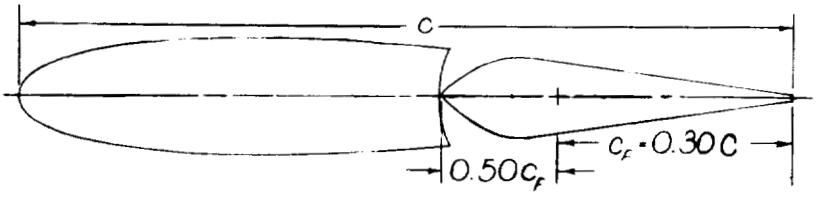

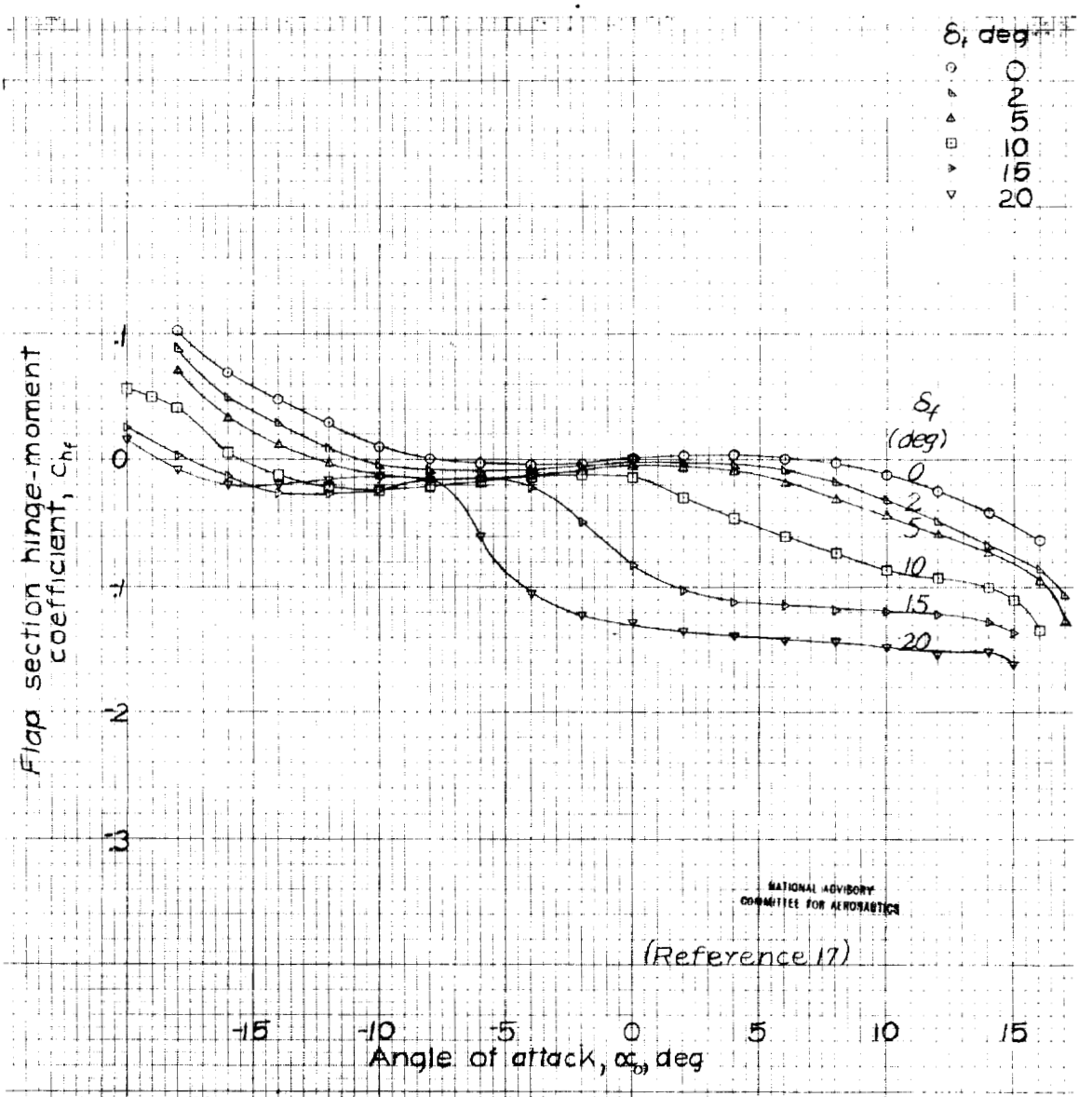

Figure 73-NACA 0015 airfoil, 0.30c straight contour flap with 0.50c_f blunt-nose overhang, modification 2, 0.005c gap.

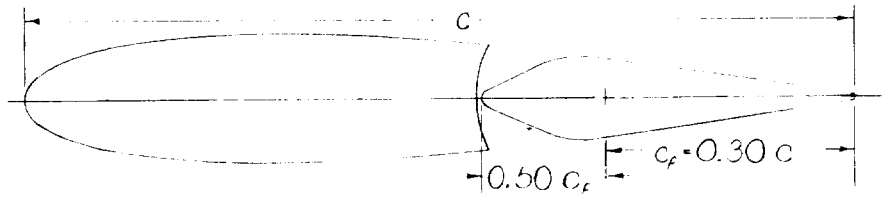

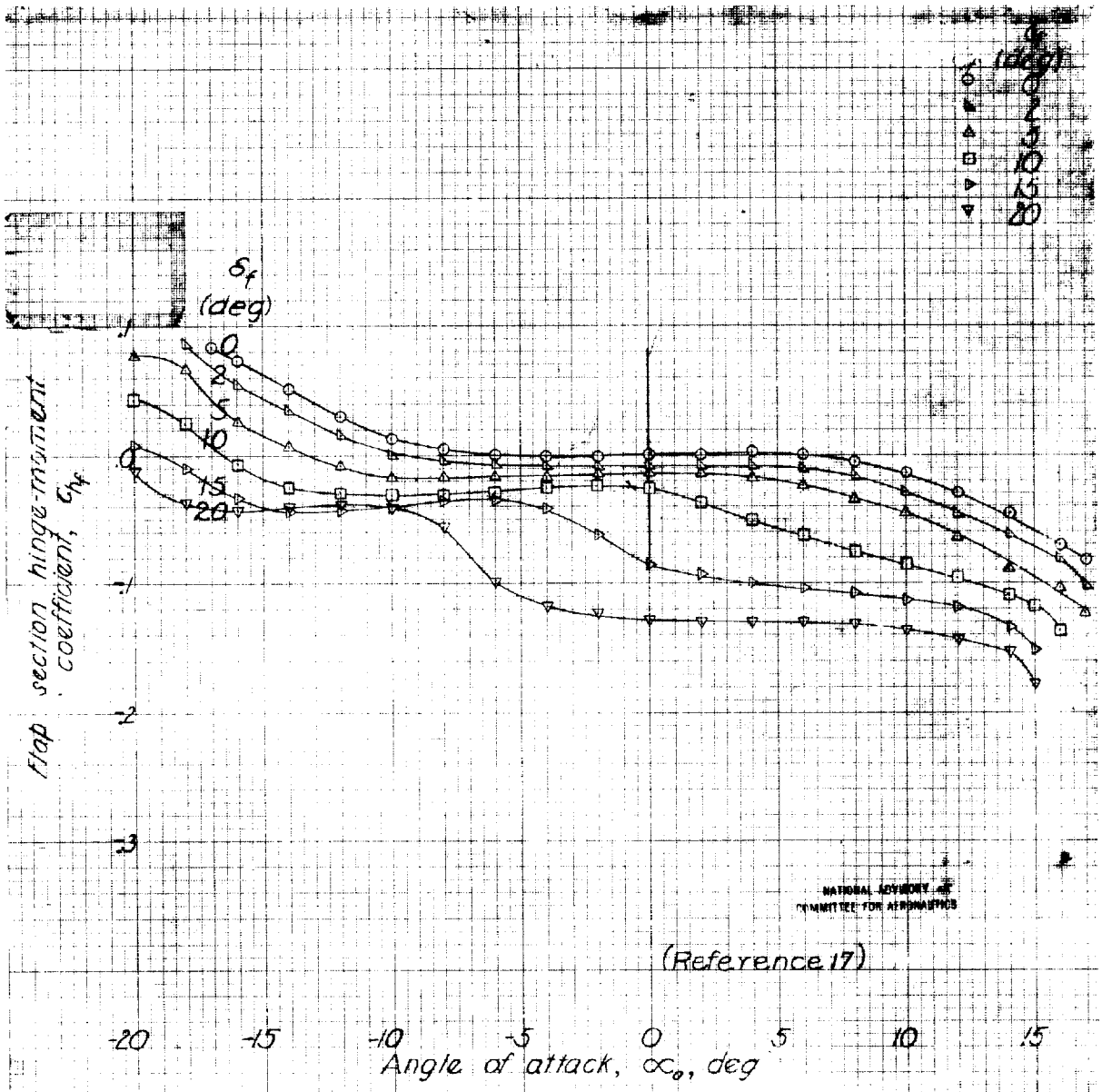

(Reference 17)

Figure 74.-NACA 0015 airfoil, 0.30c straight-contour flap with 0.50c_f blunt-nose overhang, modification 3, 0.005c gap.

L-663

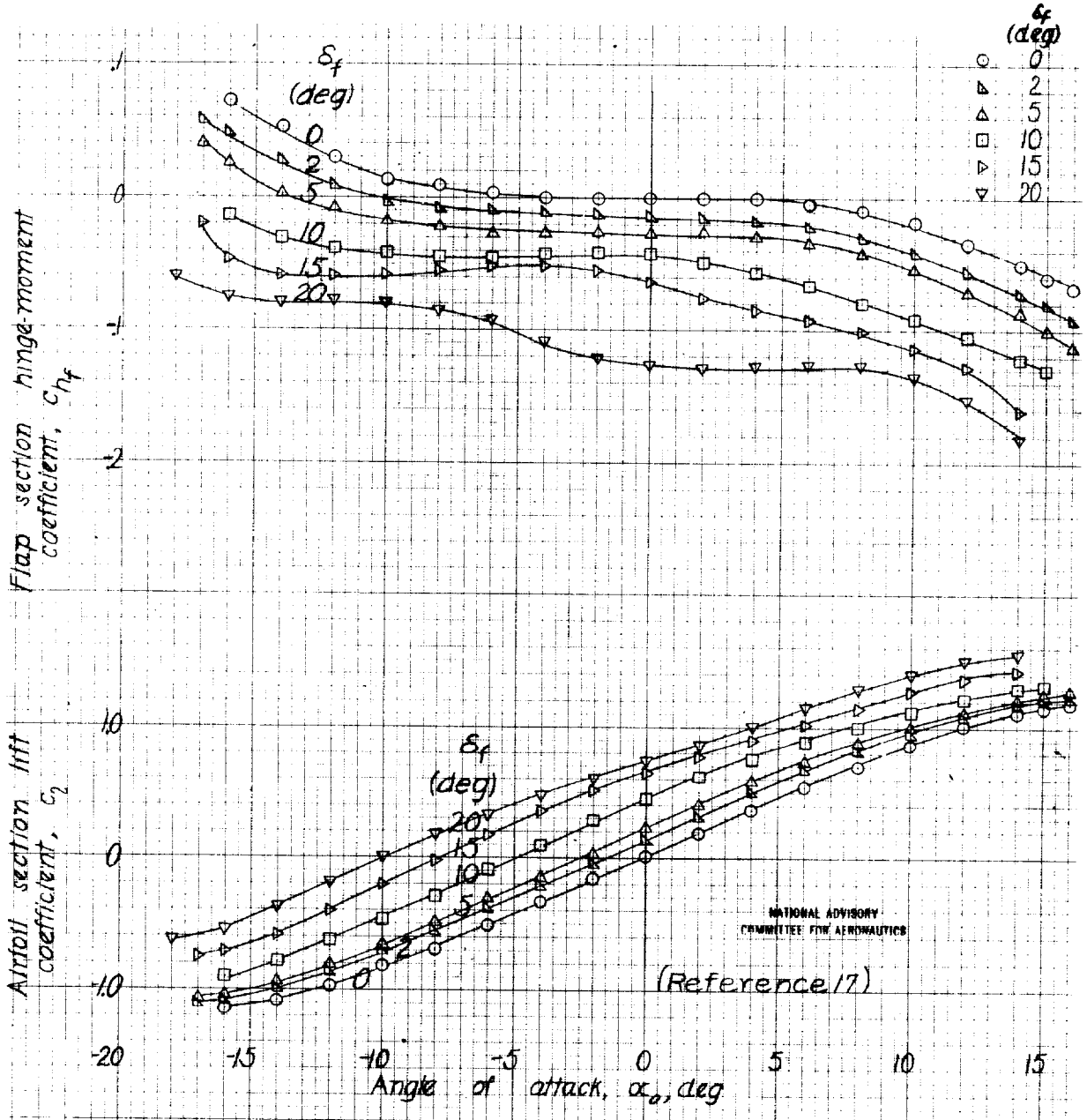

Figure 75.-NACA 0015 airfoil, 0.30c straight-contour flap with 0.50 c_f sharp-nose overhang, 0.005c gap.

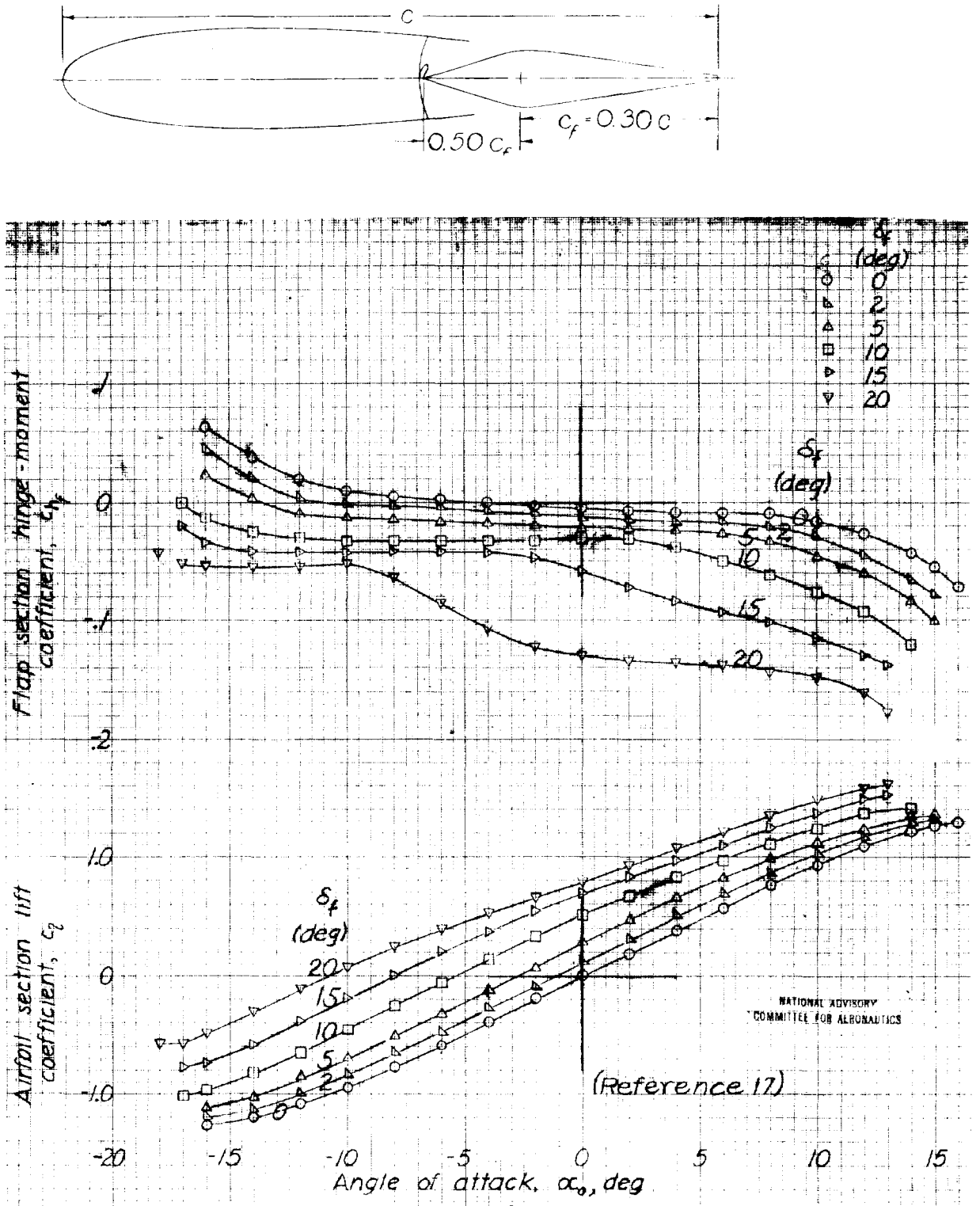

Figure 76.- NACA 0015 airfoil, 0.30c straight-contour flap with $0.50c_f$ sharp-nose overhang, narrow cover plate, sealed gap.

L-663

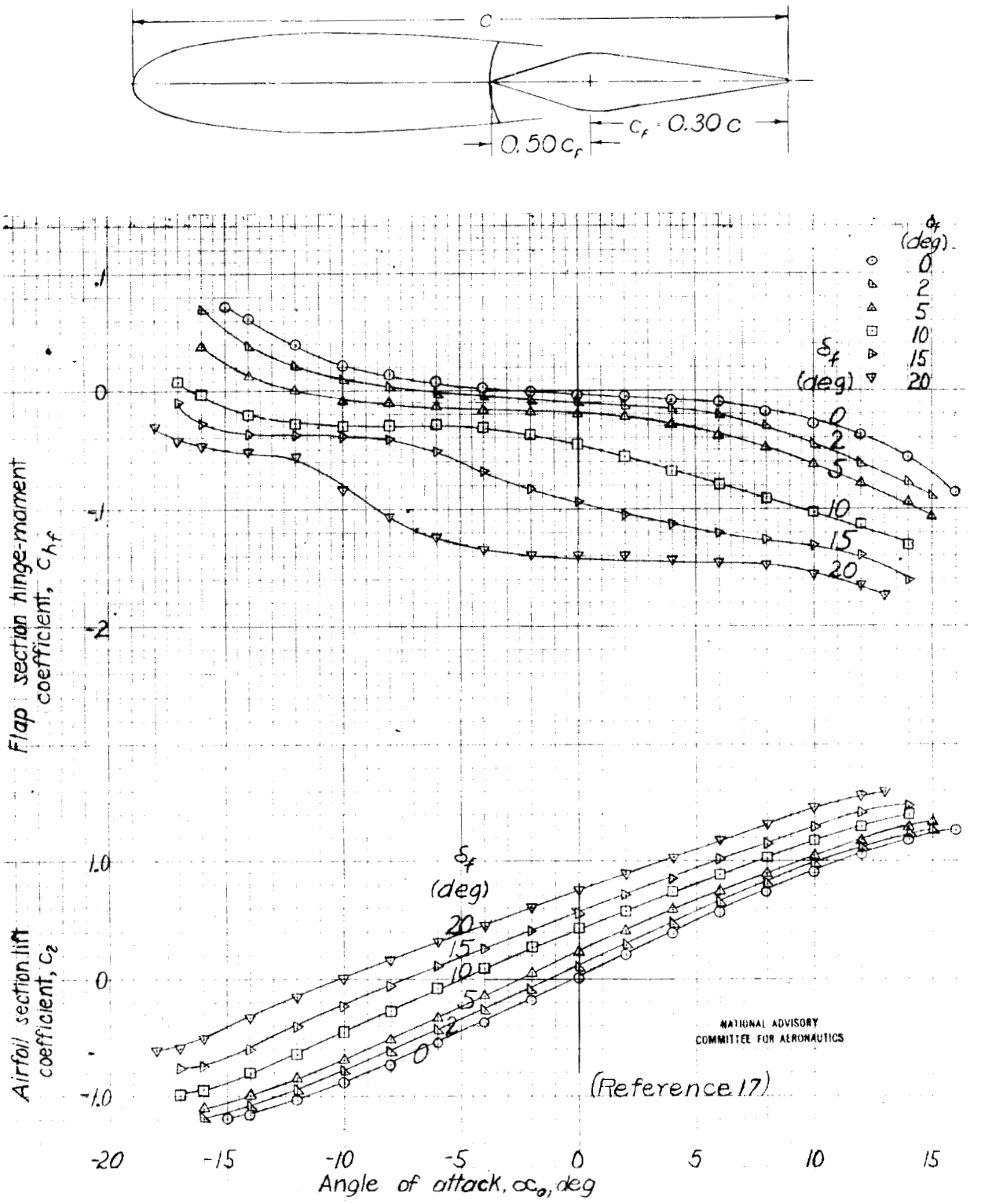

Figure 77.-NACA 0015 airfoil, 0.30c straight-contour flap with $0.50c_f$ sharp-nose overhang, narrow cover plate, 0.0011c gap.

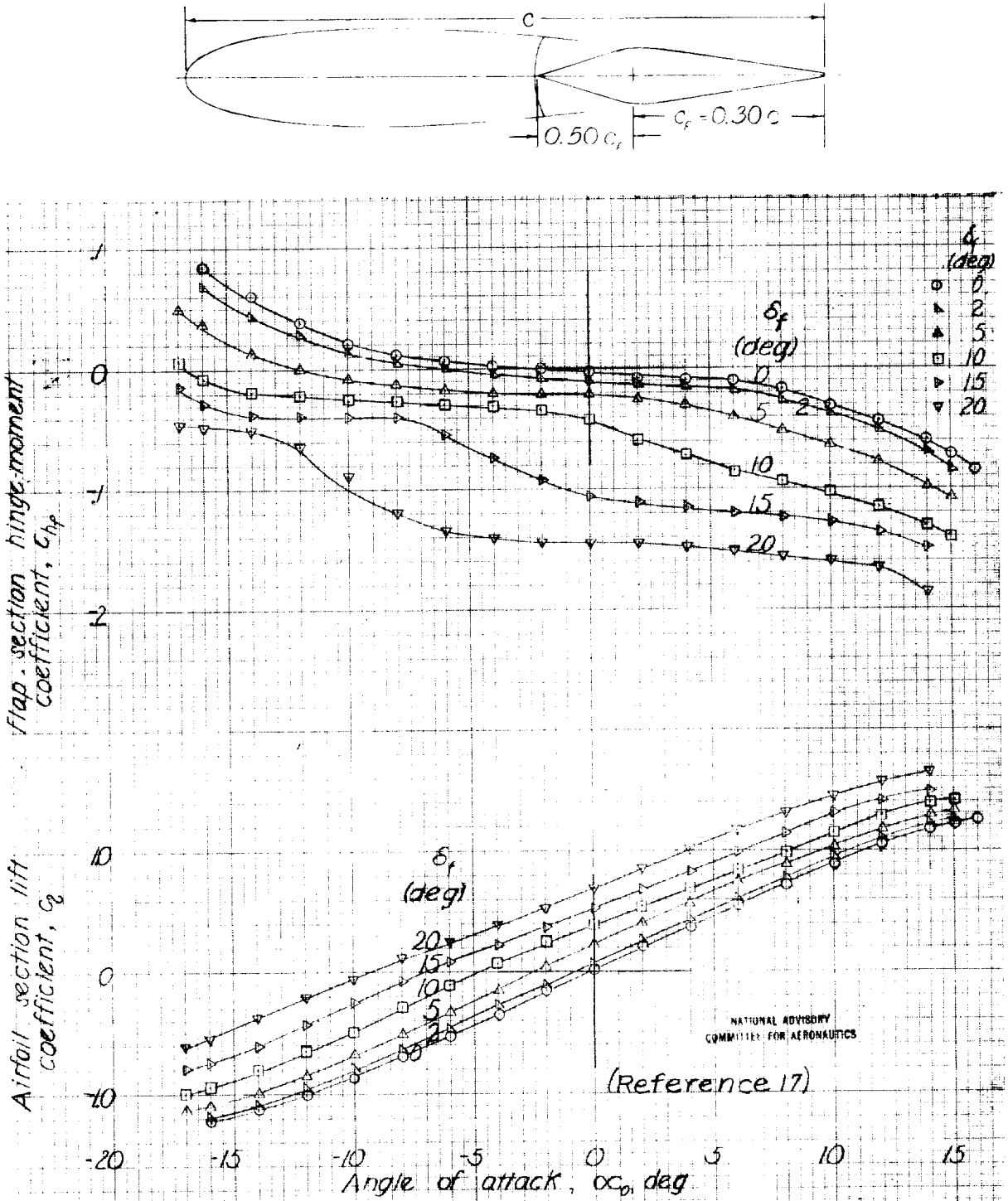

Figure 78.- NACA 0015 airfoil, 0.30c straight-contour flap with 0.50c_f sharp-nose overhang, narrow cover plate, 0.0023c gap.

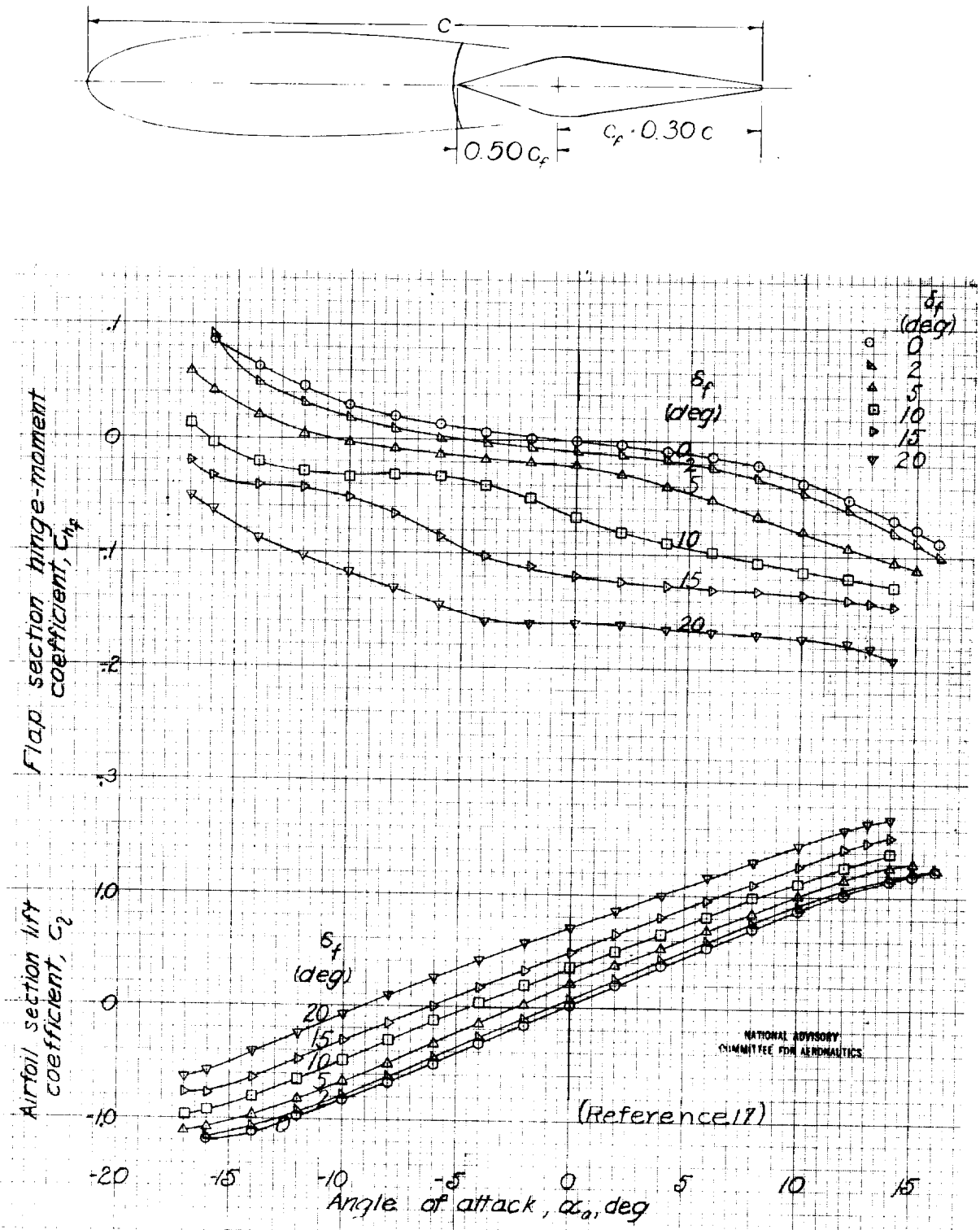

Figure 19. NACA 0015 airfoil, 0.30c straight-contour flap with 0.50 c_f sharp-nose overhang, narrow cover plate, 0.005c gap.

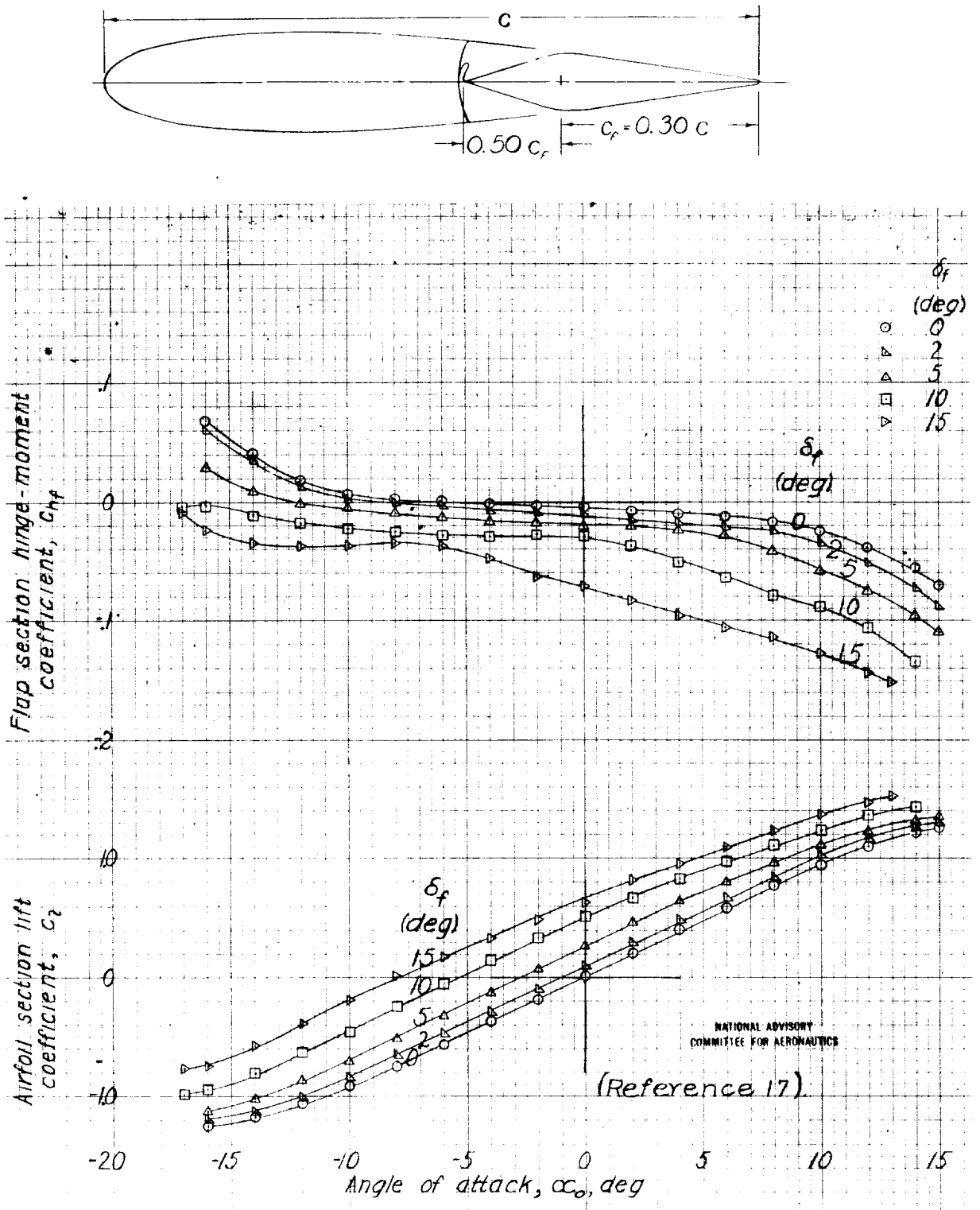

Figure 80.-NACA 0015 airfoil, 0.30c straight-contour flap with 0.50c_f sharp-nose overhang, medium cover plate, sealed gap.

L-663

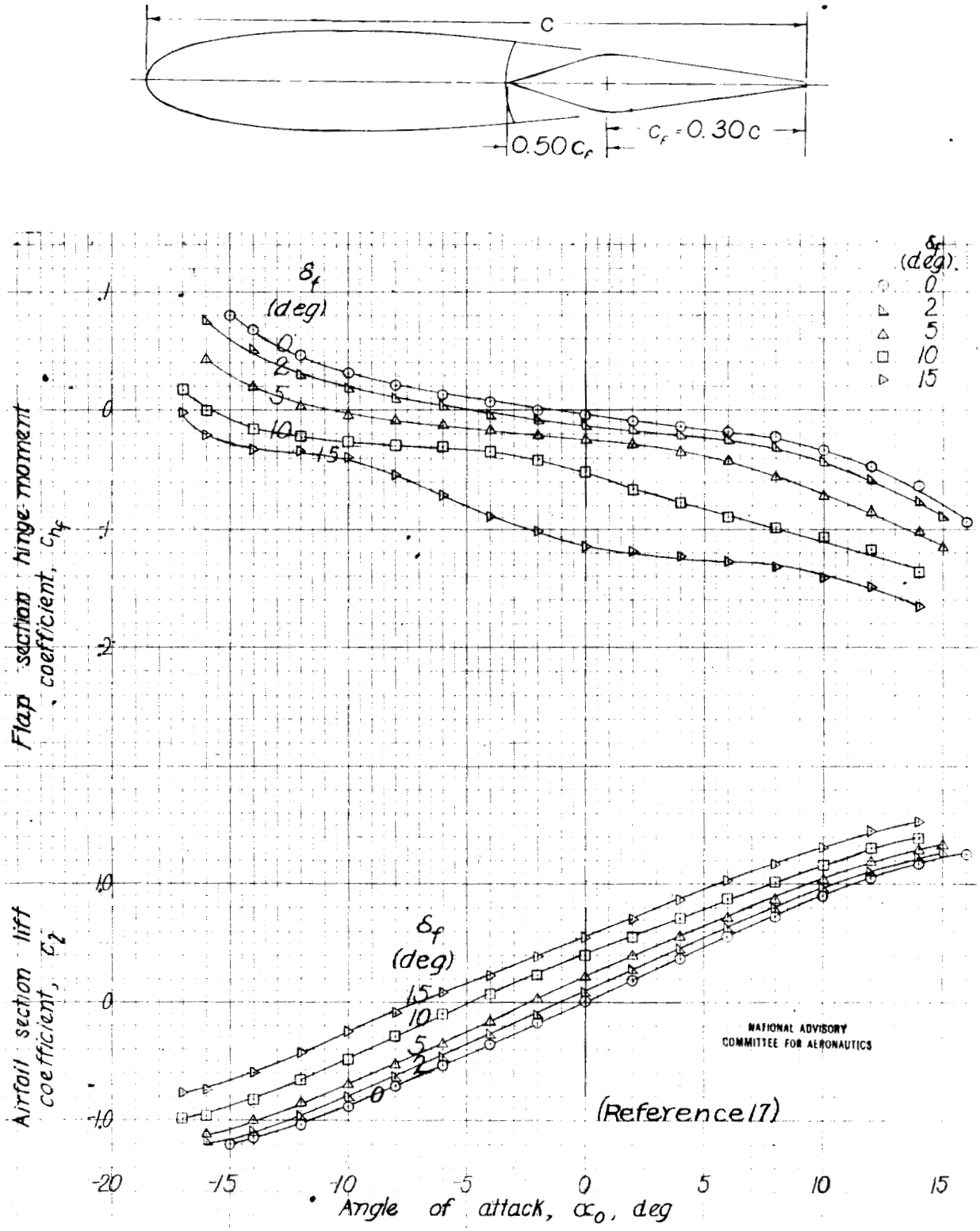

Figure 81.–NACA 0015 airfoil, 0.30c straight-contour flap with 0.50 c_f sharp-nose overhang, medium cover plate, 0.0011c gap

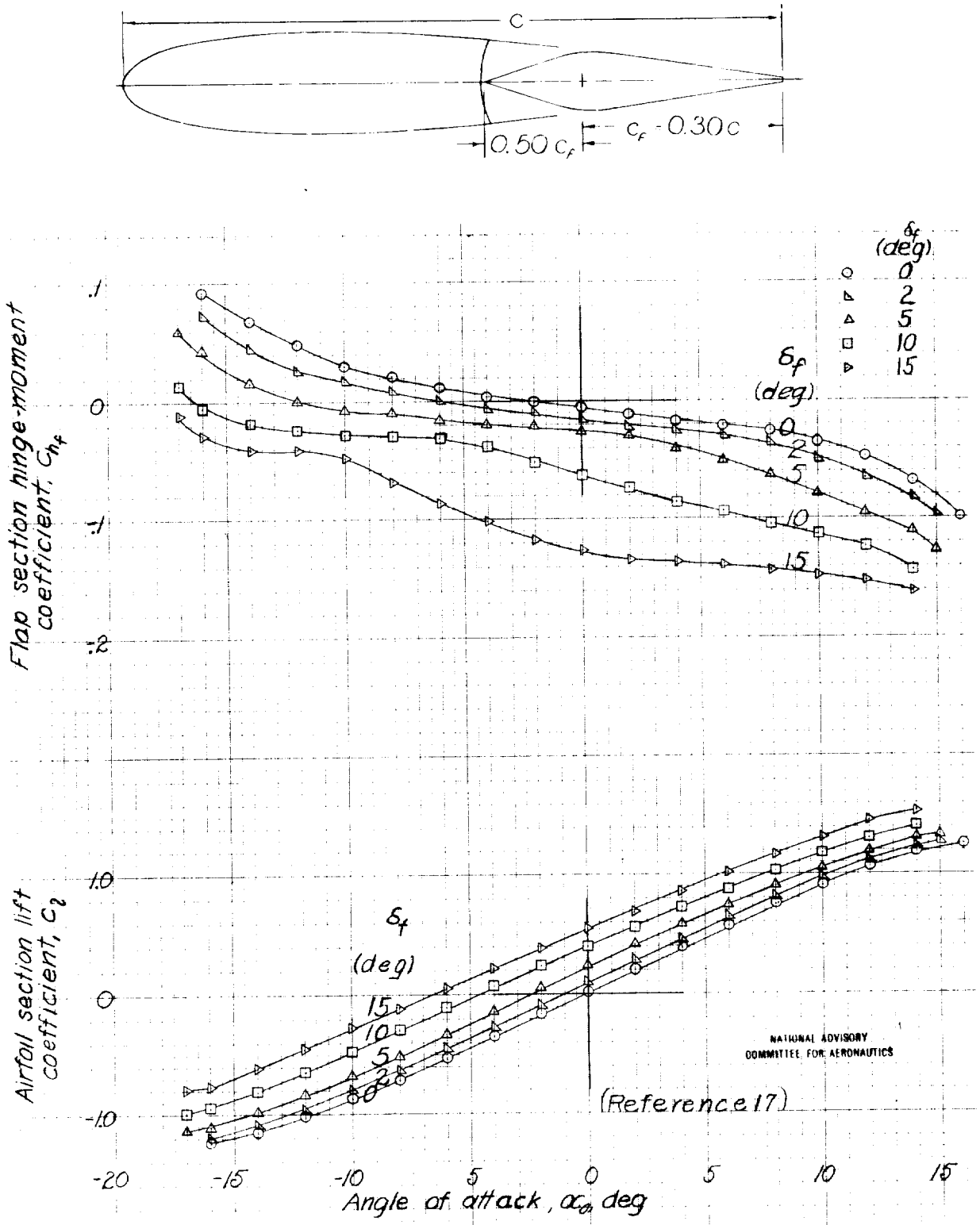

Figure 82.-NACA 0015 airfoil, 0.30c straight-contour flap, with 0.50c_f sharp-nose overhang, medium cover plate, 0.0023c gap.

L-663

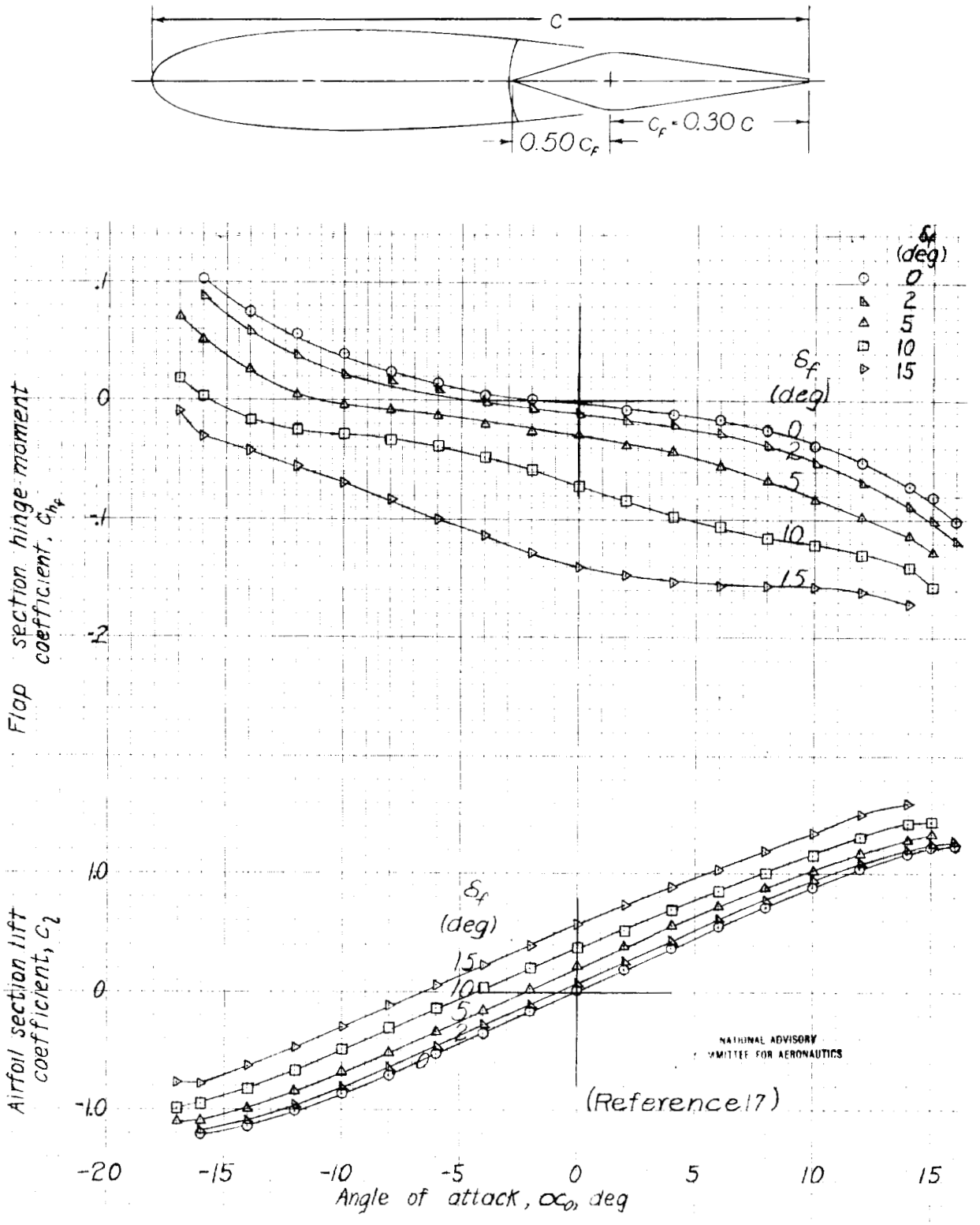

Figure 83.- NACA 0015 airfoil, 0.30c straight contour flap with 0.50 c_f sharp-nose overhang, medium cover plate, 0.005c gap.

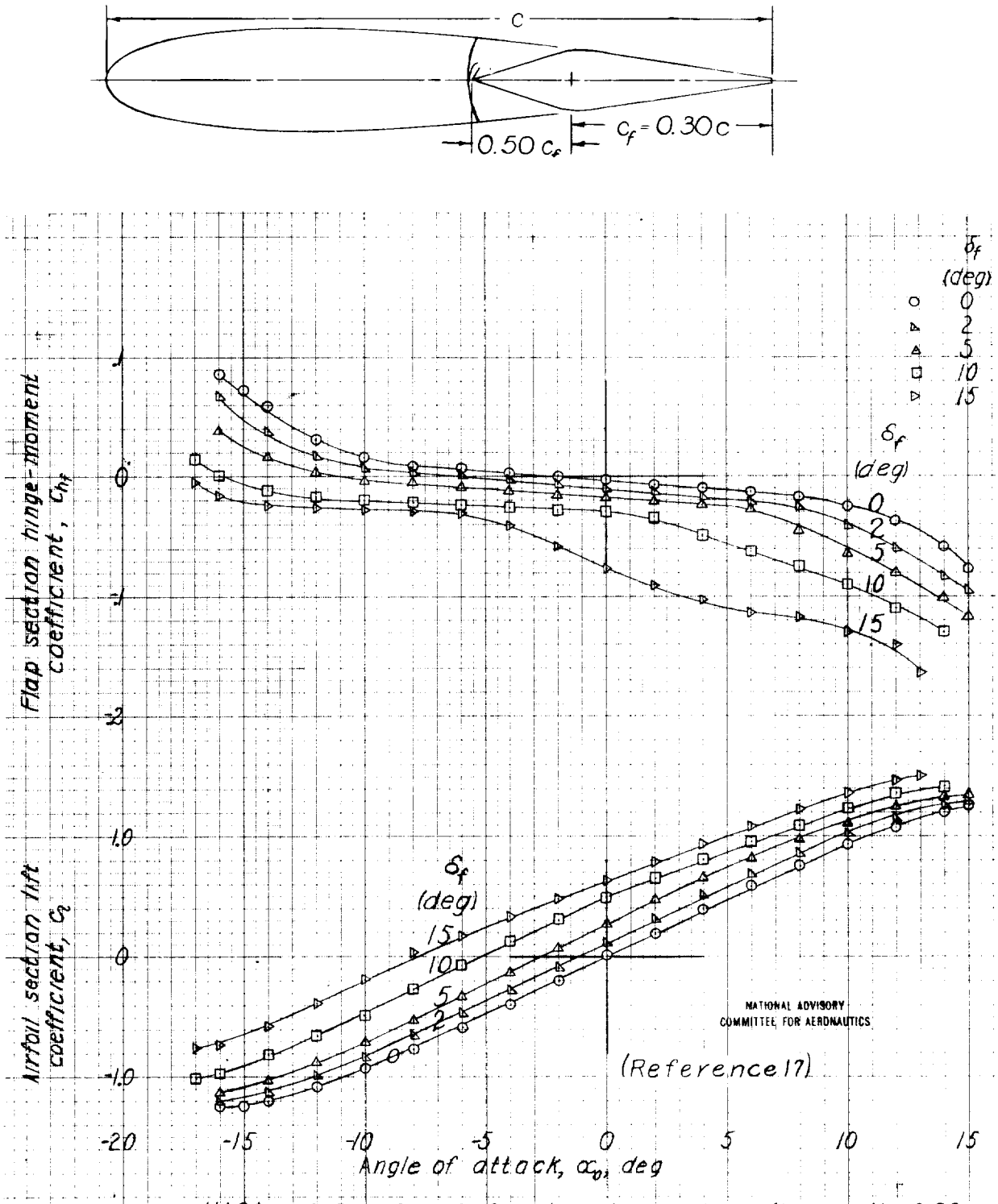

Figure 84.-NACA 0015 airfoil, 0.30c straight-contour flap with 0.50c_f sharp-nose overhang, large cover plate, sealed gap.

L-663

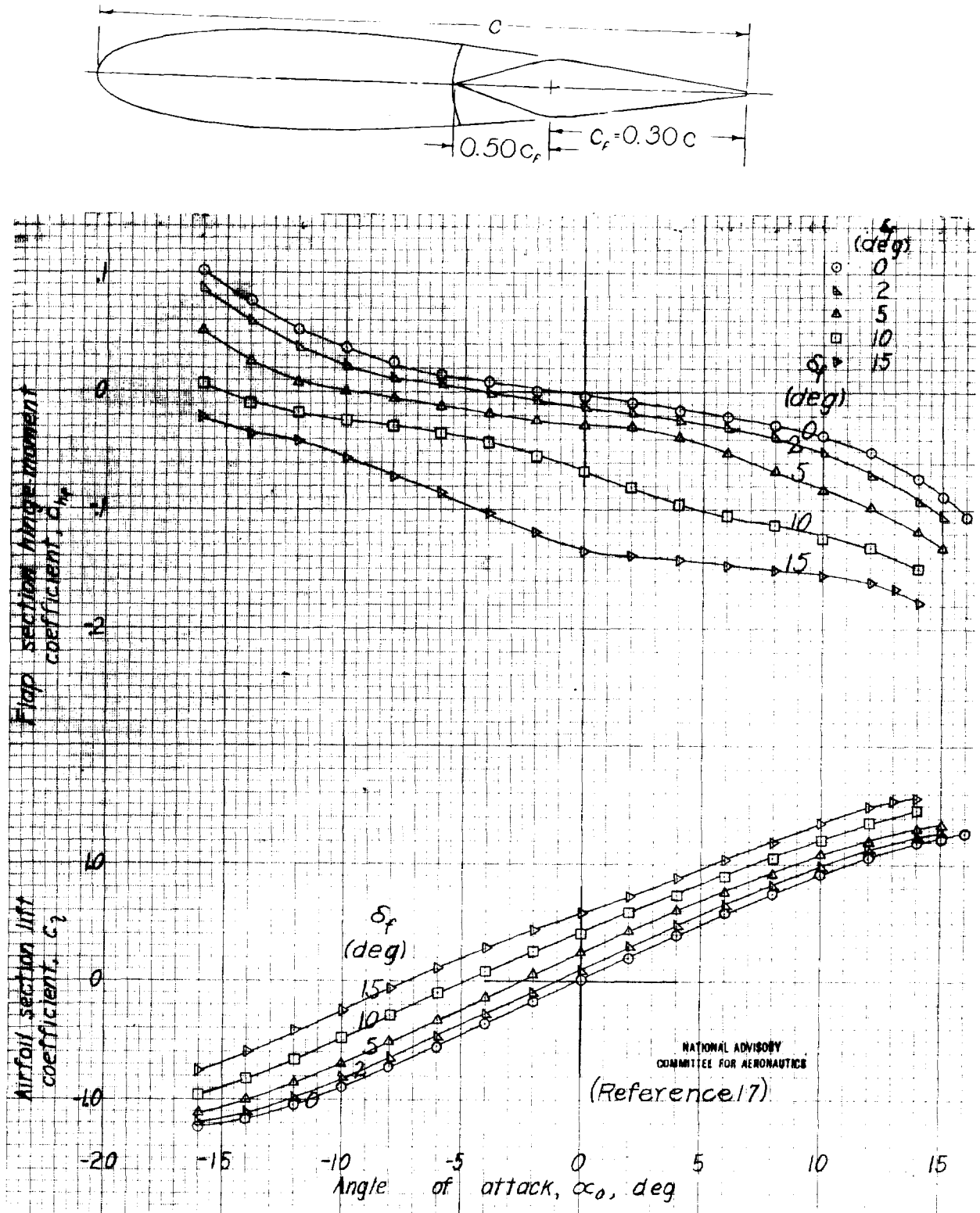

Figure 85.-NACA 0015 airfoil, 0.30c straight-contour flap with 0.50c_f sharp-nose overhang, large cover plate, 0.001lc gap.

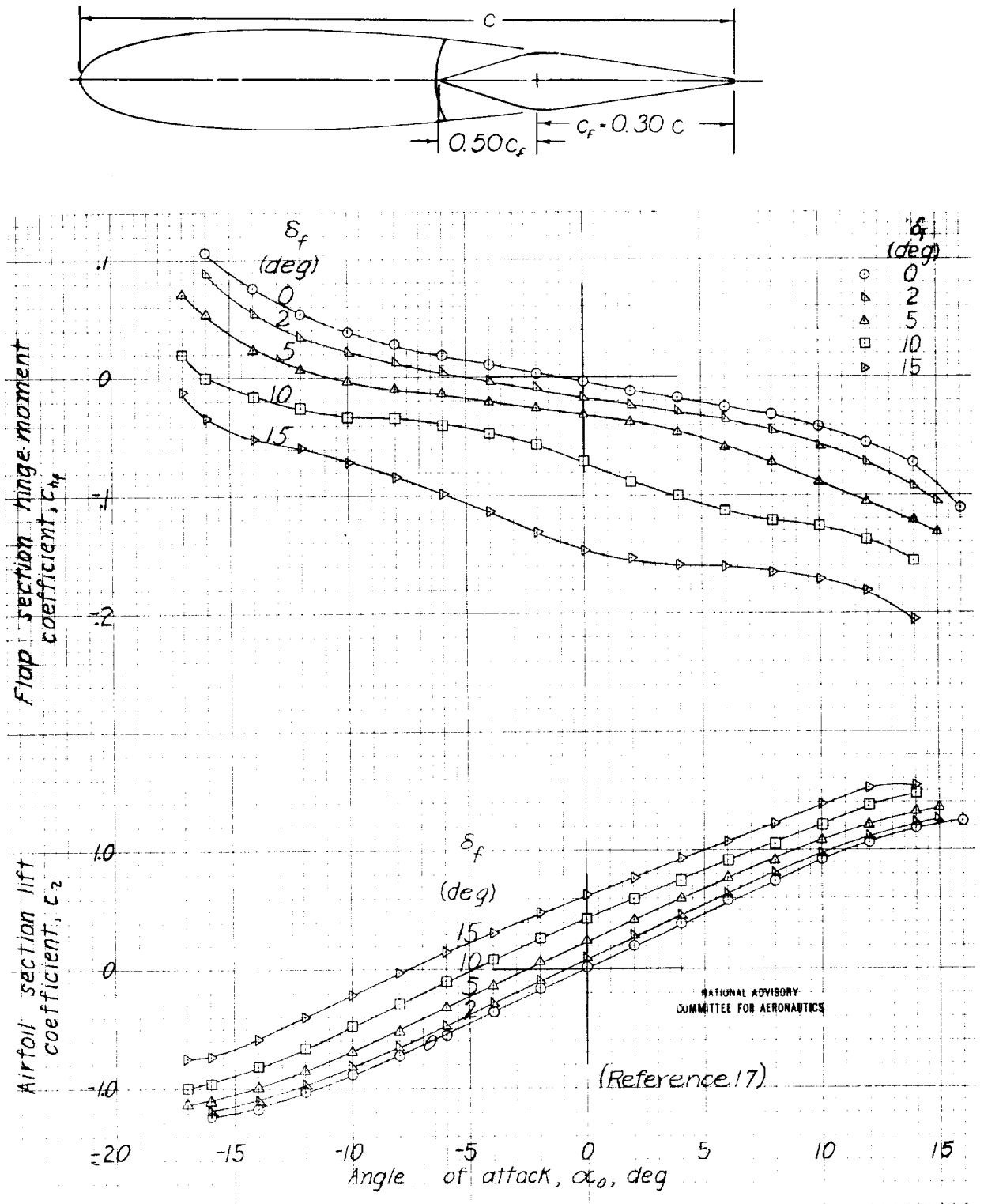

Figure 86.-NACA 0015 airfoil, 0.30c straight-contour flap with 0.50c_f sharp-nose overhang, large cover plate, 0.0023c gap.

L-663

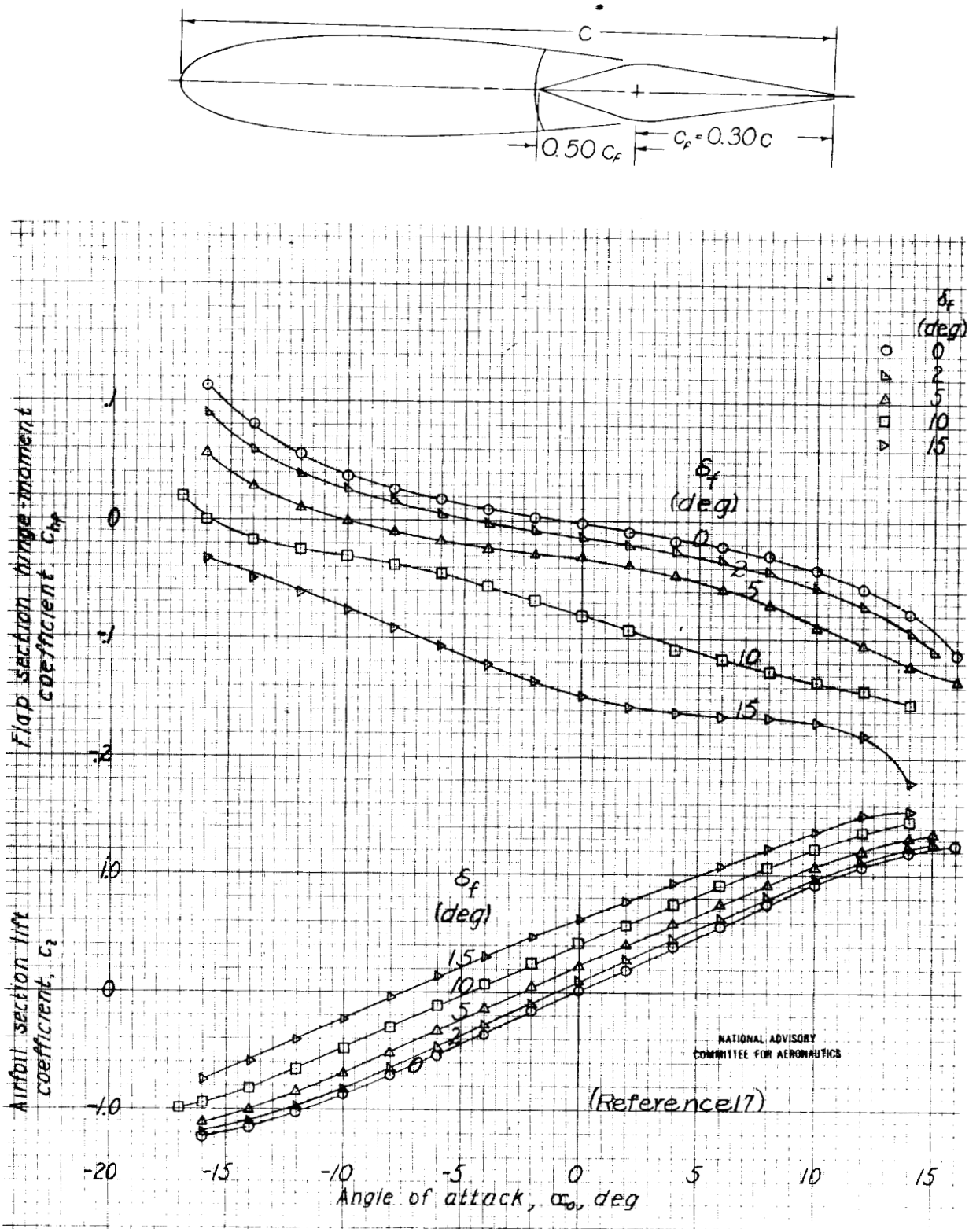

Figure 87.- NACA 0015 airfoil, 0.30c straight-contour flap with 0.50c_f sharp-nose overhang, large cover plate, 0.005c gap.

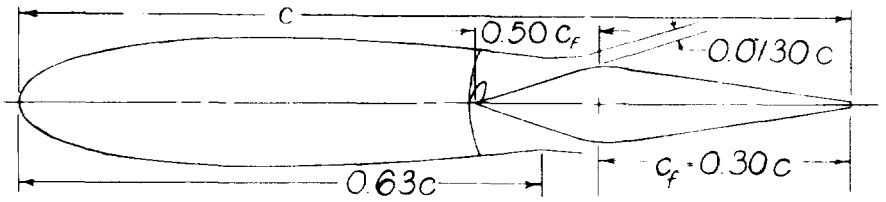

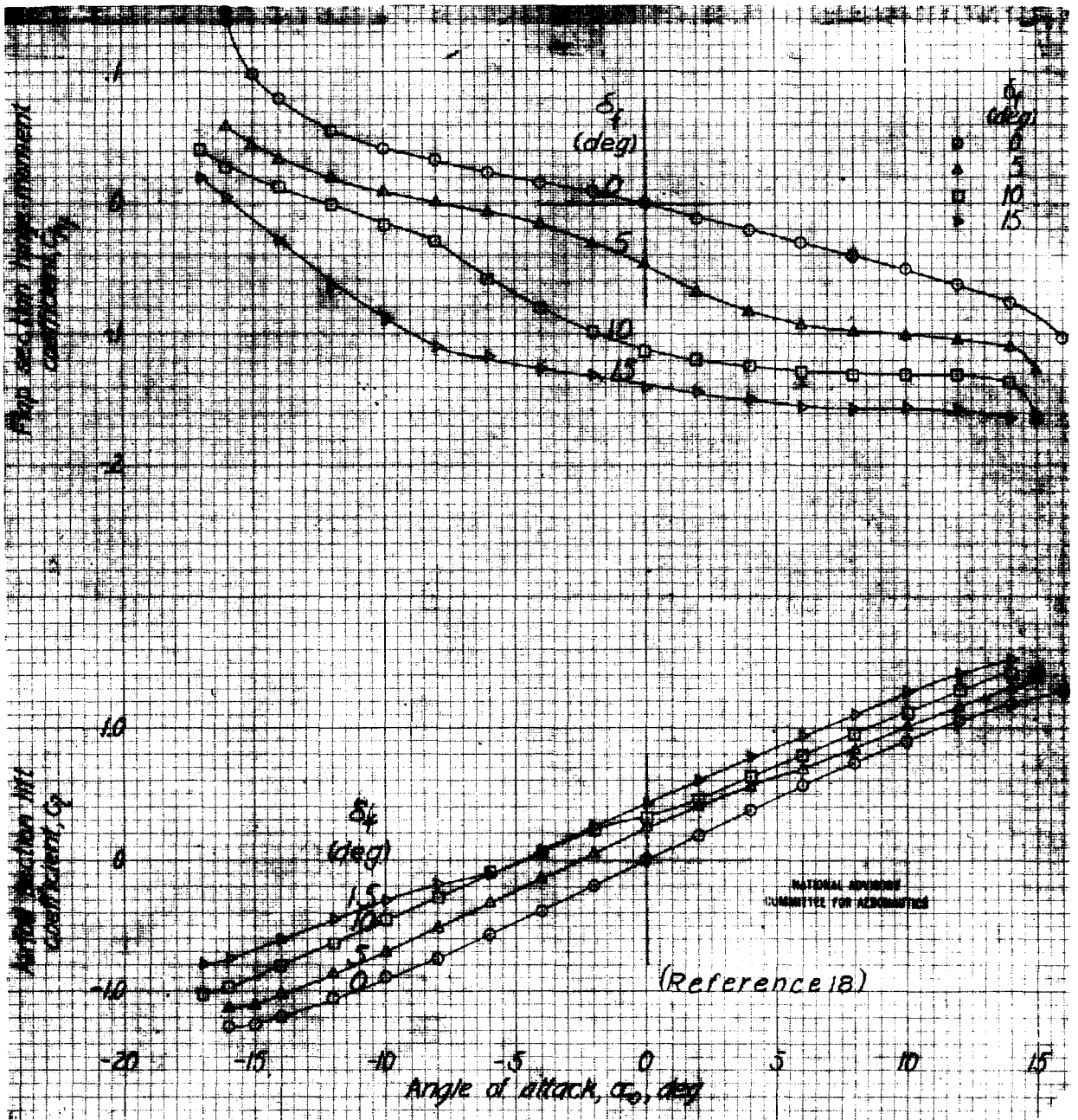

Figure 88.- NACA 0015 airfoil, 0.30c straight-camber flap with 0.50c_f internal balance, sealed gap, cover plate bent out at 0.629c station, vent size 0.0130c.

L-663

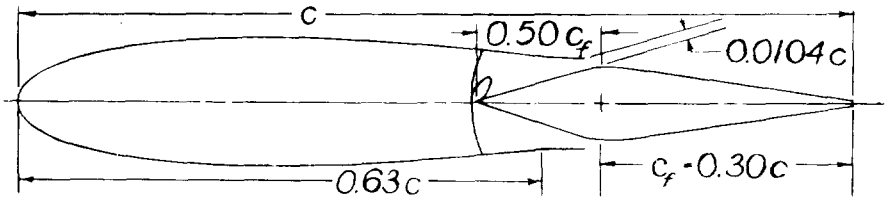

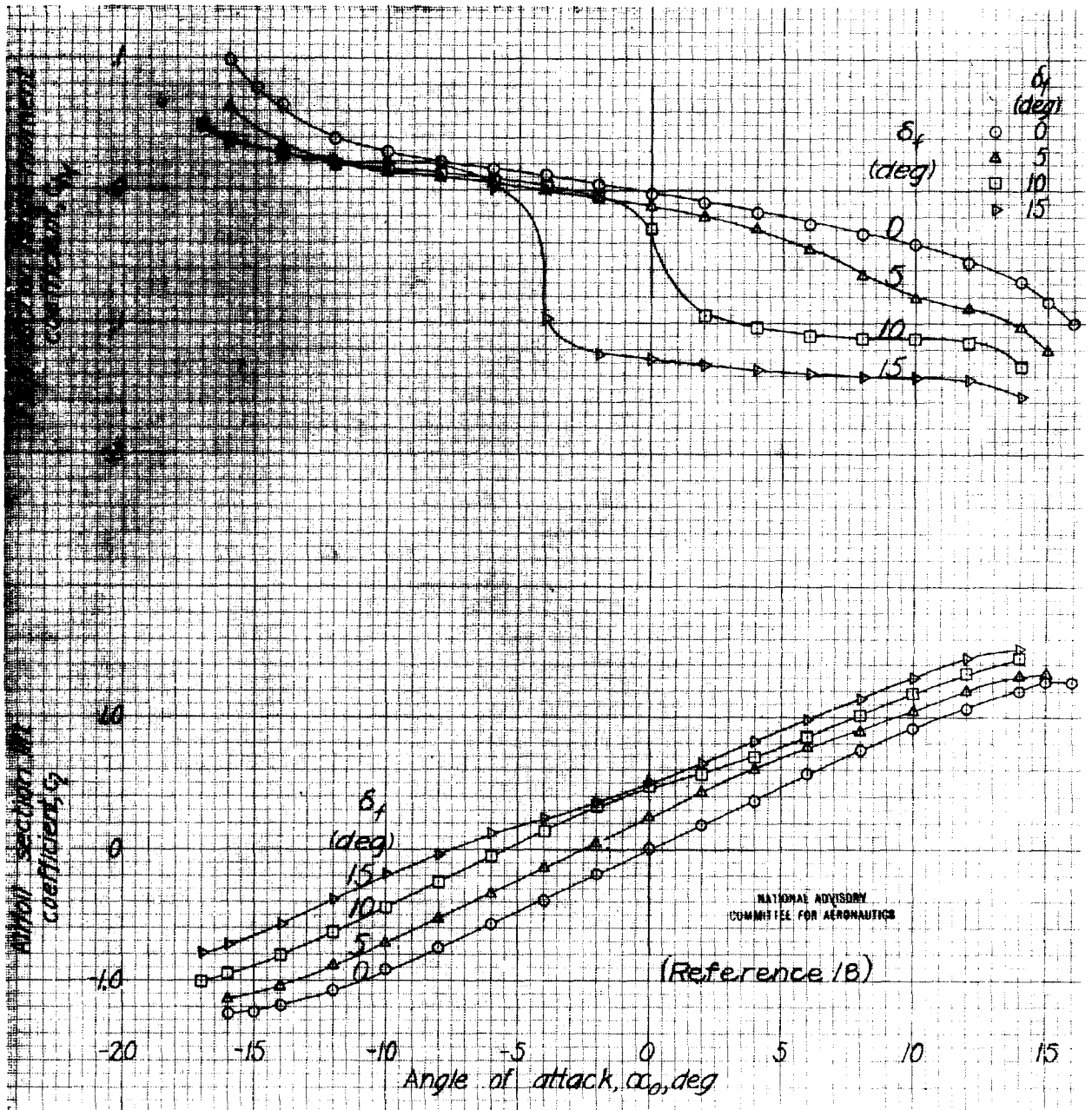

Figure 8.9.- NACA 0015 airfoil, 0.30c straight-contour flap with 0.50c_f internal balance, sealed gap, cover plate bent out at 0.629c station, vent size 0.0104c.

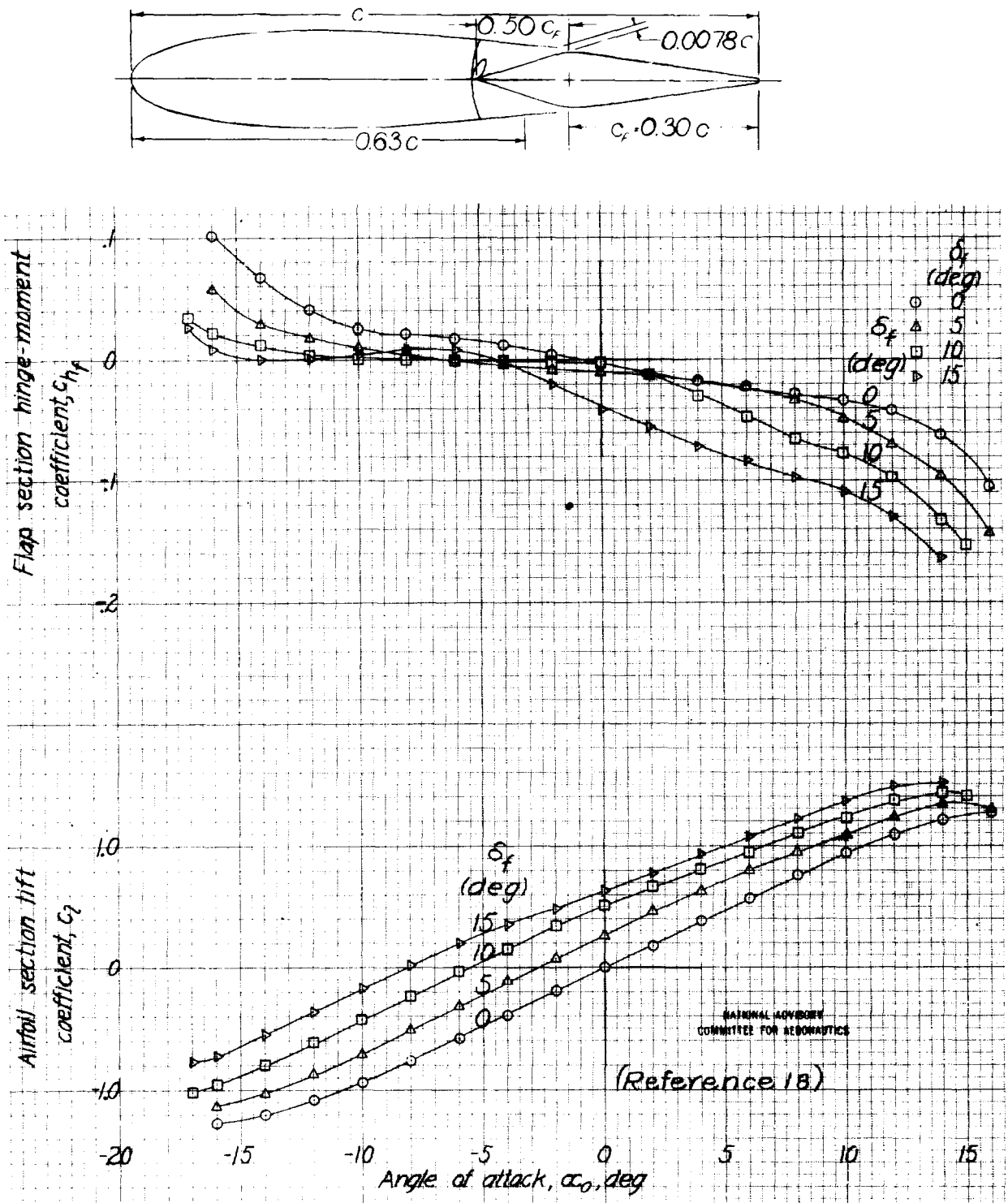

Figure 90.- NACA 0015 airfoil, 0.30c straight-contour flap with 0.50c_f internal balance sealed gap, cover plate bent out at 0.629c station, vent size 0.0078c.

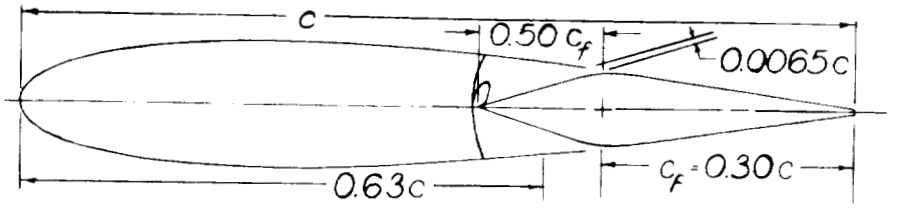

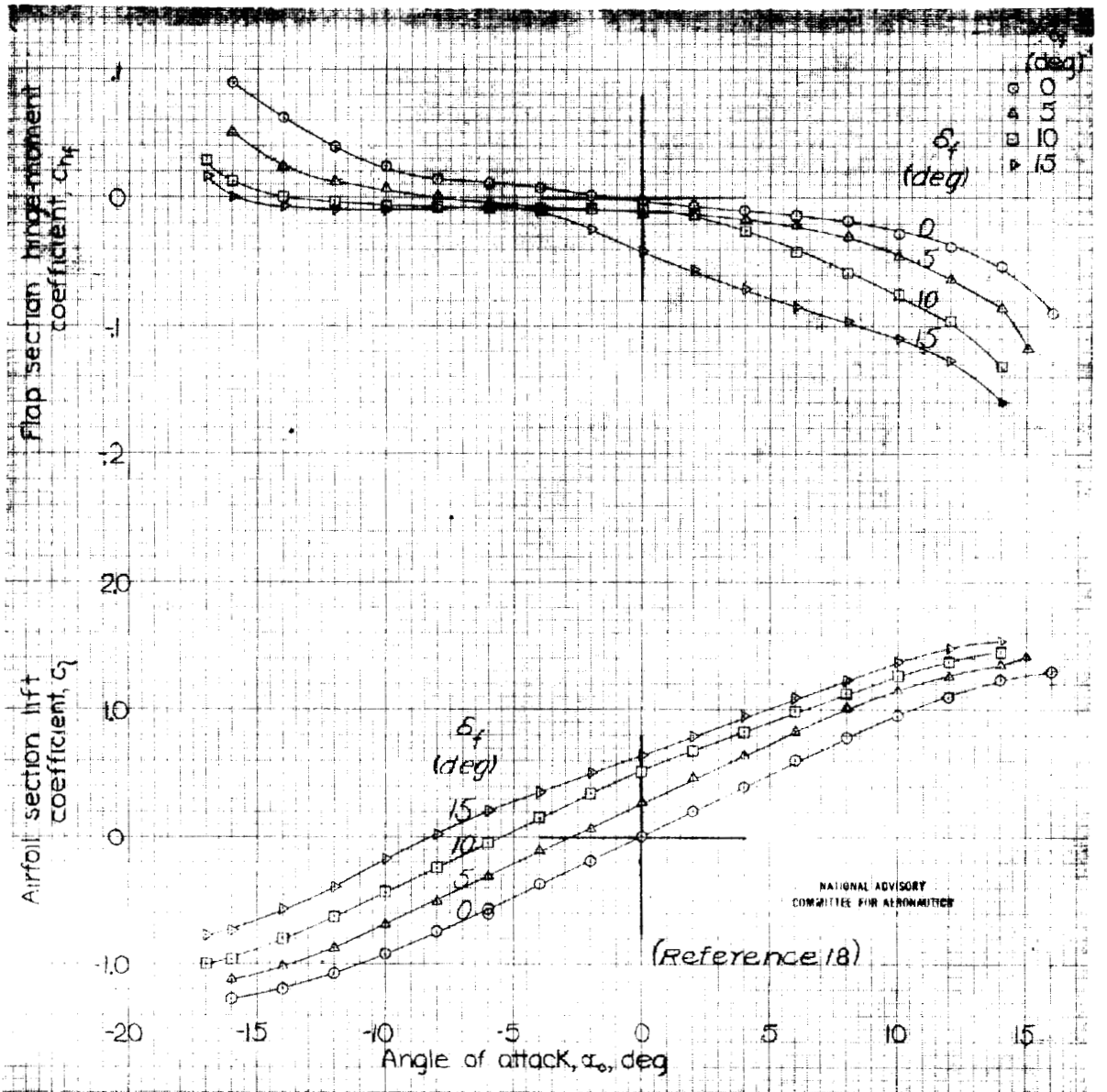

Figure 91.- NACA 0015 airfoil, 0.30c straight-contour flap with 0.50c_f internal balance, sealed gap, cover plate bent out at 0.628c station, vent size 0.0065c.

L-663

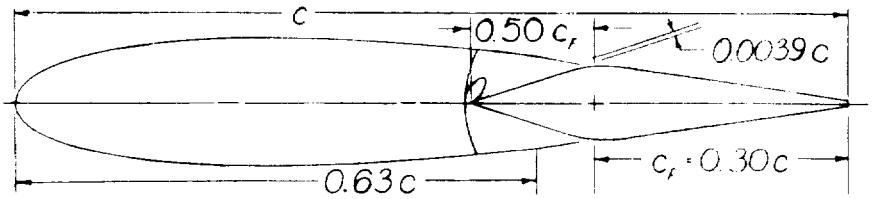

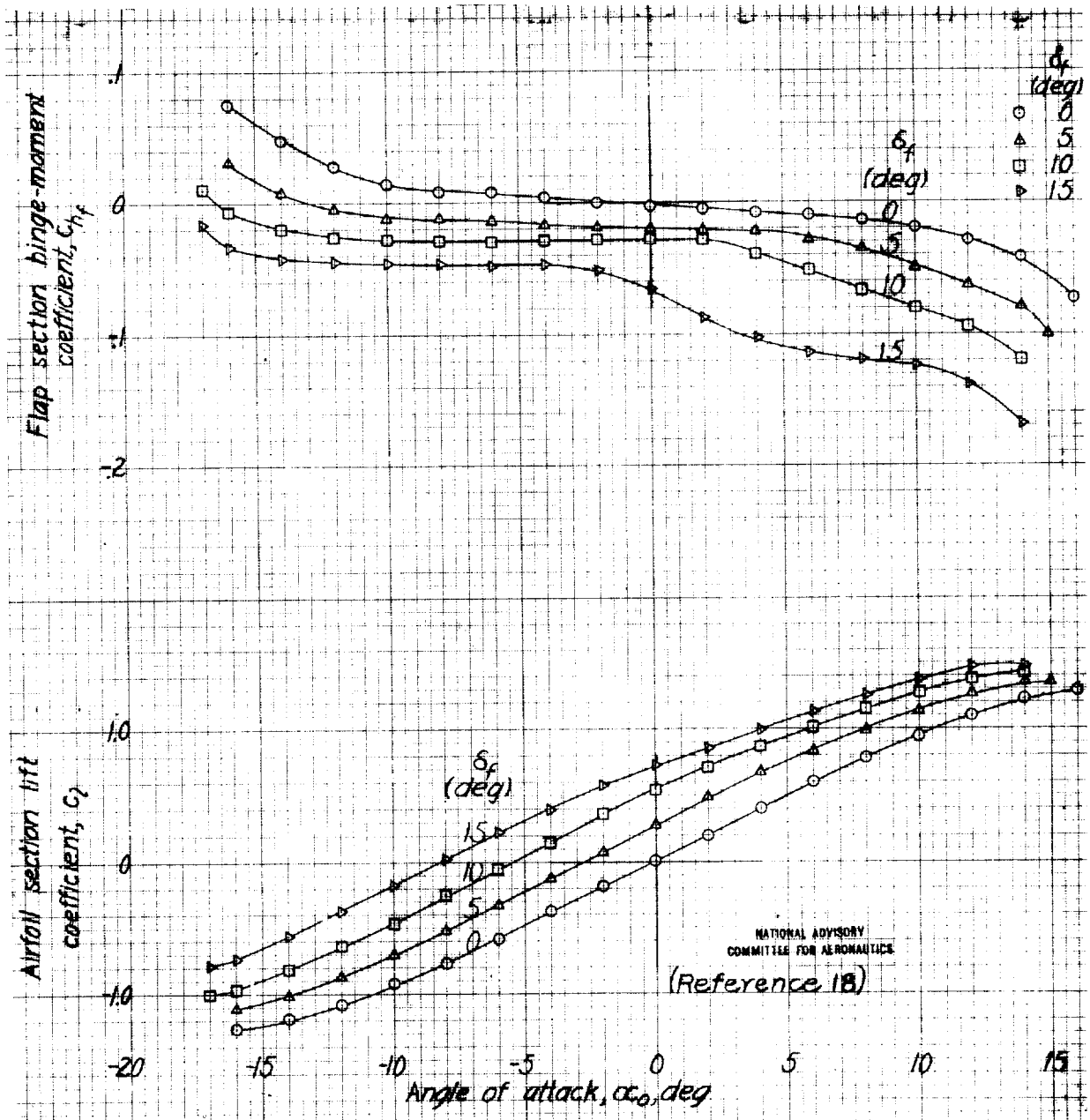

Figure 92.- NACA 0015 airfoil, 0.30c straight-contour flap with 0.50c_f internal balance, sealed gap, cover plate bent in at 0.629c station, vent size 0.0039c.

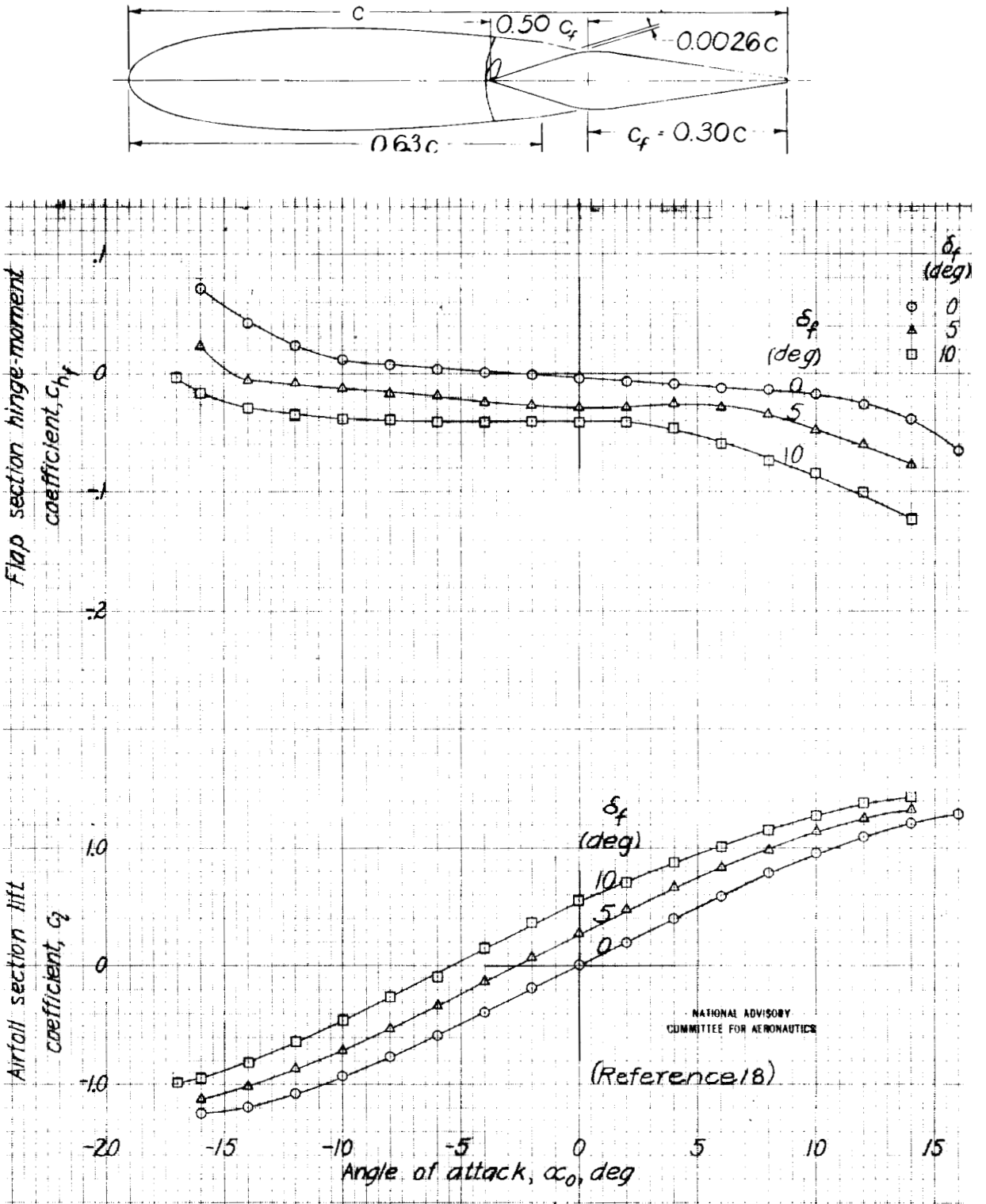

Figure 93.-NACA 0015 airfoil, 0.30c straight-contour flap with 0.50c_f internal balance, sealed gap, cover plate bent in at 0.629c station, vent size 0.0026c.

L-663

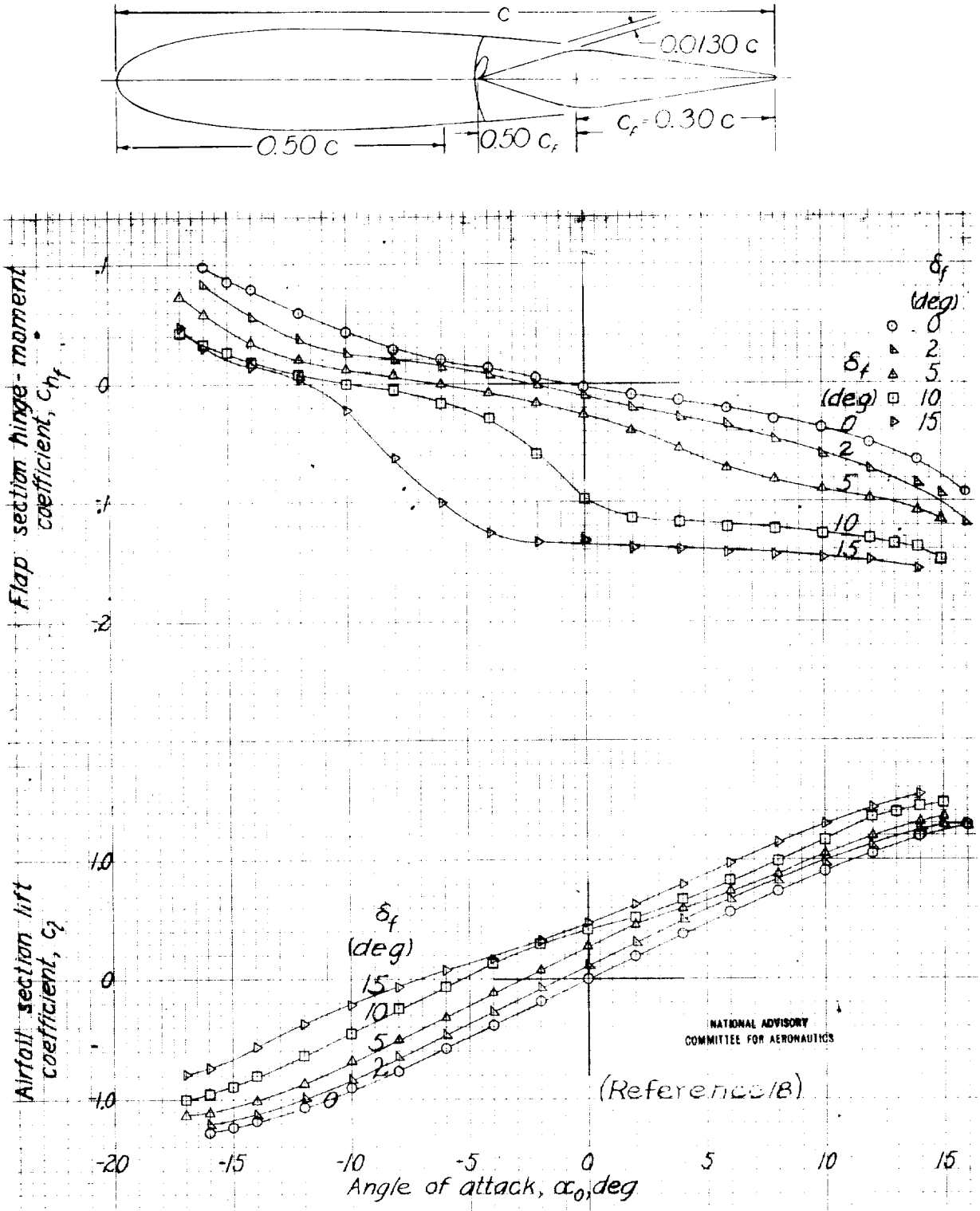

Figure 94.-NACA 0015 airfoil, 0.30c straight-contour flap with 0.50 c_f internal balance, sealed gap, cover plate bent out at 0.50c station, vent size 0.0130c.

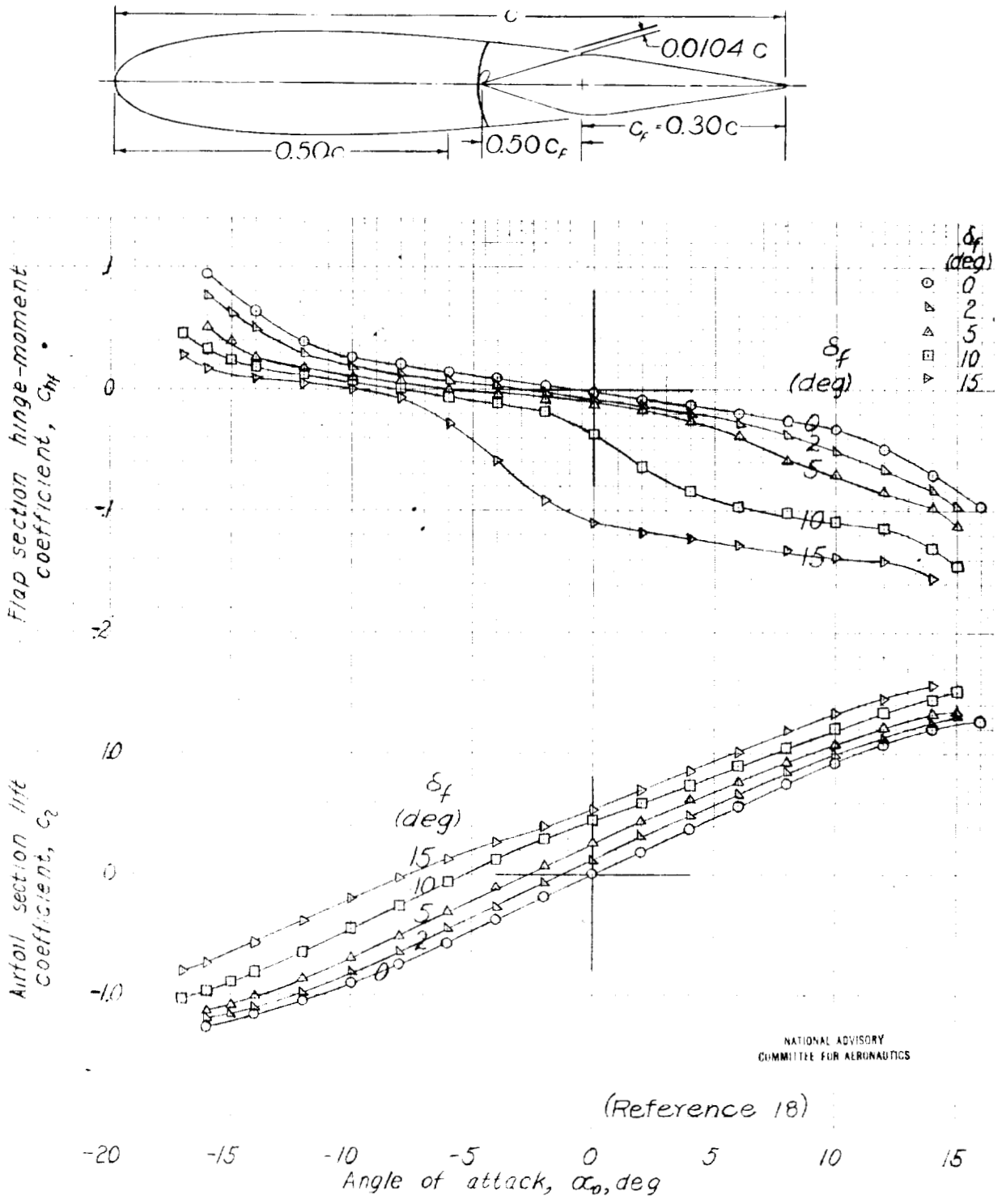

Figure 95. NACA 0015 airfoil, 0.30c straight-contour flap with 0.50c_f internal balance, sealed gap, cover plate bent out at 0.50c station; vent size 0.01046c.

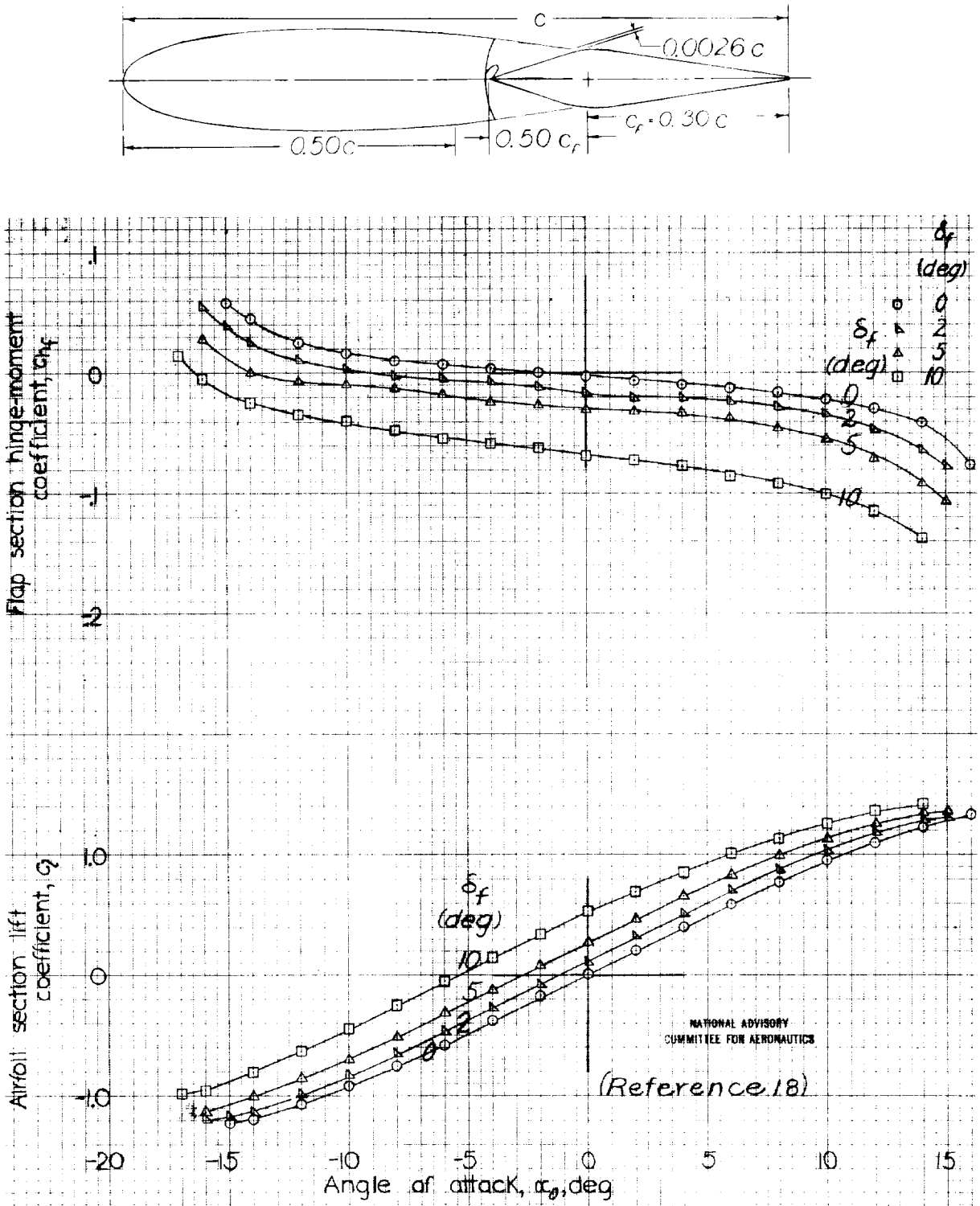

Figure 96.- NACA 0015 airfoil, 0.30c straight-contour flap with 0.50c_f internal balance, sealed gap, cover plate bent in at 0.50c station, vent size 0.0026c.

L-663

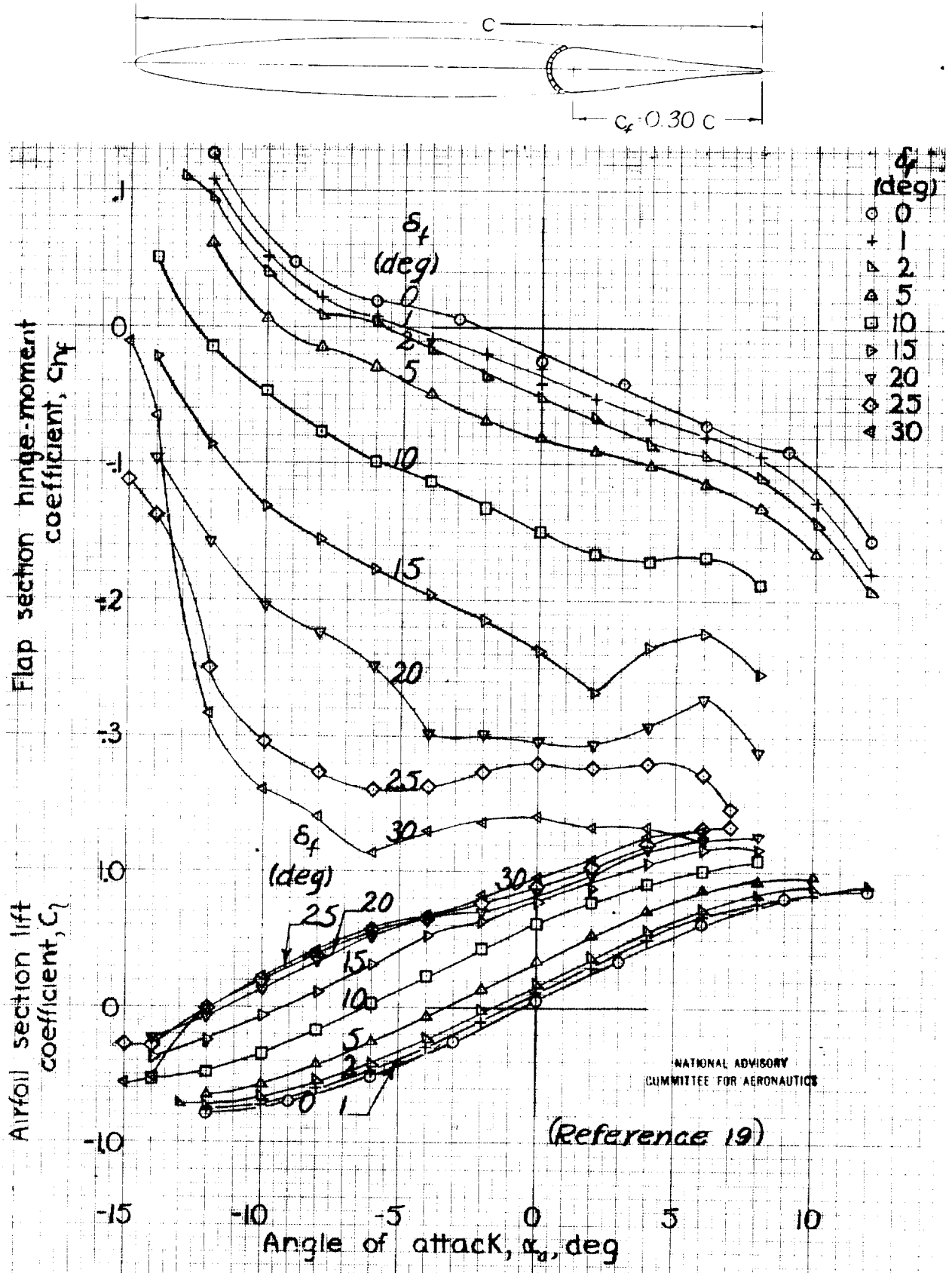

Figure 97.- NACA 66-009 airfoil, 0.30c plain flap, sealed gap.

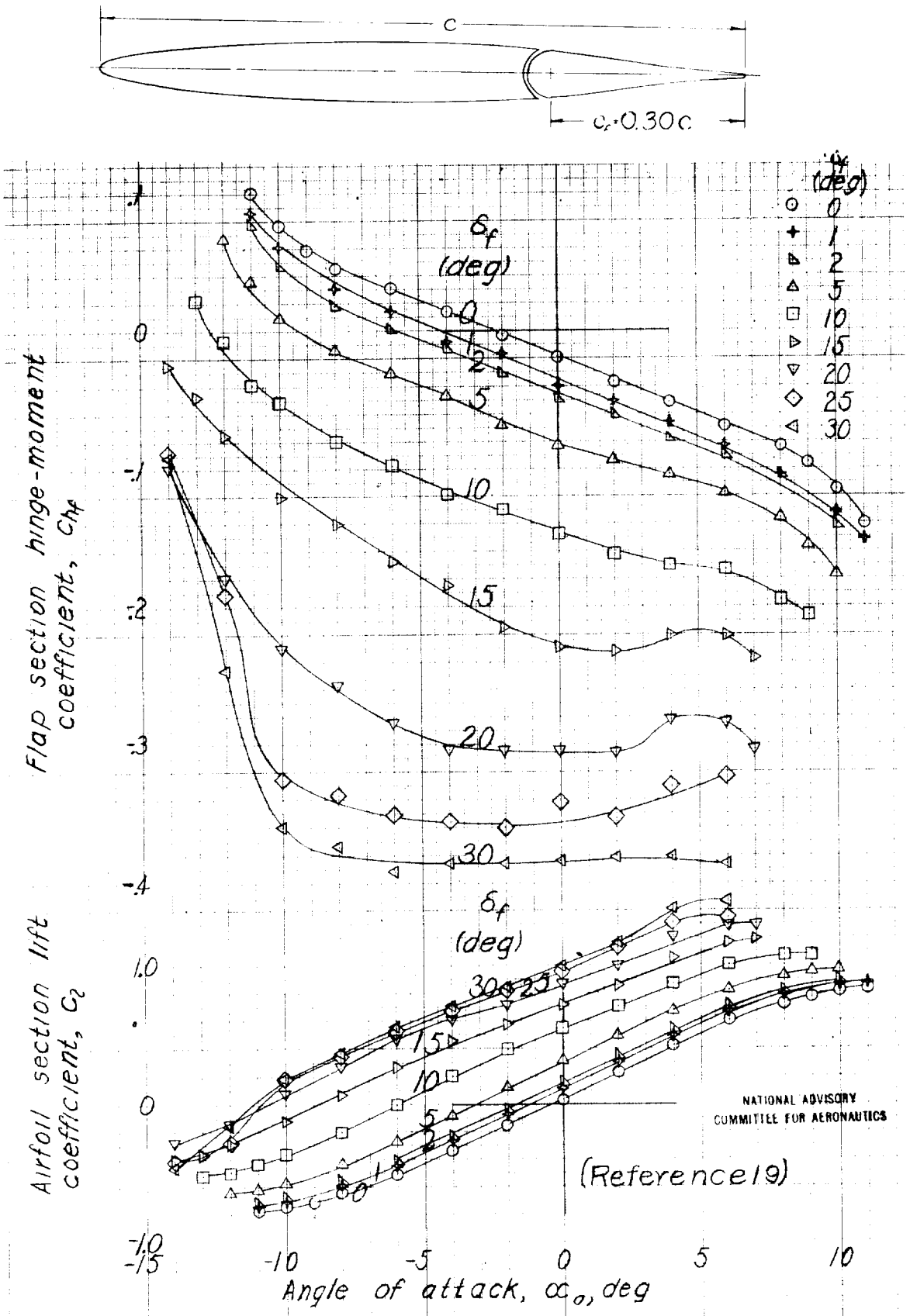

Figure 98.-NACA 66-009 airfoil, 0.30c plain flap, 0.005c gap.

L-663

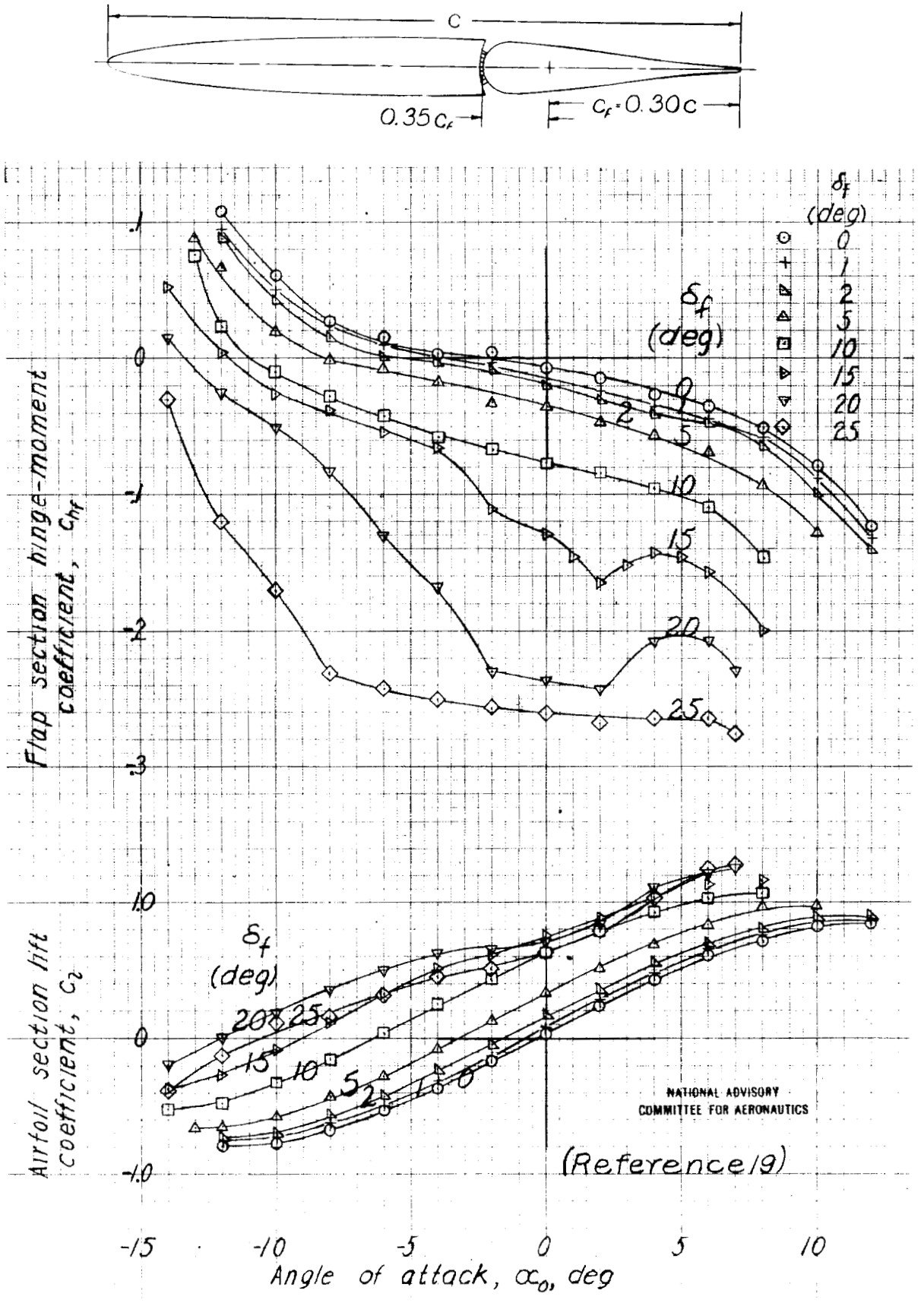

Figure 99.- NACA 66-009 airfoil, 0.30c flap with 0.35c_f blunt-nose overhang, sealed gap.

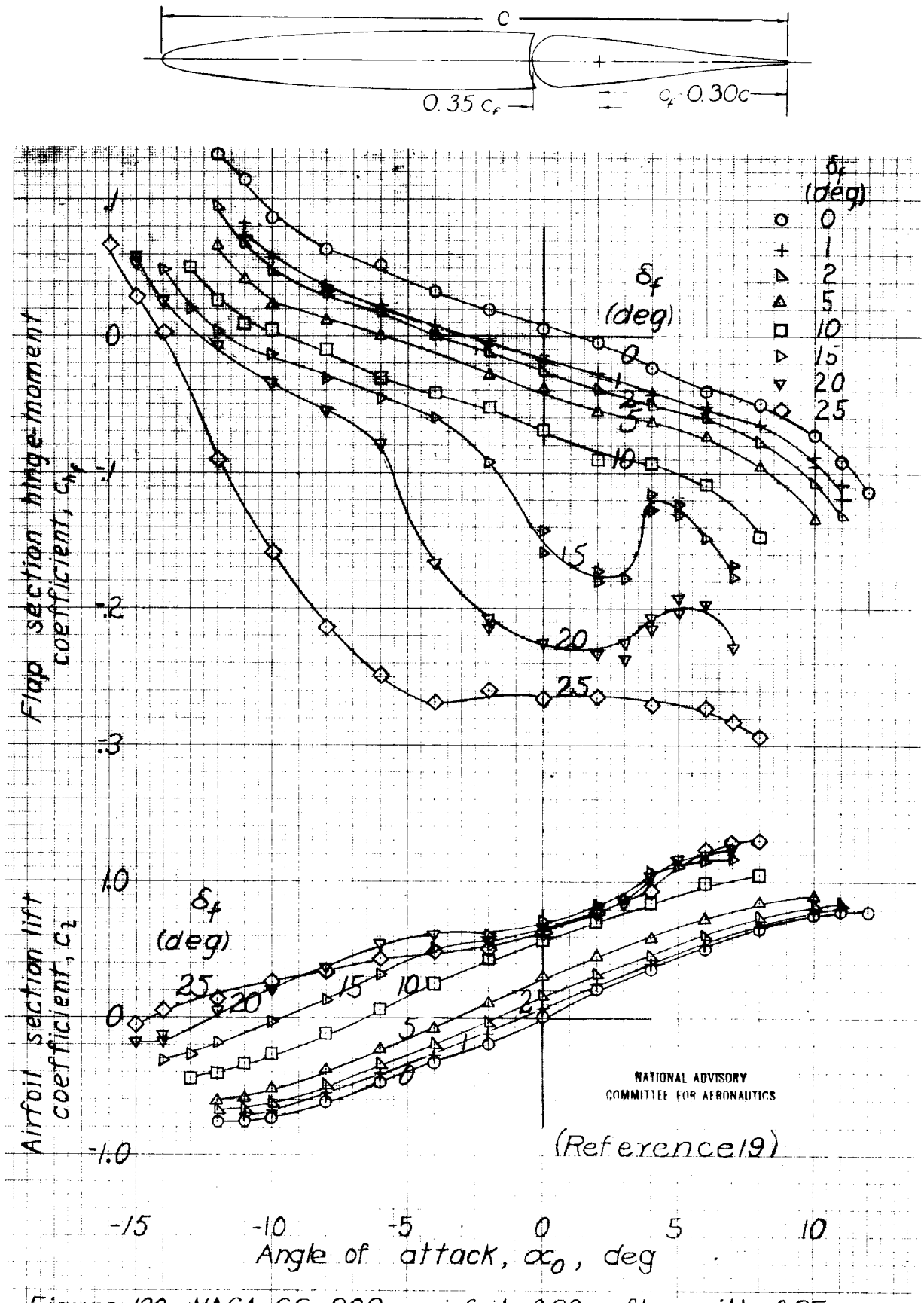

Figure 100.- NACA 66-009 airfoil, 0.30c flap with 0.35c_f blunt-nose overhang, 0.005c gap.

L-663

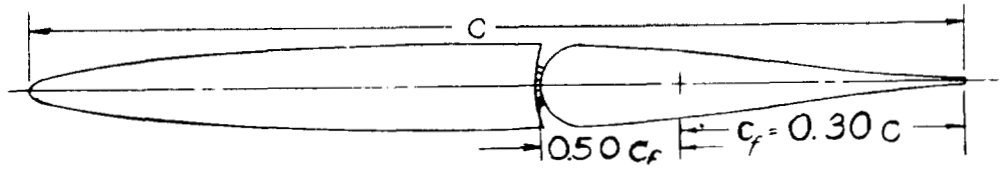

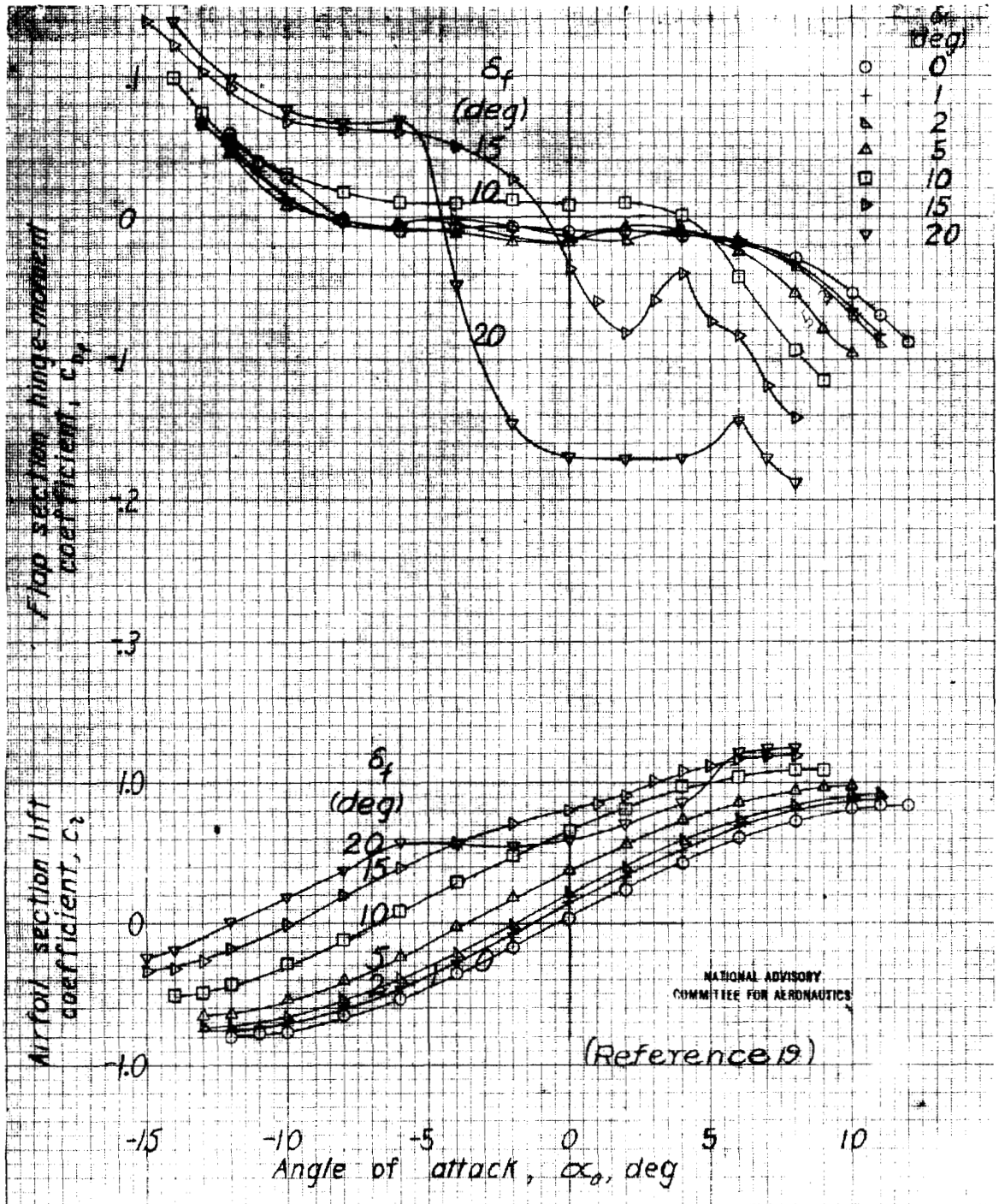

Figure 101.- NACA 66-009 airfoil, 0.30c flap with 0.50c_f blunt-nose overhang, sealed gap.

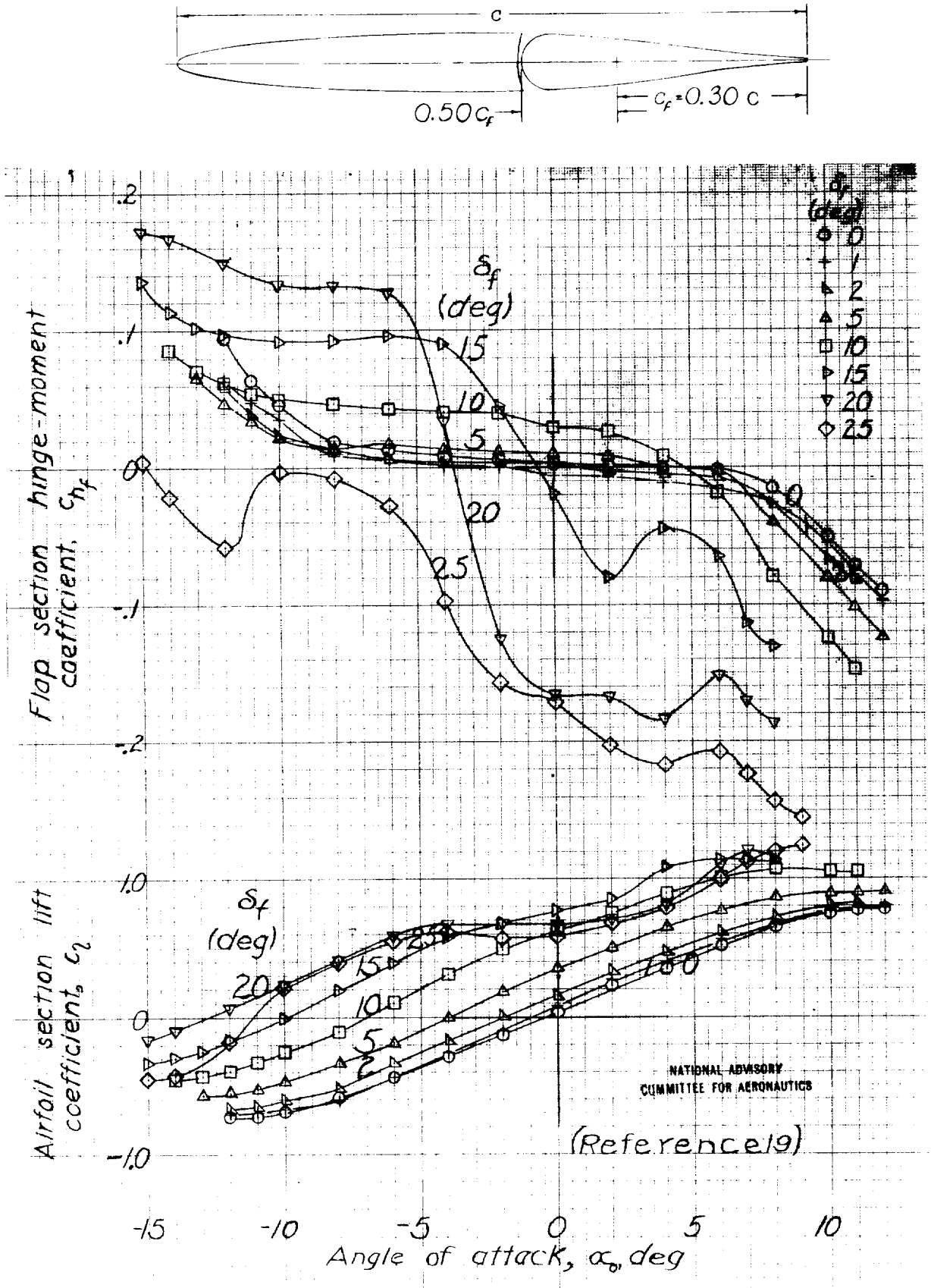

Figure 102.- NACA 66-009 airfoil, 0.30c flap with 0.50c_f blunt-nose overhang, 0.005c gap

L-663

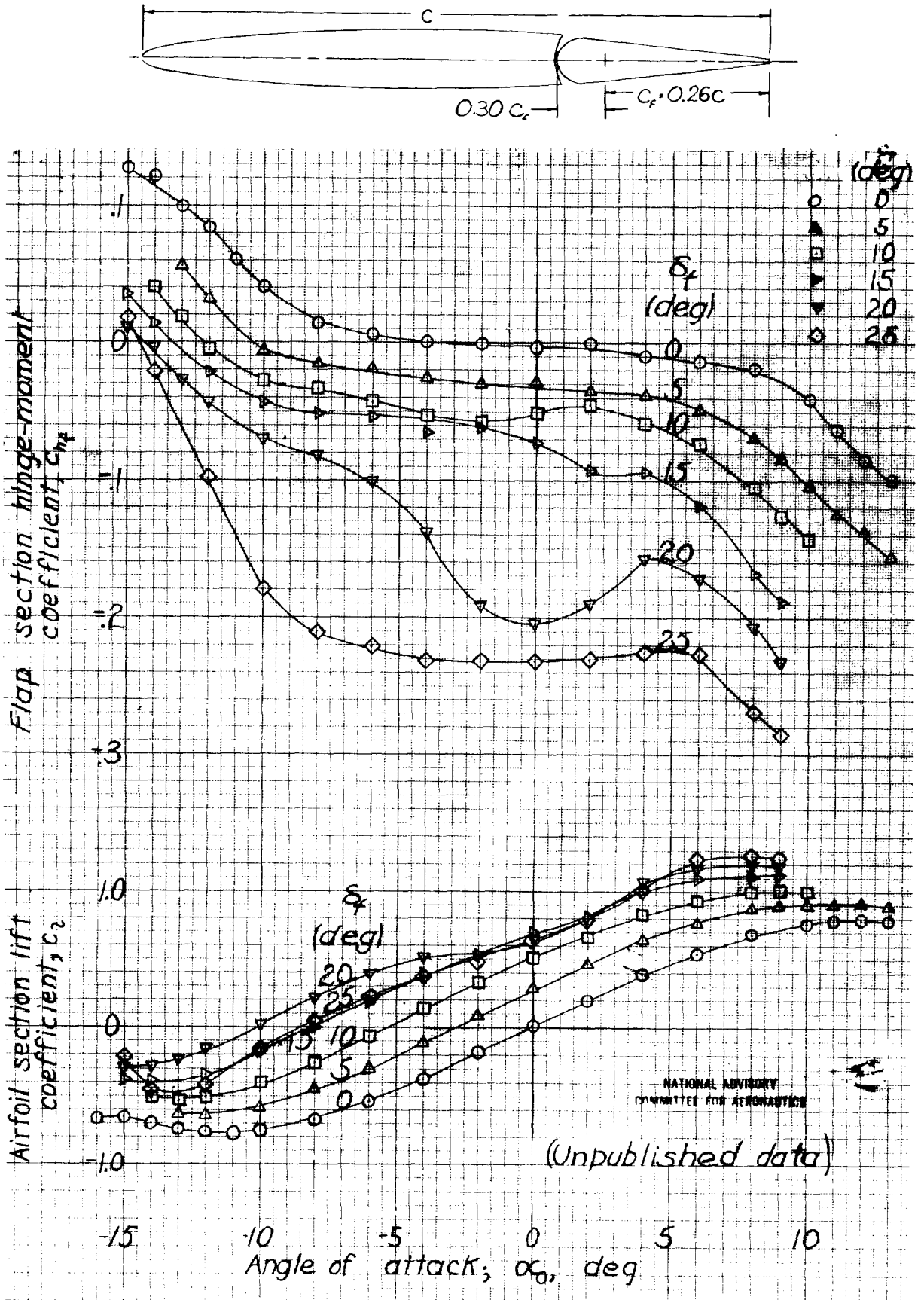

Figure 103-NACA 66-009 airfoil, 0.26c straight-contour flap with 0.30c_f blunt-nose overhang, sealed gap.

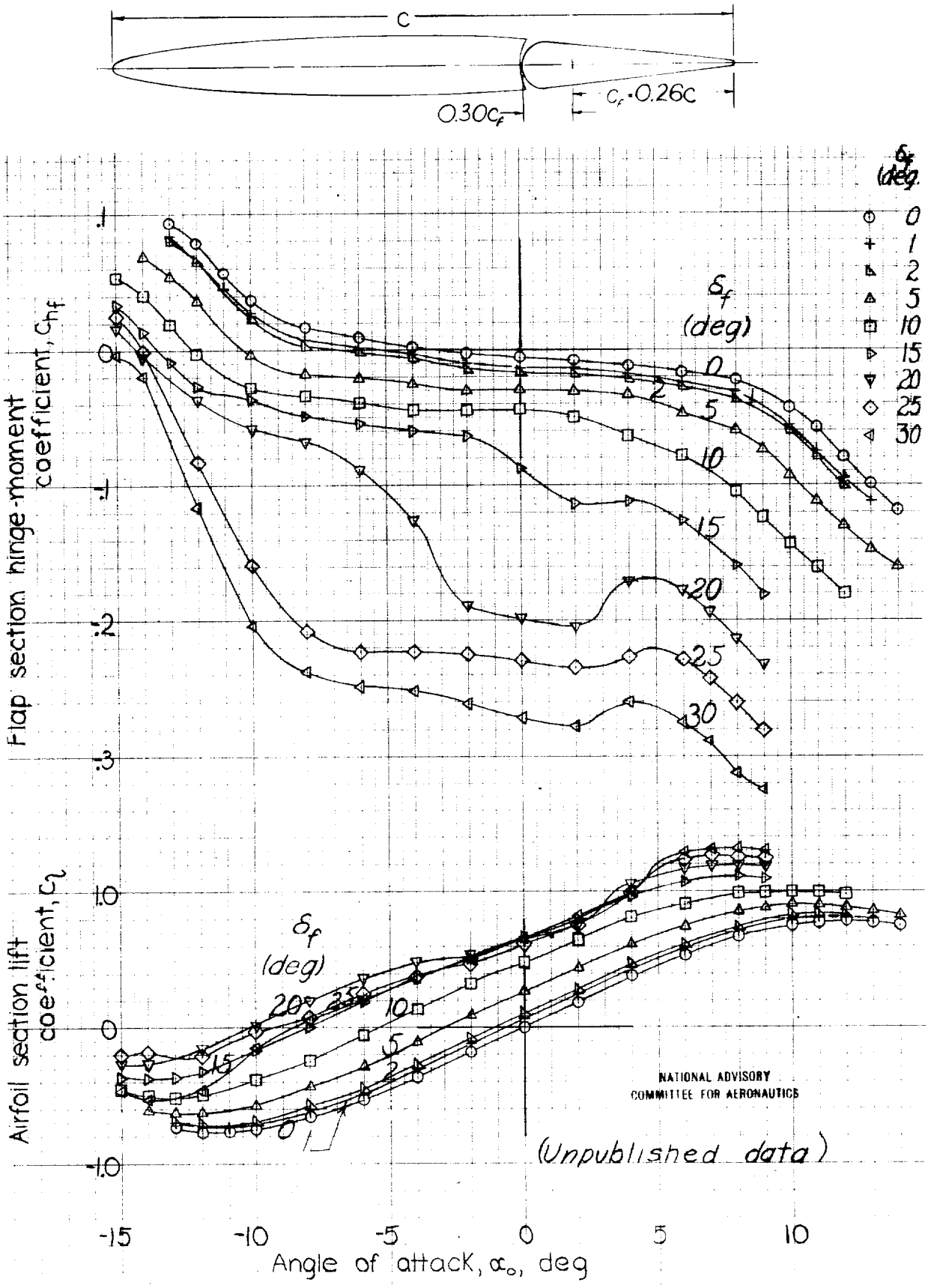

Figure 104.-NACA 66-009 airfoil, 0.26c straight-contour flap with $0.30c_f$ blunt-nose overhang, 0.001c gap.

L-663

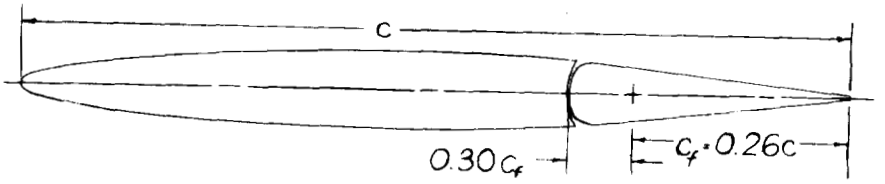

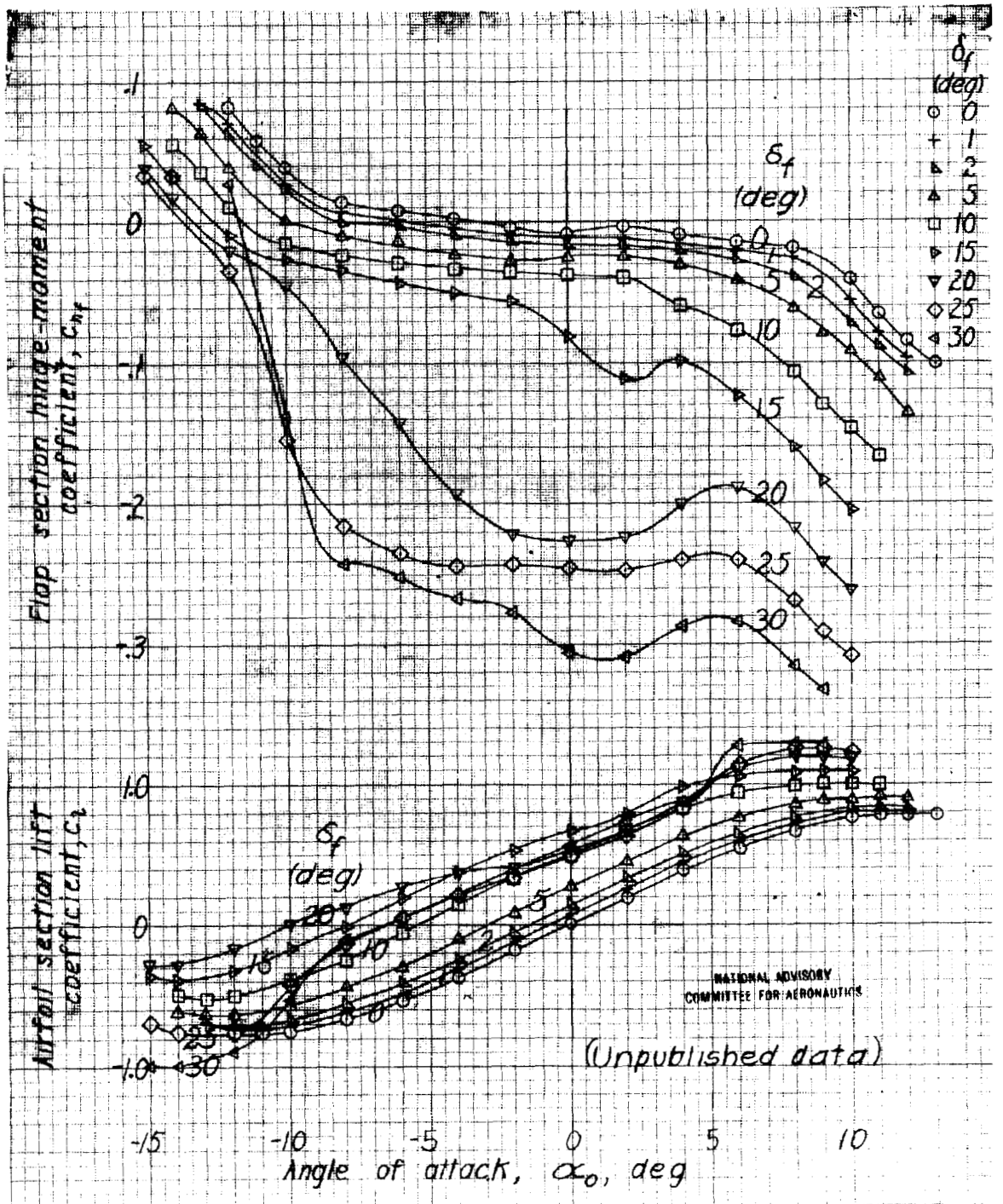

Figure 105.-NACA 66-009 airfoil, 0.26c straight-contour flap with 0.30c_f modified blunt-nose overhang, 0.001c gap

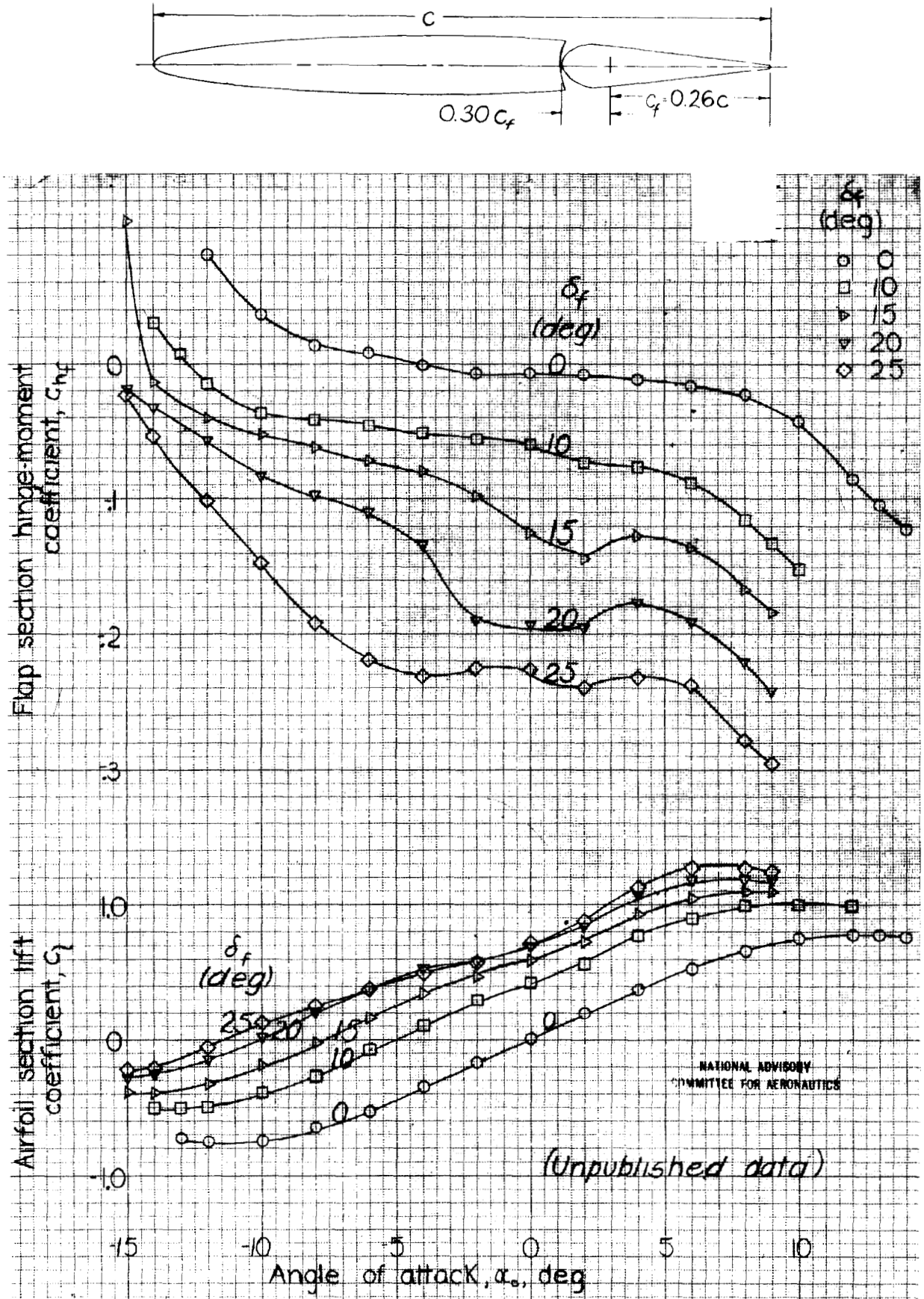

Figure 106.-NACA 66-009 airfoil, 0.26c straight-contour flap with 0.30c_f medium-nose overhang, 0.001c gap.

L-663

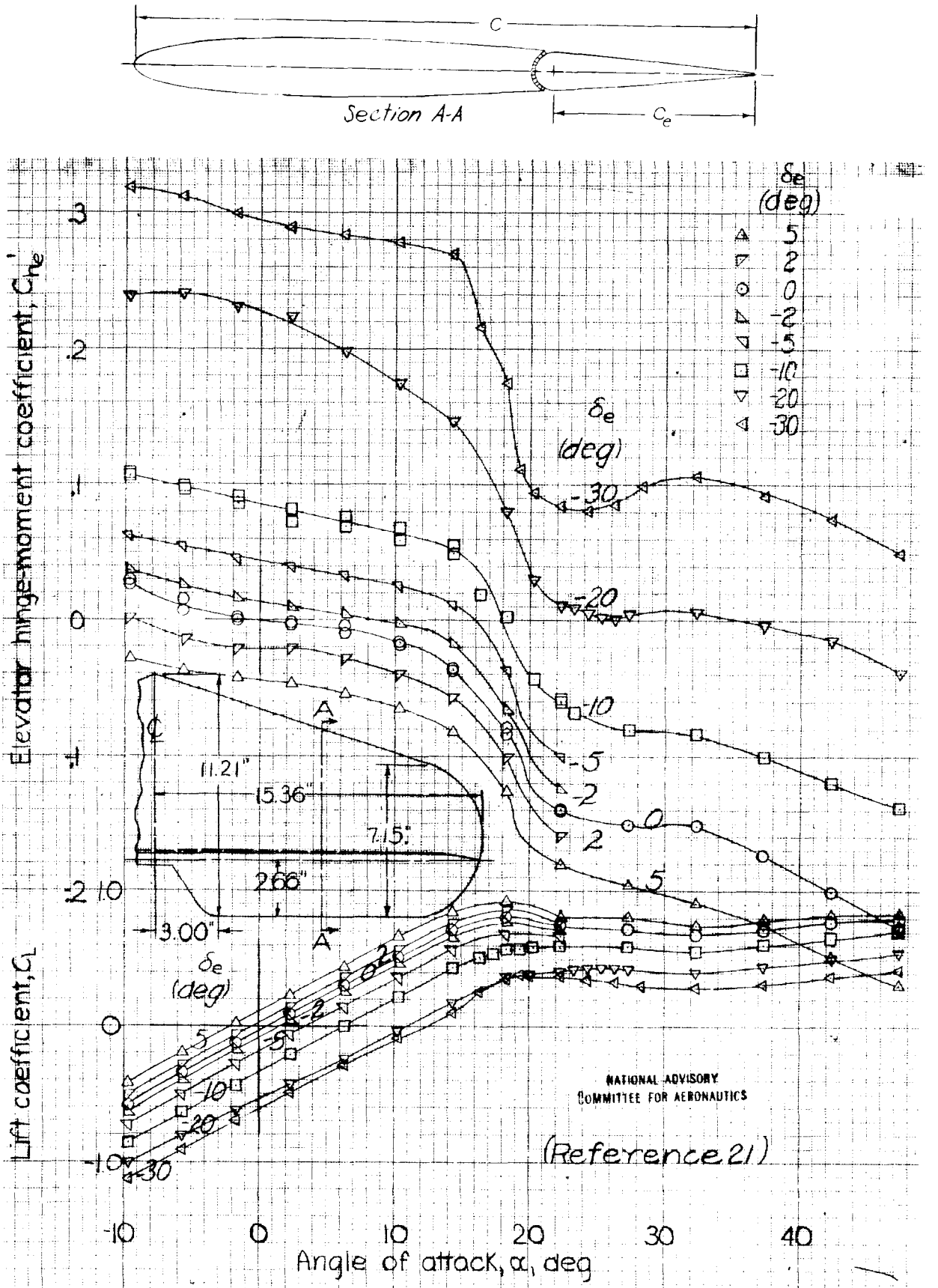

Figure 107.- Unbalanced elevator on pursuit fuselage, NACA 0009 airfoil section, $S_e/S = 0.27$, $A = 3.7$, sealed gap.

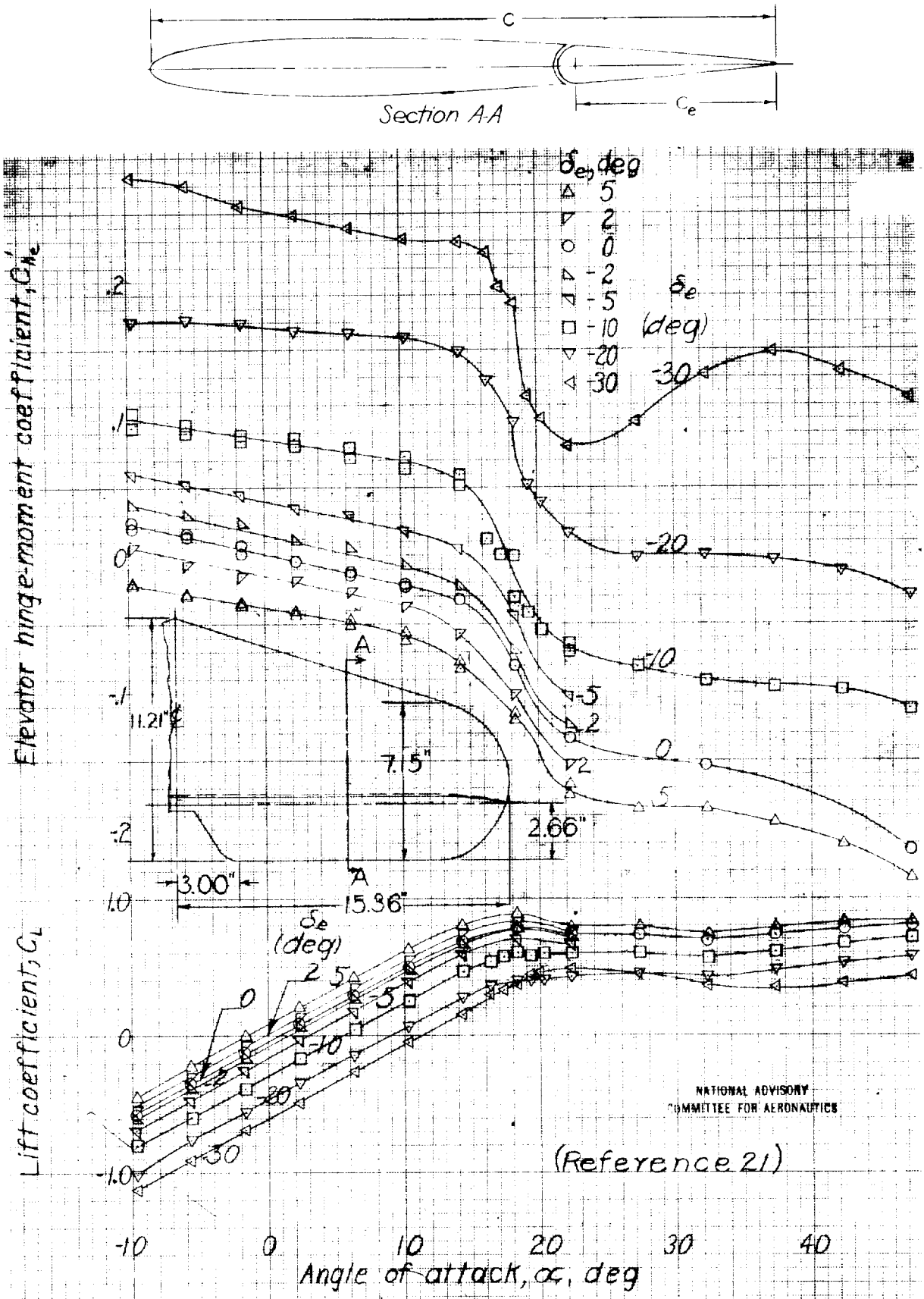

Figure 108.- Unbalanced elevator on pursuit fuselage, NACA 0009 airfoil section, $S_e/S = 0.27$, $A = 3.7$, 0.005c gap.

L-663

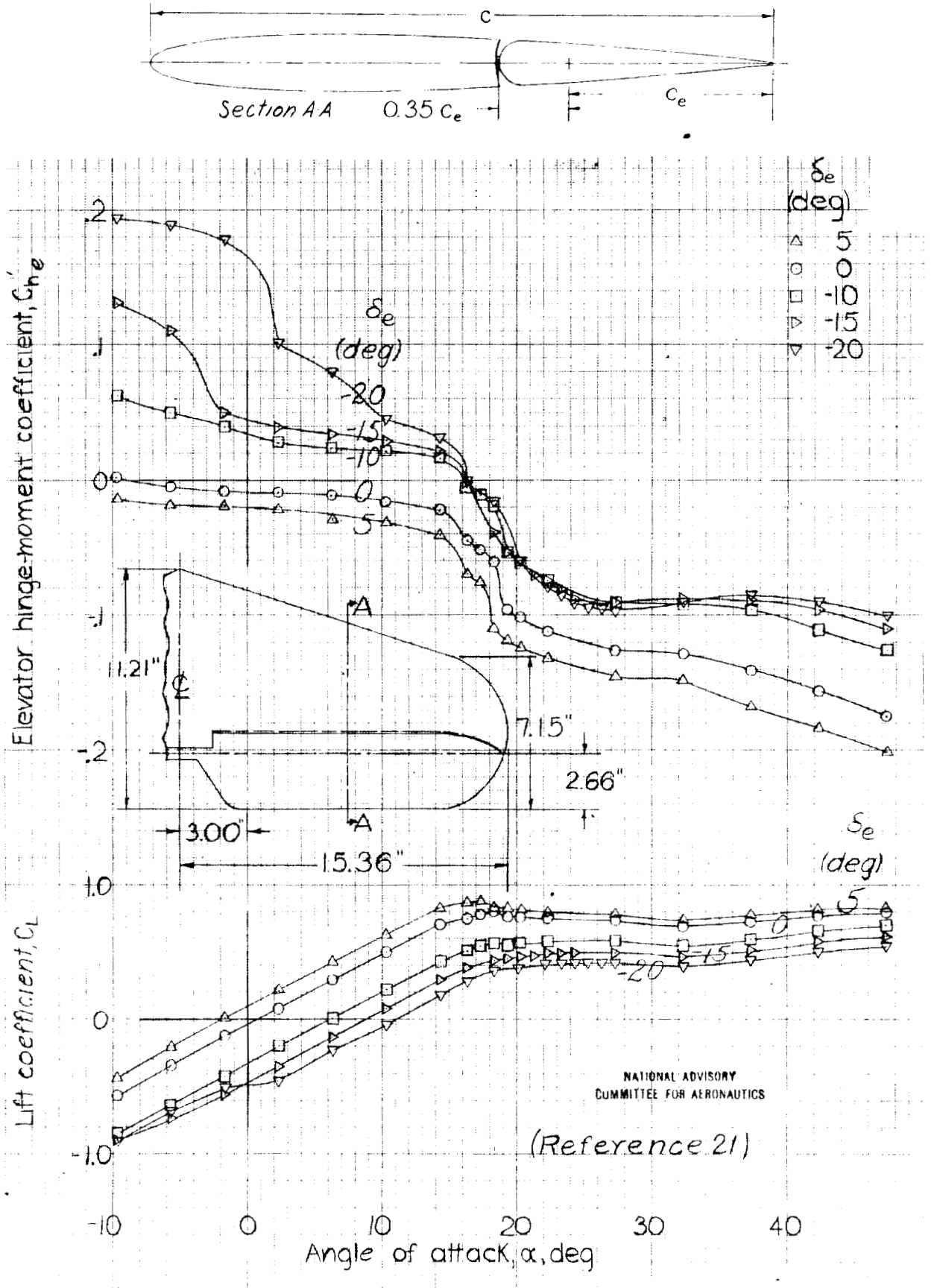

Figure 109. Balanced elevator on pursuit fuselage, NACA 0009 airfoil section $S_e/S = 0.27$, $A = 3.7$, $0.35c_e$ blunt-nose overhang, sealed gap.

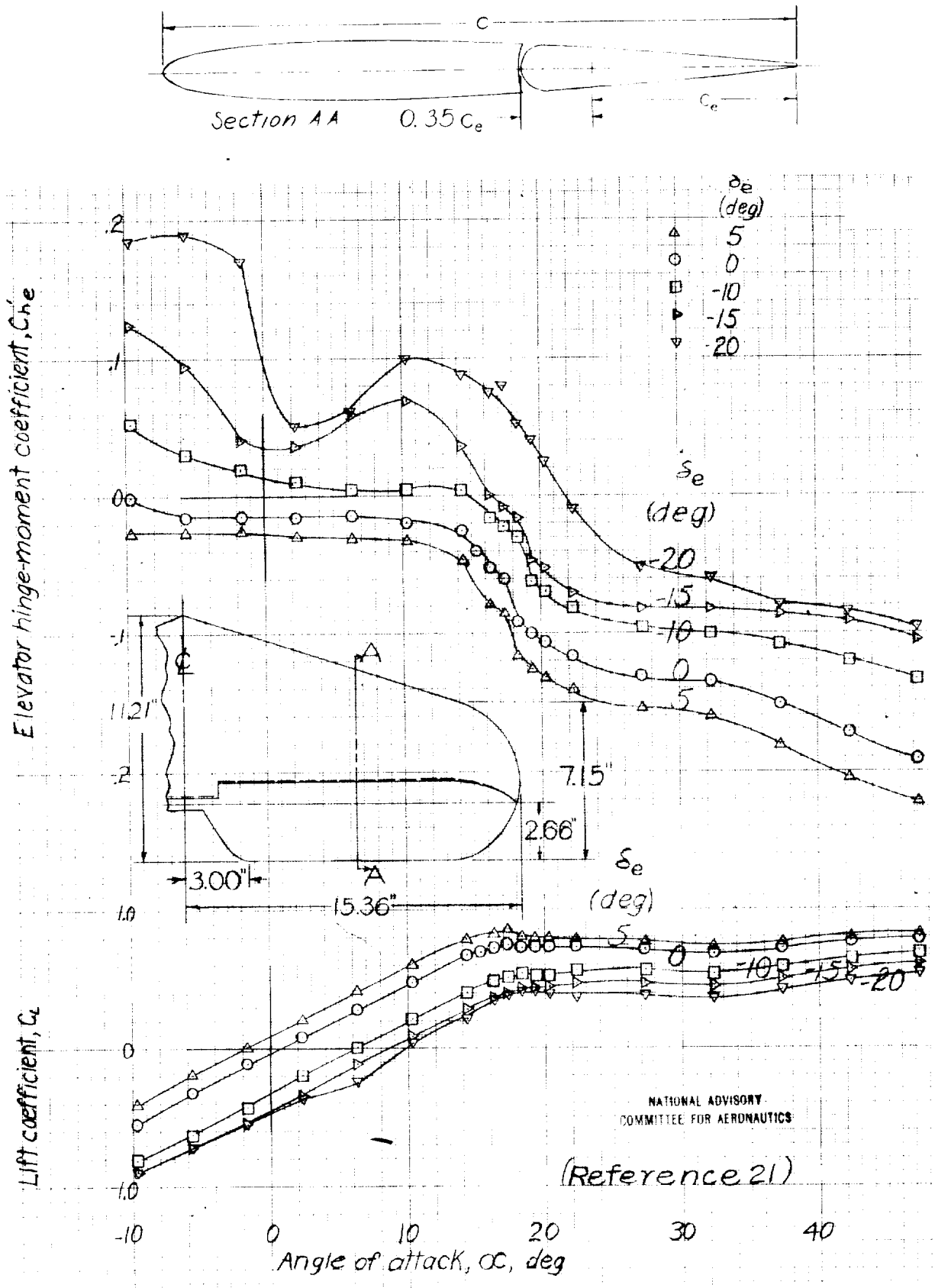

Figure 110.- Balanced elevator on pursuit fuselage, NACA 0009 airfoil section, $S_e/S = 0.27$, $A = 3.7$, $0.35c_e$ blunt-nose overhang, 0.005 gap.

L-663

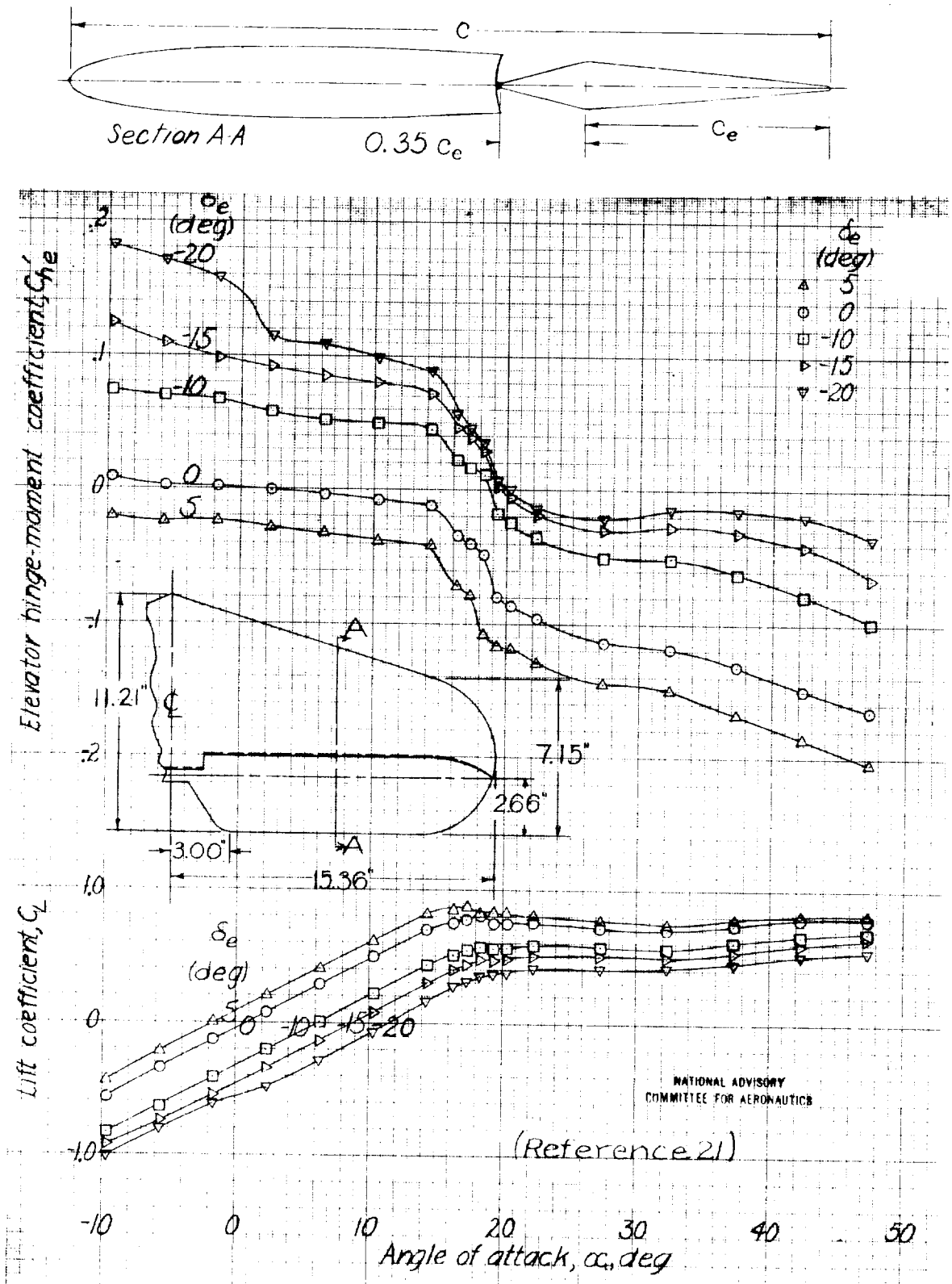

Figure 111.-Balanced elevator on pursuit fuselage, NACA 0009 airfoil section, S_e/S 0.27, A=3.7, sealed gap, 0.35c_e sharp nose overhang.

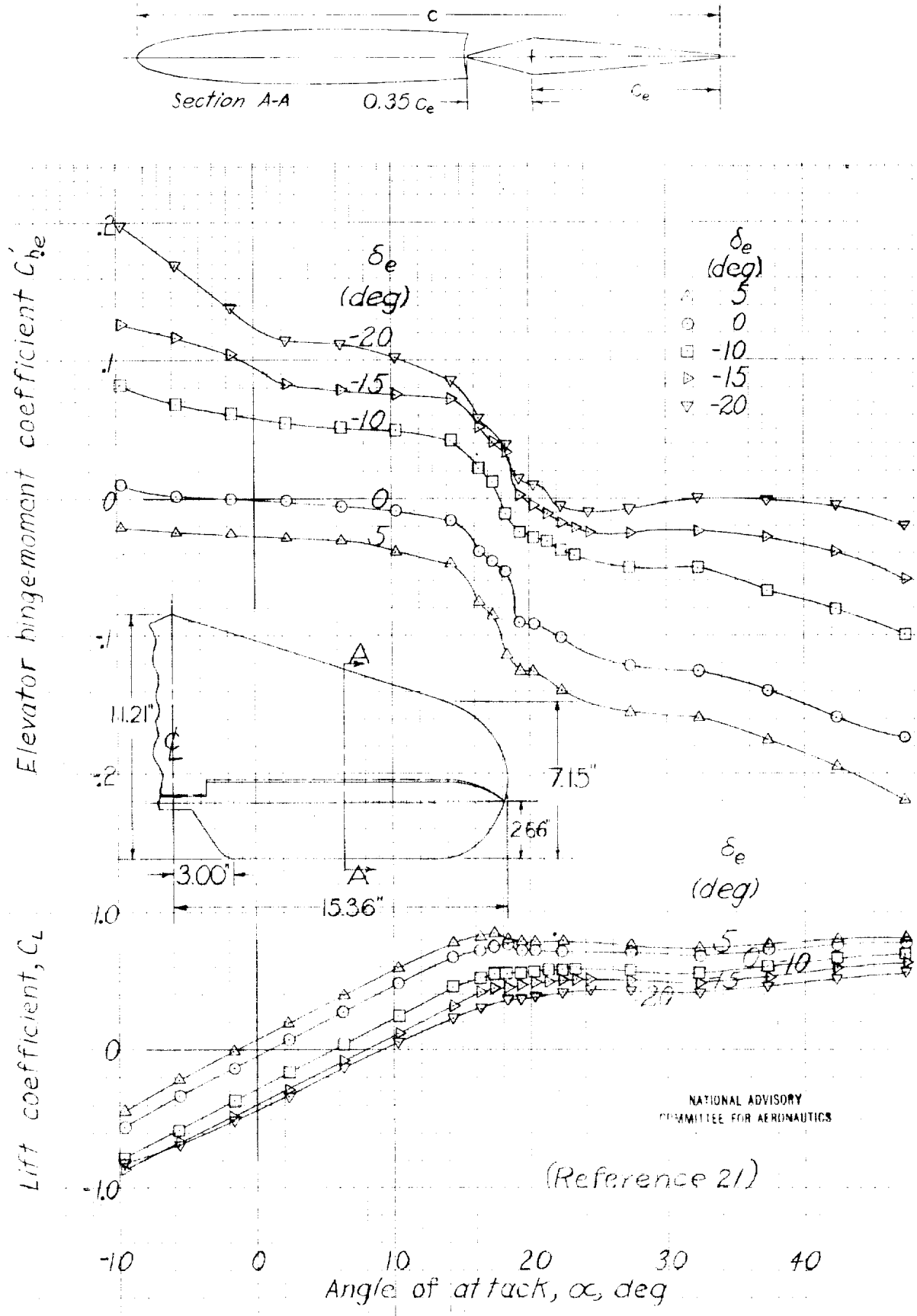

Figure 112.- Balanced elevator on pursuit fuselage, NACA 0009 airfoil section, $S_e/S=0.27$, $A=3.1$, 0.005c gap, 0.35c_e sharp-nose overhang.

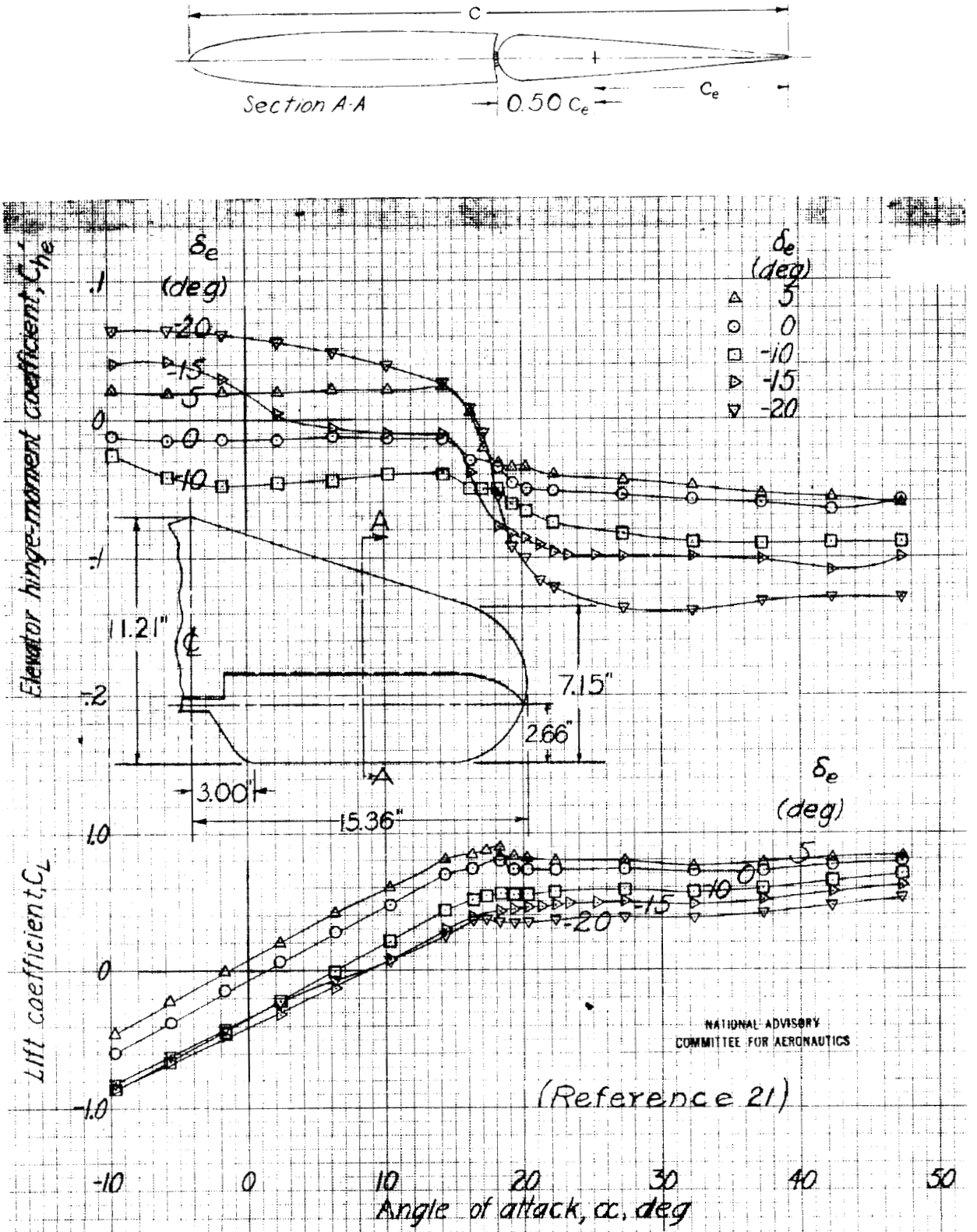

Figure 113.- Balanced elevator on pursuit fuselage, NACA 0009 airfoil section, $S_e/S = 0.27$, $A = 3.7$, sealed gap, $0.50c_e$ blunt-nose overhang.

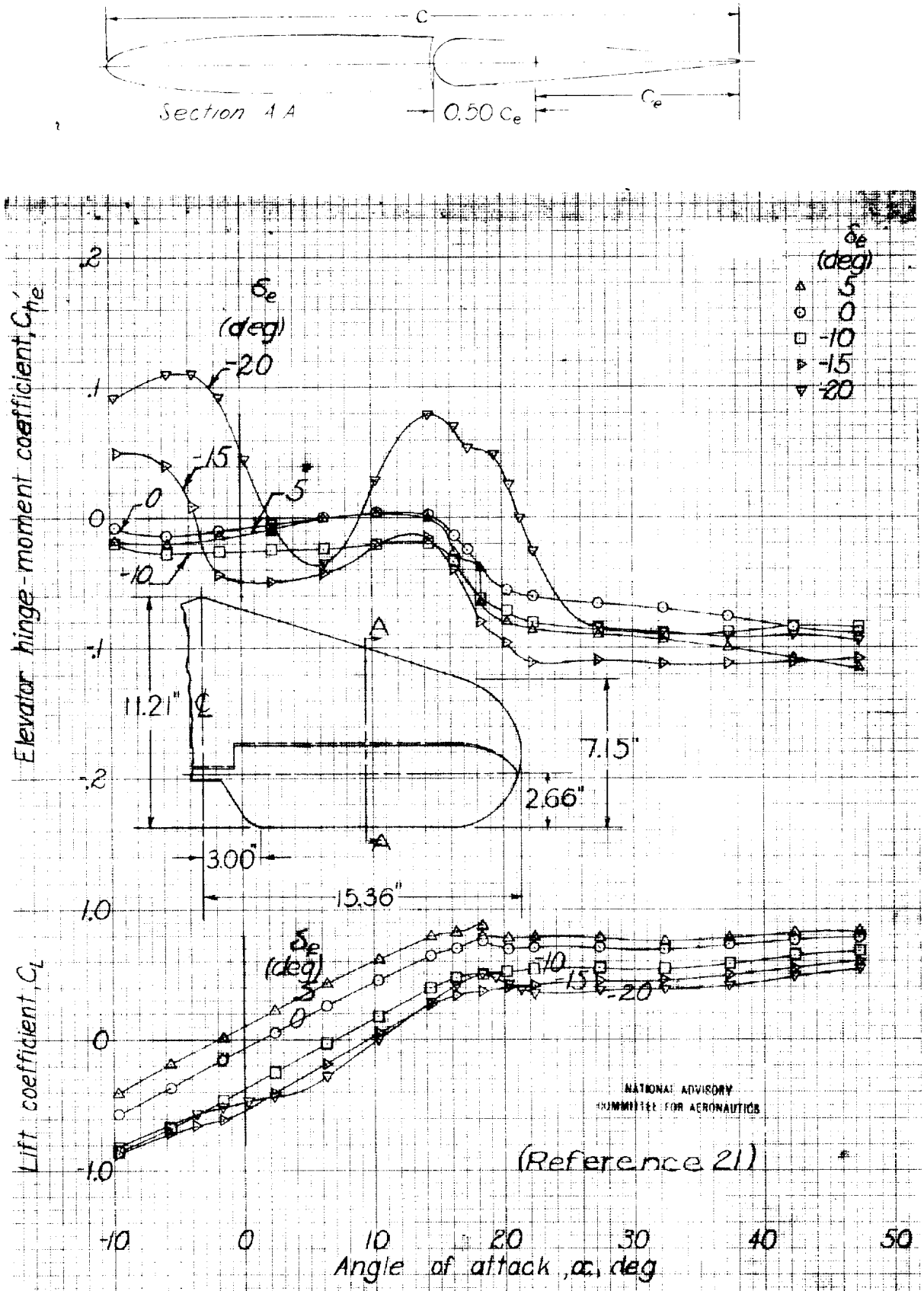

Figure 114.- Balanced elevator on pursuit fuselage, NACA 0009 airfoil section, $S_e/S = 0.27$, $A = 3.7$, 0.005c gap, 0.50 c_e blunt nose overhang.

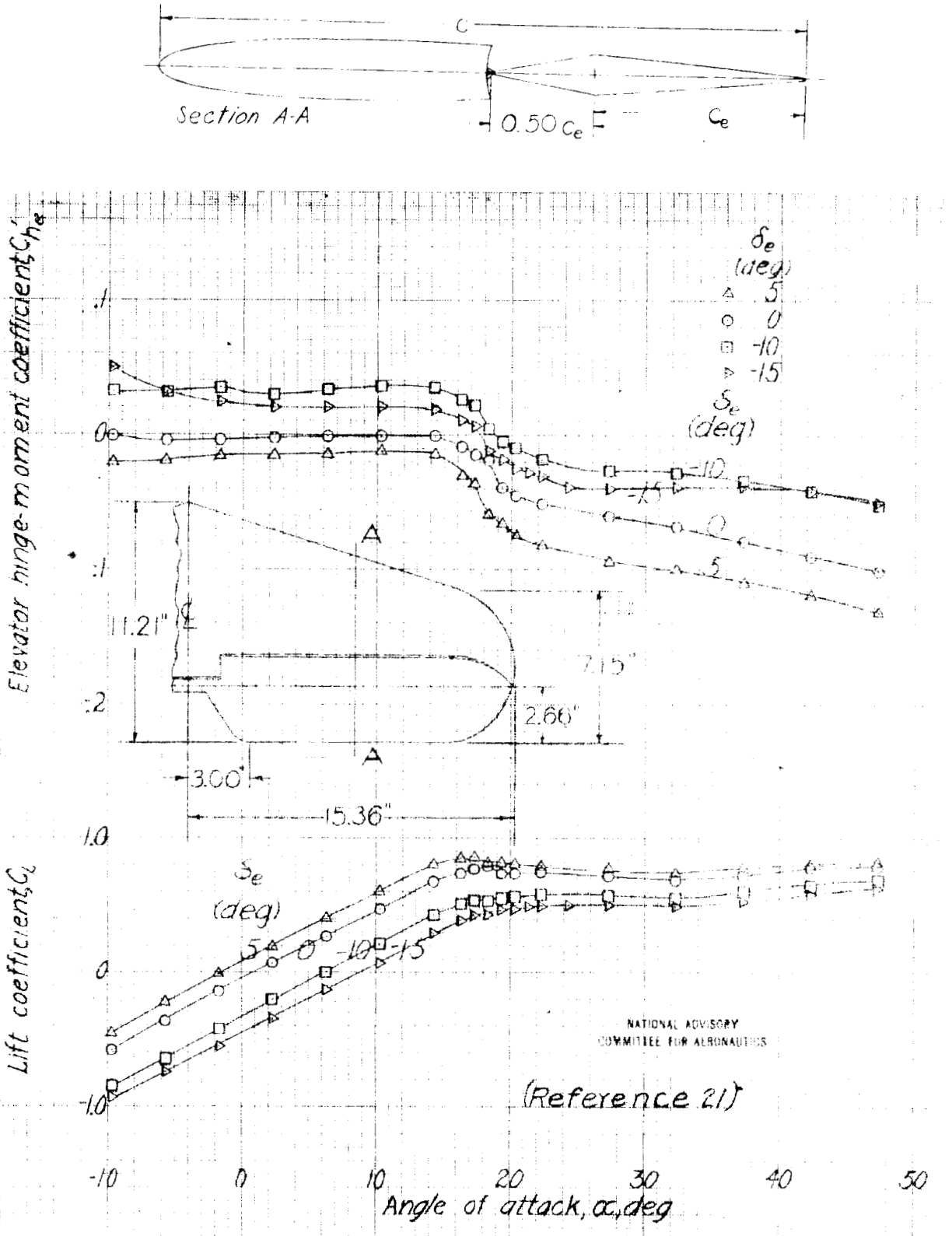

Figure 115.- Balanced elevator on pursuit fuselage, NACA 0009 airfoil section, $S_e/S = 0.27$, A-3.7, sealed gap, $0.50c_e$ sharp-nose overhang.

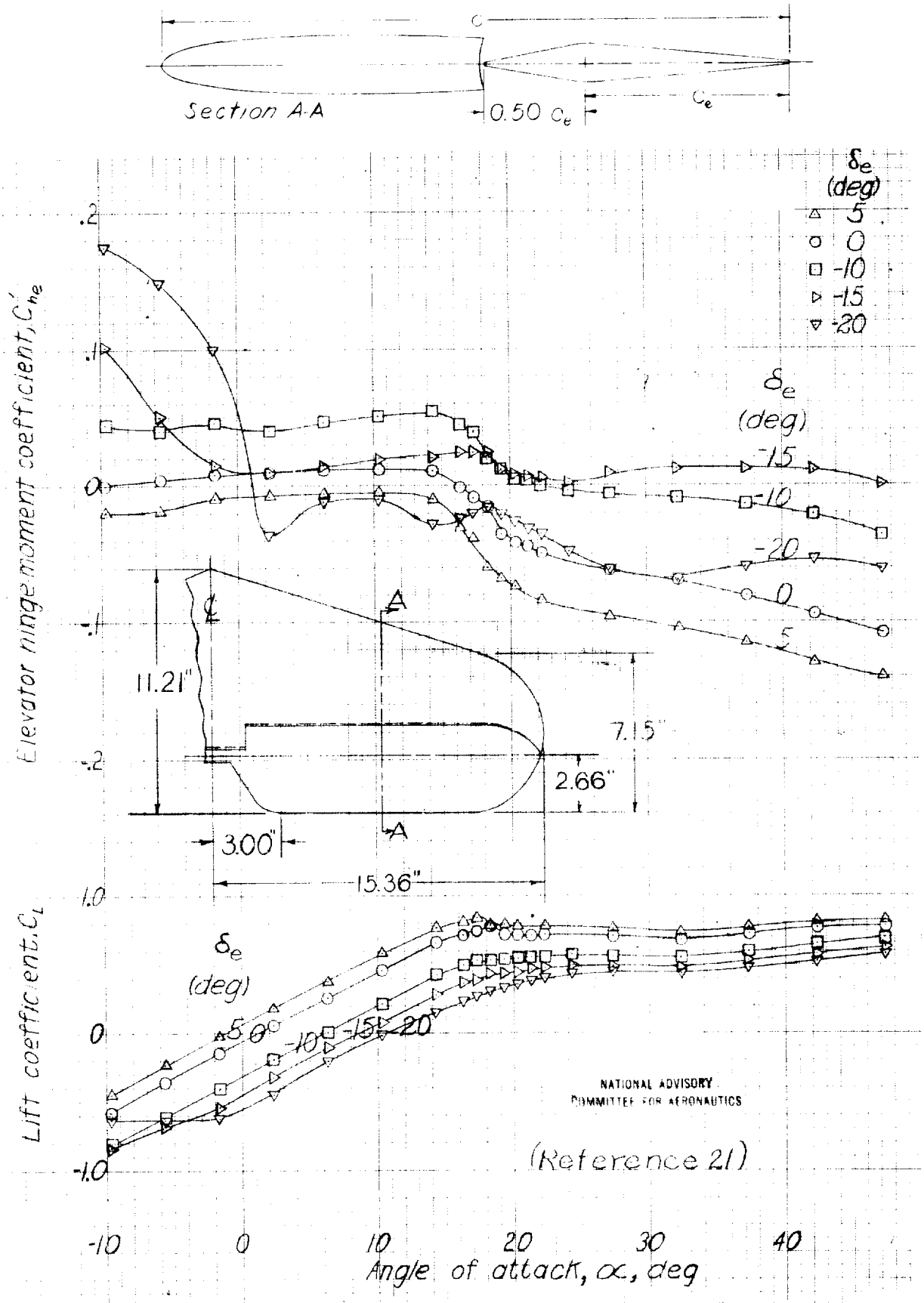

Figure 116.- Balanced elevator on pursuit fuselage, NACA 0009 airfoil section, $S_e/S = 0.27$, $A = 3.7$, 0.005c gap, 0.50c_e sharp-nose overhang.

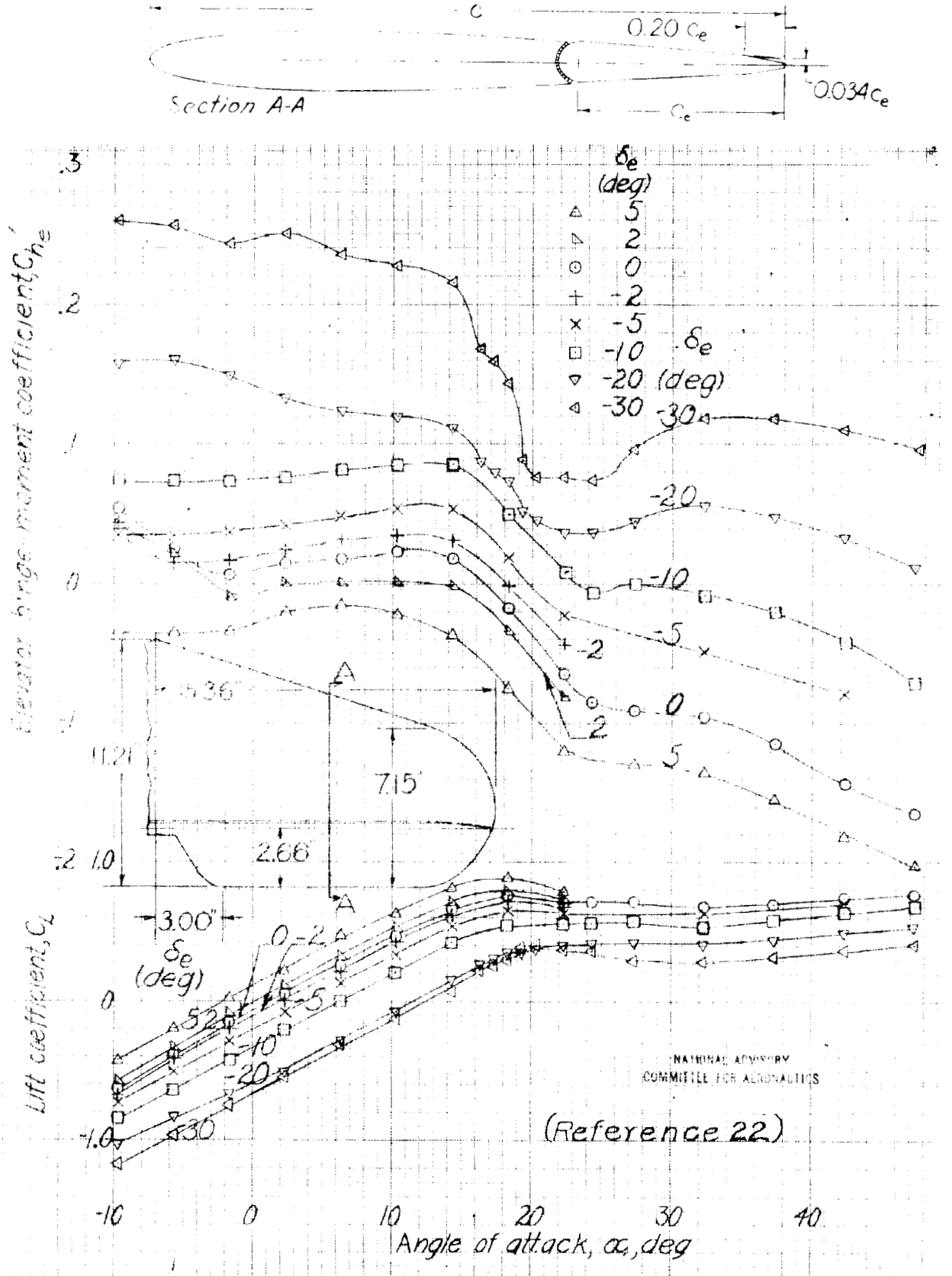

Figure 117.- Beveled trailing-edge elevator on pursuit fuselage, NACA 0009 airfoil section, $S_e/S = 0.27$, $A = 3.7$, sealed gap, $0.20c_e$ bevel.

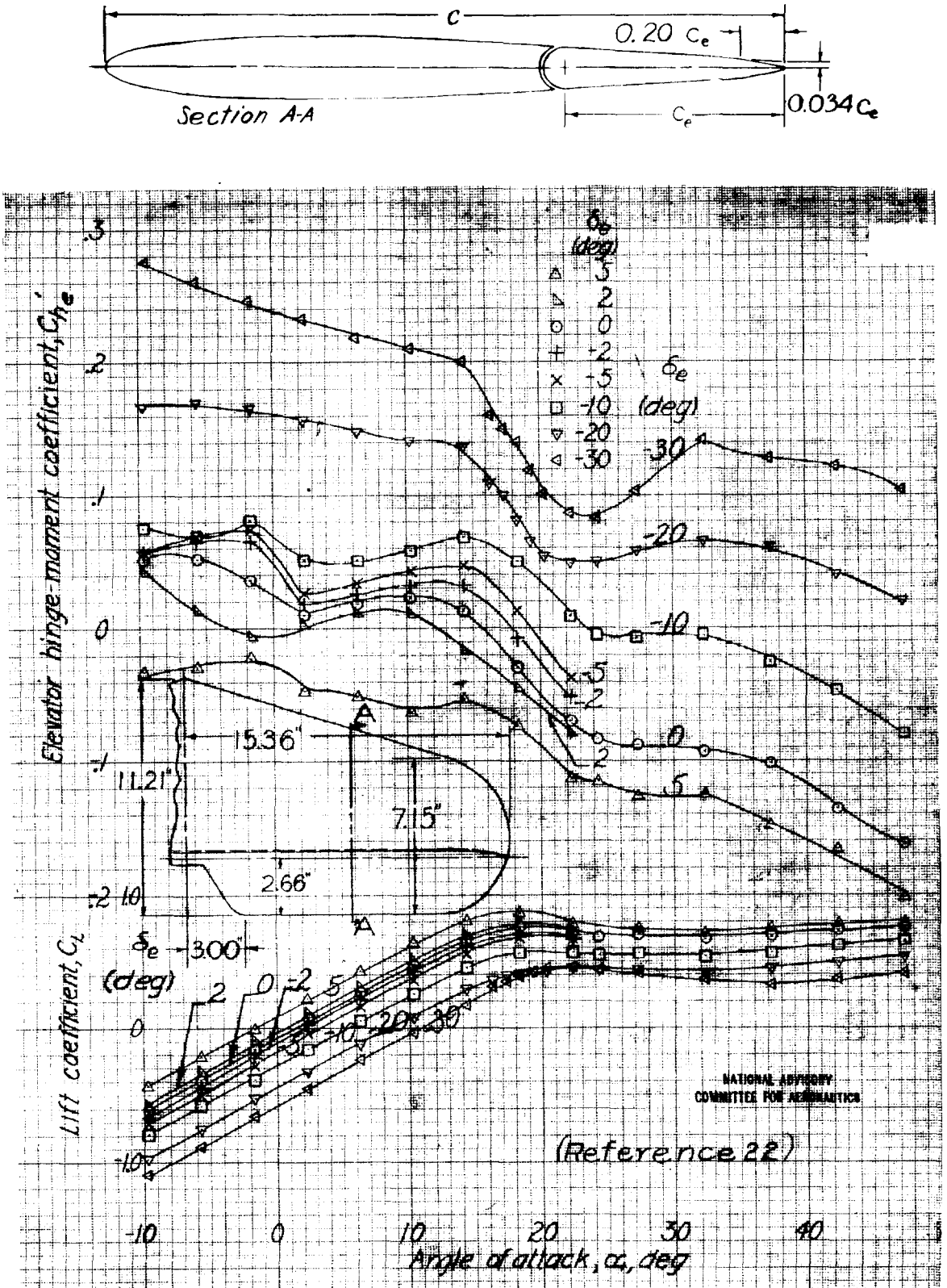

Figure 118.- Beveled trailing-edge elevator on pursuit fuselage, NACA 0009 airfoil section, S_e/S=0.27, A=3.7, 0.005c gap, 0.20c_e bevel.

L-663

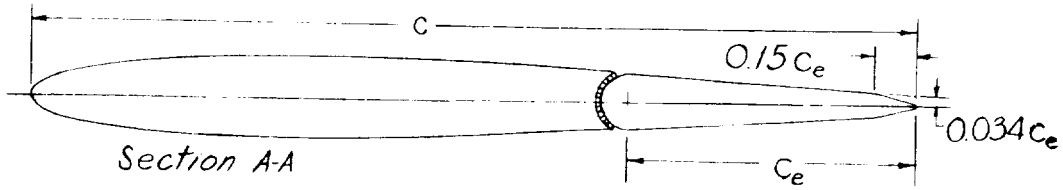

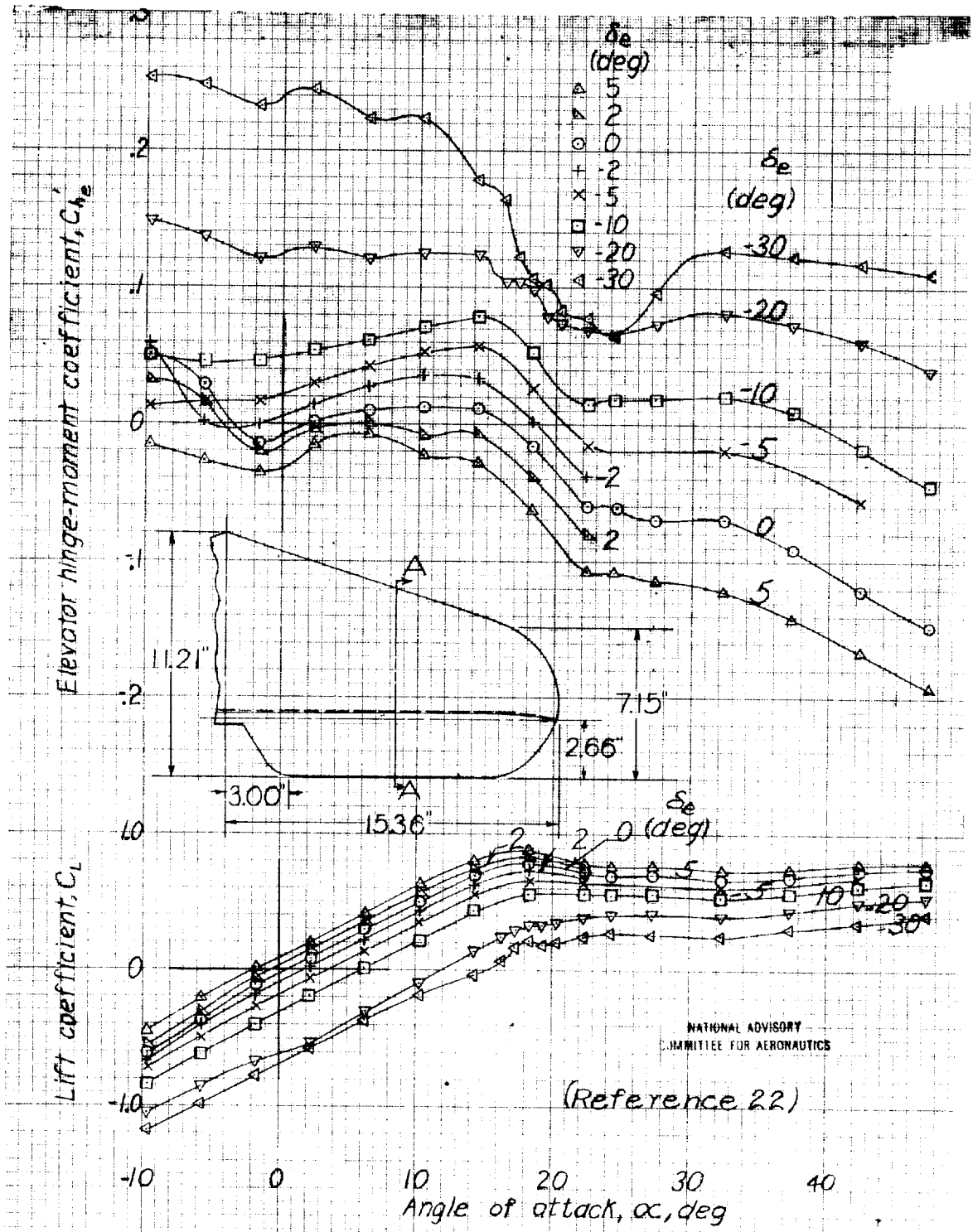

Figure 119.-Beveled trailing-edge elevator on pursuit fuselage, NACA 0009 airfoil section, $S_e/S = 0.27$, $A = 3.7$, sealed gap, $0.15c_e$ bevel.

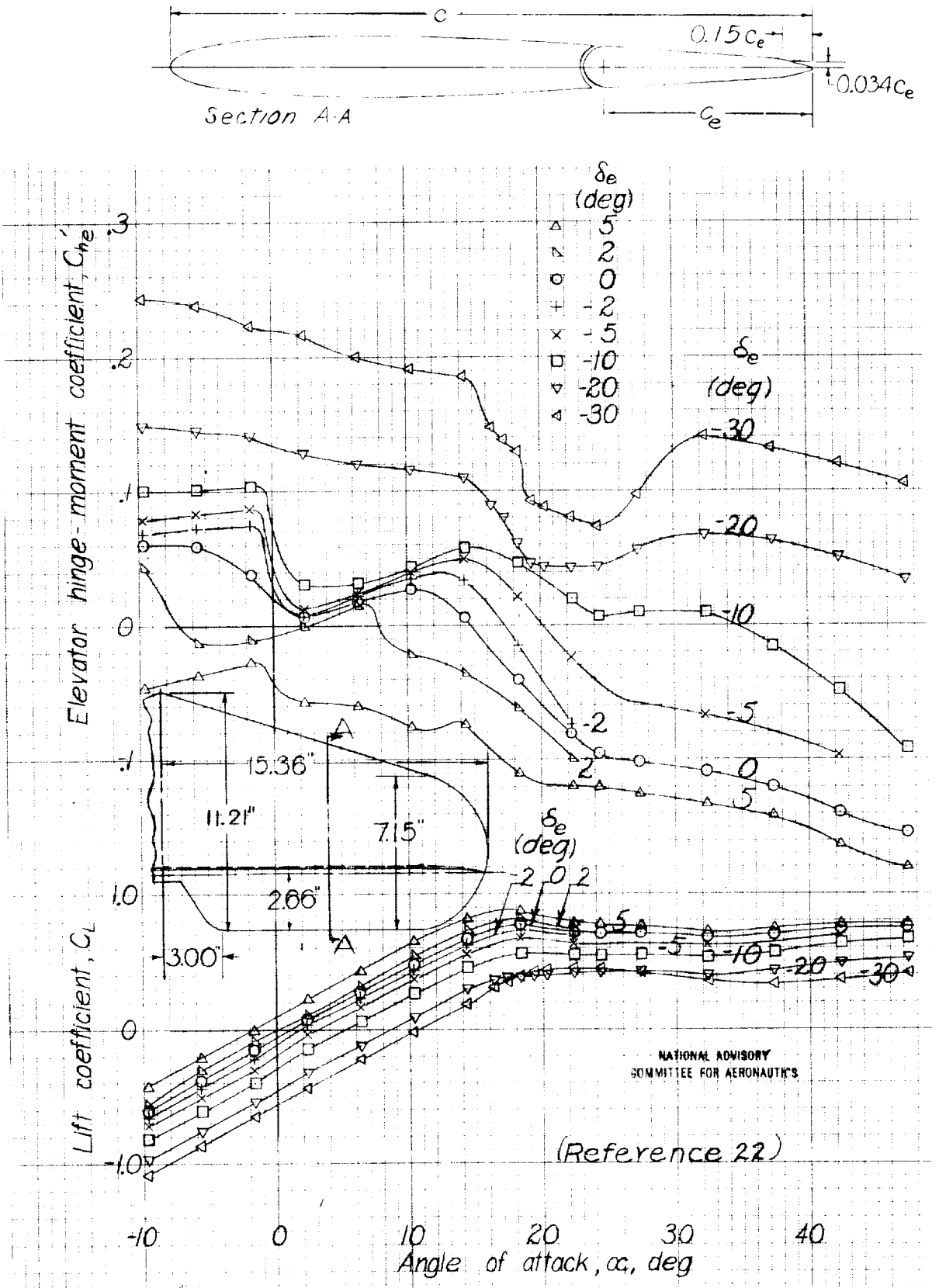

Figure 120. - Beveled trailing-edge elevator on pursuit fuselage, NACA 0009 airfoil section, $S_e/S = 0.27$, $A = 3.7$, 0.005c gap, 0.15c_e bevel.

L-663

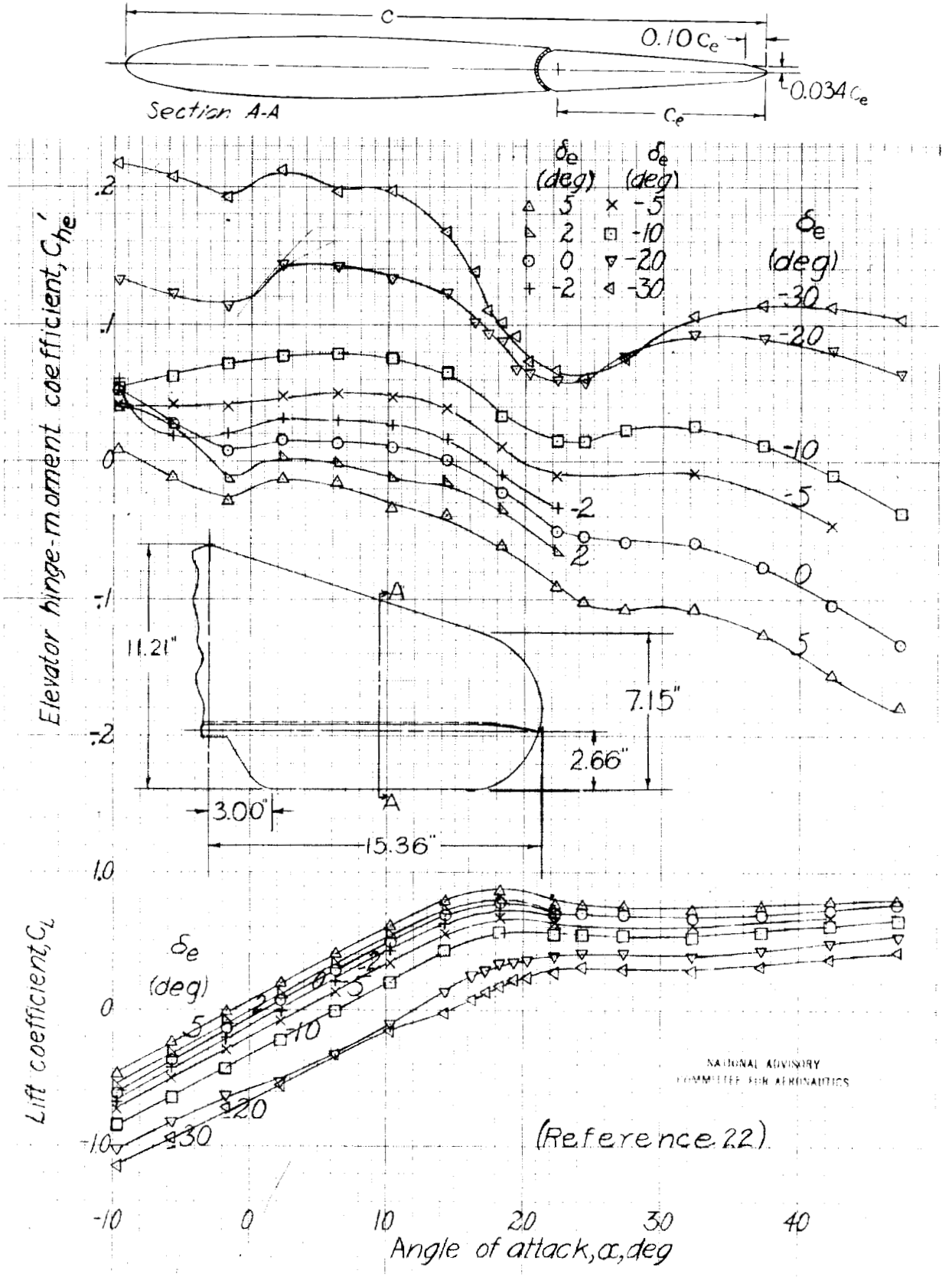

Figure 121. Beveled trailing-edge elevator on pursuit fuselage, NACA 0009 airfoil section, $S_e/S = 0.27$, $A = 3.7$, sealed gap, $0.10c_e$ bevel.

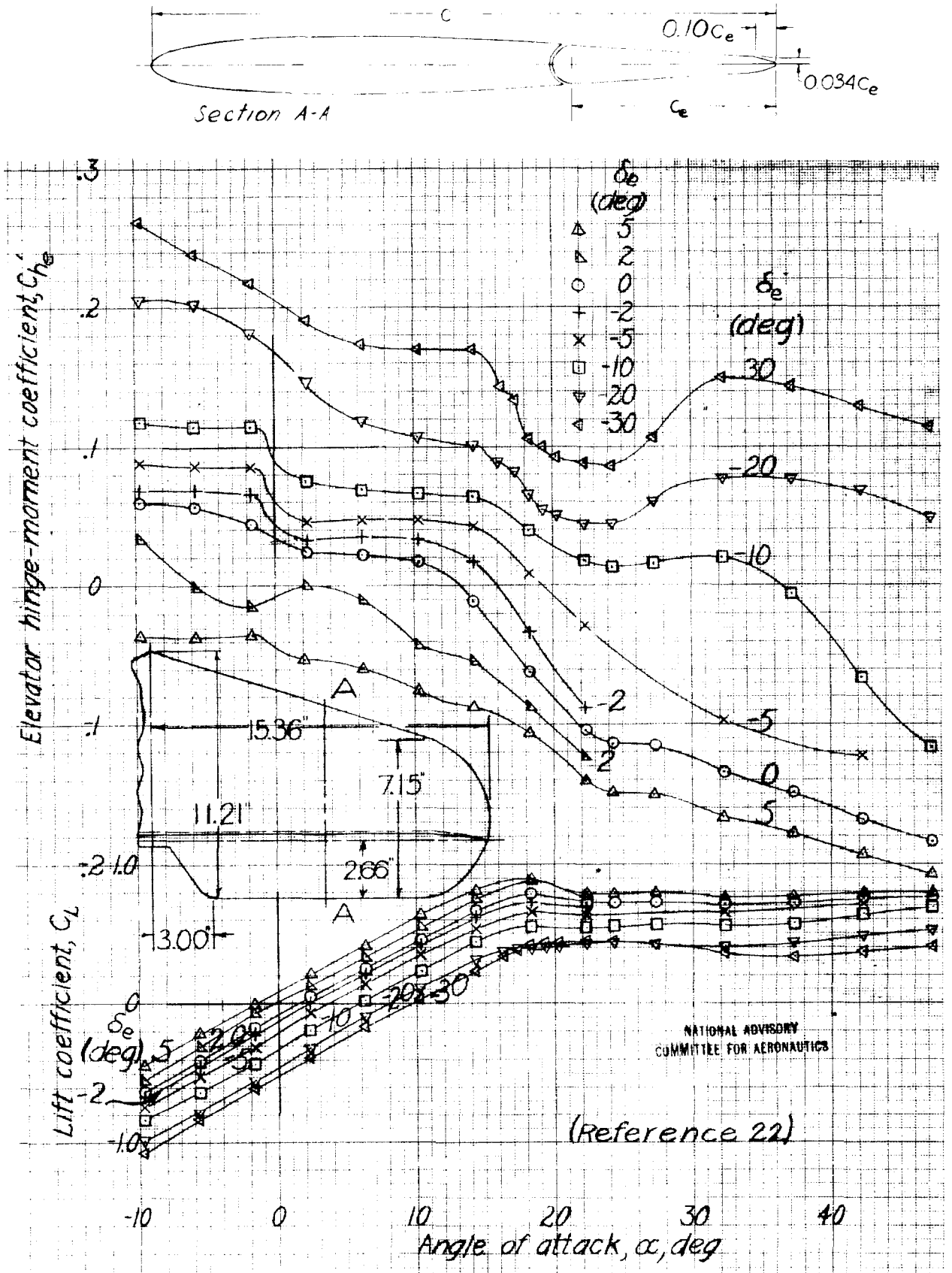

Figure 122. -Beveled trailing-edge elevator on pursuit fuselage, NACA 0009 airfoil section, $S_e/S = 0.27$, $A = 3.7$, 0.005c gap, 0.10c_e bevel.

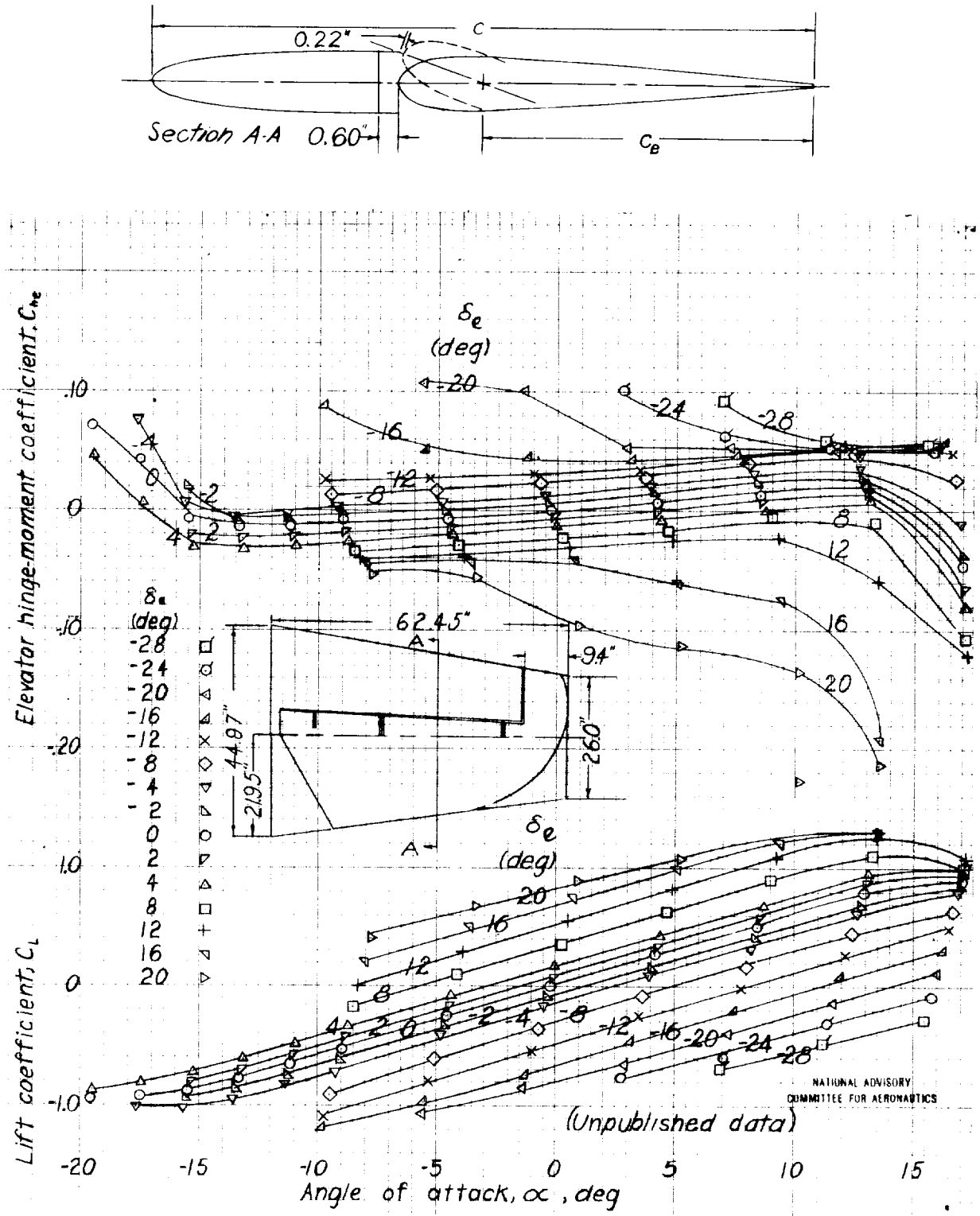

Figure 123.- Semispan horizontal tail surface, horn I, $S_e/S = 0.433$, $A = 3.96$, $S_b/S = 0.179$, gap = 0.02c.

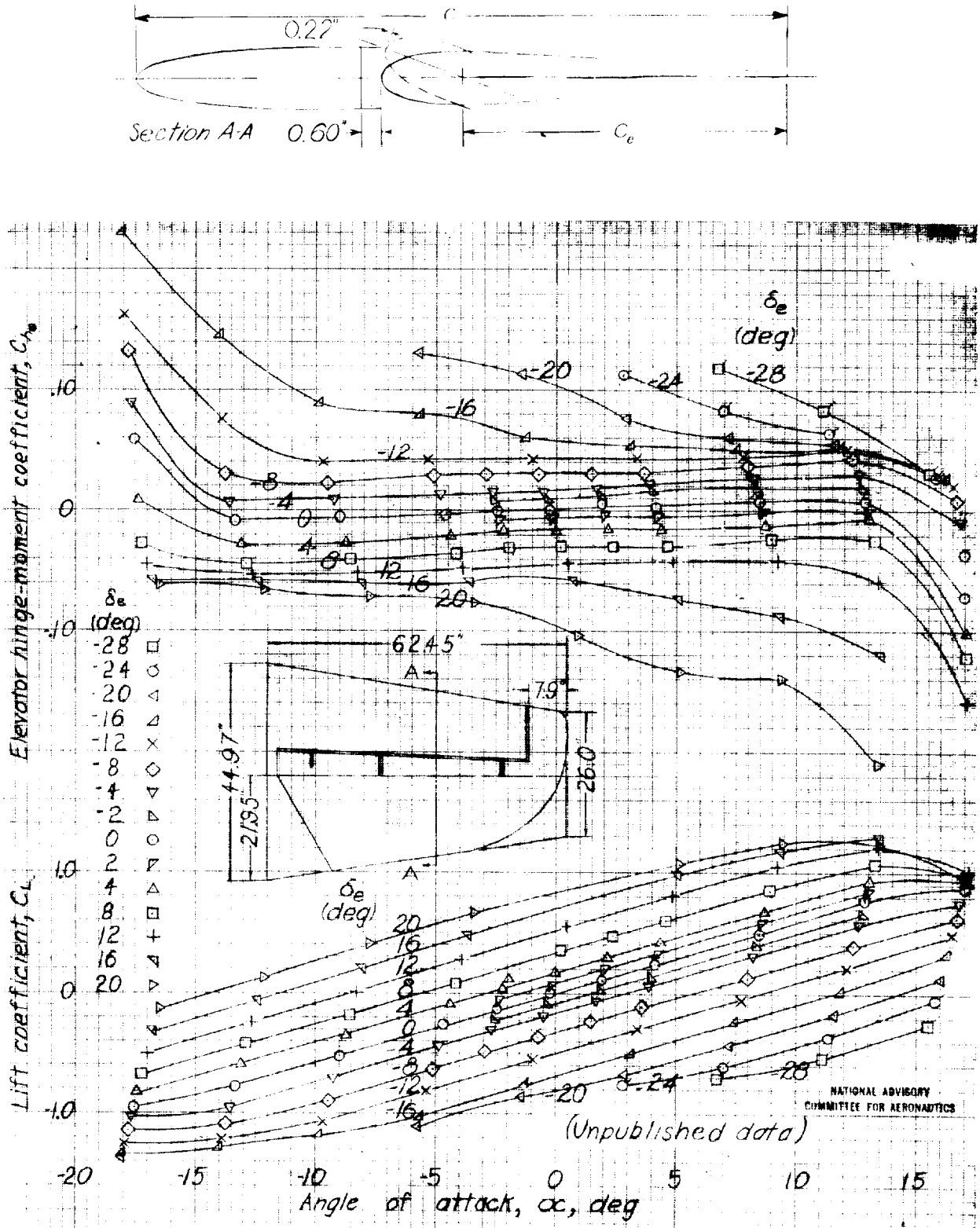

Figure 124.- Semispan horizontal tail surface, horn 2, $S_e/S = 0.433$, $\lambda = 3.96$, $S_t/S = 0.171$, gap = 0.02c.

L-663

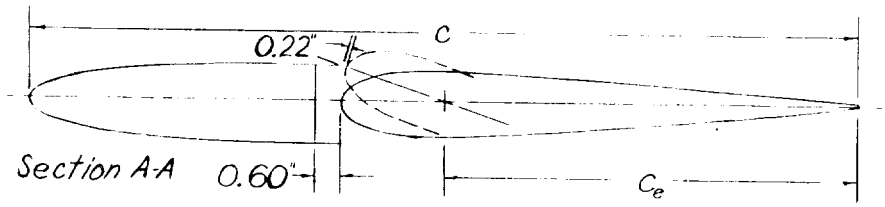

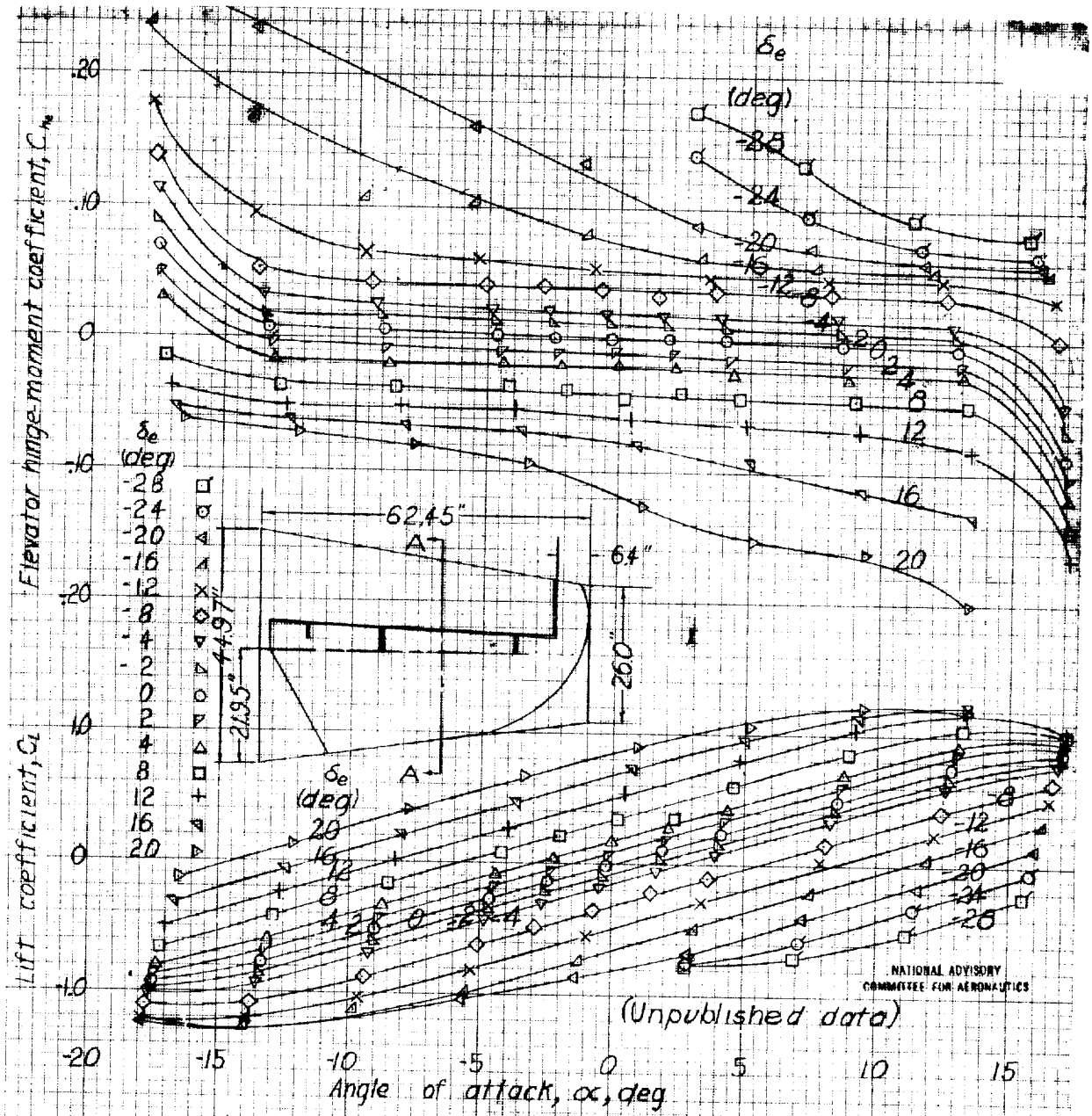

Figure 12.5- Semispan horizontal tail surface, horn 3, $S_e/S = 0.433$, $A = 3.96$, $S_h/S = 0.163$, gap = 0.02c.

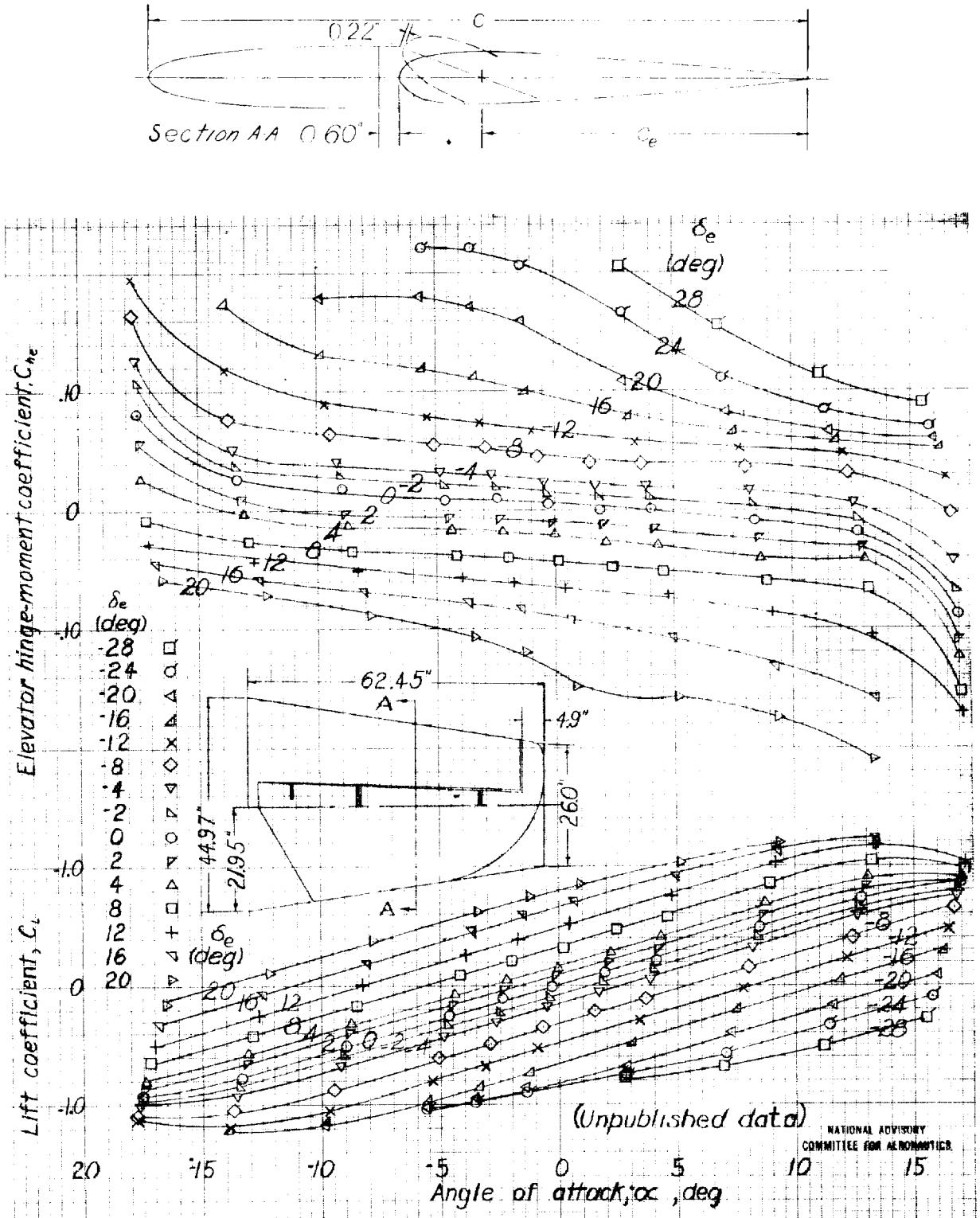

Figure 126.- Semispan horizontal tail surface, horn 4, $S_e/S = 0.433$, $A = 3.96$, $S_t/S = 0.155$, gap = 0.02c.

L-663

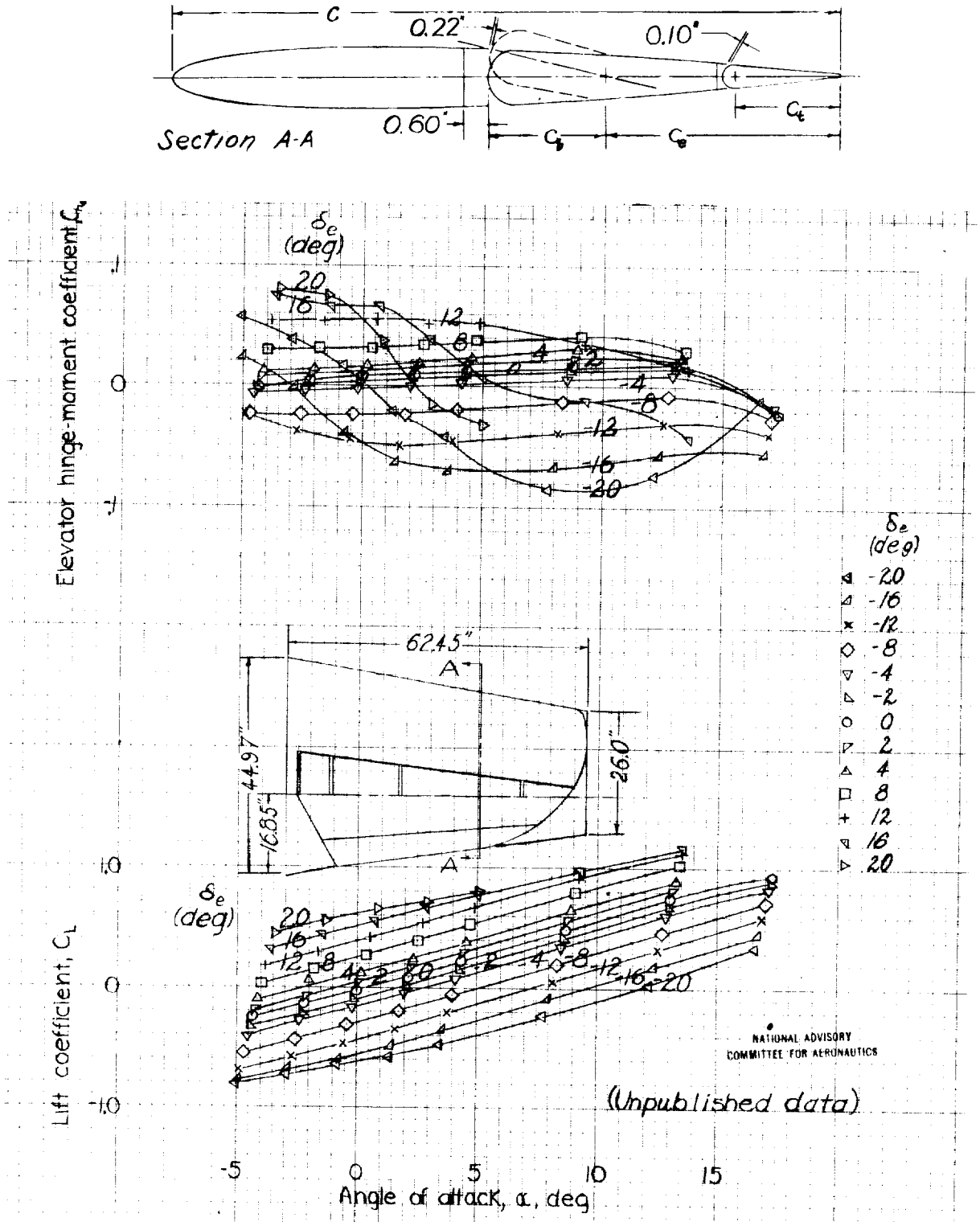

Figure 127.- Semispan horizontal tail surface, $S_e/S = 0.30$, $S_t/S = 0.10$, $S_e/S_t = 0.50$, $A = 3.96$, $\partial\alpha_t/\partial\delta_e = 0$, gap = 0.02 c.

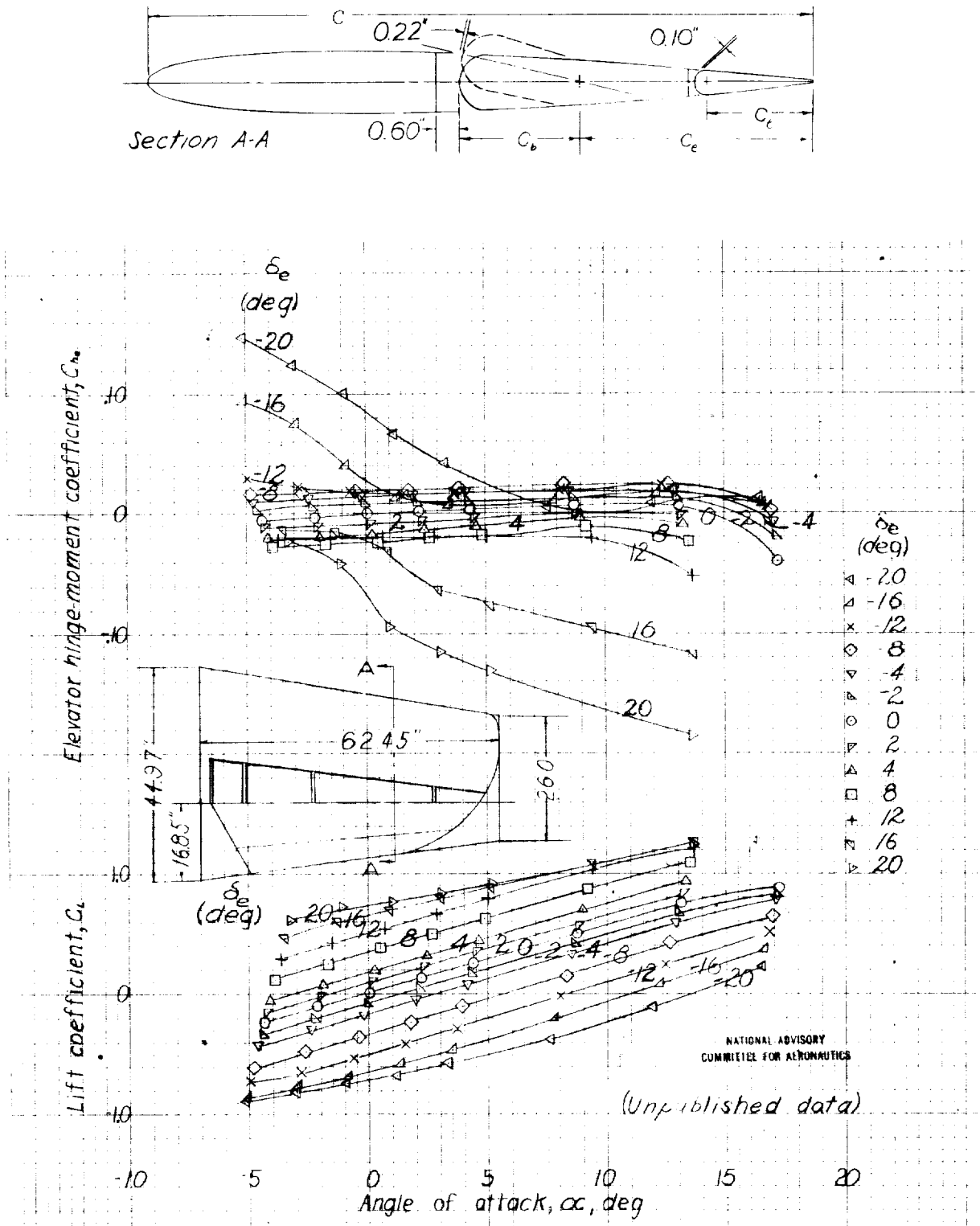

Figure 128.- Semispan horizontal tail surface, $S_e/S = 0.30$, $S_t/S = 0.10$, $S_L/S_e = 0.50$, $A = 3.96$, $\partial\delta_L/\partial\delta_e = 0.50$, gap = 0.02.

L-663

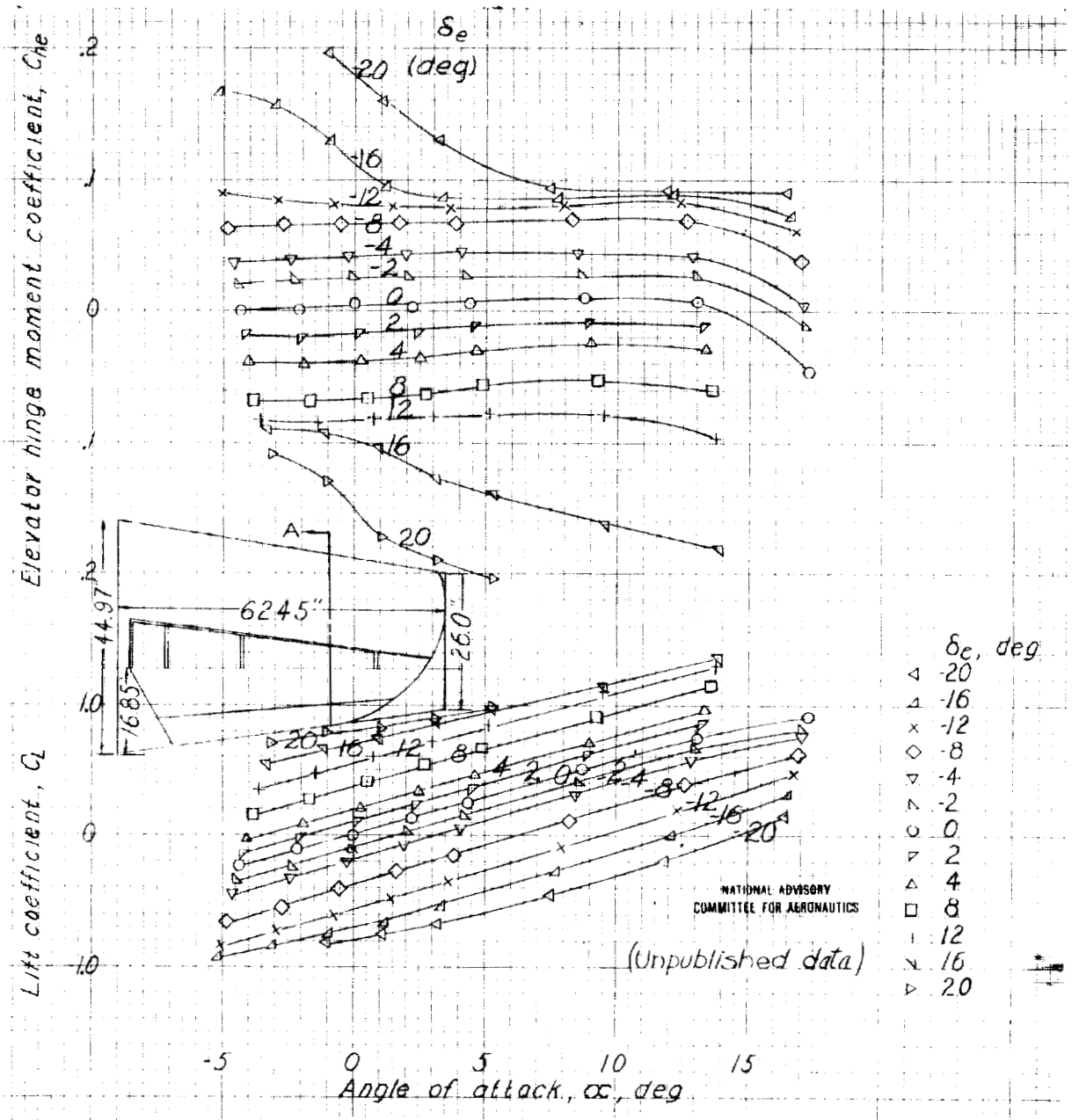

Figure 129.- Semispan horizontal tail surface, $S_e/S = 0.30$, $S_t/S = 0.10$, $S_b/S_e = 0.50$, $A = 3.96$, $\partial\delta_t/\partial\delta_e = 1.0$, gap = 0.02c.

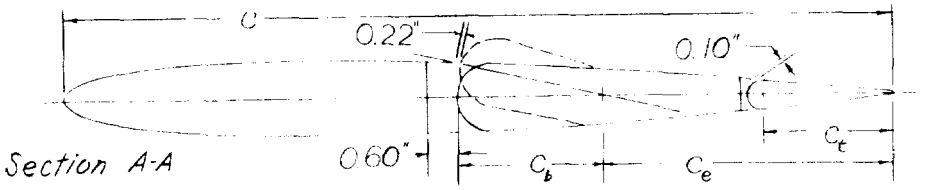

Note:- Plan-form same as that of figures 127 to 129.

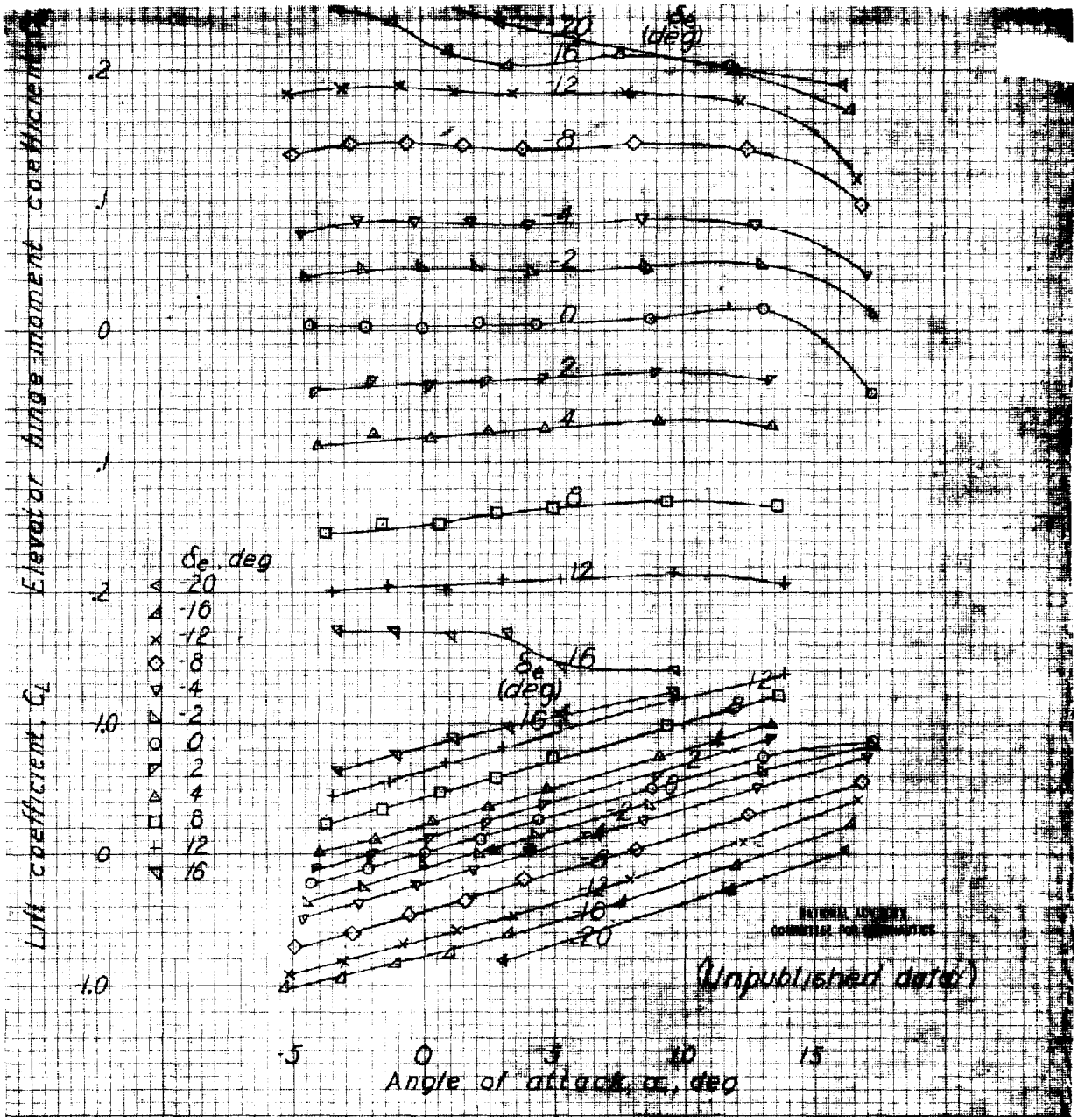

Figure 130.- Semispan horizontal tail surface, $S_e/S=0.30$, $S_t/S=0.10$, $S_b/S_e=0.50$, $A=3.98$, $2b_e/2b_t=2$, gap=0.02c.

L-663

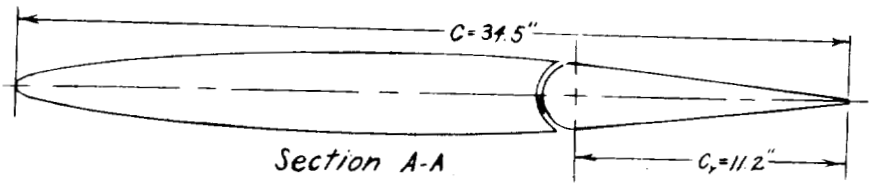

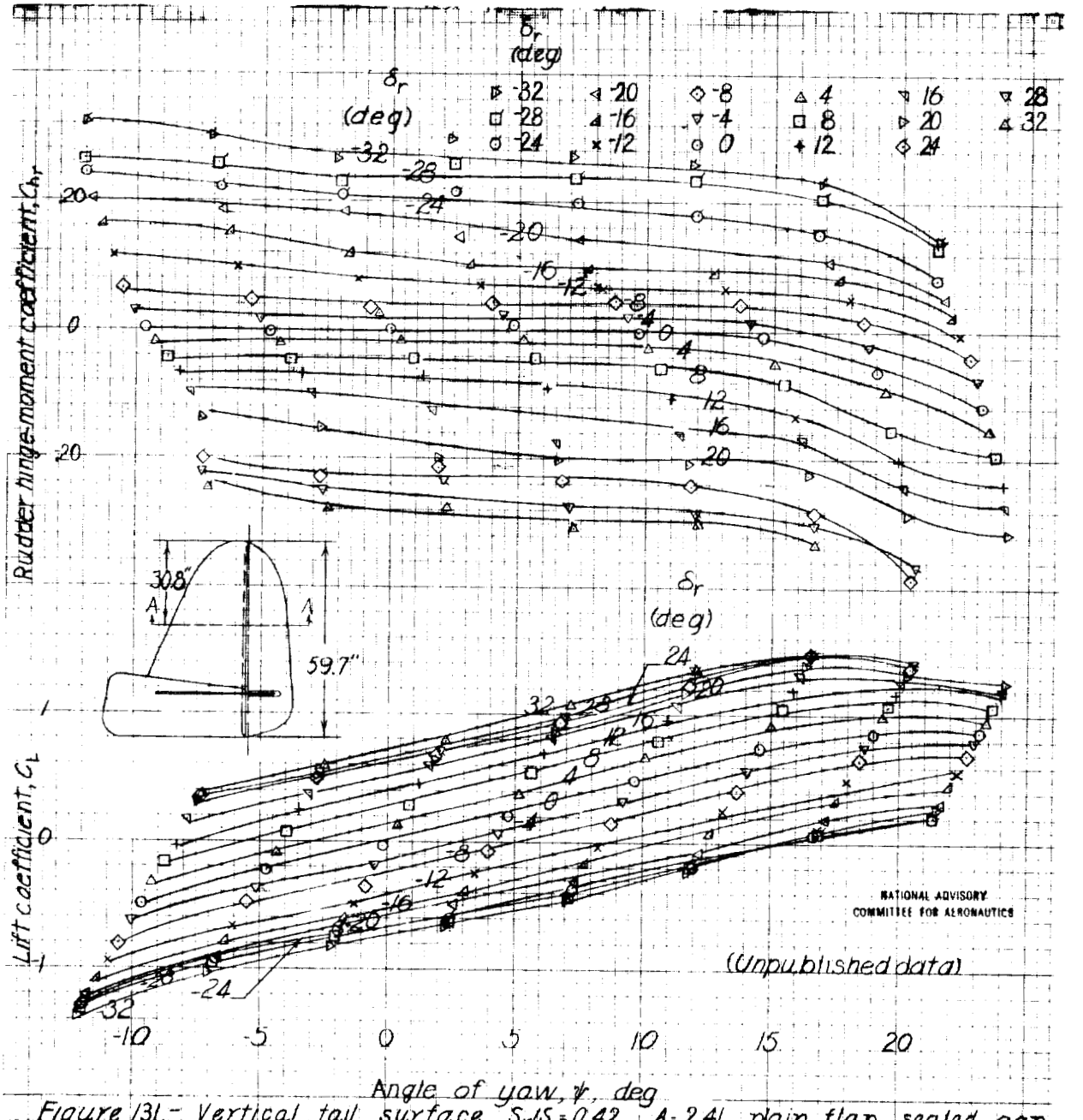

Figure 131.- Vertical tail surface, $S_r/S = 0.42$, $A = 2.41$, plain flap, sealed gap.

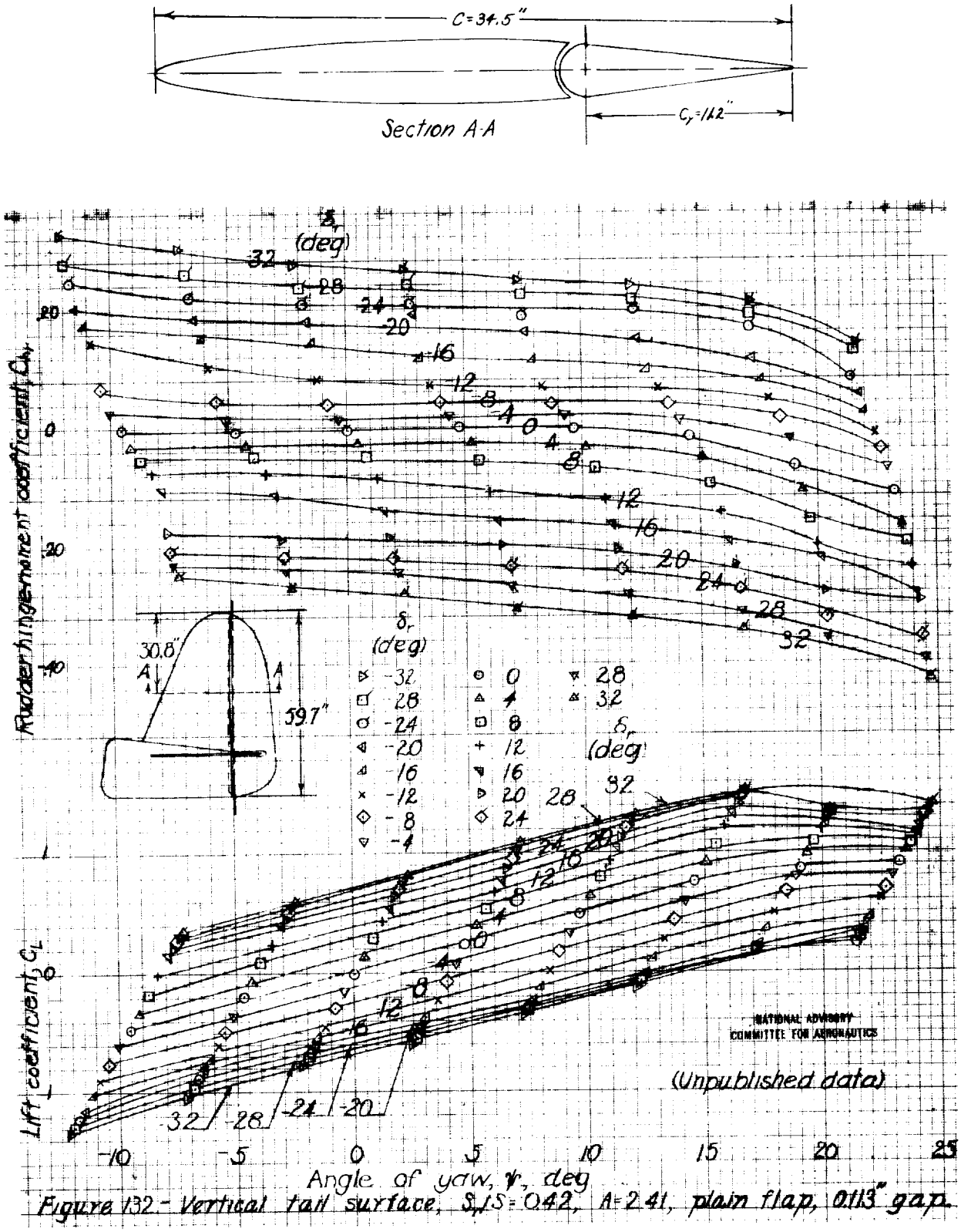

Figure 132 - Vertical tail surface, S_t/S = 0.42, A = 2.41, plain flap, 0.113" gap.

L-663

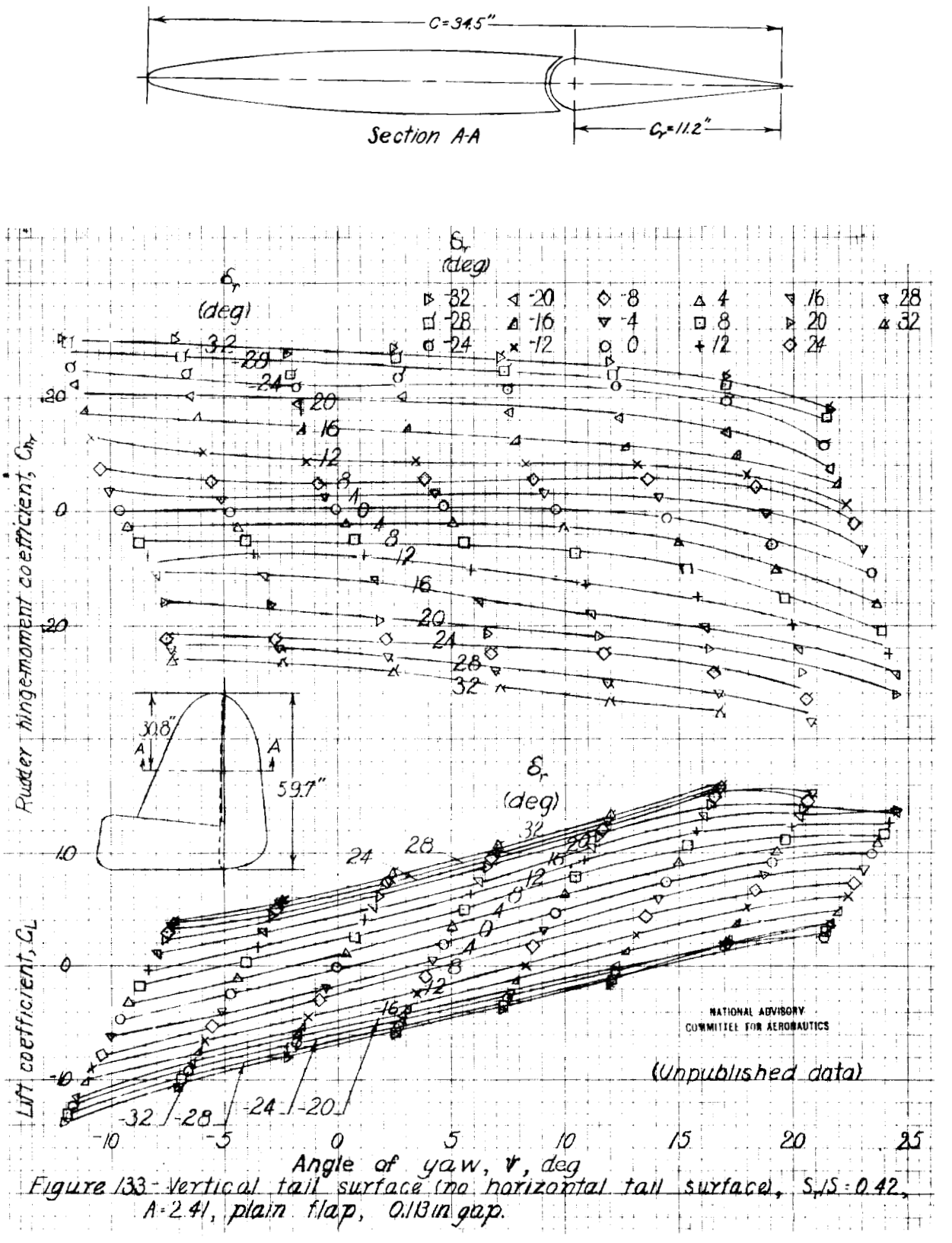

Figure 133 - Vertical tail surface (no horizontal tail surface), $S_r/S = 0.42$, A = 2.41, plain flap, 0.113 in gap.

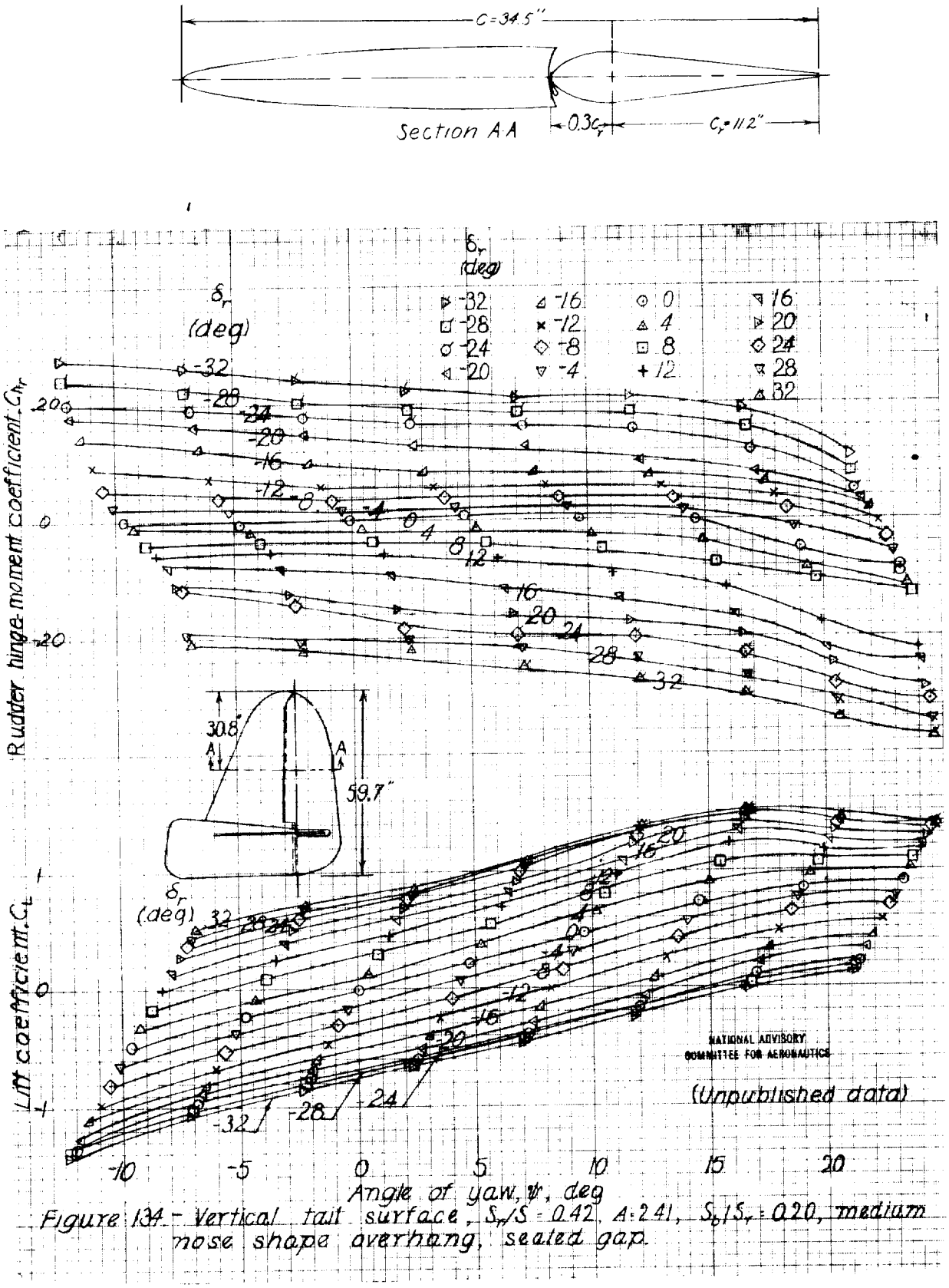

Figure 134 - Vertical tail surface, $S_r/S = 0.42$, $A = 2.41$, $S_b/S_r = 0.20$, medium nose shape overhang, sealed gap.

L-663

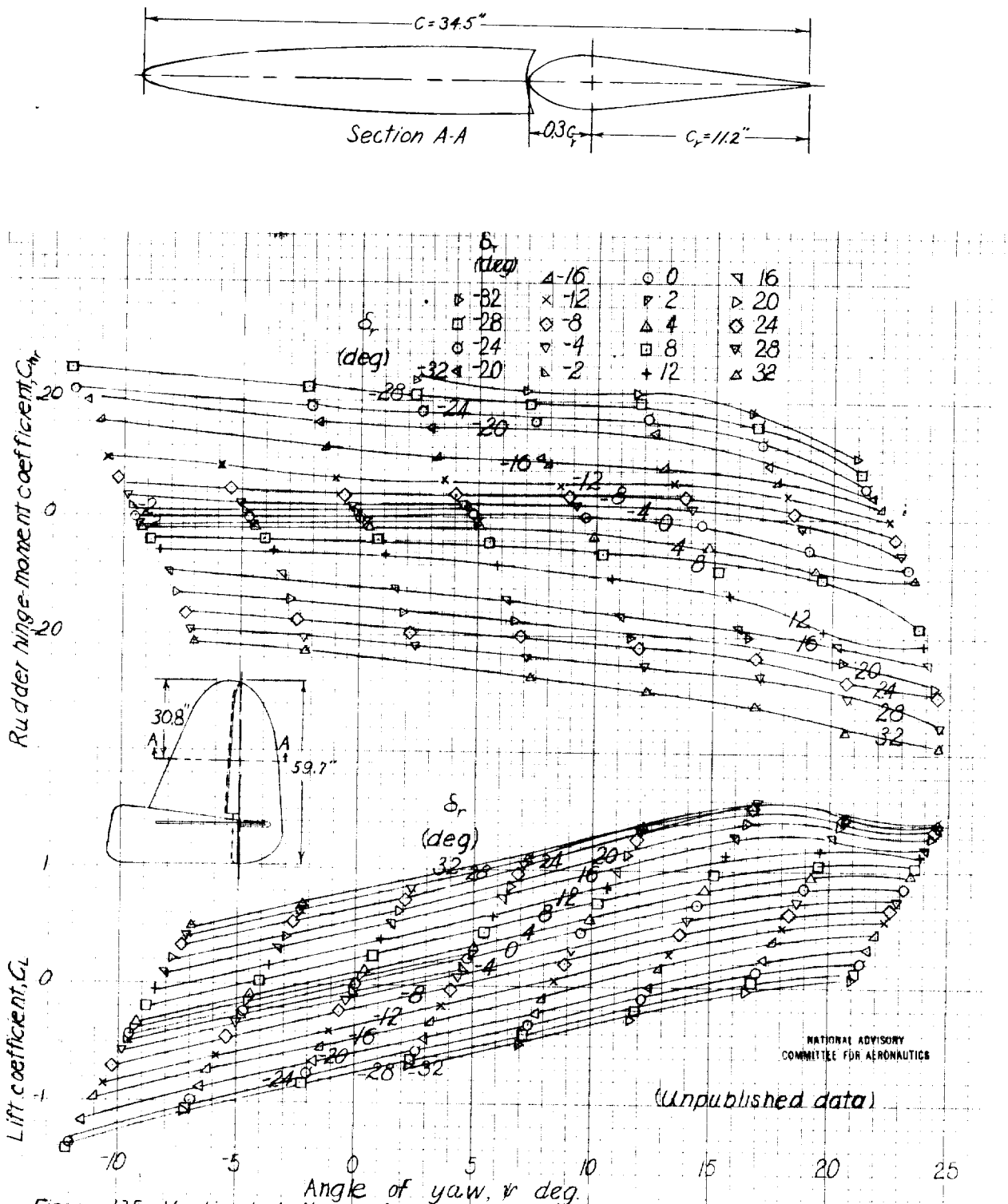

Figure 135.- Vertical tail surface $S_t/S = 0.42$, $A = 2.41$, $S_b/S_r = 0.20$, medium nose shape overhang, 0.113 in gap.

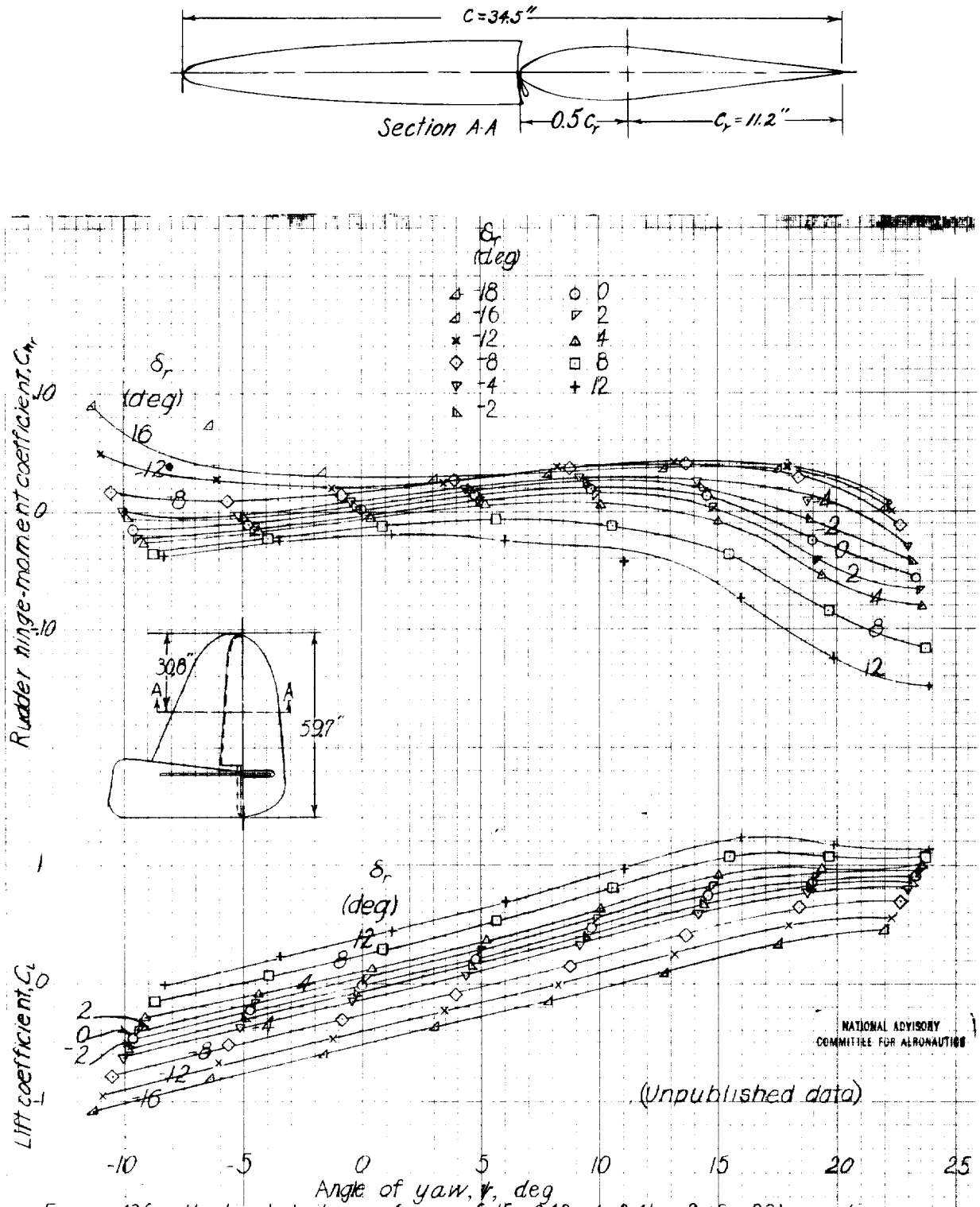

Figure 136.- Vertical tail surface, $S_r/S = 0.42$, $A = 2.41$, $S_h/S_r = 0.31$, medium nose shape overhang, sealed gap.

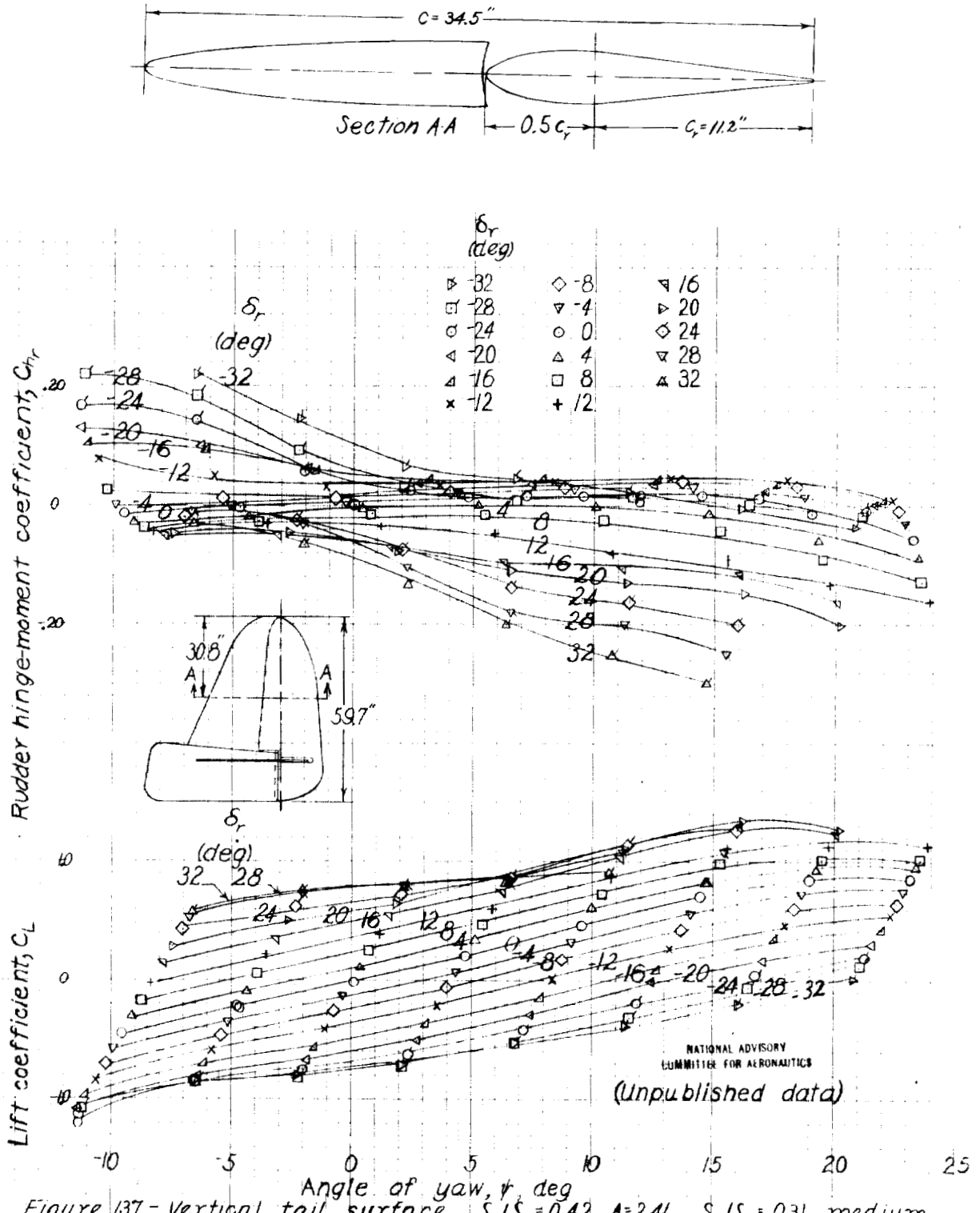

Figure 137.- Vertical tail surface, S_r/S = 0.42, A = 2.41, S_b/S_r = 0.31, medium nose shape overhang, 0.113 in gap.

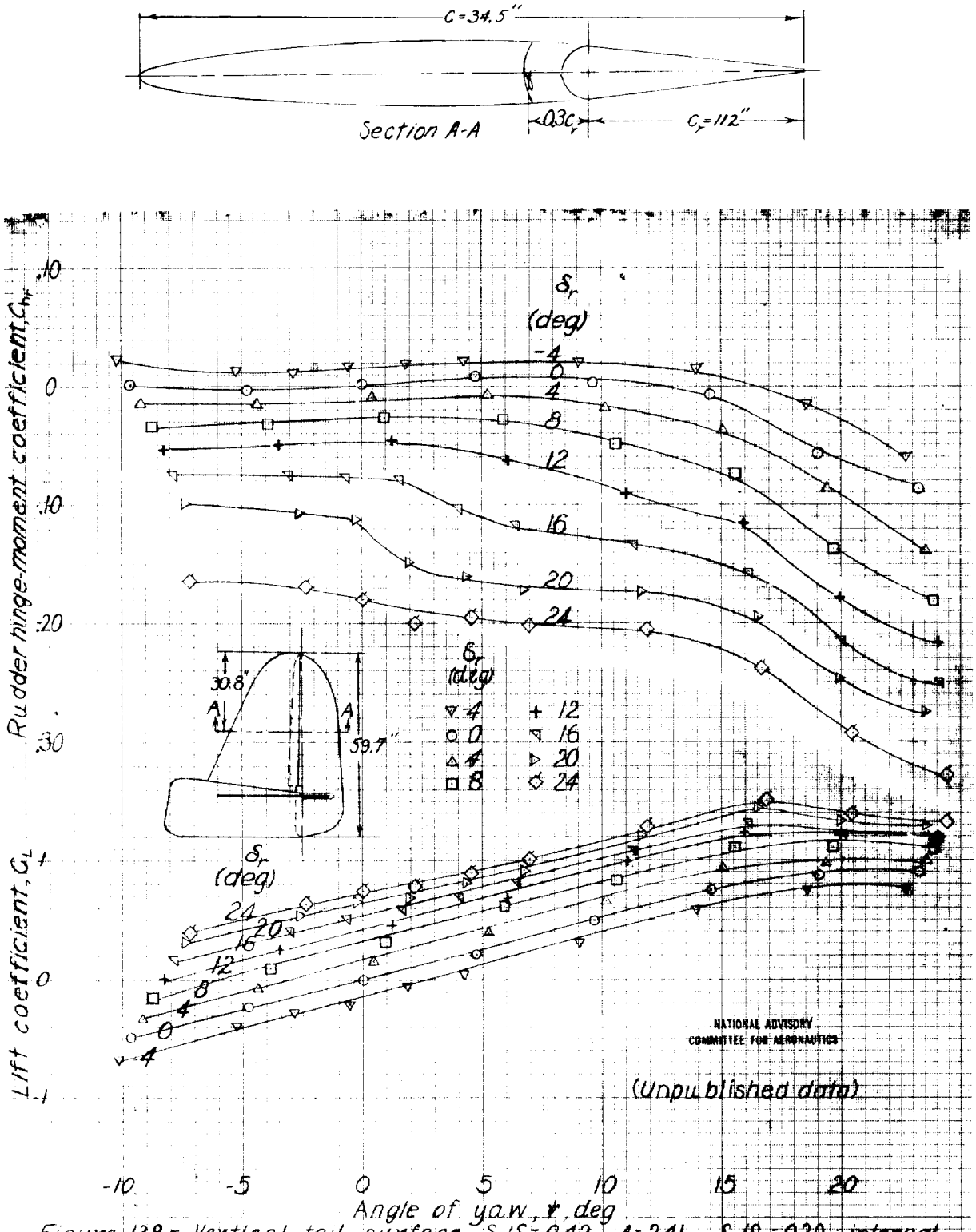

Figure 138.- Vertical tail surface, $S_r/S = 0.42$, $A = 2.41$, $S_b/S_r = 0.20$, internal balance, sealed gap, Hinges sealed.

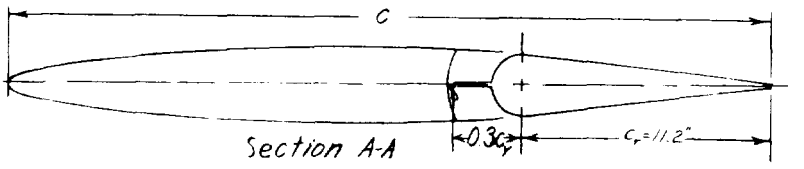

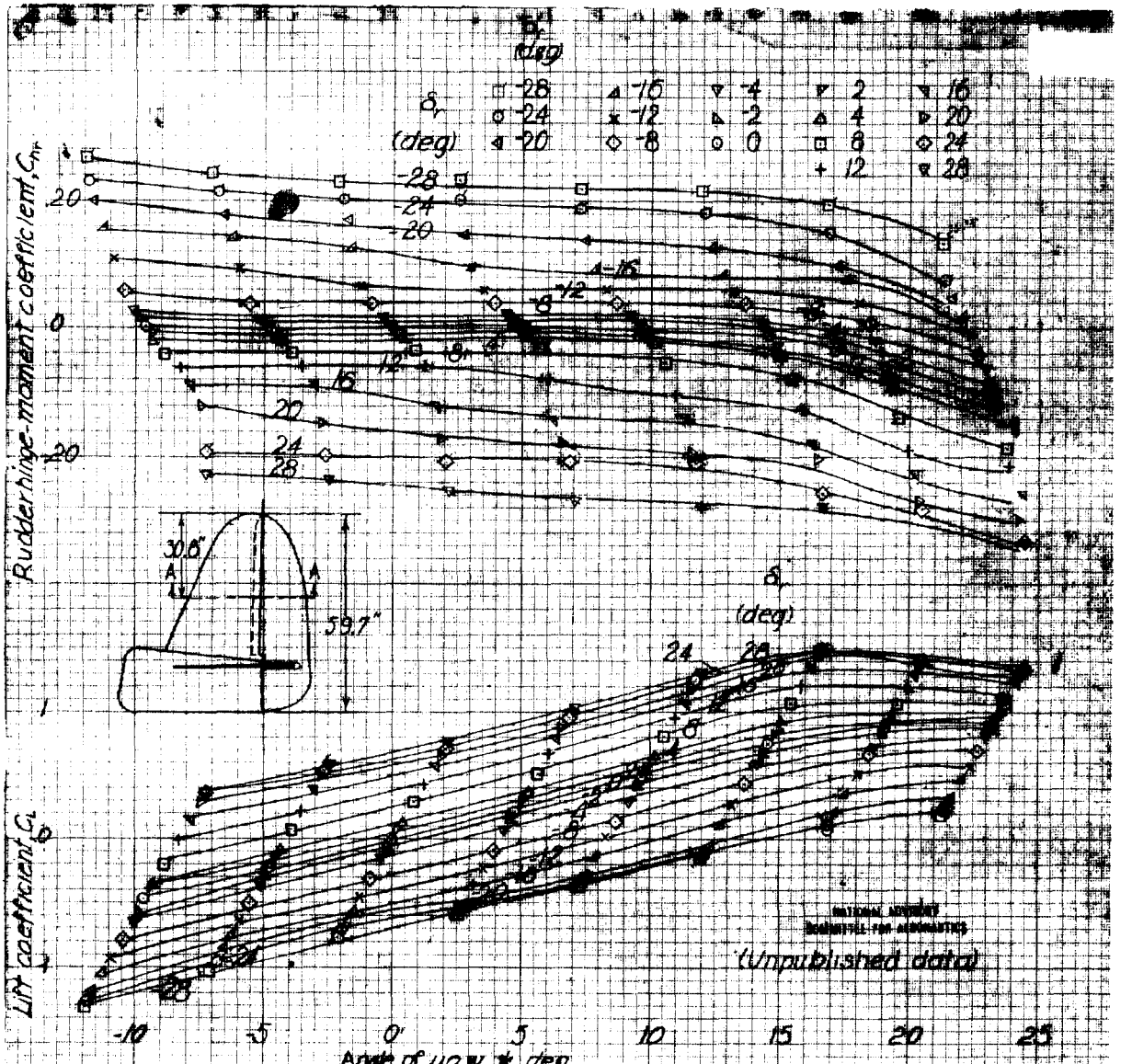

Figure 139.- Vertical tail surface, $S_v/S = 0.42$, $A = 2.41$, $S_r/S_v = 0.20$, internal balance, Sealed gap, Hinges unsealed.

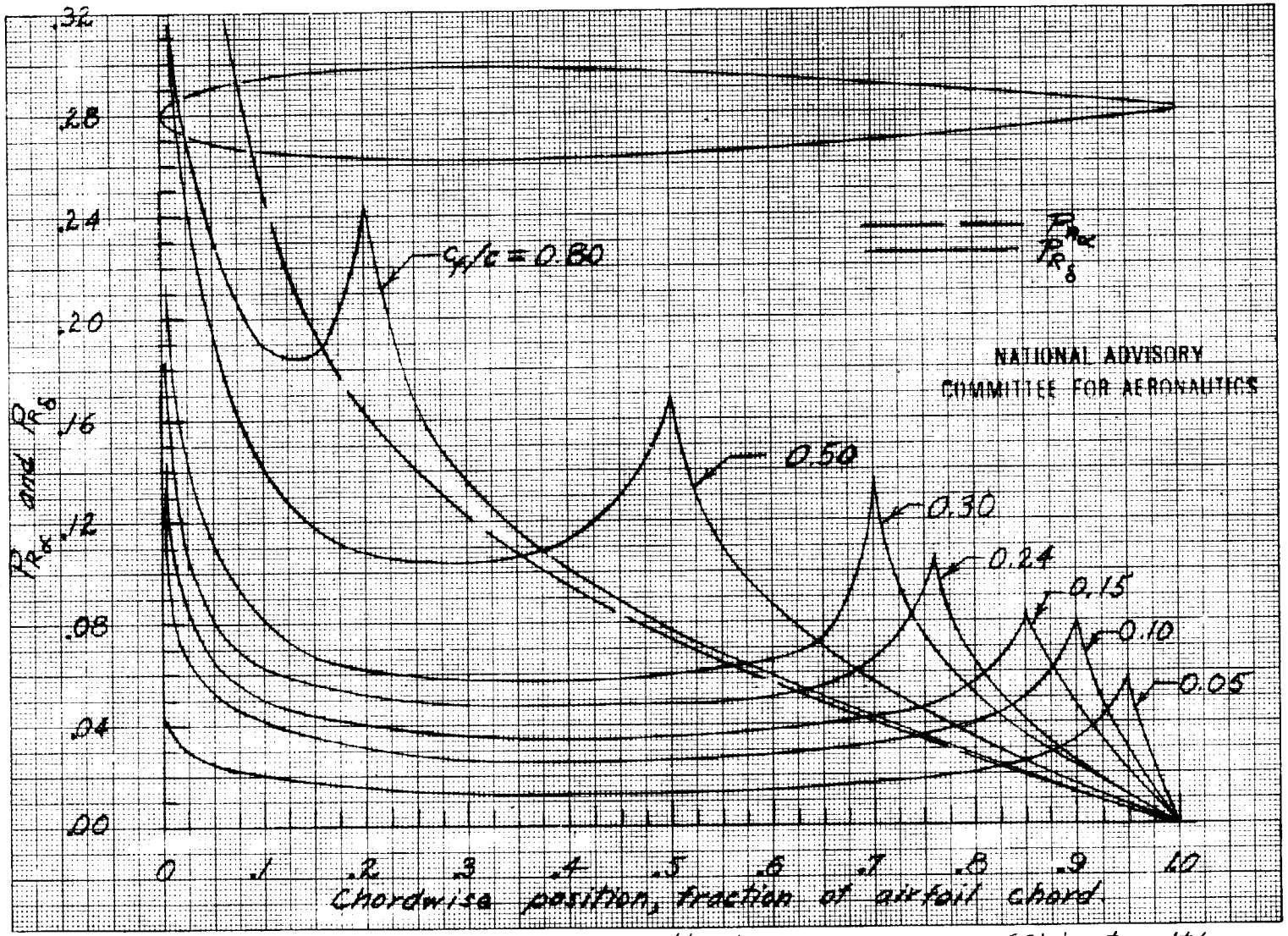

Figure 140.-Rate of change of resultant pressure coefficient with angle of attack and with flap deflection as a function of chordwise position. NACA 0009 airfoil; plain flaps; sealed gaps; section data.

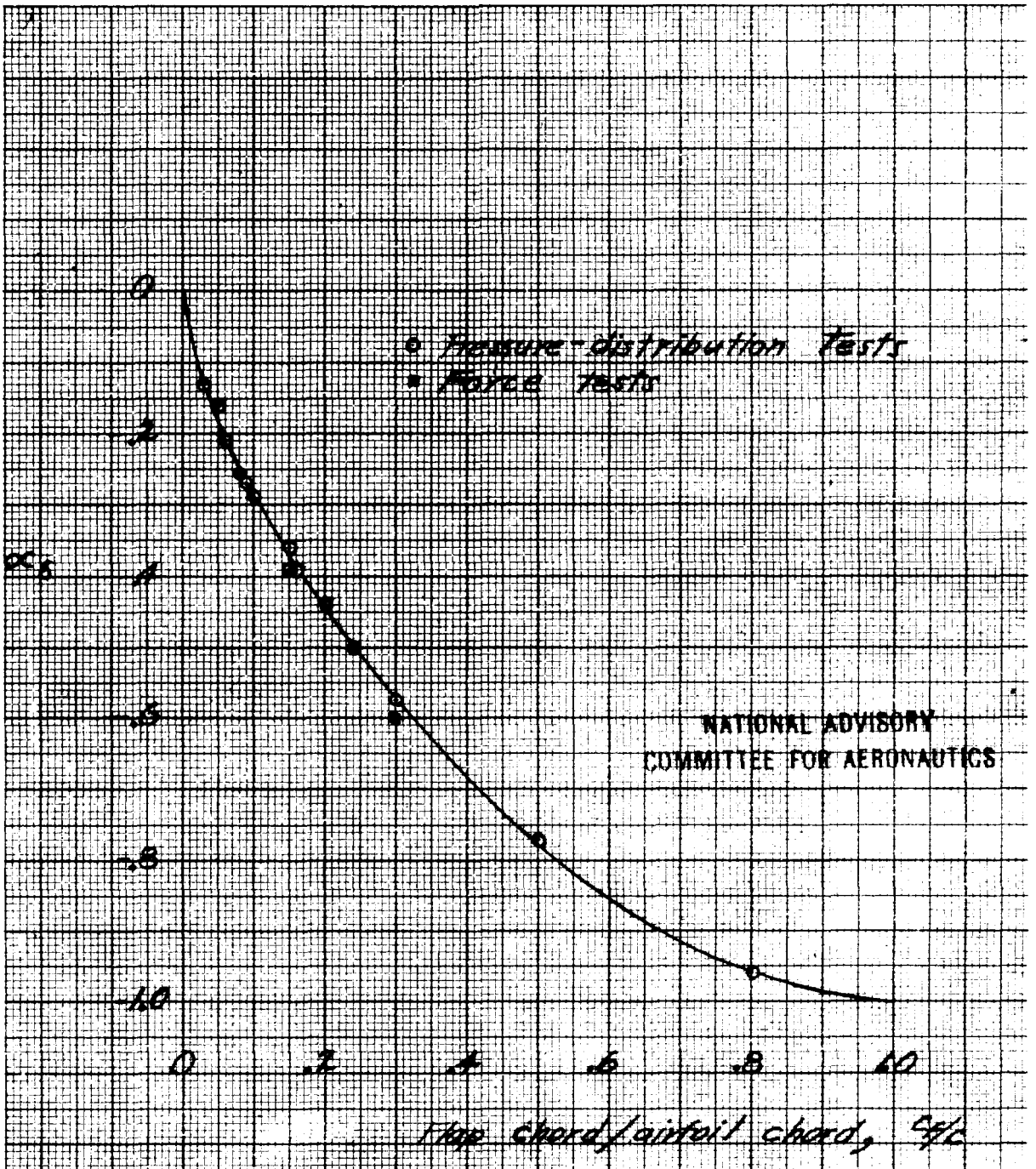

Figure 141.- Variation of lift effectiveness parameter with ratio of flap chord to airfoil chord. Plain flaps with sealed gaps on NACA 0009 airfoil.

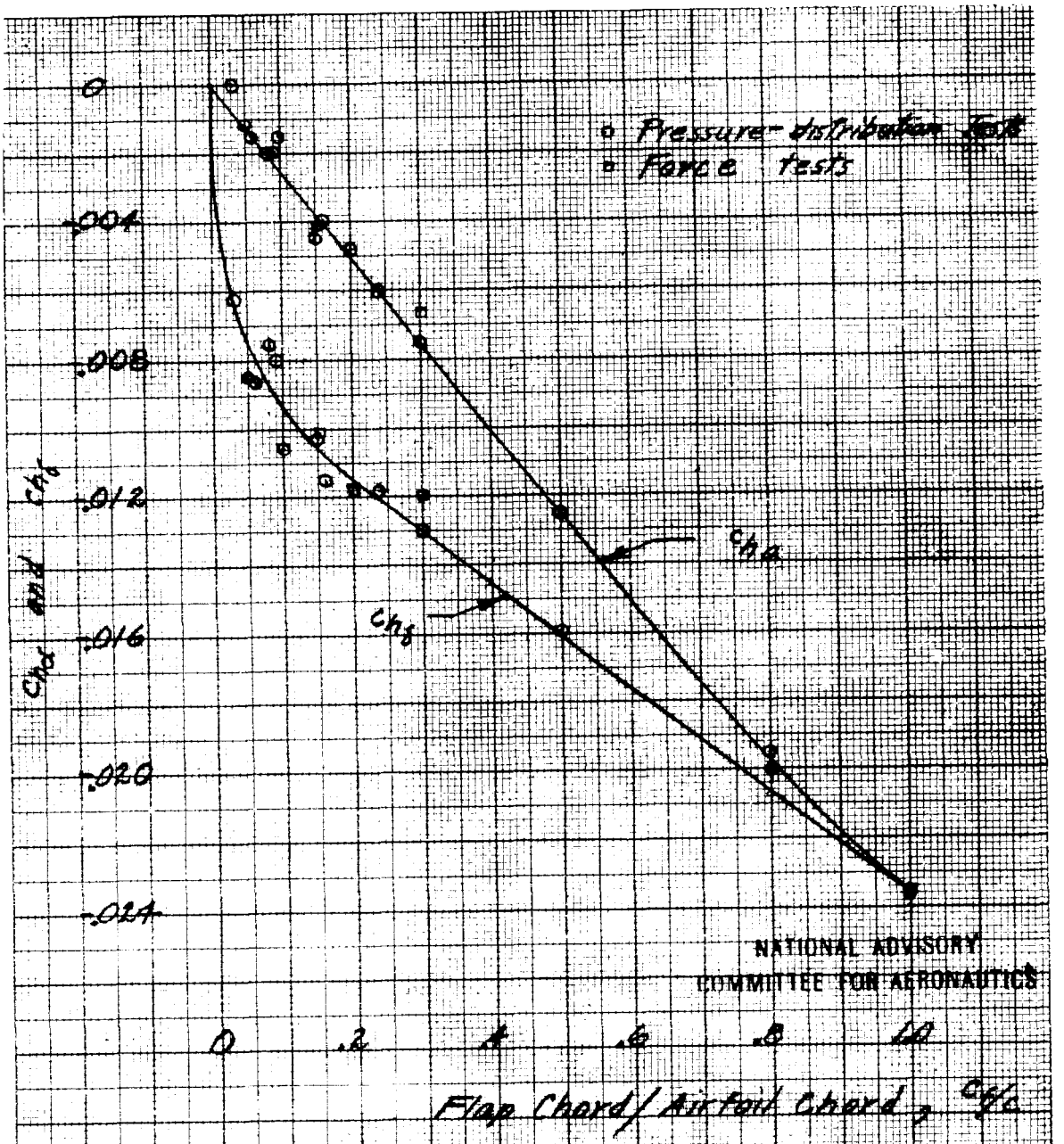

Figure 142.- Variation of flap section hinge-moment parameters with ratio of flap chord to airfoil chord. Plain flaps with sealed gaps on NACA 0009 airfoil.

L-663

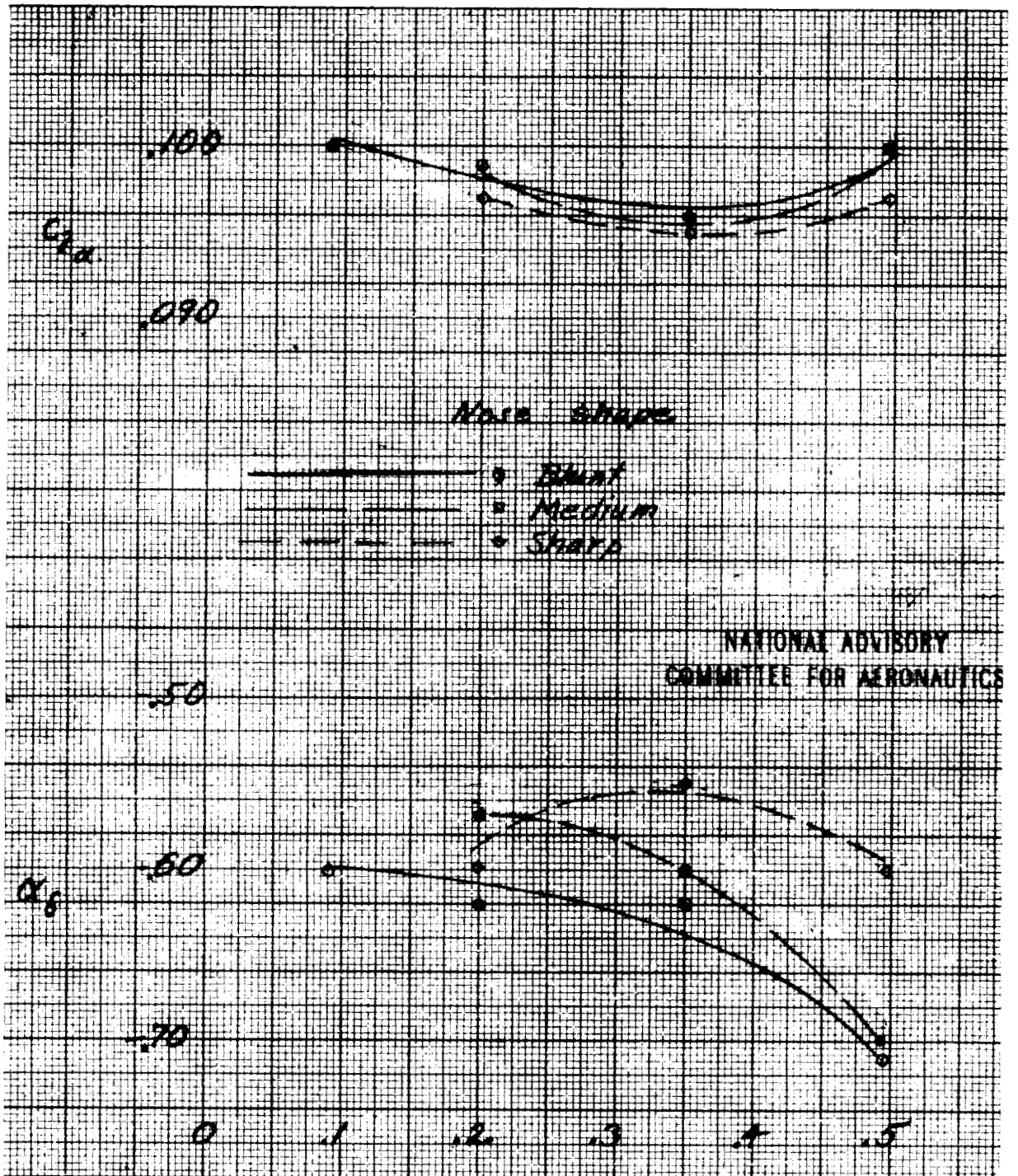

(a) NACA 0009 airfoil, sealed gap.

Figure 143.- Variation of airfoil section lift parameters with overhang. 0.30 c flap.

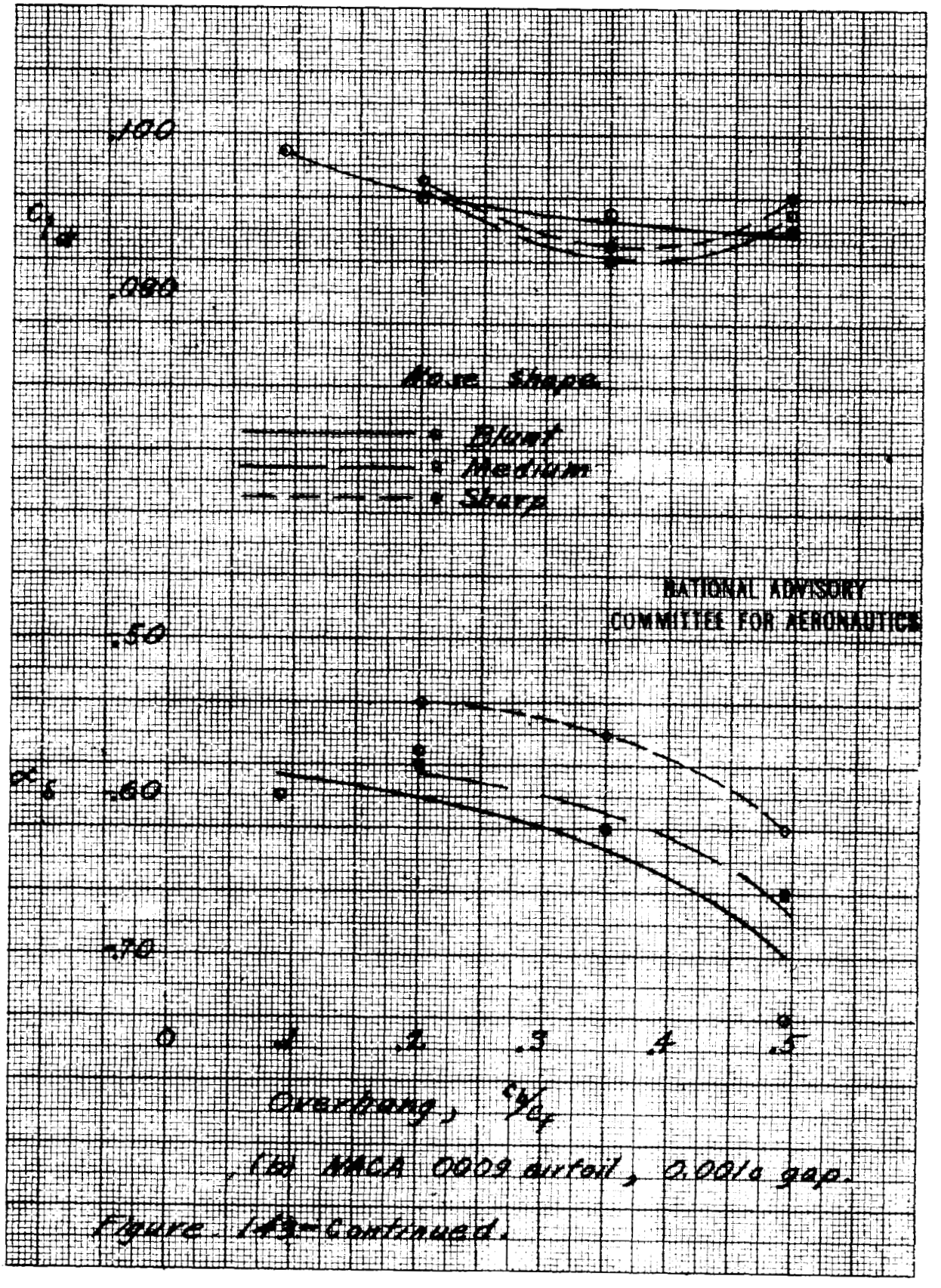

(b) NACA 0009 airfoil, 0.001c gap.

Figure 14.—Continued.

L-663

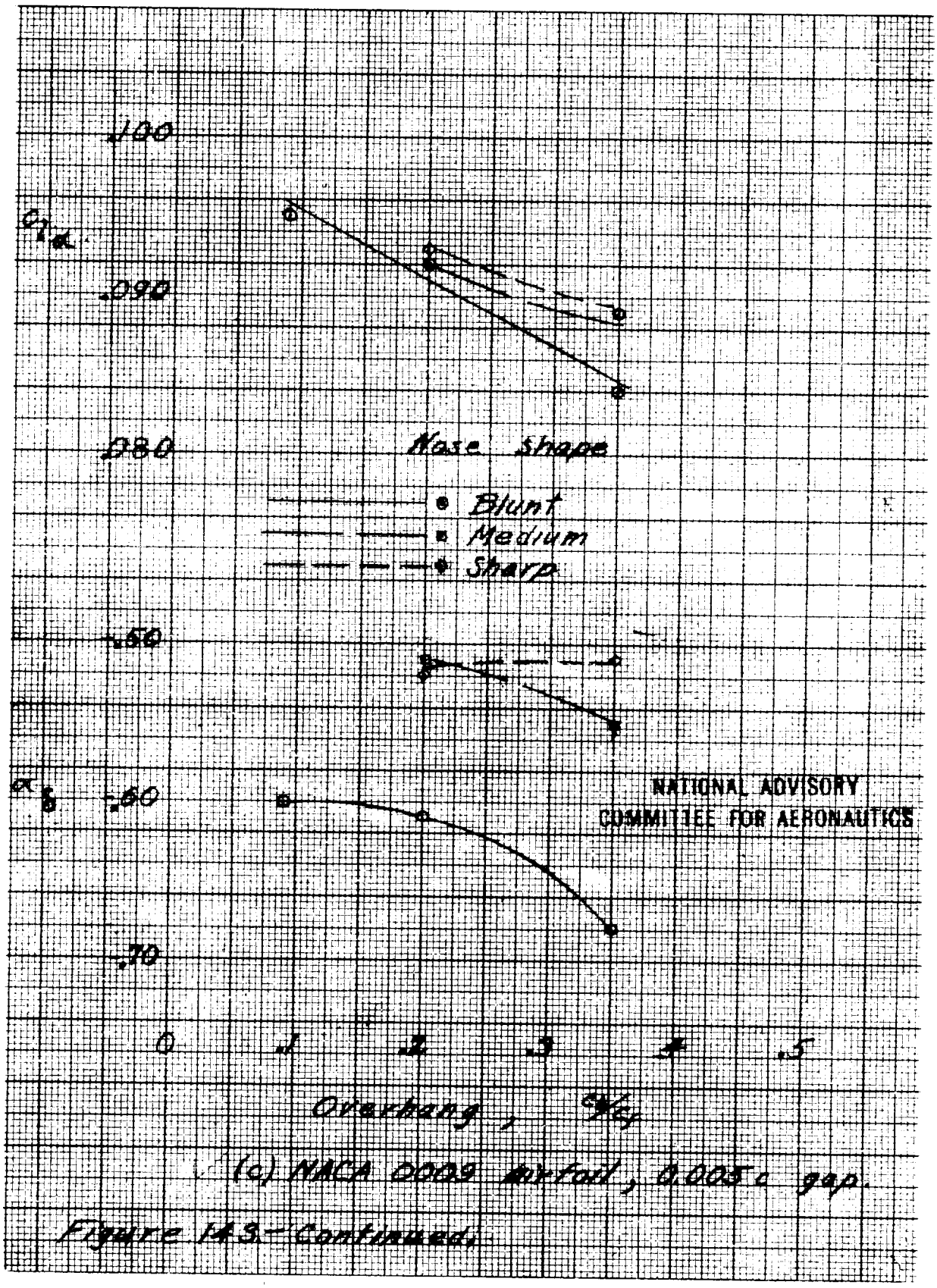

(c) NACA 0009 airfoil, 0.005 c gap.

Figure 143.- Continued.

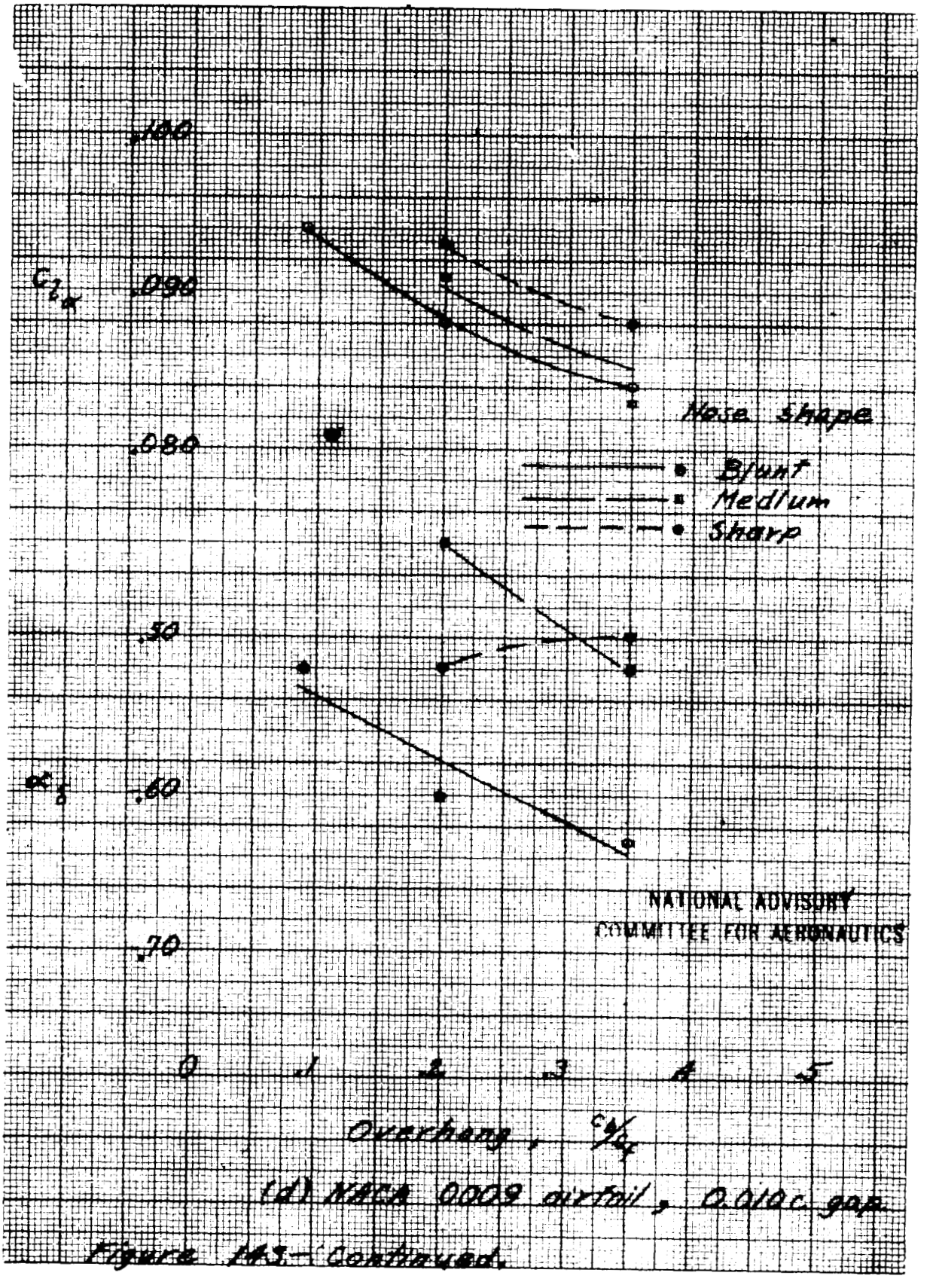

(d) NACA 0009 airfoil, 0.010c gap.

Figure 145.—Continued.

L-663

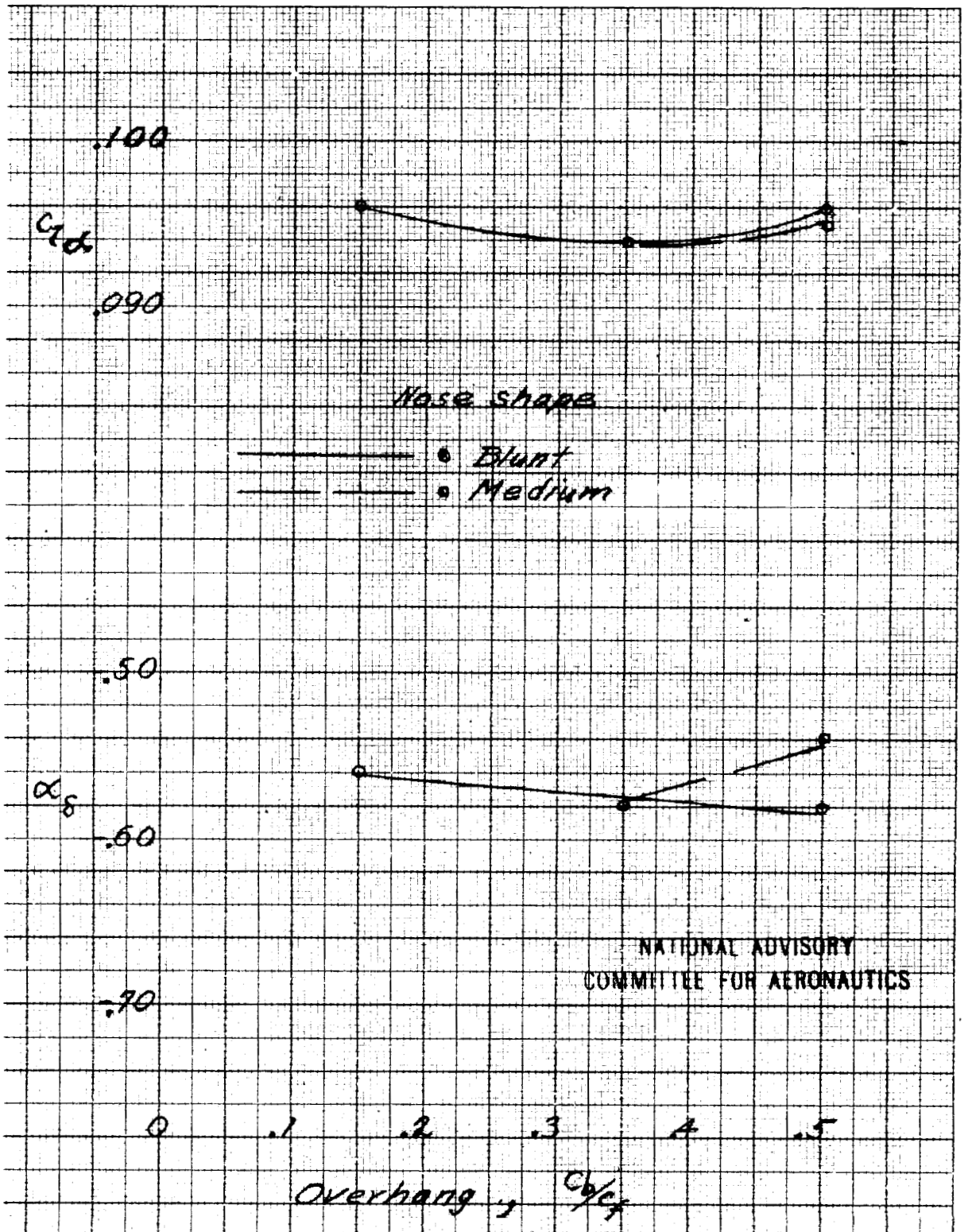

(e) NACA 0015 airfoil, sealed gap.

Figure 143.- Continued.

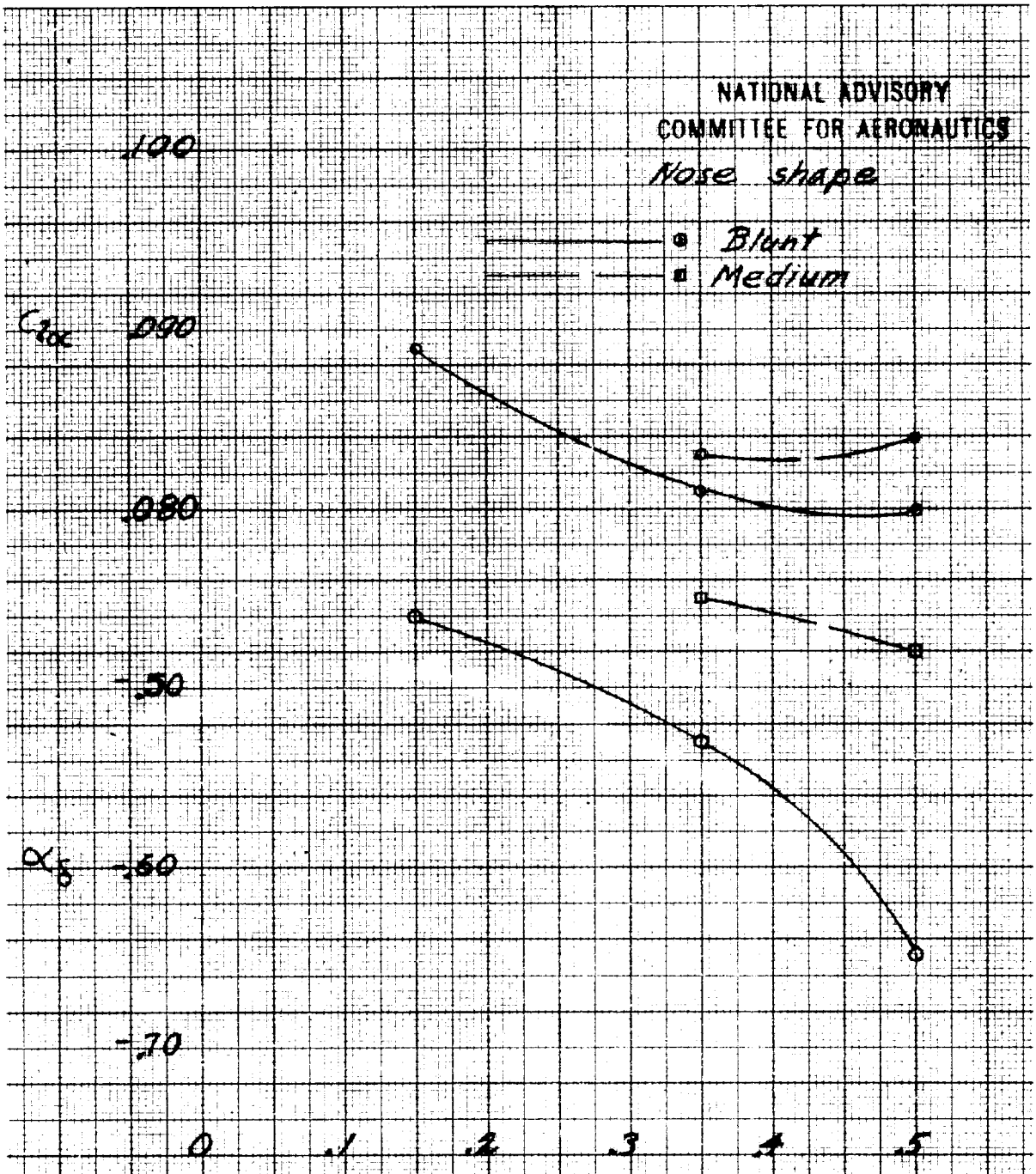

(f) NACA 0015 airfoil, 0.005c gap.

Figure 143.- Continued.

L-663

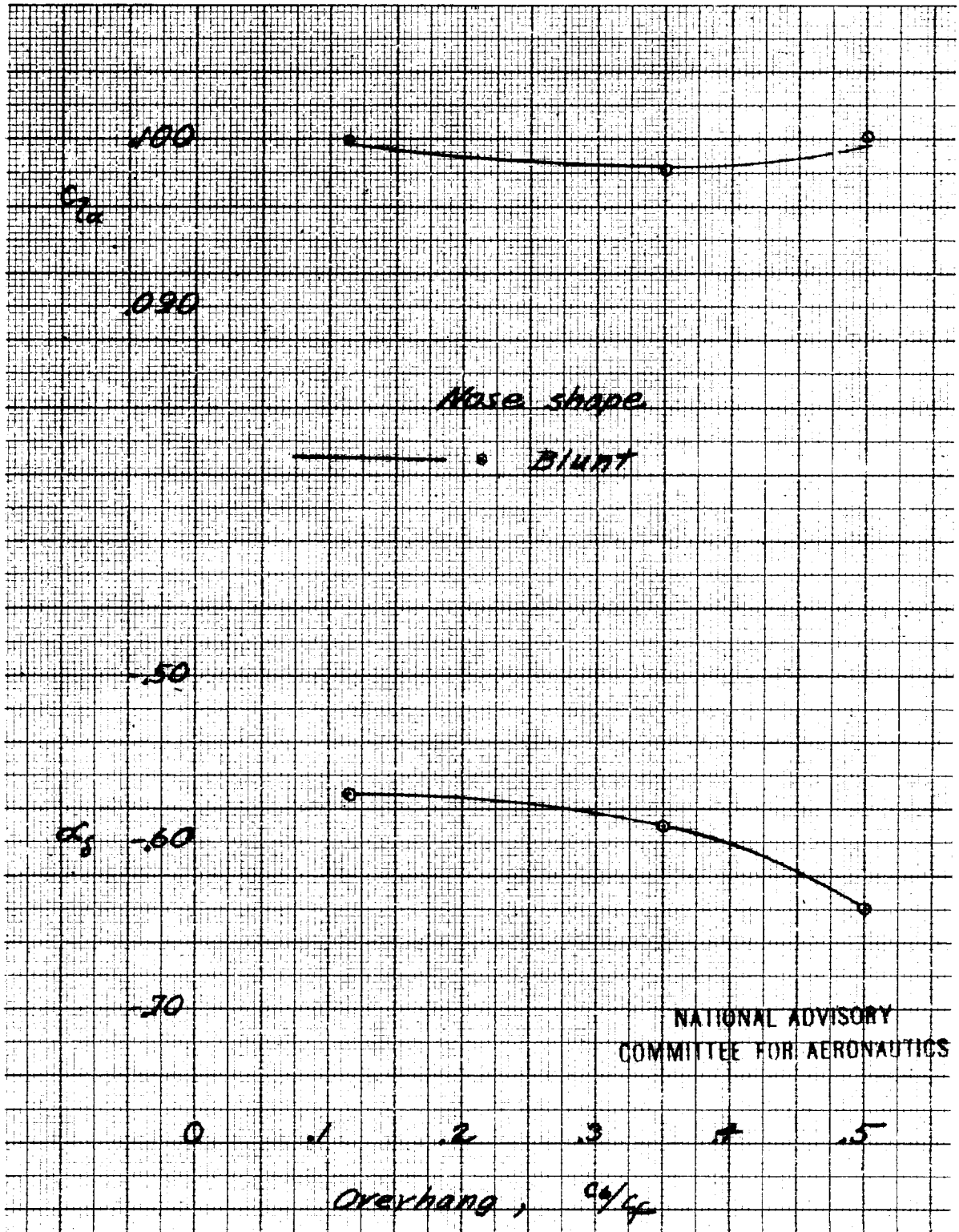

(g) NACA 66-009 airfoil, sealed gap.

Figure 143.- Continued.

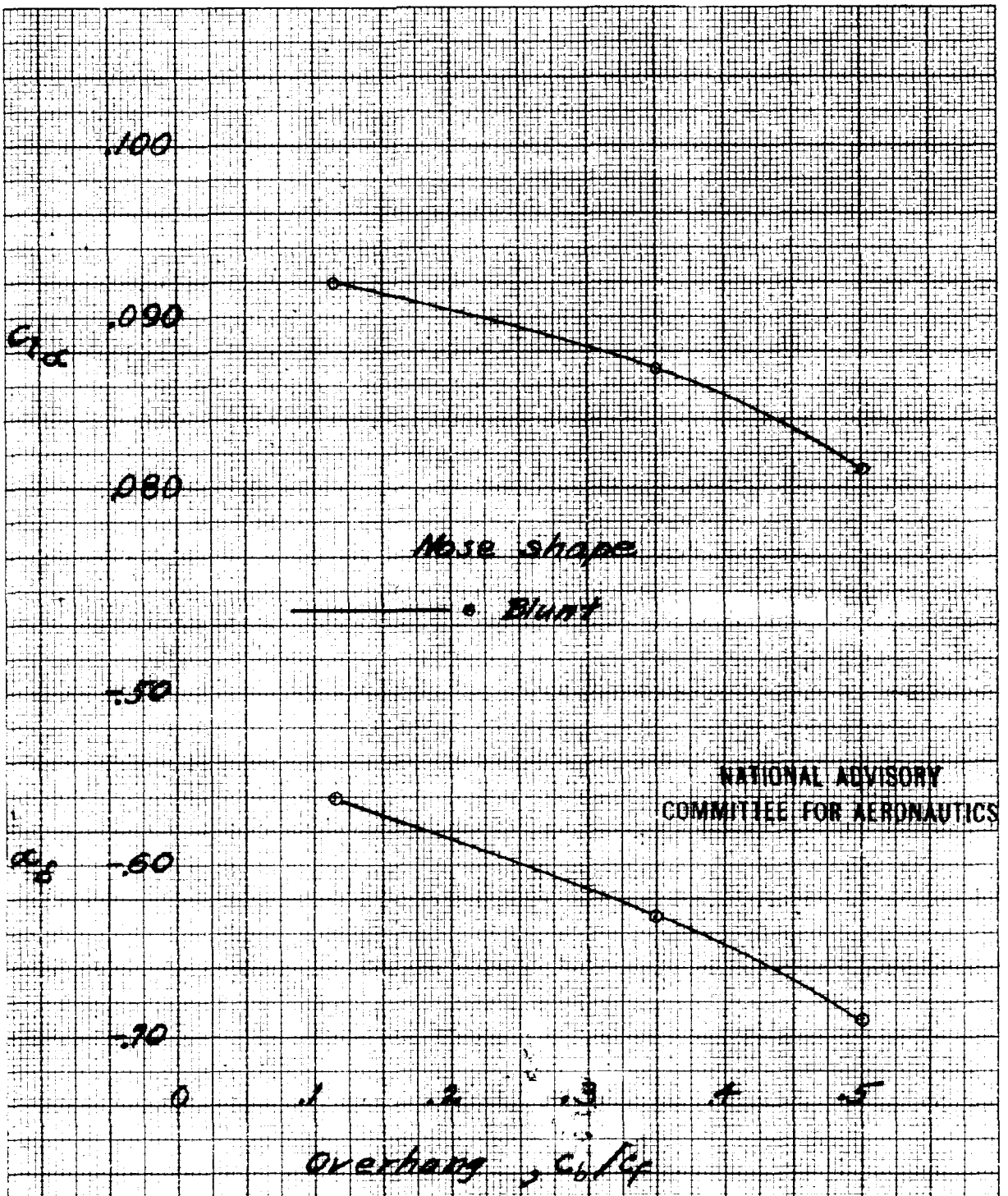

(h) NACA 66-009 airfoil, 0.005c gap.

Figure 143.- Concluded.

L-663

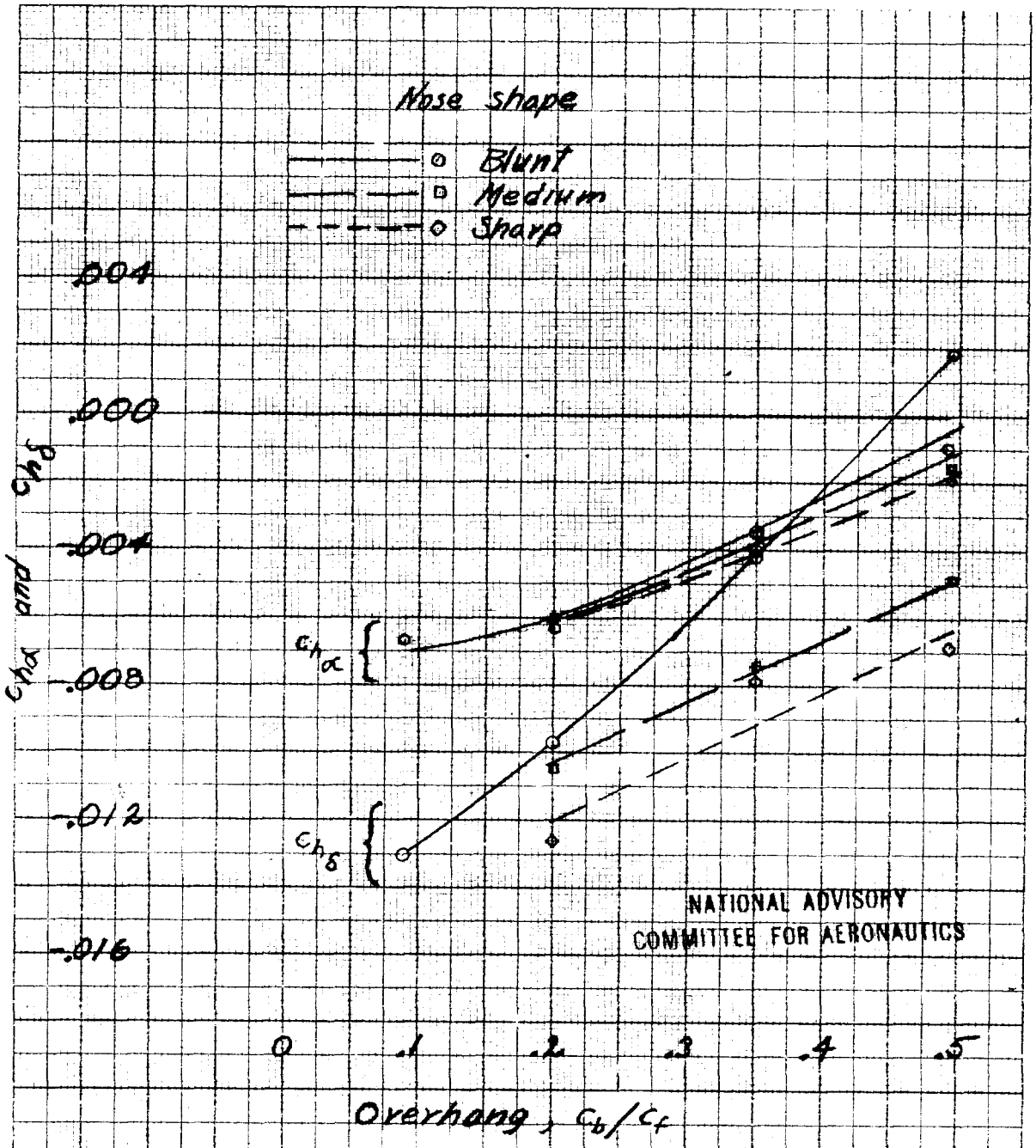

(a) NACA 0009 airfoil, sealed gap.

Figure 144.- Variation of flap section hinge-moment parameters with overhang. 0.30c flap.

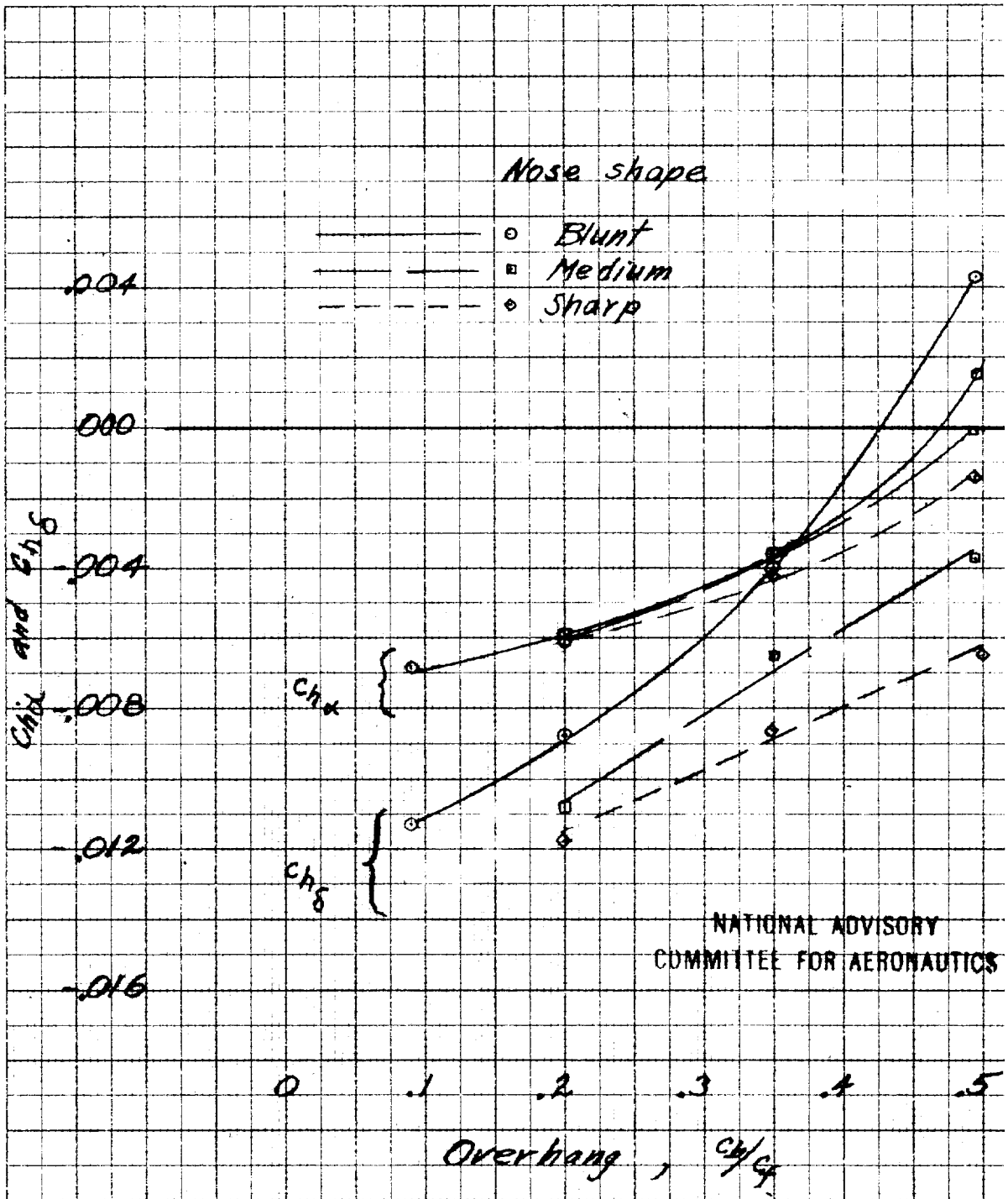

(b) NACA 0009 airfoil, 0.001c gap.

Figure 144.-Continued.

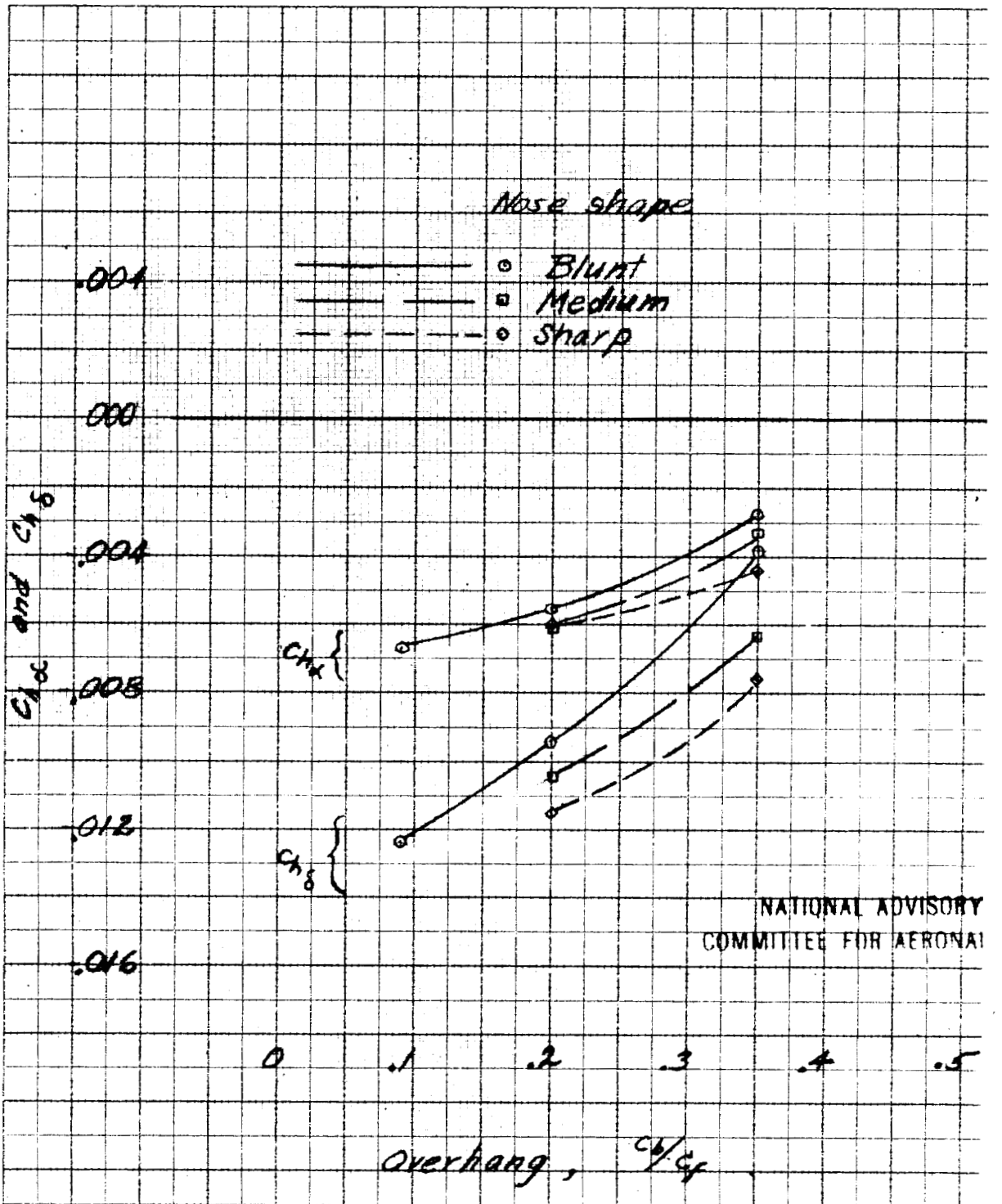

NATIONAL ADVISORY
COMMITTEE FOR AERONAU

(c) NACA 0009 airfoil, 0.005c gap.

Figure 144.- Continued.

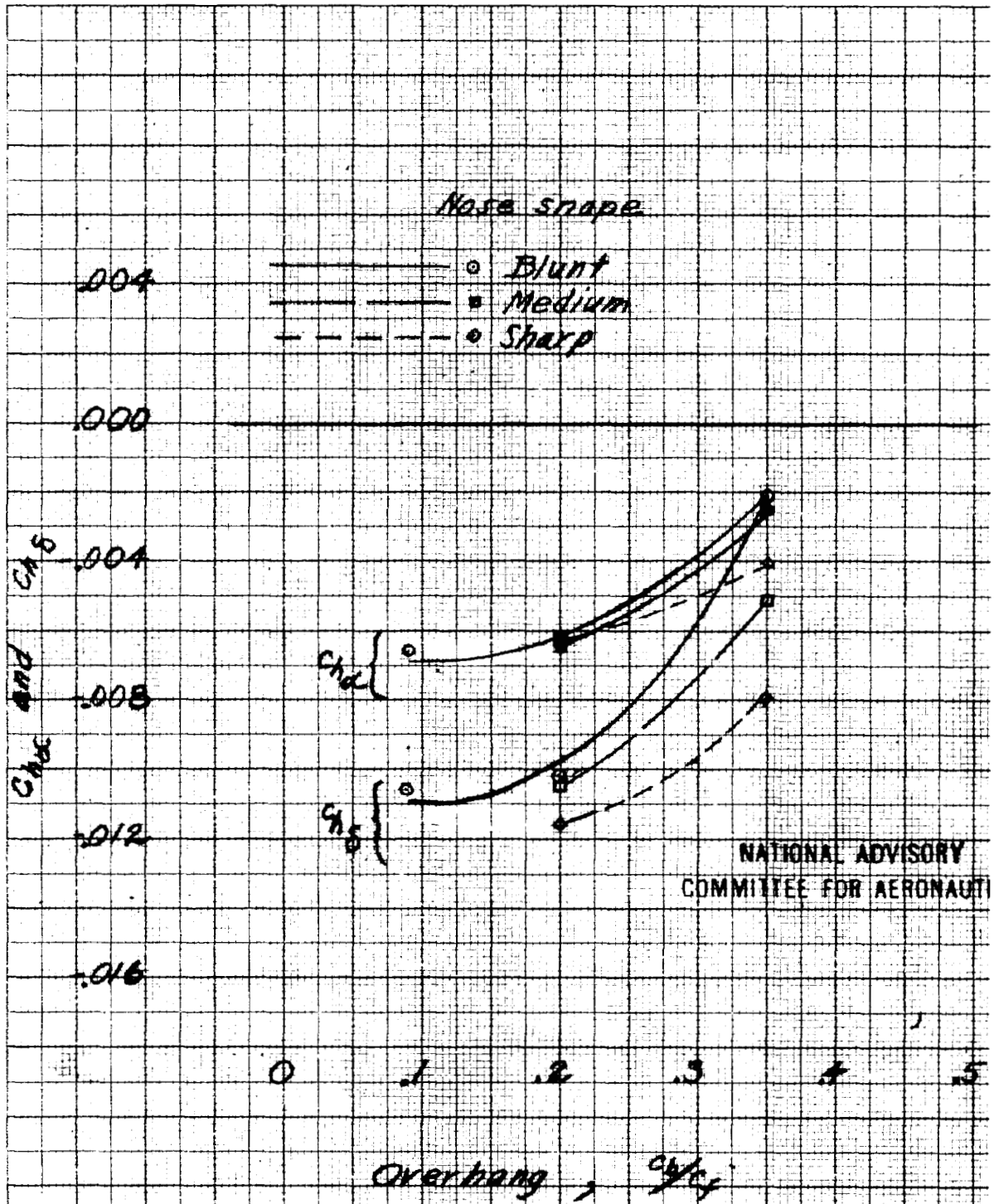

(d) NACA 0009 airfoil, 0.010c gap.

Figure 144.-Continued.

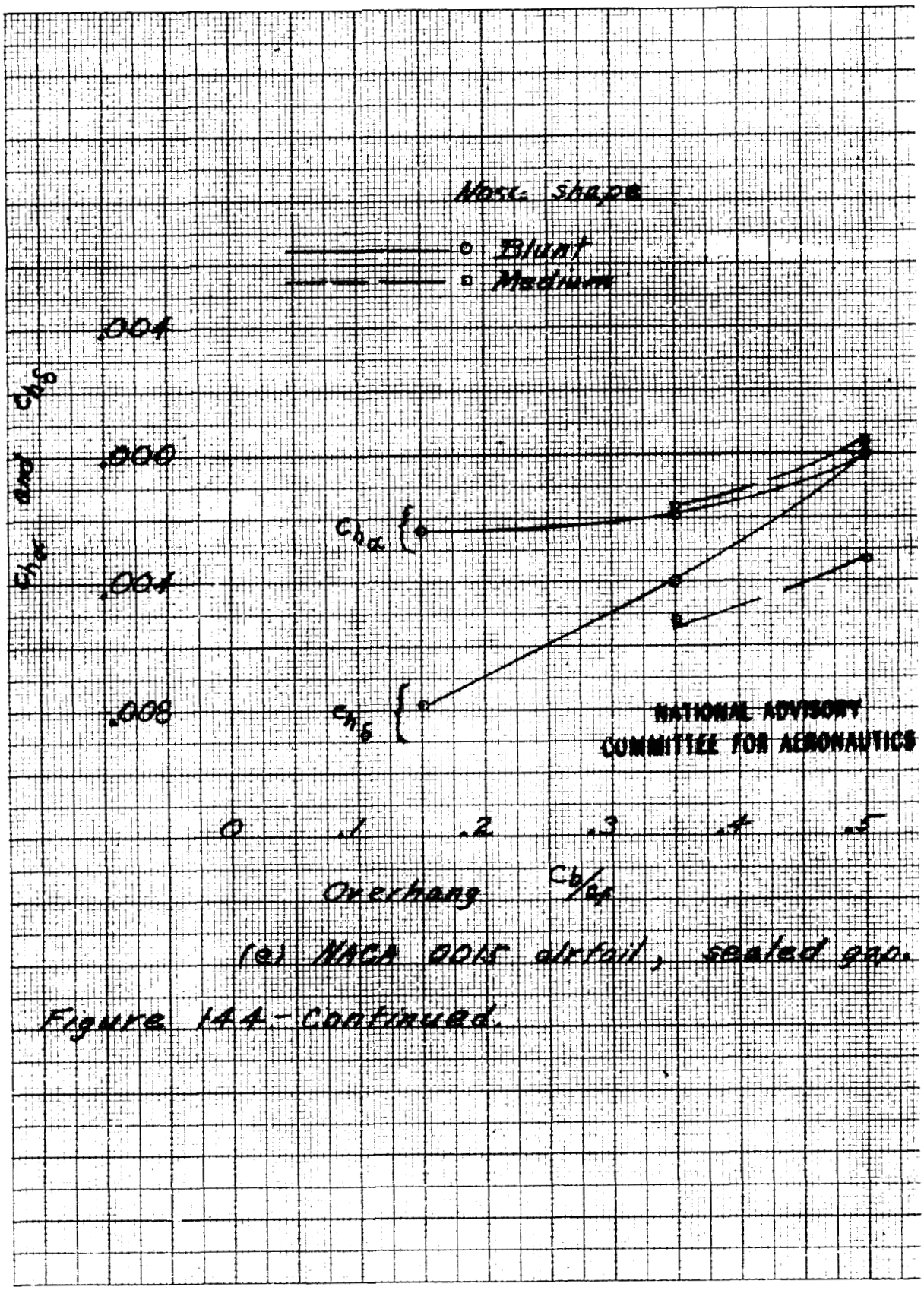

(e) NACA 2015 airfoil, sealed gap.

Figure 144.- Continued.

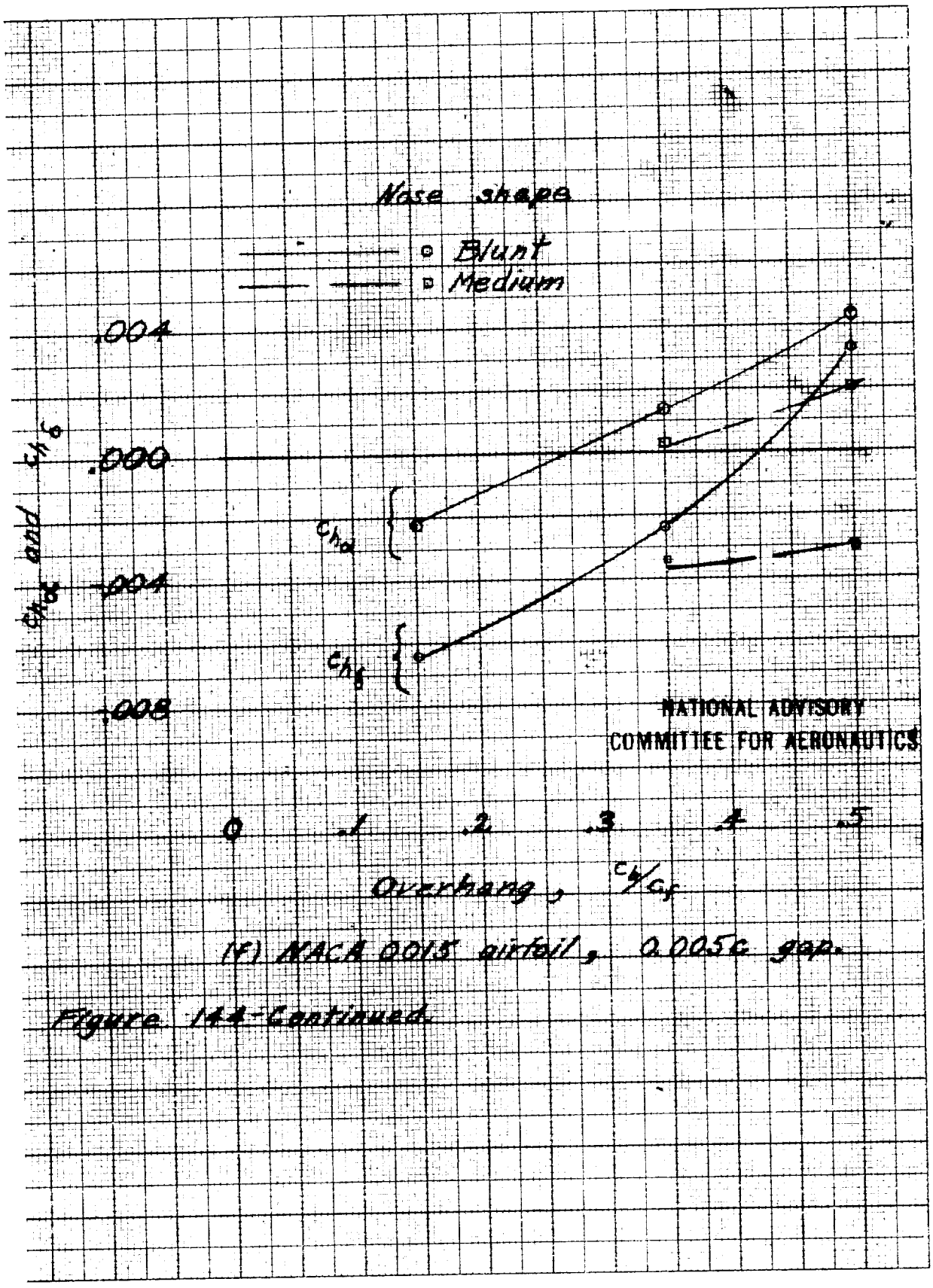

(f) NACA 0015 airfoil, 0.005c gap.

Figure 144-Continued.

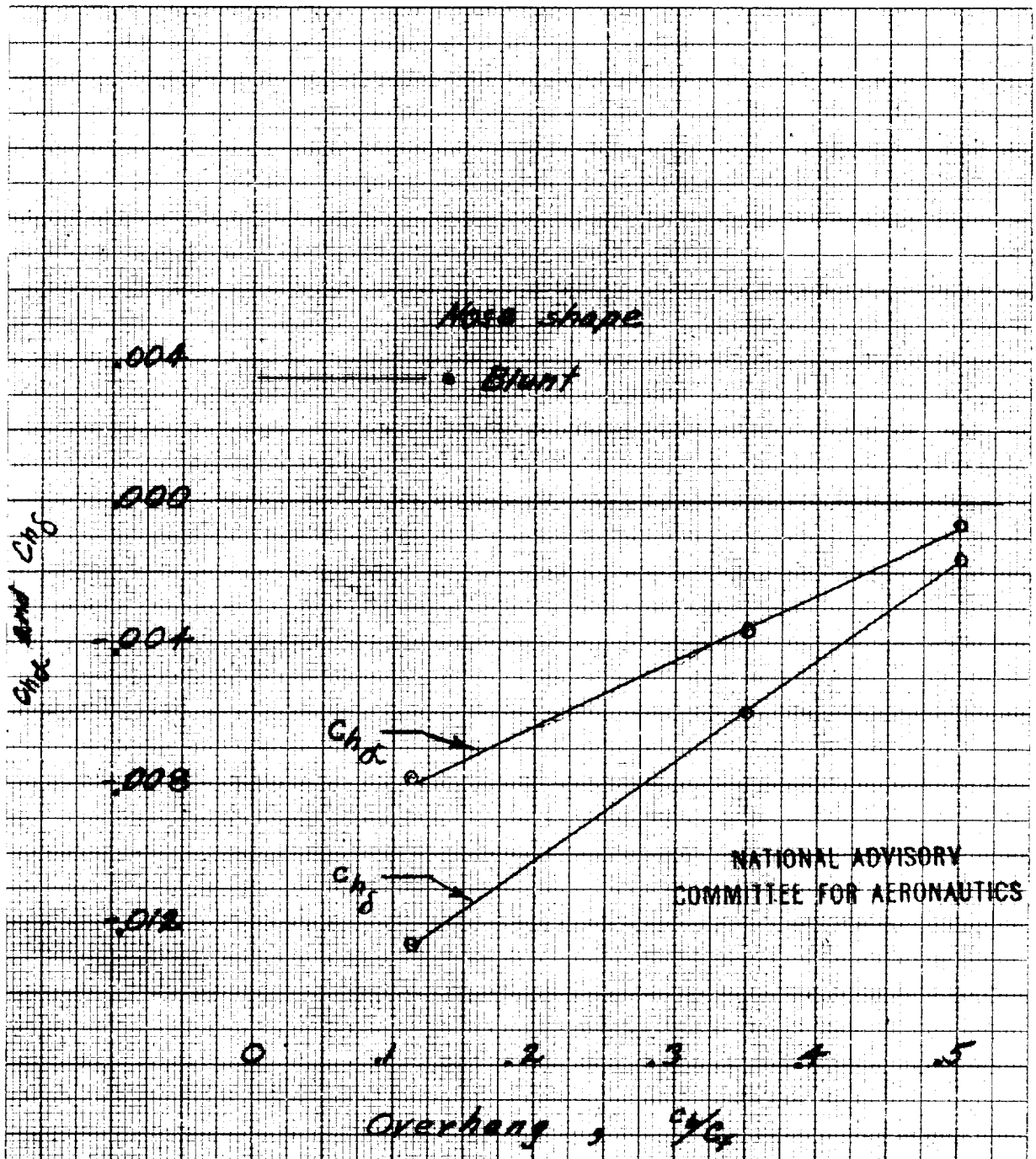

(g) NACA 66-009 airfoil, sealed gap.

Figure 144.-Continued.

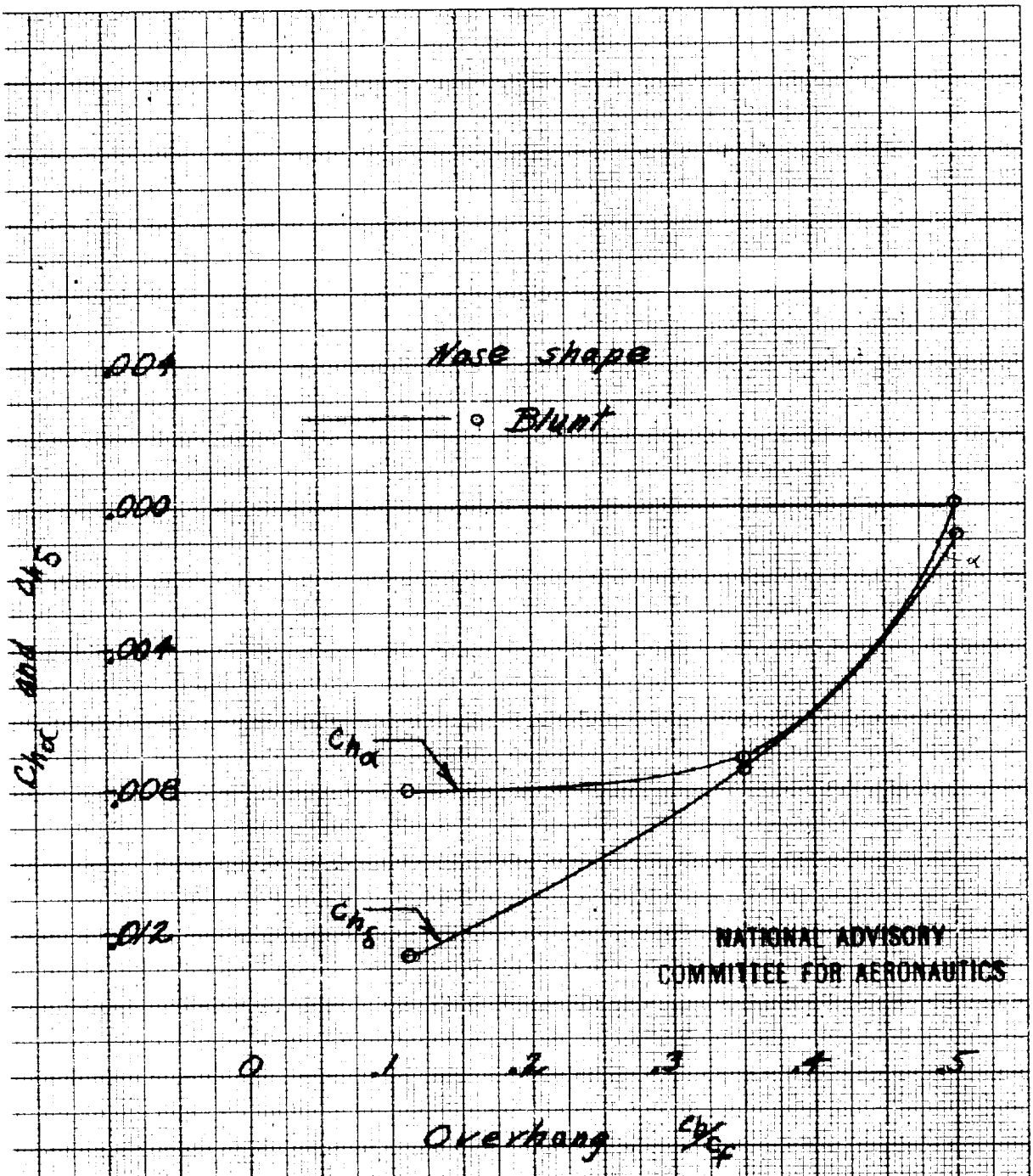

NATIONAL ADVISORY
COMMITTEE FOR AERONAUTICS

(h) NACA 66-009 airfoil, 0.005c gap.

Figure 144 - Concluded.

L-663

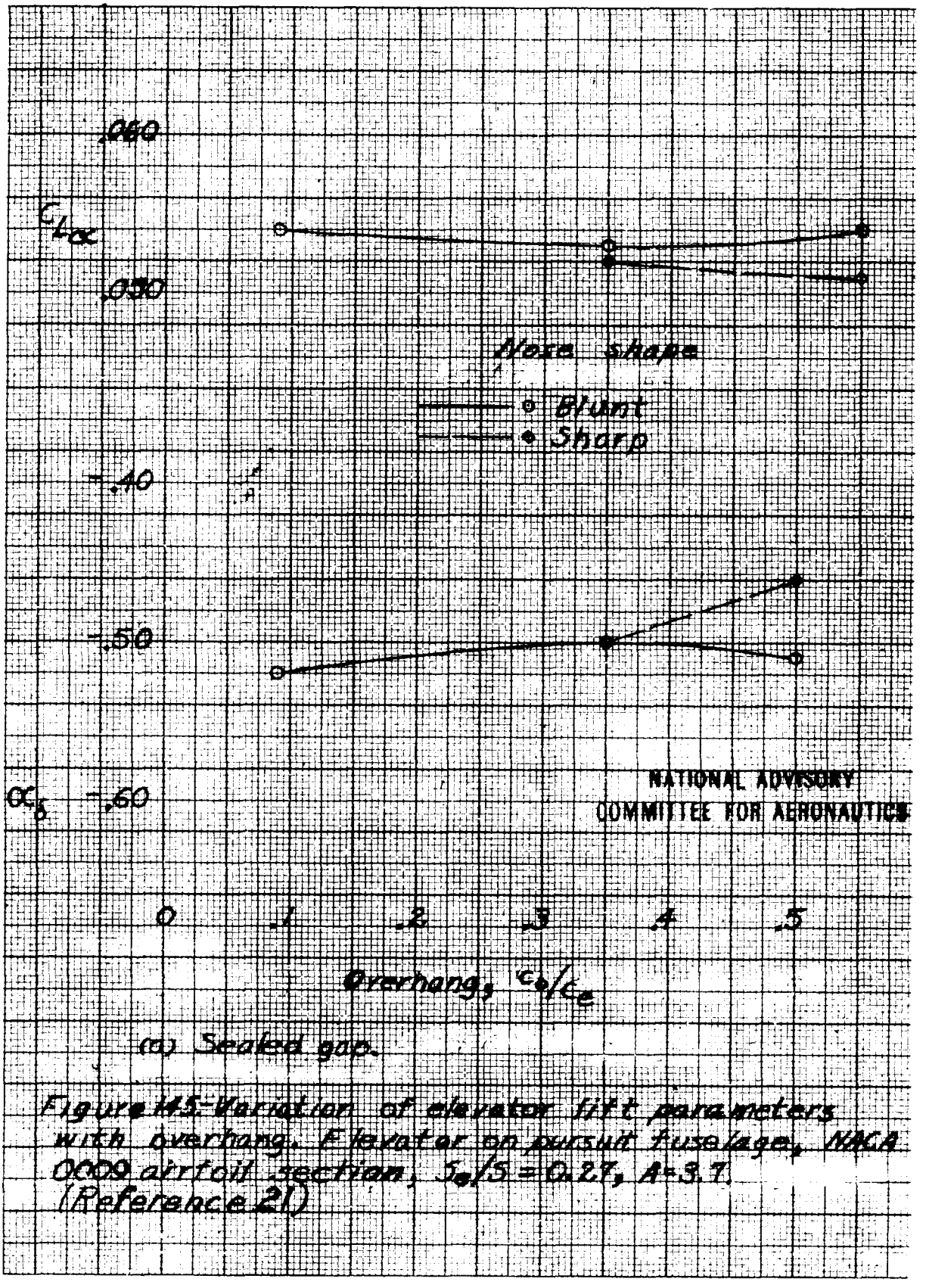

(a) Sealed gap.

Figure 45.- Variation of elevator lift parameters with overhang. Elevator on pursuit fuselage, NACA 0009 airfoil section, $S_e/S = 0.27$, $A = 3.7$. (Reference 21)

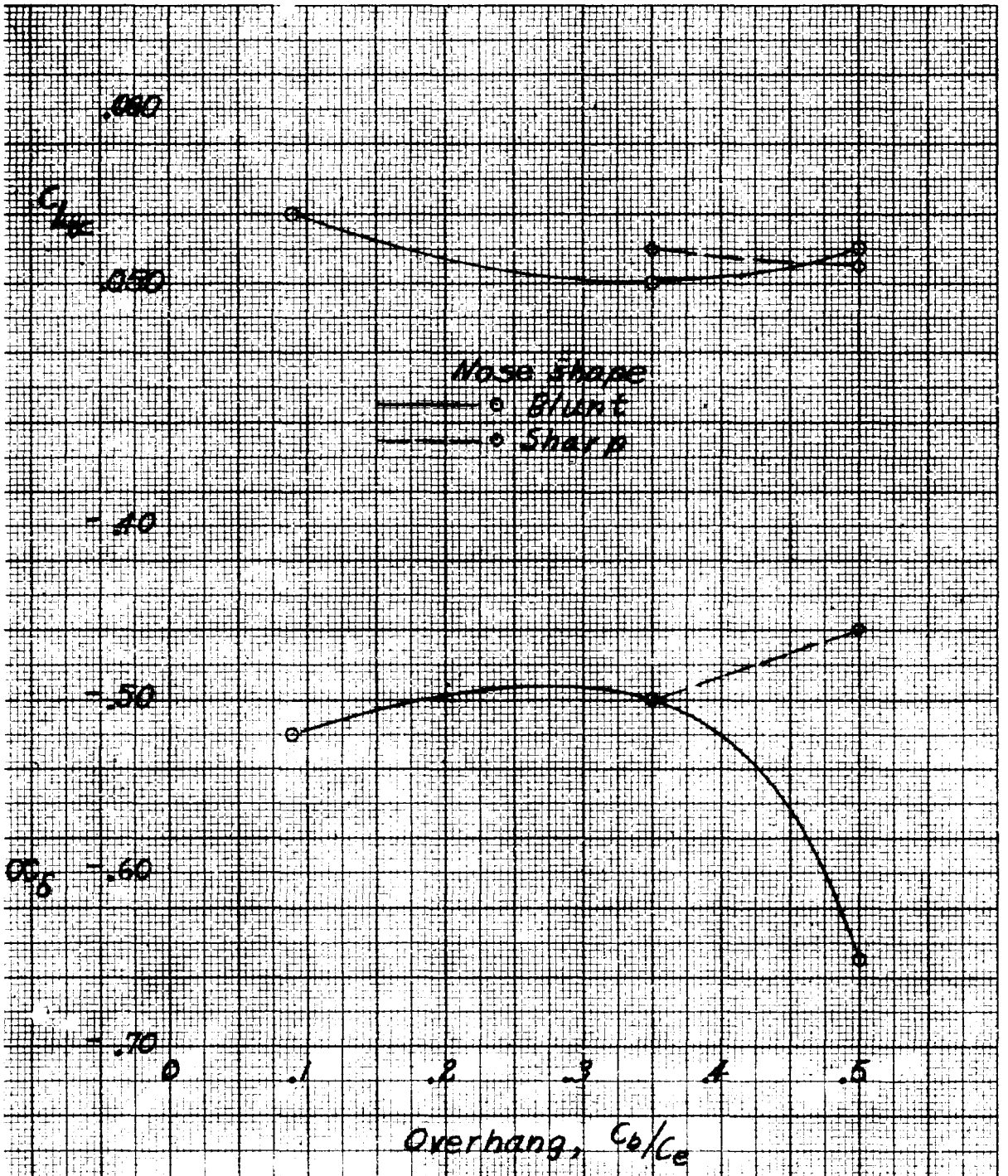

(b) 0.005c gap.

NATIONAL ADVISORY COMMITTEE FOR AERONAUTICS

Figure 146-Concluded.

L-663

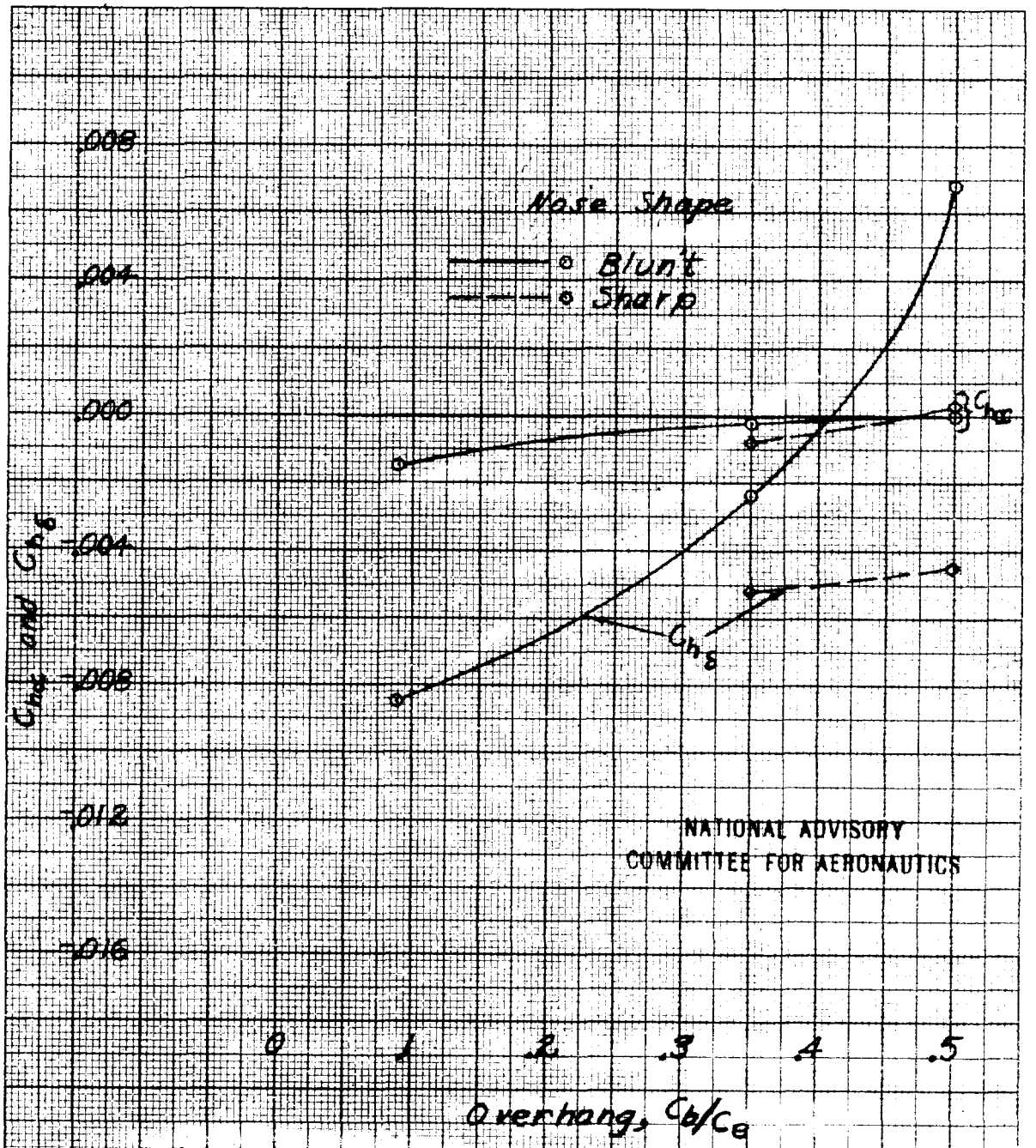

(a) Sealed gap.

Figure 146-Variation of elevator hinge-moment parameters with overhang. Elevator on pursuit fuselage, NACA 0009 airfoil section, $S_e/S = 0.27$, $A = 3.7$. (Reference 21)

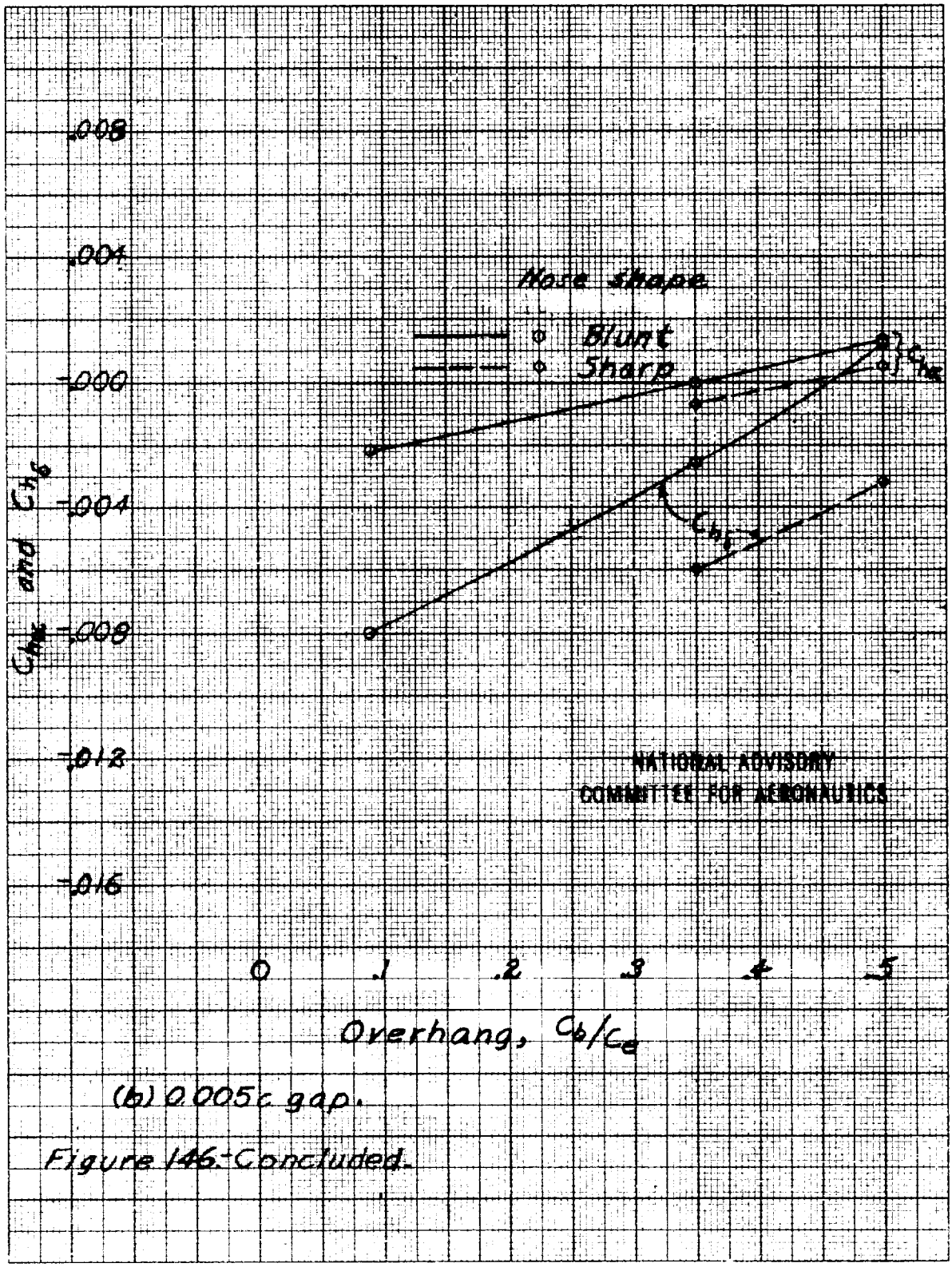

(b) 0.005c gap.

Figure 146.-Concluded.

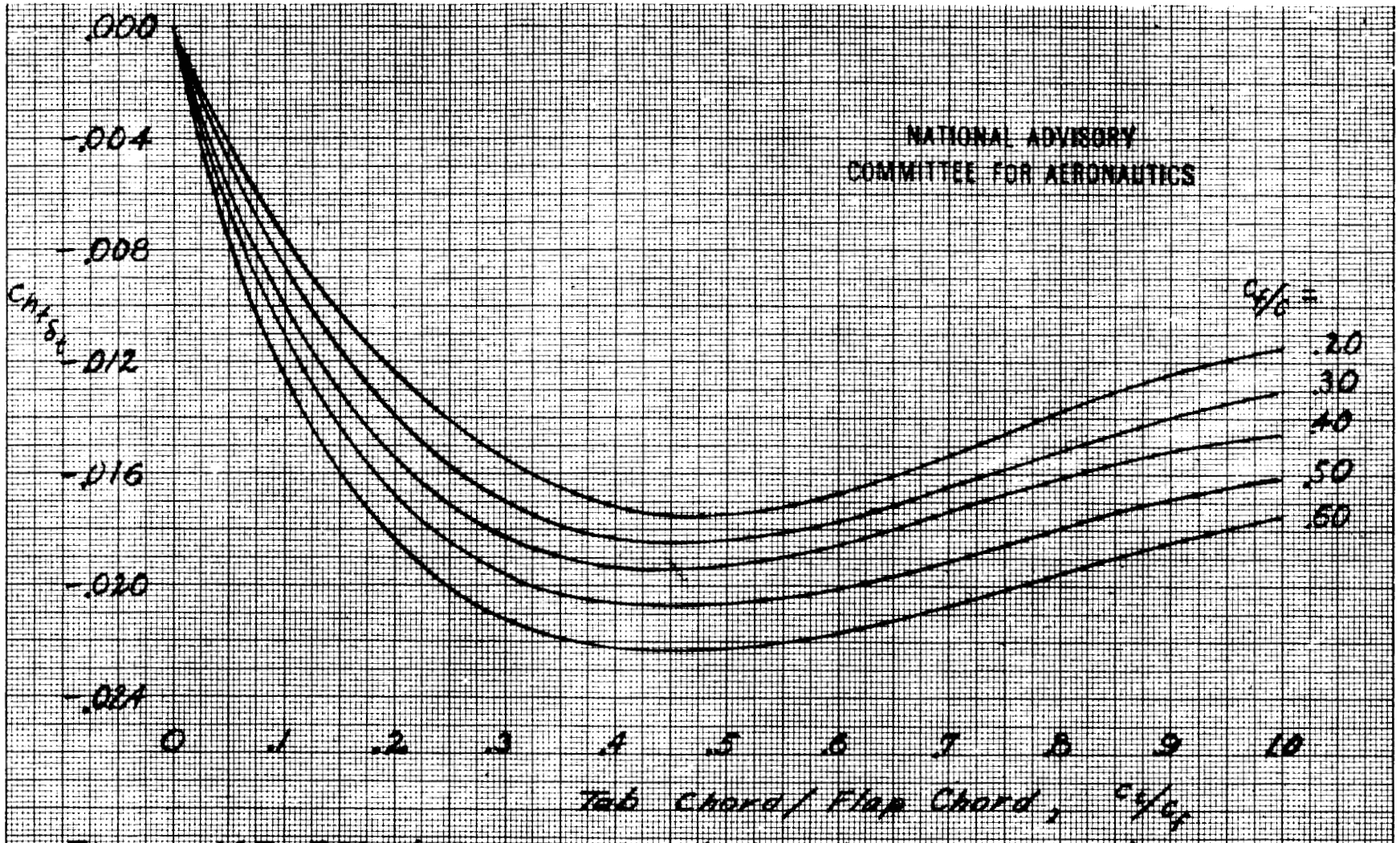

Figure 147.-Effectiveness of tab in changing flap hinge-moment as a function of tab size. Data from pressure-distribution investigation of NACA 0009 airfoil in two dimensional flow. Plain flaps and tabs with sealed gaps.

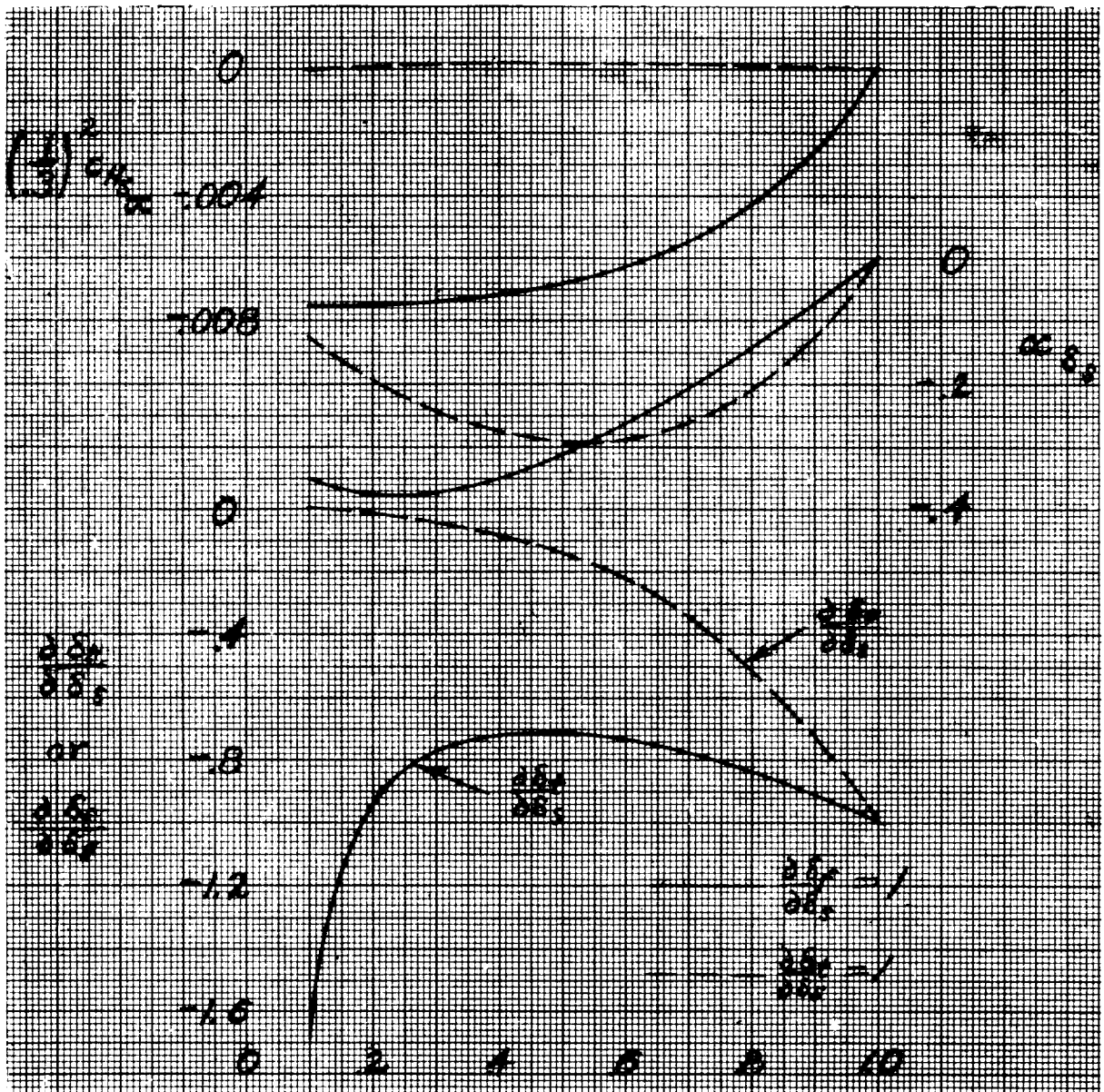

(a) 0.30c flap

Figure 148.- Characteristics of an NACA 0009 airfoil with various arrangements of flaps and balancing tabs to give $c_{H_{\delta_s}} = 0$.

$$c_{H_{\delta_s}} = c_{H_{\delta_f}}\left(\frac{\partial \delta_f}{\partial \delta_s}\right)^2 + \left(c_{H_{\delta_t}} + c_{H_{\delta_f}}\right)\frac{\partial \delta_f}{\partial \delta_s}\frac{\partial \delta_t}{\partial \delta_s} + c_{H_{\delta_t}}\left(\frac{\partial \delta_t}{\partial \delta_s}\right)^2$$

$$c_{H_\alpha} = c_{H_{\delta_f}}\left(\frac{\partial \delta_f}{\partial \delta_s}\right) + c_{H_{\delta_t}}\left(\frac{\partial \delta_t}{\partial \delta_s}\right)$$

$$\alpha_{\delta_s} = \alpha_{\delta_f}\left(\frac{\partial \delta_f}{\partial \delta_s}\right) + \alpha_{\delta_t}\left(\frac{\partial \delta_t}{\partial \delta_s}\right)$$

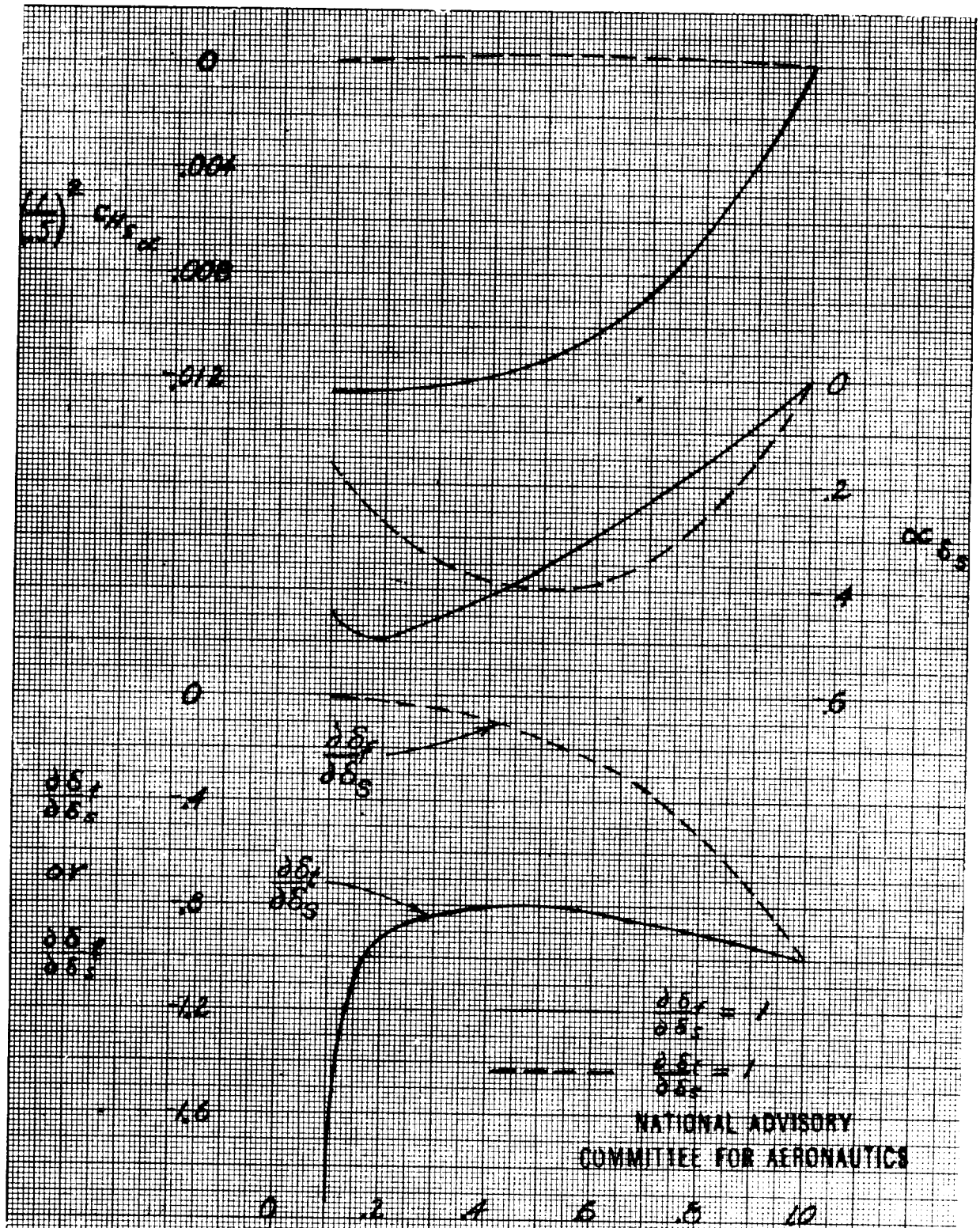

(b) 0.50 c flap.

Figure 148.- Concluded.

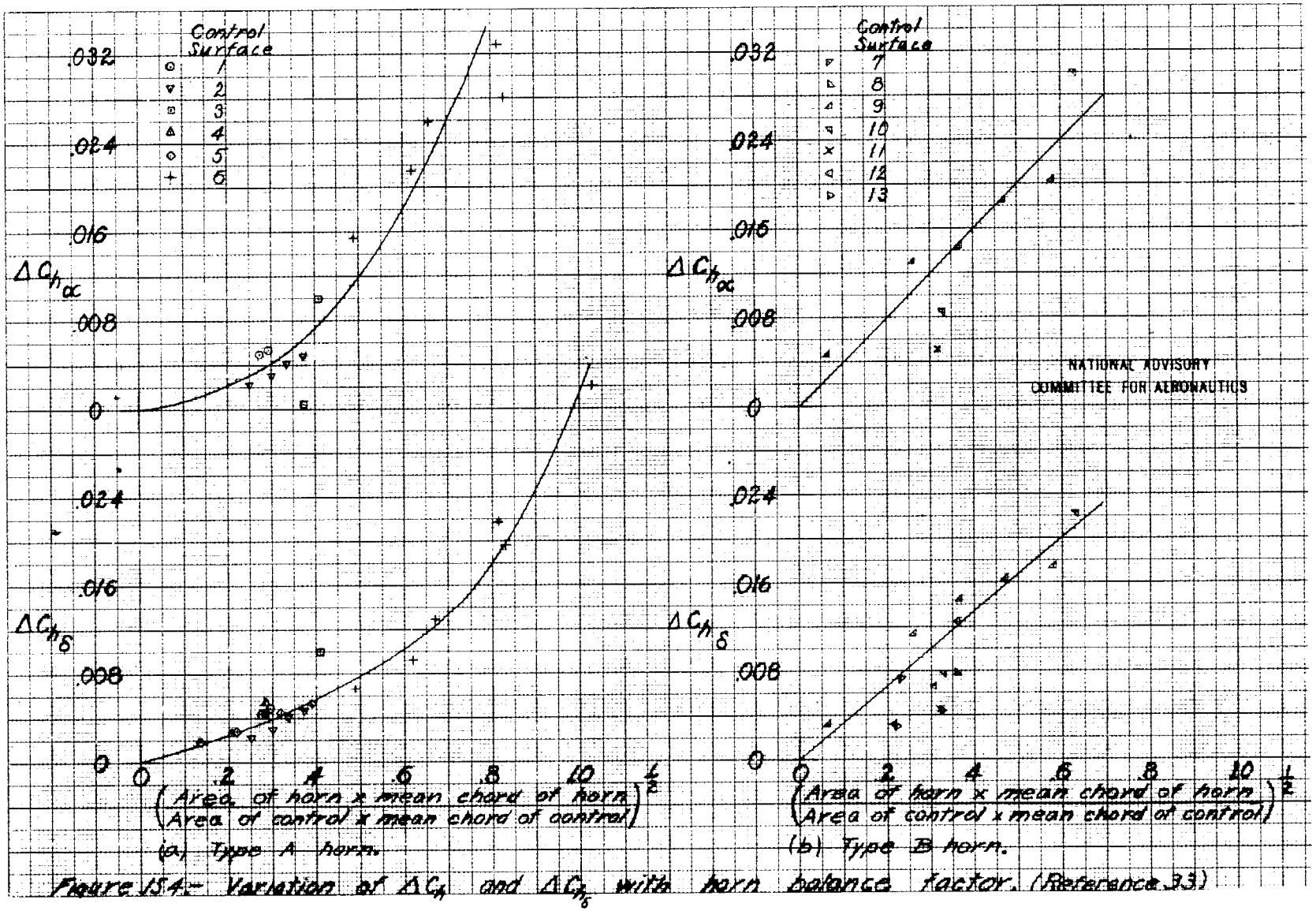

(a) Type A horn.

(b) Type B horn.

Figure 154.- Variation of ΔC_{h_α} and ΔC_{h_δ} with horn balance factor. (Reference 33)

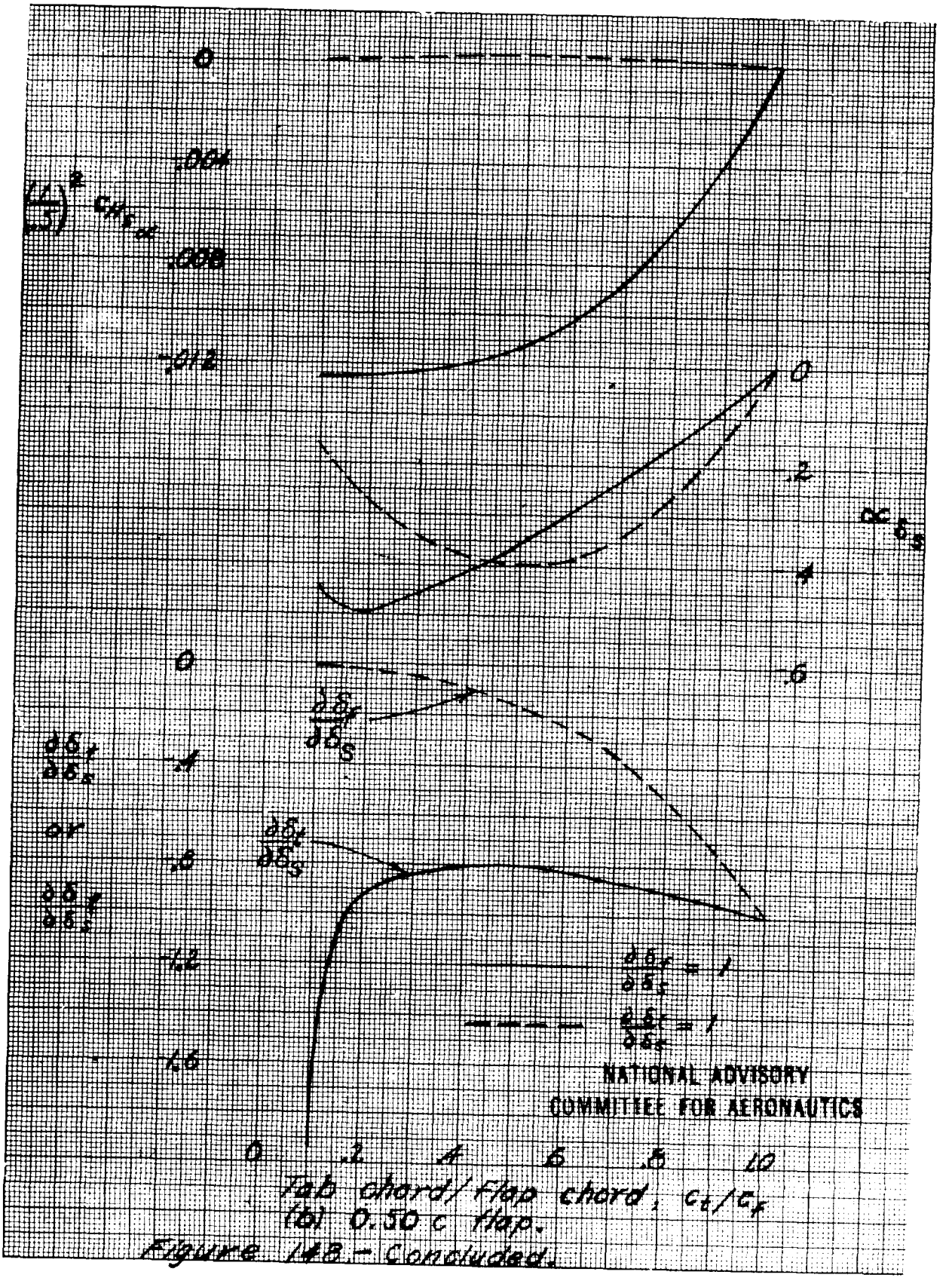

(b) 0.50 c flap.

Figure 148.- Concluded.

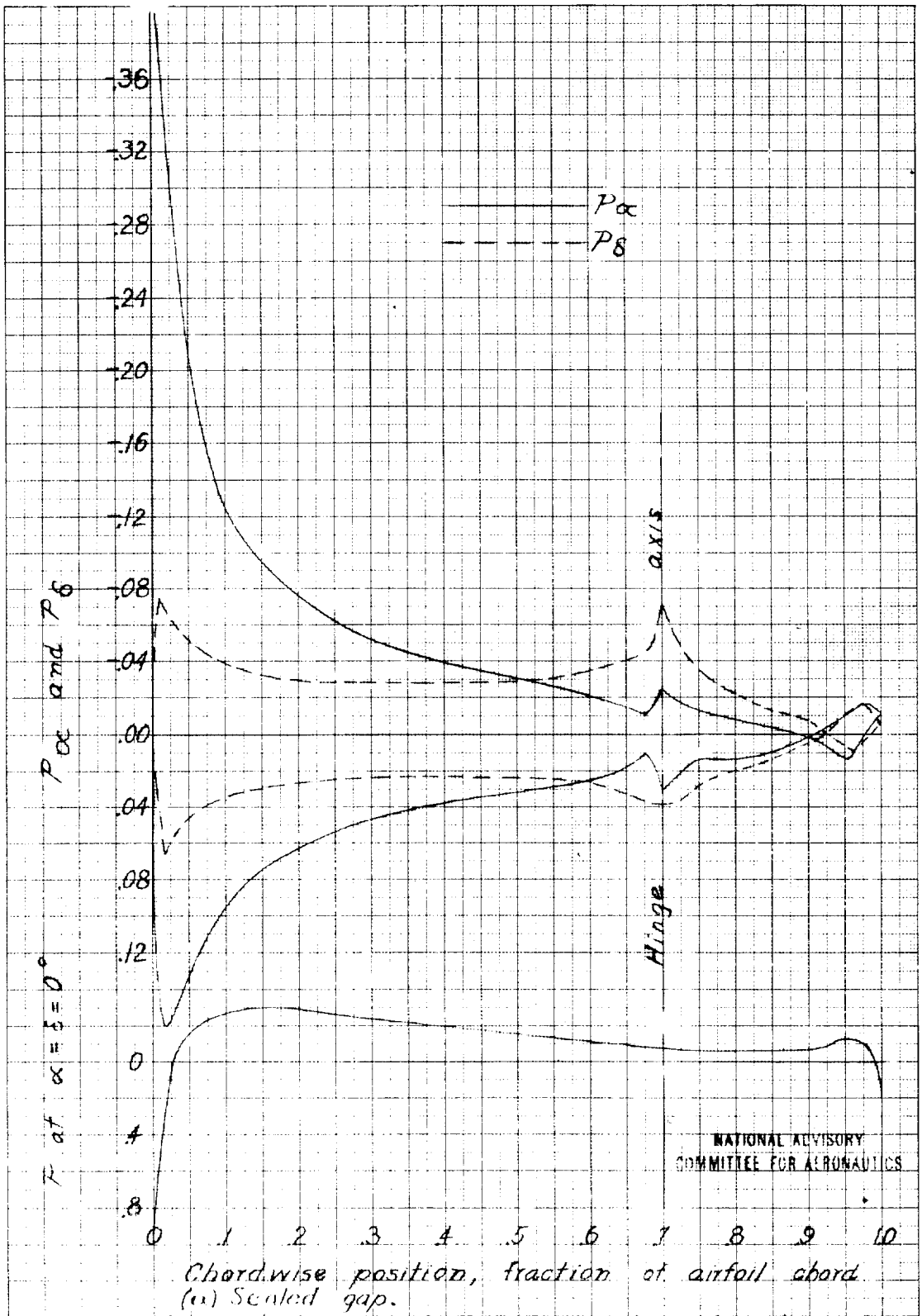

Chordwise position, fraction of airfoil chord.

(a) Sealed gap.

Figure 149.- Pressure distribution characteristics of an NACA 0009 airfoil with a 0.30c flap having a 30° beveled trailing edge. (Unpublished data.)

L-663

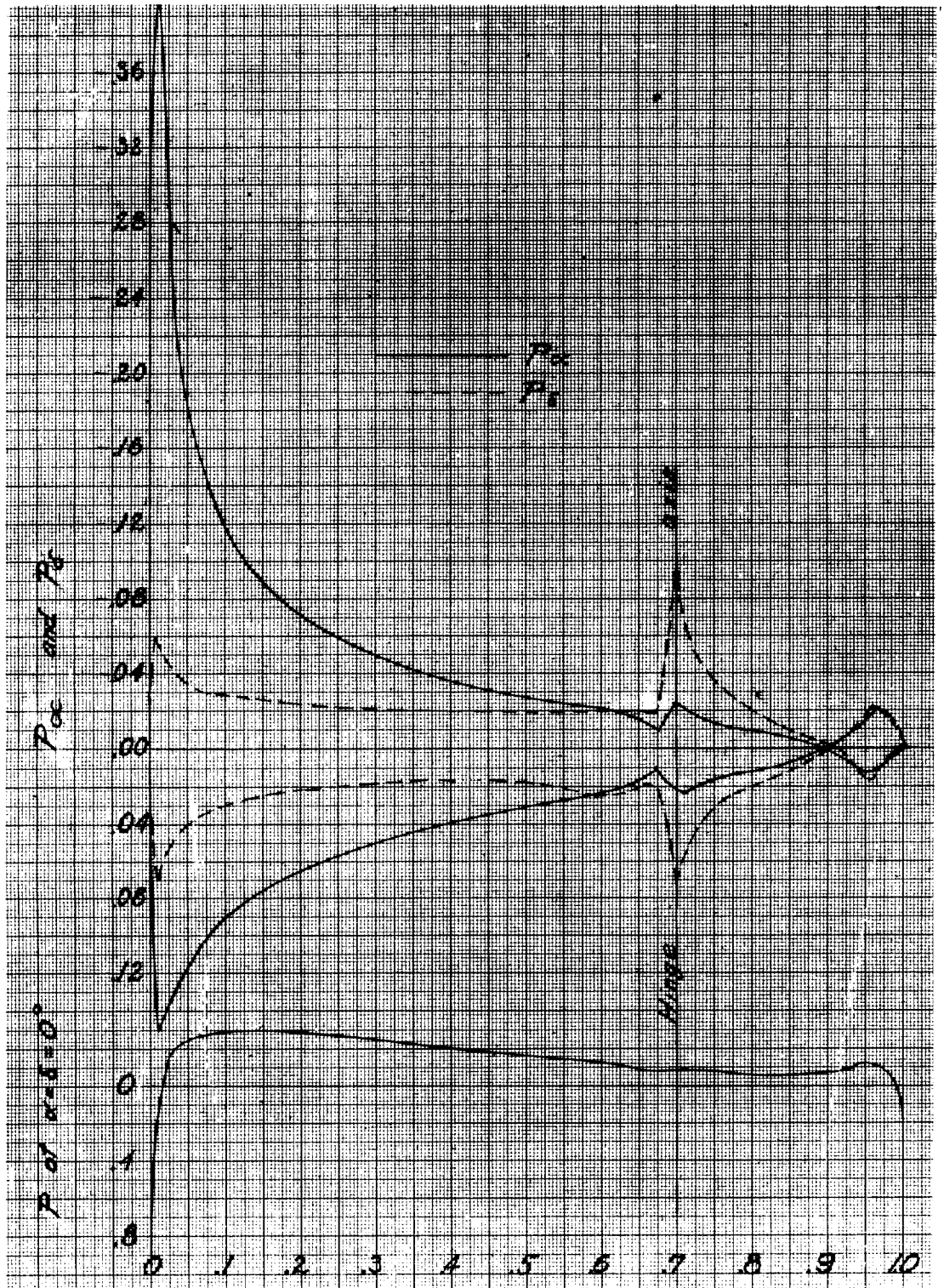

(b) 0.005 c gap.

Figure 149.— Concluded.

NATIONAL ADVISORY
COMMITTEE FOR AERONAUTICS

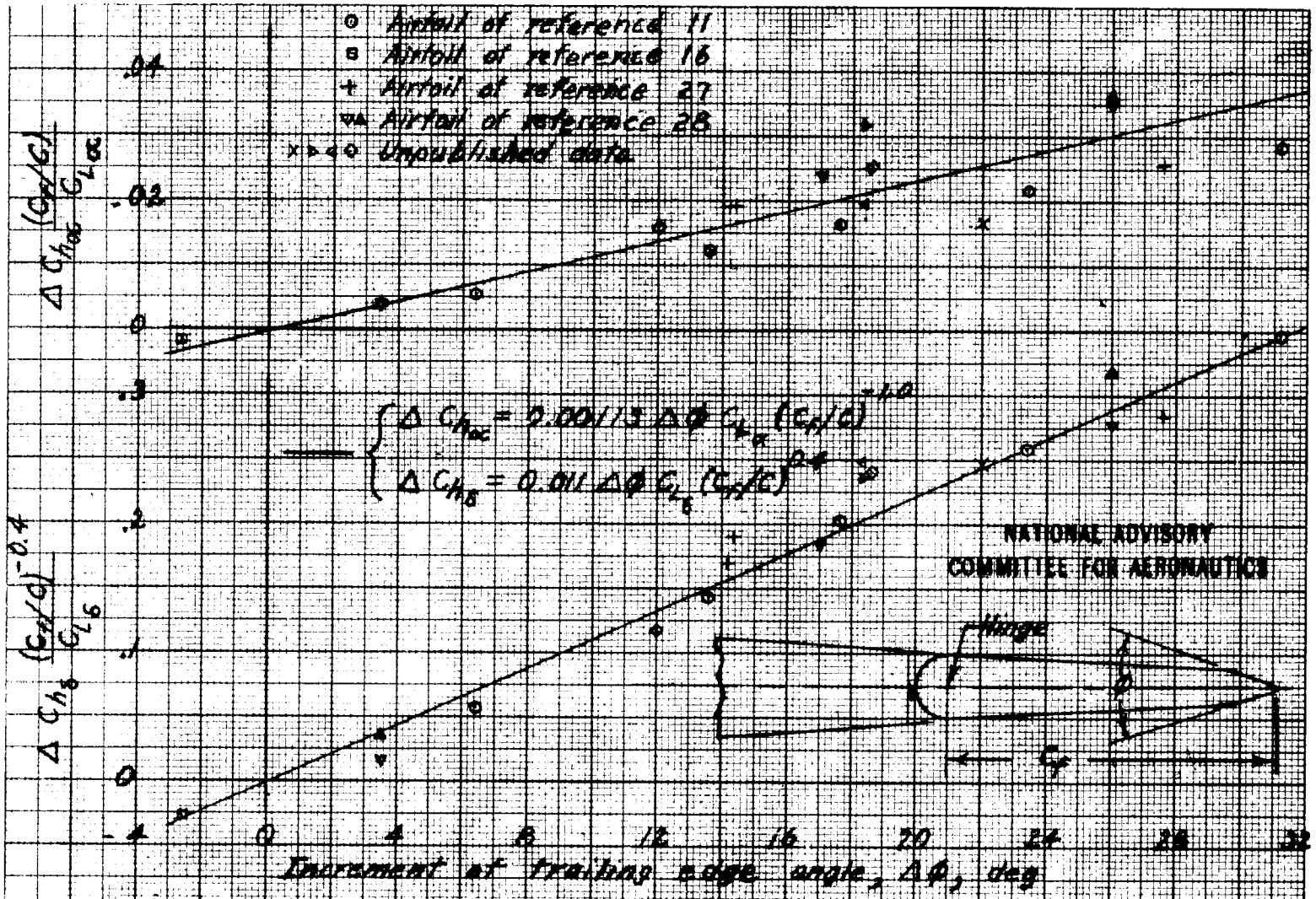

NATIONAL ADVISORY
COMMITTEE FOR AERONAUTICS

Figure 150.- Correlation of hinge moment parameters of beveled trailing-edge flaps on the basis of trailing edge angle. Data adapted from reference 26. Sealed gap.

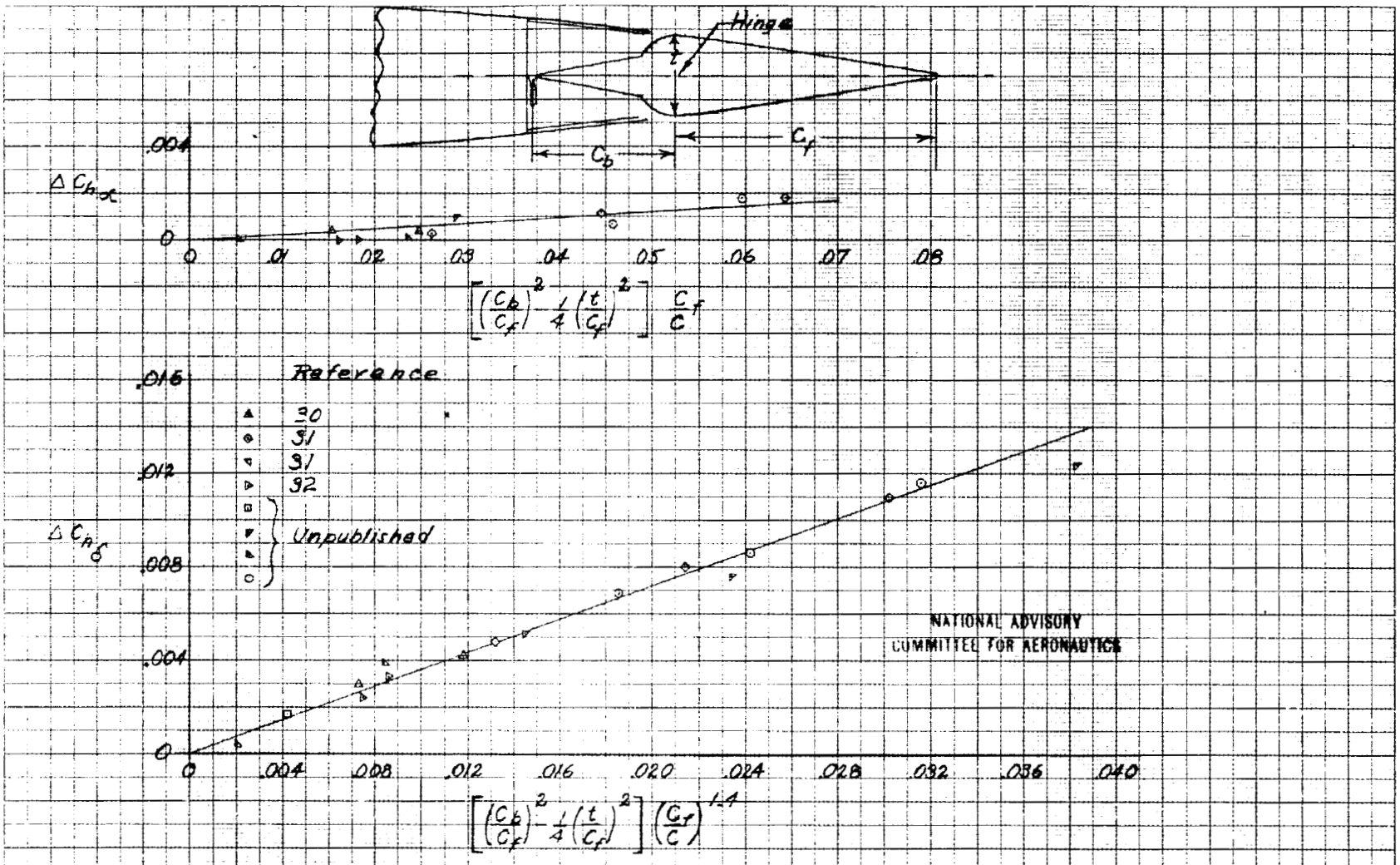

Figure 151.- Correlation of hinge-moment parameters of flaps with internal balance. (Reference 29)

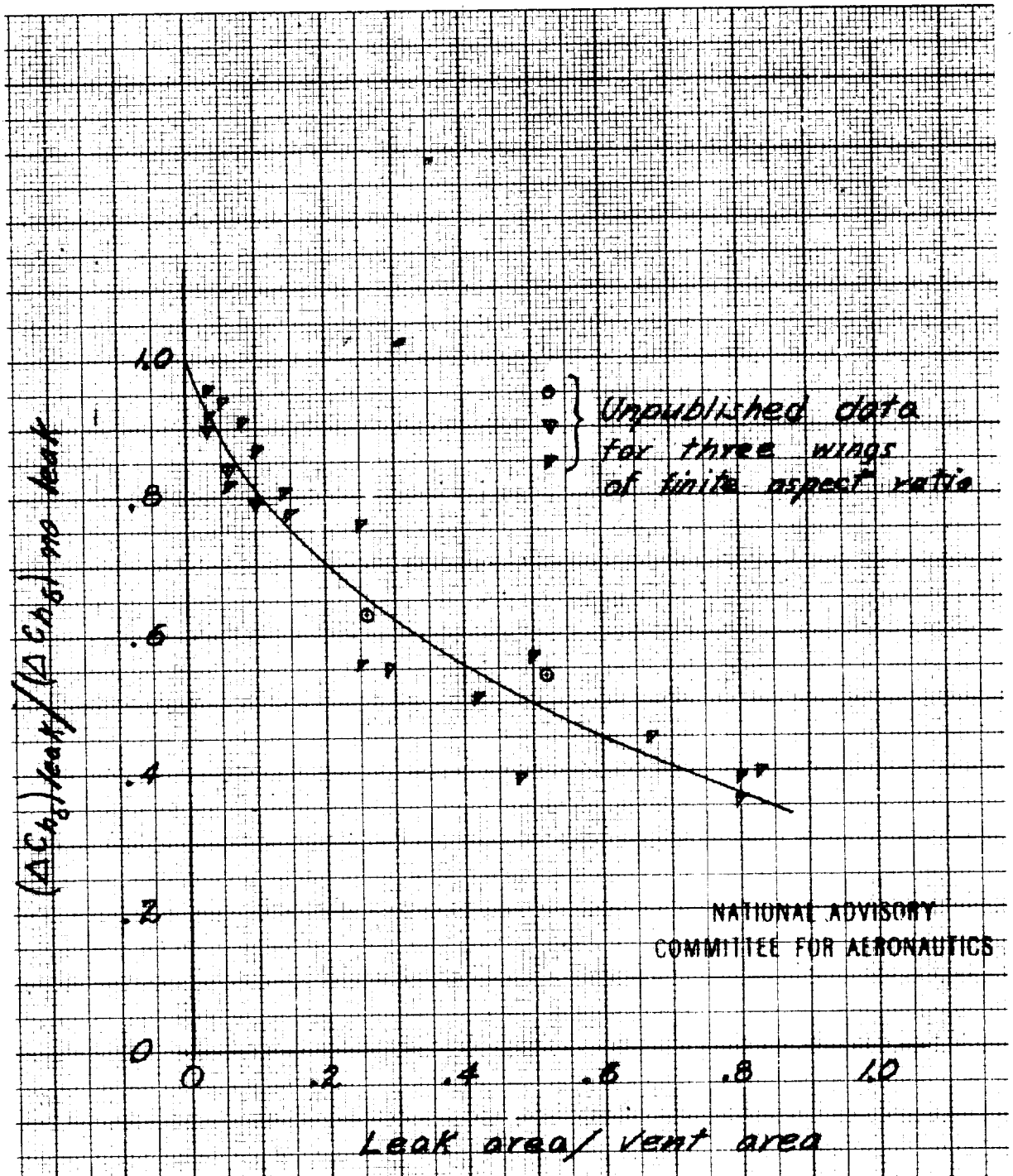

Figure 152.- Effect of ratio of leak area to vent area on hinge moment parameter for flaps with internal type of aerodynamic balance. (Reference 29)

L-663

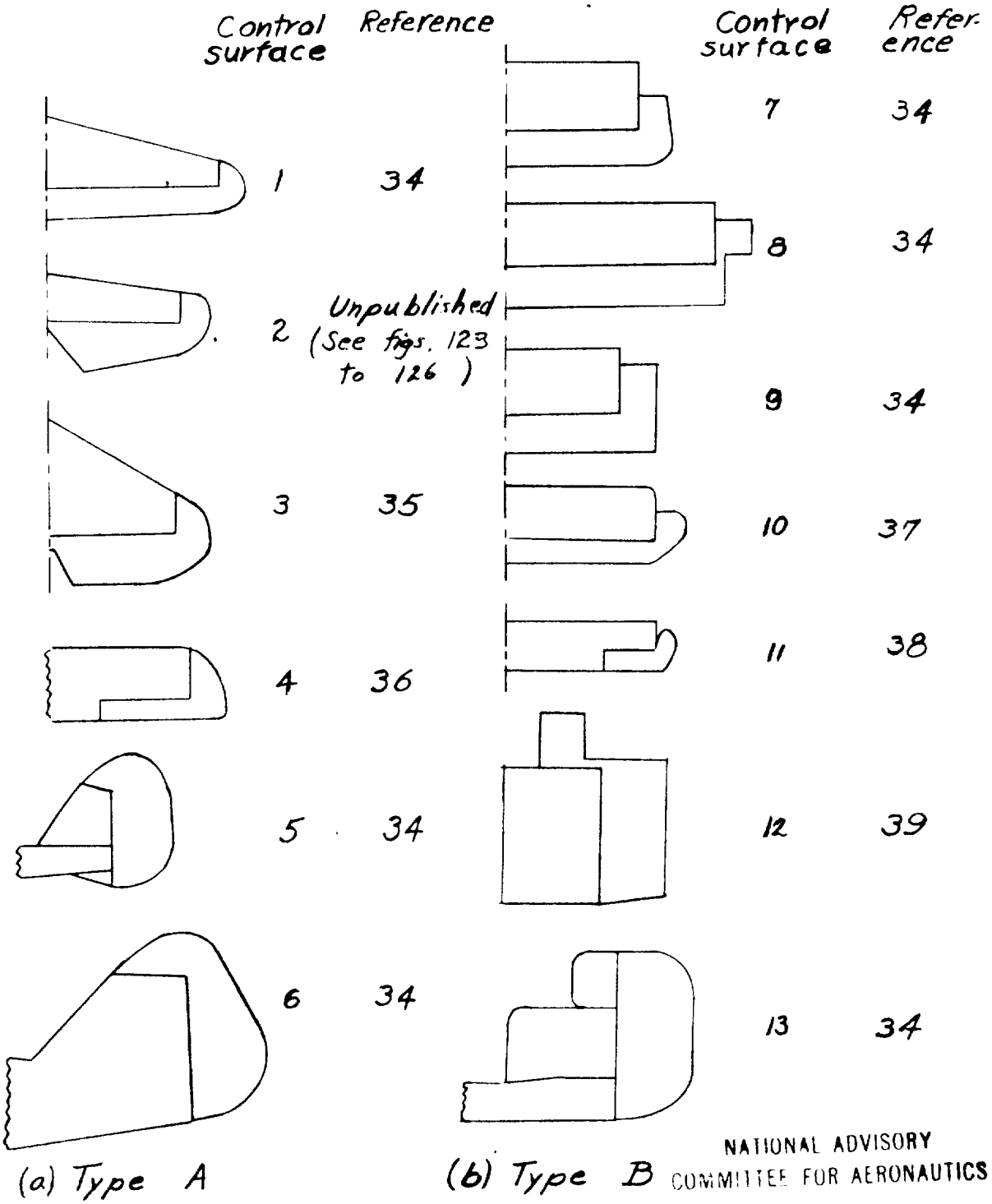

NATIONAL ADVISORY COMMITTEE FOR AERONAUTICS

Figure 153.— Control surfaces with horn type of aerodynamic balance.

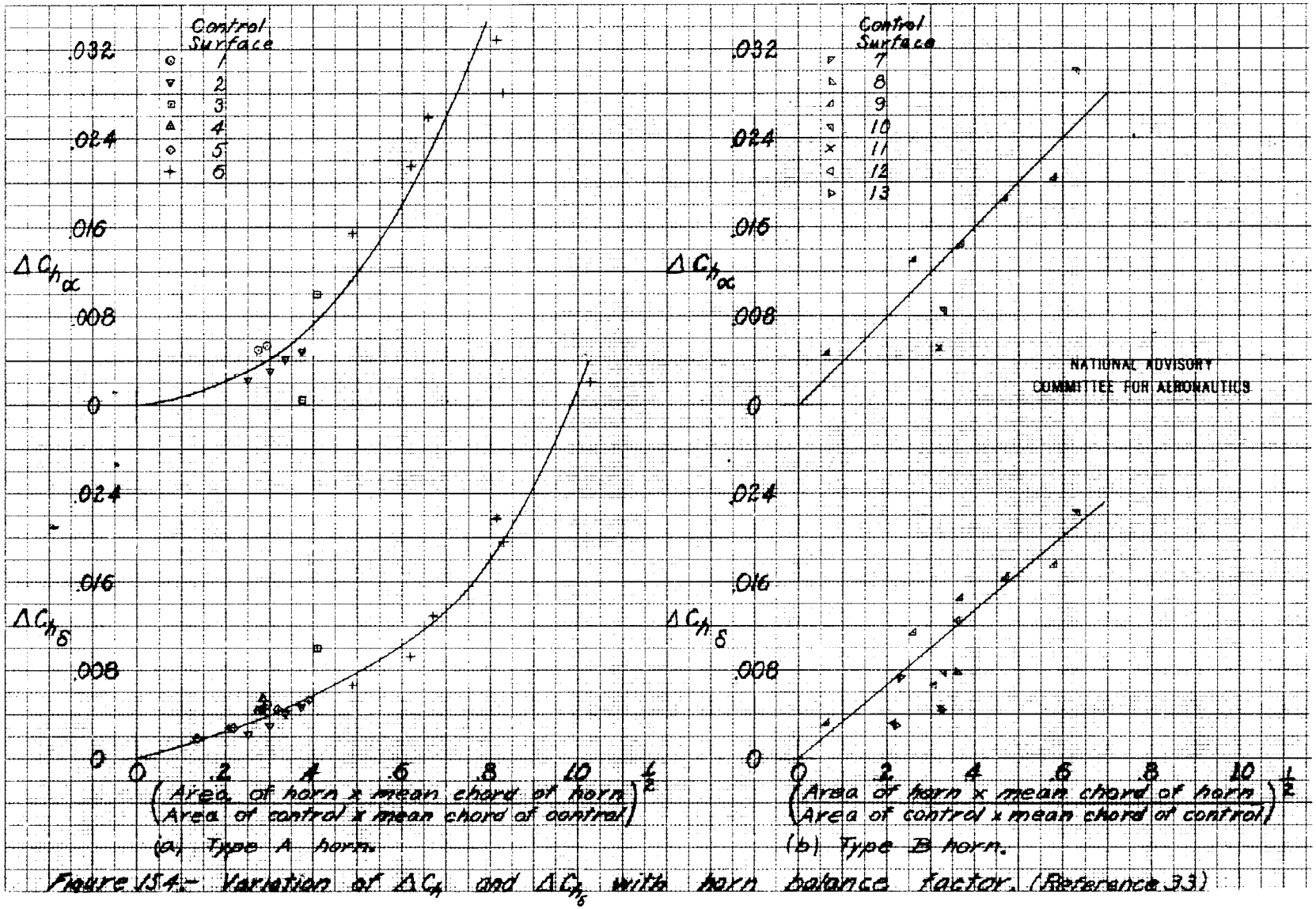

(a) Type A horn.

(b) Type B horn.

Figure 154.- Variation of ΔC_{h_α} and ΔC_{h_δ} with horn balance factor. (Reference 33)

L-663

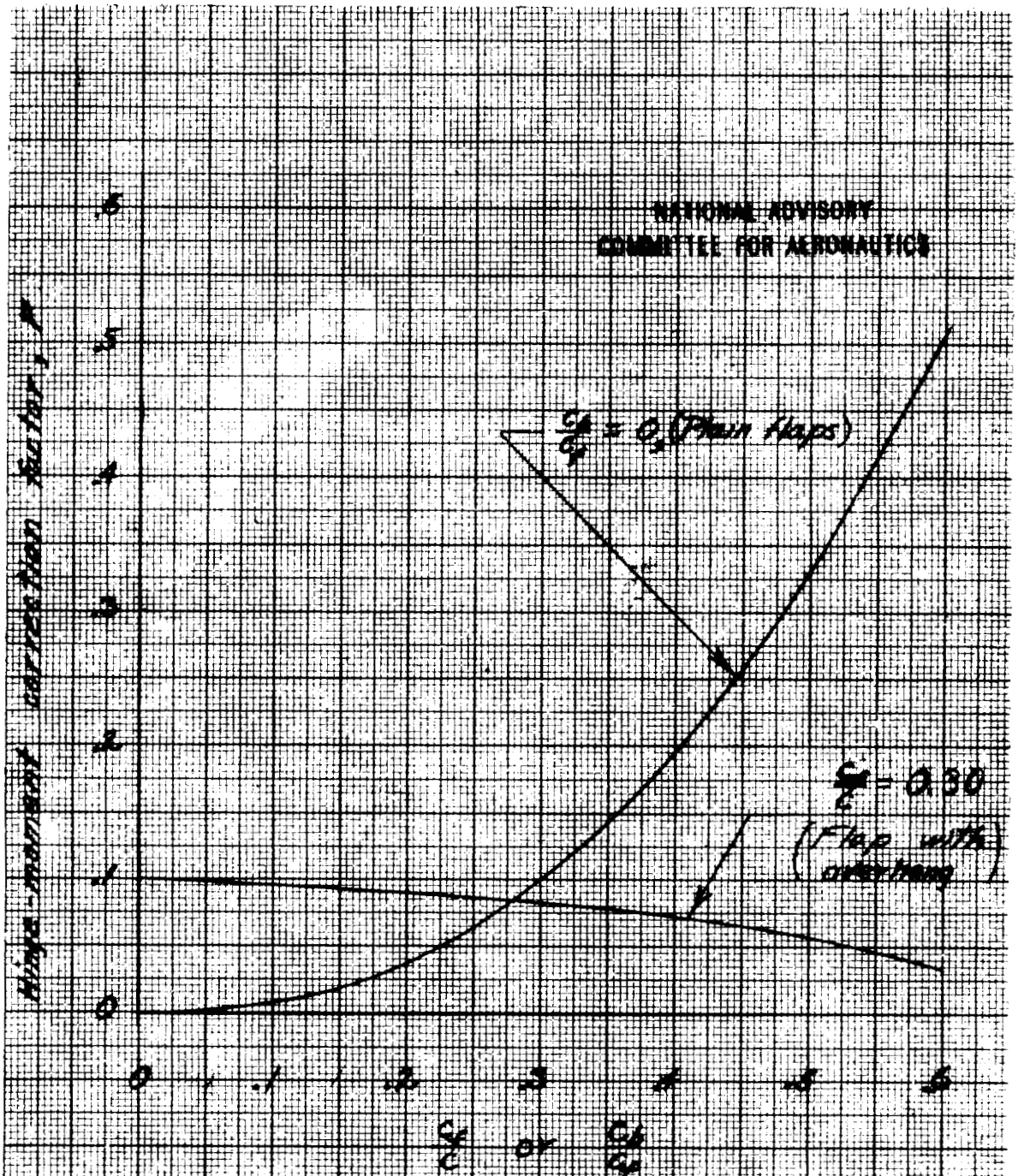

Figure 155.- Variation of hinge-moment, tunnel correction factor F with c_f/c for plain flaps and with c_f/c_p for a 0.30 c flap with overhang. (From reference 40)